



National Library  
of Canada

Bibliothèque nationale  
du Canada

Canadian Theses Service

Service des thèses canadiennes

Ottawa, Canada  
K1A 0N4

## NOTICE

The quality of this microform is heavily dependent upon the quality of the original thesis submitted for microfilming. Every effort has been made to ensure the highest quality of reproduction possible.

If pages are missing, contact the university which granted the degree.

Some pages may have indistinct print especially if the original pages were typed with a poor typewriter ribbon or if the university sent us an inferior photocopy.

Reproduction in full or in part of this microform is governed by the Canadian Copyright Act, R.S.C. 1970, c. C-30, and subsequent amendments.

## AVIS

La qualité de cette microforme dépend grandement de la qualité de la thèse soumise au microfilmage. Nous avons tout fait pour assurer une qualité supérieure de reproduction.

S'il manque des pages, veuillez communiquer avec l'université qui a conféré le grade.

La qualité d'impression de certaines pages peut laisser à désirer, surtout si les pages originales ont été dactylographiées à l'aide d'un ruban usé ou si l'université nous a fait parvenir une photocopie de qualité inférieure.

La reproduction, même partielle, de cette microforme est soumise à la Loi canadienne sur le droit d'auteur, SRC 1970, c. C-30, et ses amendements subséquents.

**NMR Line Shape Studies of Solids:  
Probing Molecular and Electronic Structure  
*via* Experiment and Simulation**

by

William Patrick Power

Submitted in partial fulfilment of the requirements

for the degree of Doctor of Philosophy

at

Dalhousie University

Halifax, Nova Scotia

September, 1991

© Copyright by William Patrick Power 1991



National Library  
of Canada

Bibliothèque nationale  
du Canada

Canadian Theses Service    Service des thèses canadiennes

Ottawa, Canada  
K1A 0N4

The author has granted an irrevocable non-exclusive licence allowing the National Library of Canada to reproduce, loan, distribute or sell copies of his/her thesis by any means and in any form or format, making this thesis available to interested persons.

L'auteur a accordé une licence irrévocable et non exclusive permettant à la Bibliothèque nationale du Canada de reproduire, prêter, distribuer ou vendre des copies de sa thèse de quelque manière et sous quelque forme que ce soit pour mettre des exemplaires de cette thèse à la disposition des personnes intéressées.

The author retains ownership of the copyright in his/her thesis. Neither the thesis nor substantial extracts from it may be printed or otherwise reproduced without his/her permission.

L'auteur conserve la propriété du droit d'auteur qui protège sa thèse. Ni la thèse ni des extraits substantiels de celle-ci ne doivent être imprimés ou autrement reproduits sans son autorisation.

ISBN 0-315-71564-2

Canada

*What we observe is not nature itself  
but nature exposed to our method of questioning.*

- Werner Heisenberg

*The world doesn't yield to us directly,  
the description of the world stands in between.*

- Carlos Castaneda

## Table of Contents

Table of Contents . . . . .	v
List of Figures . . . . .	ix
List of Tables . . . . .	xii
Abstract . . . . .	xiii
List of Symbols . . . . .	xiv
Acknowledgments . . . . .	xviii
Chapter 1	
Introductory Remarks . . . . .	1
Chapter 2	
Background Theory . . . . .	4
2.1 The Field of View . . . . .	4
2.2 The NMR Interactions . . . . .	10
2.2.1 The Zeeman Interaction . . . . .	10
2.2.2 The Radiofrequency Interaction . . . . .	11
2.2.3 The Direct Dipolar Interaction . . . . .	12
2.2.4 The Chemical Shielding Interaction . . . . .	15
2.2.5 The Indirect Spin-Spin Interaction . . . . .	19

2.2.6	The Quadrupolar Interaction . . . . .	20
2.3	Tensors . . . . .	22
2.4	Origin of Powder Line Shapes . . . . .	25
2.5	Multiple-Interaction Line Shapes . . . . .	30
2.5.1	Dipolar - Chemical Shift NMR Line Shapes . . . . .	30
2.5.2	Influence of Isotropic and Anisotropic Indirect Coupling . . . . .	35
2.6	Analysis of Spinning Sidebands in MAS Spectra . . . . .	39

### Chapter 3

	Anisotropic Indirect Spin-Spin Coupling in Solid Mercury Phosphines, [HgPR <sub>3</sub> (NO <sub>3</sub> ) <sub>2</sub> ] <sub>2</sub> . . . . .	41
3.1	Introduction . . . . .	41
3.2	Experimental . . . . .	46
3.3	Results . . . . .	47
3.4	Discussion . . . . .	58
3.5	Conclusion . . . . .	62

### Chapter 4

	Solid-State <sup>31</sup> P NMR Studies of Mercury(II) Phosphonates. Anisotropies of the <sup>31</sup> P Chemical Shift and the <sup>31</sup> P- <sup>199</sup> Hg Indirect Spin-Spin Coupling . . . . .	63
4.1	Introduction . . . . .	63
4.2	Experimental . . . . .	66

4.3	Results and Discussion	68
4.3.1	(EtO) <sub>2</sub> P(O) <sup>14/15</sup> NHPh	68
4.3.2	(EtO) <sub>2</sub> P(O)HgX Complexes	72
4.4	Conclusions	84

## Chapter 5

Anisotropies of the <sup>31</sup> P Chemical Shift and <sup>31</sup> P- <sup>195</sup> Pt Indirect Spin-Spin Coupling in Platinum Phosphines		85
5.1	Introduction	85
5.2	Experimental	89
5.3	Results	90
5.3.1	MAS Spectra	90
5.3.2	Static Spectra	97
5.4	Discussion	105
5.5	Conclusion	110

## Chapter 6

Simulation of NMR Powder Line Shapes of Quadrupolar Nuclei with Half-Integer Spin at Low-Symmetry Sites		111
6.1	Introduction	111
6.2	Theory	116
6.3	Experimental	121

6.4	Results and Discussion . . . . .	122
6.4.1	First-Order Quadrupolar - Chemical Shielding Line Shapes . . . . .	122
6.4.2	Cesium-133 NMR Powder Spectrum of Cs <sub>2</sub> CrO <sub>4</sub> . . . . .	127
6.4.3	Second-Order Quadrupolar - Chemical Shielding Effects on the Central Transition . . . . .	136
6.5	Conclusion . . . . .	140
Chapter 7		
	Concluding Remarks . . . . .	141
Appendix 1		
	<sup>133</sup> Cs Single Crystal NMR Results for Cs <sub>2</sub> CrO <sub>4</sub> . . . . .	143
A.1.1	Introduction . . . . .	143
A.1.2	Experimental Preparation and Operation . . . . .	144
A.1.3	Idiosyncrasies of the Bruker MSL-200 at Dalhousie . . . . .	146
A.1.4	Data Analysis . . . . .	148
A.1.5	Chemical Shielding Parameters . . . . .	151
A.1.6	Quadrupolar Parameters . . . . .	157
Appendix 2		
	Complete FORTRAN-77 Listings of NMR Line Shape Simulation Programs . . . . .	164
	References . . . . .	195

## List of Figures

1. The characteristic "Pake pattern" that arises between two dipolar coupled nuclei	14
2. The orientation of $B_0$ in the principal axis system of the chemical shielding tensor	17
3. Calculated powder line shapes due to chemical shielding	18
4. Stereographic representations of the unit sphere	27
5. Octahedral model of the unit sphere used in the POWDER simulation routine	29
6. Definition of the Euler angles $\alpha$ and $\beta$	33
7. Calculated nmr line shapes for chemical shielding alone and with direct dipolar coupling	34
8. Calculated nmr spectra for one nucleus of a heteronuclear spin-pair	38
9. Phosphorus-31 solid-state nmr spectra of $[\text{HgP}(m\text{-tolyl})_3(\text{NO}_3)_2]_2$	48
10. Phosphorus-31 solid-state nmr spectra of $[\text{HgP}(p\text{-methoxyphenyl})_3(\text{NO}_3)_2]_2$	53
11. Phosphorus-31 solid-state nmr line shapes of $[\text{HgP}(p\text{-tolyl})_3(\text{NO}_3)_2]_2$	55
12. Calculated $^{31}\text{P}$ nmr line shapes of $[\text{HgP}(o\text{-tolyl})_3(\text{NO}_3)_2]_2$	57
13. Experimental and calculated $^{31}\text{P}$ static nmr spectra of $(\text{EtO})_2\text{P}(\text{O})\text{NHPH}$	69
14. Phosphorus-31 CPMAS spectra of two mercury phosphonate compounds	73
15. Phosphorus-31 static nmr spectra of $(\text{EtO})_2\text{P}(\text{O})\text{HgO}_2\text{CCH}_3$	79
16. Phosphorus-31 static nmr spectrum of $(\text{EtO})_2\text{P}(\text{O})\text{HgO}_2\text{CCH}_3$	80

17. Phosphorus-31 CPMAS spectrum of <i>cis</i> -Pt(PPh <sub>3</sub> ) <sub>2</sub> Cl <sub>2</sub>	93
18. Variation of the peak-to-peak splitting with spinning rate of the two isotropic signals of <i>cis</i> -Pt(PEt <sub>3</sub> ) <sub>2</sub> Cl <sub>2</sub>	96
19. Phosphorus-31 static nmr spectra of the <i>trans</i> isomers	100
20. Phosphorus-31 powder nmr line shapes for <i>trans</i> -Pt(PPh <sub>3</sub> ) <sub>2</sub> Cl <sub>2</sub>	102
21. The magnetic field vector, B <sub>0</sub> , oriented in the quadrupolar tensor and in the chemical shielding tensor	119
22. Chemical shielding, quadrupolar, and chemical shielding with quadrupolar calculated nmr spectra for a <sup>133</sup> Cs (I = 7/2) nucleus	123
23. Effect on the calculated <sup>133</sup> Cs nmr line shape of varying the angle β	125
24. Parameters for the two <sup>133</sup> Cs sites in Cs <sub>2</sub> CrO <sub>4</sub>	129
25. Cesium-133 nmr powder spectrum with magic-angle spinning at 4 kHz	130
26. Calculated <sup>133</sup> Cs nmr of each site, their sum, and the experimental <sup>133</sup> Cs nmr spectrum of Cs <sub>2</sub> CrO <sub>4</sub> powder at 26.247 MHz (B <sub>0</sub> = 4.7 T)	132
27. Calculated and experimental <sup>133</sup> Cs nmr powder spectra of Cs <sub>2</sub> CrO <sub>4</sub>	134
28. Calculated nmr powder line shapes of the central transition as the angle β is increased	137
29. Cesium-133 single crystal nmr data and least-squares curves for the central (1/2 ↔ -1/2) transition of Cs <sub>2</sub> CrO <sub>4</sub> for rotations about the X cube axis	152
30. Cesium-133 single crystal nmr data and least-squares curves for the central (1/2 ↔ -1/2) transition of Cs <sub>2</sub> CrO <sub>4</sub> for rotations about the Y cube axis	153

31. Cesium-133 single crystal nmr data and least-squares curves for the central  
( $1/2 \leftrightarrow -1/2$ ) transition of  $\text{Cs}_2\text{CrO}_4$  for rotations about the Z cube axis 154
32. Cesium-133 single crystal nmr data and least-squares curves for the average  
( $7/2 \leftrightarrow -7/2$ ) quadrupolar splittings of  $\text{Cs}_2\text{CrO}_4$  for rotations about the X  
cube axis 158
33. Cesium-133 single crystal nmr data and least-squares curves for the average  
( $7/2 \leftrightarrow -7/2$ ) quadrupolar splittings of  $\text{Cs}_2\text{CrO}_4$  for rotations about the Y  
cube axis 159
34. Cesium-133 single crystal nmr data and least-squares curves for the average  
( $7/2 \leftrightarrow -7/2$ ) quadrupolar splittings of  $\text{Cs}_2\text{CrO}_4$  for rotations about the Z  
cube axis 160

## List of Tables

1. Phosphorus-31 nmr parameters for solid $[\text{HgPR}_3(\text{NO}_3)_2]_2$	49
2. Isotropic $^{31}\text{P}$ chemical shifts and $^{31}\text{P}$ - $^{199}\text{Hg}$ indirect spin-spin coupling constants for the mercury phosphonates	74
3. Phosphorus-31 chemical shift tensor components and anisotropies in $^{31}\text{P}$ - $^{199}\text{Hg}$ indirect spin-spin coupling for the mercury phosphonates	77
4. Phosphorus-31 solid-state nmr spectral parameters for the platinum phosphines from $^{31}\text{P}$ MAS spectra	91
5. Phosphorus-31 solid-state anisotropic nmr spectral parameters for the platinum phosphines	98
6. Average isotropic and anisotropic values of the observed (J) and reduced (K) indirect spin-spin coupling tensors	108
7. Observed and calculated best-fit frequencies for $^{133}\text{Cs}$ nmr spectra of $\text{Cs}_2\text{CrO}_4$ powder	133
8. Cesium-133 chemical shielding (central transition) parameters from the least-squares fits of the rotation plots for the two sites in $\text{Cs}_2\text{CrO}_4$	155
9. Cesium-133 quadrupolar ( $\Delta\nu(7/2)$ splitting) parameters from the least-squares fits of the rotation plots for the two sites (two for each site) in $\text{Cs}_2\text{CrO}_4$	161

## Abstract

The nuclear magnetic resonance line shapes of solid compounds are used to gain new and fundamental information on several chemical systems. Analysis of the  $^{31}\text{P}$  nmr line shapes of several metal-phosphorus systems is used to characterize the anisotropic nature of the  $^{31}\text{P}$  chemical shielding and metal-phosphorus indirect spin-spin coupling. This work has revealed that substantial anisotropies exist in the indirect spin-spin coupling between  $^{31}\text{P}$  and  $^{199}\text{Hg}$  or  $^{195}\text{Pt}$ . In the mercury(II) phosphines,  $[\text{HgPR}_3(\text{NO}_3)_2]_2$ , these anisotropies are quite large, of the order of 5 kHz, for couplings that possess isotropic values of approximately 10 kHz. Although the isotropic  $^{31}\text{P}$ - $^{199}\text{Hg}$  indirect spin-spin couplings are larger in the mercury(II) phosphonates,  $\text{HgP}(\text{O})(\text{OEt})_2\text{X}$ , this study indicates that the anisotropies in these couplings are much smaller. In the square-planar platinum(II) bisphosphine complexes,  $\text{Pt}(\text{PR}_3)_2\text{Cl}_2$ , the  $^{31}\text{P}$ - $^{195}\text{Pt}$  indirect couplings are found to possess anisotropies in the indirect spin-spin couplings of at least 1 to 2 kHz, although a dependence of these values on the geometry of the complex cannot be determined. These findings are significant as they demonstrate that the indirect spin-spin coupling between  $^{31}\text{P}$  and some metal nuclei is not dominated by the Fermi contact mechanism, as has been commonly assumed. The nmr line shapes of half-integer spin quadrupolar nuclei are found to be sensitive to the relative orientation of the chemical shielding and quadrupolar interactions, and a method to interpret such line shapes is proposed. This is used to simulate the  $^{133}\text{Cs}$  nmr powder spectra of  $\text{Cs}_2\text{CrO}_4$  at four magnetic fields, as these interactions are not aligned in this compound.

## List of Symbols

$\alpha, \beta, \gamma$	-	Euler angles
$B_0$	-	applied static magnetic field
$B_{rf}$	-	applied radiofrequency field
CP	-	cross-polarization
CS	-	chemical shielding
Cy	-	cyclohexyl
$c_{in}$	-	coefficient of $n$ atomic orbital to $i$ molecular orbital
$\gamma_n$	-	magnetogyric ratio of nucleus $n$
DD	-	direct dipolar
$\Delta J$	-	anisotropy of indirect spin-spin coupling
$\Delta K$	-	anisotropy of reduced indirect spin-spin coupling
$\Delta\nu$	-	frequency difference or splitting
$\Delta\sigma$	-	chemical shielding anisotropy
${}^3\Delta E$	-	triplet excitation energy
$\delta_{iso}$	-	isotropic chemical shift
$\delta_{11}, \delta_{22}, \delta_{33}$	-	principal components of the chemical shift tensor
$\mathcal{E}fg$	-	electric field gradient
Et	-	ethyl
$eQ$	-	nuclear quadrupole moment
eq	-	electric field gradient

$\mathcal{H}$	-	Hamiltonian
$\eta_Q$	-	asymmetry in nuclear quadrupolar coupling
$\eta_\sigma$	-	asymmetry in chemical shielding
$I, S$	-	general nuclear spins
$\mathbf{I}, \mathbf{S}$	-	general nuclear spin vectors
$I_z, S_z$	-	nuclear spin vector components along static magnetic field
$I_+, S_+$	-	nuclear spin raising operators
$I_-, S_-$	-	nuclear spin lowering operators
$J$	-	indirect spin-spin
$\mathbf{J}$	-	indirect spin-spin coupling tensor
$J_{\text{iso}}$	-	isotropic indirect spin-spin coupling constant
$J_{\parallel}, J_{\perp}$	-	components of indirect spin-spin coupling tensor along and perpendicular to internuclear vector
$K_{\text{iso}}$	-	isotropic reduced indirect spin-spin coupling constant
$M$	-	general metal nucleus
$MO$	-	molecular orbital
$\text{mes}$	-	mesityl
$m_I$	-	spin state of nucleus I
$\mu$	-	magnetic moment
$\text{nmr}$	-	nuclear magnetic resonance
$\text{nqr}$	-	nuclear quadrupole resonance
$\nu$	-	frequency

$\nu_0$	-	Larmor frequency
$\nu_{DJ}$	-	coupling frequency
$\nu_Q$	-	quadrupolar frequency
$\nu_\sigma$	-	chemical shielding frequency
$\theta, \phi, \vartheta, \varphi$	-	orientation angles
$\theta_m$	-	magic angle
PAS	-	principal axis system
Ph	-	phenyl
Q	-	quadrupolar
$Q_2$	-	second-order quadrupolar term
R	-	general alkyl or aryl group
$R_{DD}$	-	direct dipolar coupling constant
$R_{\text{eff}}$	-	effective dipolar coupling constant
rf	-	radiofrequency
$r_{IS}$	-	I-S internuclear separation
$\mathbf{r}_{IS}$	-	I-S internuclear vector
$\rho(m)$	-	intensity of the $m$ transition
$\mathbf{S}^D$	-	orientational order tensor
$s_n(0)$	-	value of $s$ orbital at nucleus $n$
$\sigma$	-	chemical shielding tensor
$\sigma_{\text{iso}}$	-	isotropic chemical shielding constant
$\sigma_{11}, \sigma_{22}, \sigma_{33}$	-	principal components of chemical shielding tensor

$t$	-	time
tot	-	total
$\mathbf{V}$	-	electric field gradient tensor
$V_{11}, V_{22}, V_{33}$	-	principal components of electric field gradient tensor
$\omega$	-	angular frequency
$\chi$	-	quadrupolar coupling constant
$Z$	-	Zeeman
§	-	section

All other symbols correspond to their standard usage.

## Acknowledgments

Before all others, I must sincerely thank my supervisor, Prof. Rod Wasylshen. "The Boss" has been a constant source of training, support, patience and encouragement over the time I have spent in his lab. He places Science, then his students, before all else, and I hope the work contained herein is a good reflection of the high standards he holds for his own research and all that study with him.

Next, I must thank my coworkers on the projects that are detailed in the thesis. Mike Lumsden possessed the synthetic capabilities that provided the mercury-phosphorus compounds used in Chapters 3 and 4. Dr. Ron Curtis spent considerable time training this experimental neophyte in the practical side of solid-state nmr, and obtained some of the preliminary spectra for the platinum phosphines in Chapter 5. Dr. Arnold Kentgens of the University of Nijmegen and Dr. Alan Berger of the Naval Surface Weapons Centre in Maryland provided the programs to perform sideband analysis of MAS spectra. Dr. Sandra Mooibroek of Bruker Canada and Profs. Brian Pettitt and Werner Danchura of the University of Winnipeg helped identify the problem and potential solutions concerning the generalization of the nmr line shape theory for quadrupolar nuclei in Chapter 6. Sandra, Dr. John Walter of NRC-Halifax and Dr. Laima Baltusis of Varian Associates also provided the  $^{133}\text{Cs}$  nmr spectra of polycrystalline  $\text{Cs}_2\text{CrO}_4$  at magnetic fields other than 4.7 T. Prof. Stan Cameron provided the crystallographic expertise and equipment needed to characterize the unit cell axes in the single crystal of  $\text{Cs}_2\text{CrO}_4$ , described in the Appendix. The efforts of all these people are greatly appreciated.

The other members of the nmr group have continuously given me support, education and encouragement, especially Prof. Glenn Penner, Dr. Marco Gruwel, Mark MacIntosh, Gang Wu, and Dr. Klaus Eichele. Thanks for all the discussions, and remember, Klaus, just one! Thanks are also due to Prof. Don Hooper and the Atlantic Region Magnetic Resonance Centre, where most of the spectra contained in this thesis were acquired.

Financial support was provided by NSERC, the Killam Trust, the Walter Sumner Foundation, and Dalhousie University, including specifically the Department of Chemistry, and I thank them for their support.

Outside of the lab, the friendship of several special people made my time at Dalhousie particularly enjoyable, and I am grateful to Dr. Bruce Royan, Kevin McMaHon, Phil Elliott, Andrew Nurse and Ed (the man...) Stoddard for dragging me out of the lab when I needed it. Dean Hopkins and "the boys" provided much amusement, except late in the season, when they could only trigger frustration. Let's go, Citadels!!!

I must also thank my parents and my sister, for always encouraging my studies, even when I bored them talking about it, and for all the home cooking.

The final word is reserved for Patricia, who, besides proof-reading this document, has been a part of much of the last 5 years, and will be a big part of everything to come. Thanks for your patience and caring, it would have been a lonely time without you, even at a 1000-mile distance. I hope it has been worth the wait! *Amor vincit omnia!*

# Chapter 1

## Introductory Remarks

This thesis is concerned with the interpretation of the line shapes obtained in the nuclear magnetic resonance (nmr) experiment of solid compounds. Various nuclear, electronic and structural characteristics of a solid compound can influence the nmr line shape. These effects often do not occur alone, but are superimposed on each other, resulting in complicated nmr spectra. The goal of the research described in this thesis is to decipher these complex line shapes in order to gain new and fundamental information about not only the compounds, but also the various perturbing influences themselves.

There are two main accomplishments in the research related in this thesis. The first is the determination of substantial anisotropies in the indirect spin-spin coupling (or  $J$  coupling) between phosphorus and metal nuclei in several metal-phosphorus compounds. This provides the best experimental evidence to date that mechanisms other than the Fermi contact contribute to the electron-mediated transmission of spin information between the two nuclei. This result is important because many of the existing explanations for the trends in the values of  $J_{iso}$  begin by assuming the complete domination of the Fermi contact term. Clearly, these interpretations will have to be reconsidered.

The second accomplishment is the complete generalization of the nmr line shape theory for half-integer spin quadrupolar nuclei. Until recently, the accepted theory did

not allow the two contributing interactions, nuclear quadrupolar coupling and anisotropic chemical shielding, to be non-coincident, as may occur for nuclei at low-symmetry sites in solid compounds. This drawback was recognized and removed in the course of the research outlined in this thesis. This also is a significant advancement, as the solid-state nmr spectra of quadrupolar nuclei are receiving increasing attention recently.

The study of nmr line shapes, of which this thesis becomes a part, has a distinguished history. Pake<sup>1</sup> made the first significant contribution in 1948 when he was able to determine the <sup>1</sup>H-<sup>1</sup>H separation in H<sub>2</sub>O for the hydrating water in gypsum, CaSO<sub>4</sub>·2H<sub>2</sub>O. From the width of the <sup>1</sup>H nmr powder line shape, he derived a value of 1.58 Å ± 2%. Until recently, this represented one of the most precise investigations of the structure of the water molecule. Pake's study was followed two years later by a consideration of the effects of nuclear quadrupolar coupling on the nmr line shape by Pound.<sup>2</sup> As well as providing the necessary theory to understand such line shapes, he gave several experimental nmr powder spectra for <sup>7</sup>Li, <sup>23</sup>Na and <sup>27</sup>Al, all of which are quadrupolar and possess a nuclear spin of 3/2.

The first interpretation of a multiple-interaction nmr line shape appeared in 1955 in a detailed report by Bloembergen and Rowland<sup>3</sup> of the <sup>203</sup>Tl and <sup>205</sup>Tl nmr powder spectra of metallic Tl and Tl<sub>2</sub>O<sub>3</sub>. The most significant feature of this investigation was the observation and analysis of the effects of direct dipolar coupling, anisotropic chemical shielding and anisotropic indirect spin-spin coupling, especially when one considers that neither anisotropic chemical shielding nor anisotropic indirect coupling had been observed previously. Since this time, the nmr powder line shapes of many systems have attracted

the interest of chemists, physicists and biologists. Technical advances in nmr instrumentation as well as more detailed line shape theories have increased the accuracy and applicability of solid-state nmr to a variety of systems. Some of these applications are outlined in this thesis.

The thesis begins with a consideration of the necessary theoretical background, in terms of the frequency response of the various nmr interactions, and their manifestations in the observed nmr line shapes. The effects of multiple interactions have been treated explicitly, as this is a central theme of the thesis. Chapters 3 through 5 detail the investigations of the  $^{31}\text{P}$  nmr powder line shapes of mercury(II) phosphines and phosphonates and platinum(II) bisphosphine complexes. These three chapters constitute the significant results concerning the characterization of anisotropic J coupling. Chapter 6 describes the improved line shape theory for quadrupolar nuclei with half-integer spin, and provides an experimental example of such influences on the  $^{133}\text{Cs}$  nmr powder spectra of  $\text{Cs}_2\text{CrO}_4$  at four magnetic field strengths. The experimental sections relating to each chapter are included with the chapter, rather than in a separate section. After some concluding remarks, the thesis ends with supplementary material included in two appendices. Appendix 1 describes the single crystal nmr experiment that was performed to corroborate the results of Chapter 6. Appendix 2 contains the complete Fortran-77 listings of the line shape simulation programs used exclusively throughout the thesis. It is hoped that their inclusion in the thesis will mark their birthplace and not their resting place.

## Chapter 2

### Background Theory

#### 2.1 The Field of View

Nuclear magnetic resonance (nmr) spectroscopy is based on the interaction between the magnetic moment of a nucleus and an external magnetic field. That the nucleus responds to this external influence is a consequence of it possessing a property called "spin." Not all nuclei have spin; fortunately for the nmr spectroscopist, of the first 92 elements of the periodic table, 80 have a non-radioactive isotope possessing spin. The application of a magnetic field removes the degeneracy in the  $2I+1$  energy levels corresponding to the spin  $I = \frac{n}{2}$  ( $n=1-9$ ) of the nuclear magnet; this is the Zeeman interaction. Depending on the spin of the nucleus, there may be two to ten such energy levels. The strength of the magnetic moment of a given nuclear isotope distinguishes it from all the others by the difference in its energy levels, stronger magnets having larger energy-level separations. Transitions between these levels can be stimulated by applying electromagnetic radiation of the proper energy, analogous to other forms of spectroscopy. Only transitions between adjacent levels are directly observable in nmr. What distinguishes nmr from other spectroscopic methods is its dependence on transitions between nuclear rather than electronic energy levels. In general, the transitions detected in nmr are of much lower energy than those probed in electronic spectroscopies, making sensitivity (more commonly referred to as "signal-to-noise") a constant obsession of the nmr spectroscopist. The relaxation time, or lifetime of the nucleus in a given spin state,

is also significantly longer in nmr, of the order of seconds, than those of UV or IR spectroscopies, which range from  $\mu\text{s}$  to ns time scale.<sup>4</sup> The advantage of this is clear if one considers the Uncertainty Principle,  $\Delta E \Delta t \approx h$ . If relaxation is slow, *i.e.*,  $\Delta t \approx 1\text{s}$ , typical for protons,  $\Delta E$  will be very small, allowing tremendous resolution of nuclear transitions. It is predominantly this characteristic that has led to the widespread application of nmr by chemists. Higher resolution permits greater opportunities to distinguish subtle differences in similar species. In solution studies, the main constraints on available resolution are instrumental factors, such as field inhomogeneities, rather than any "natural" influences.

If nmr detected only the simple interaction between the nuclear magnet and the applied field, it would be of little interest to the chemist, and completely in the realm of the nuclear physicist interested in nuclear structure. However, many other factors can influence the transitions between nuclear energy levels, factors which relate to the electronic structure of a compound. In this short section, the influences on the nuclear magnet that relate to such factors of chemical interest will be presented in a descriptive rather than mathematical fashion. A more rigorous description follows in §2.2.

Consider first a single isolated nucleus possessing spin  $I=1/2$ , motionless and in the absence of any electrons, in a magnetic field. The separation between its two energy levels or "spin states" (often referred to as "spin up" or "spin down" for spin- $1/2$  nuclei) is governed solely by the Zeeman interaction. Note that there is no intermediate state between "up" and "down", *i.e.*, there is no classical analogy to "spin". If one other nuclear spin is added, these two will interact in a similar fashion to two bar magnets

placed in proximity to each other. The magnets will be sensitive to the orientation of each other, and the strength of the interaction will depend on the distance between them. For the two nuclei, this results in the direct dipolar interaction. The energy transitions of each nuclear spin become slightly modified, increasing or decreasing depending on the spin state of the other nucleus (rather than spatial orientation). The strength of this interaction is measured readily as the amount of change in the nuclear energy levels of either nucleus. Using the classical expression for the interaction of two magnetic dipoles, the separation between the two nuclei can be determined from this energy change. The ability of nmr to provide this type of information has made a profound contribution to structural science, evident in the literature from 1948<sup>1</sup> to present.<sup>5</sup> Only neutron diffraction provides similar details about internuclear separations; no measurement of electron density is performed to provide this information in either technique.

If the second nucleus is replaced by an electron revolving around the first nucleus in an atomic orbital, a different situation occurs. The electron makes this an electronic paramagnetic centre, as it is unpaired. In general, nuclei at such sites are not observed in nmr due to relaxation; the short lifetime of the electronic spin state provides an efficient pathway for energy added to this system to be passed away from the nucleus. In practice, there are many other mechanisms by which relaxation can occur, for both diamagnetic and paramagnetic systems.<sup>4,6,7</sup> In general, however, this thesis will not be concerned with these phenomena other than for experimental purposes.

If electrons are added in a pairwise fashion, the effect of unpaired electronic spins

is removed. The motion of these electrons about the nucleus has an influence on the nuclear spin transitions. The electrons modify the magnetic field experienced by the nucleus, "screening" it from the applied magnetic field, therefore this interaction is called chemical shielding. Classically, this can be envisaged as a current loop that creates a weak magnetic field opposed to the applied field. In quantum mechanical terms, the electron orbital angular momentum (for electrons with  $L > 0$ ) couples with the nuclear angular momentum, resulting in a shift in the nuclear energy level spacing. The amount and direction of this shift depend on the specific electronic environment in which the nucleus is situated, although the nucleus will be most sensitive to electronic factors closest to it.<sup>8,9</sup> If the present example is expanded, so that the nucleus being considered is now part of a much larger chemical system, the potential information from observing such influences becomes obvious. Although the nuclei in a given molecule are fixed with respect to one another, the electrons are free to circulate throughout the electronic structure. In this way, the nucleus becomes sensitive to the total electronic character of its surroundings. It is here that the utility of nmr to the chemist becomes clear, as the nuclear magnet provides a probe of the electronic environment or "chemistry" of a given compound.

If a second nucleus is placed into our system, such that a bond or path of electron density exists between the two nuclei, another type of nmr interaction is observed. As in the direct dipolar interaction, this interaction makes each nucleus sensitive to the spin state of the other. However, unlike the previous case, this sensitivity is not transmitted directly through space, but is mediated by the electrons between the two nuclei. Thus

this is called the indirect spin-spin interaction, or more commonly, J coupling. In a simplistic form, this interaction can be envisaged as arising from the polarization of electrons around one nucleus in a given spin state, which is in turn transmitted to electrons near the other nucleus, modifying the field experienced by that nucleus. This polarization is sensitive to the spin state of the nucleus. The result is a nucleus $\rightarrow$ (electron) $_n$  $\rightarrow$ nucleus pathway for the transmission of nuclear spin information. Such couplings are of great interest to the chemist.<sup>10</sup> The magnitude of the nuclear spin-spin coupling between two directly-bonded atoms is intimately related to the nature of the chemical bond between the two nuclei, including factors such as bond order and stereochemistry.

One final interaction that must be introduced is the nuclear quadrupole interaction, which is only present when considering nuclei with spin greater than  $\frac{1}{2}$ . Such nuclei possess a nuclear quadrupole moment, which results from a nonsymmetrical distribution of charge within the nucleus. All the previous interactions involved couplings between a dipole and a local field; the nuclear quadrupole moment couples with the electric field gradient at the nucleus. This interaction is electrostatic in nature and varies in strength from very small or zero to very large, often much larger than the Zeeman interaction.<sup>11</sup> In these latter cases, another form of spectroscopy, nuclear quadrupole resonance (nqr),<sup>12</sup> may be performed, although, in general, it is not as wide-ranging in its applications as nmr. Variations in the strength of the nuclear quadrupole coupling rely on two factors, the size of the nuclear quadrupole moment, which is at least approximately known for most nuclei, and the electric field gradient, which will depend

on the particular chemical environment in which the nucleus is present. The quadrupolar interaction influences the nuclear energy levels by shifting them according to the particular transitions; as quadrupole effects only occur in nuclei of spin  $I=1$  or greater, there will be at least two different one-level transitions possible. The different transitions no longer will be equal in energy.

Each of these interactions described can occur alone, or in company with the others. Isotropic motion of the molecule in which the nucleus of interest is present will reduce the observed values of these interactions to their average values; for the direct dipolar and nuclear quadrupolar interactions, this will be zero, whereas it may be some observable scalar quantity for the others. In the solid state, these interactions in general will have an orientation dependence, *i.e.*, the energy required to induce transitions between perturbed nuclear-spin energy levels may change as the orientation of the molecule in the magnetic field is varied, unless such characteristics are prohibited by the symmetry at the nucleus. This property of orientation dependence is due to the tensorial nature of the nmr interactions. A tensor is a matrix that describes the relation between the magnitude of a particular interaction and the orientation of the molecule or crystal, of which the nucleus is a part, with respect to some vector, usually the applied magnetic field. A wealth of information is available if the magnitudes of these various interactions can be assigned to specific orientations of the compound of interest. It is the pursuit of knowledge of this type that is the focus of this thesis.

## 2.2 The NMR Interactions

The full nuclear spin Hamiltonian in a diamagnetic nonconducting material is made up of the following terms,<sup>13</sup>

$$\hat{\mathcal{H}}_{tot} = \hat{\mathcal{H}}_Z + \hat{\mathcal{H}}_{rf} + \hat{\mathcal{H}}_{DD} + \hat{\mathcal{H}}_{CS} + \hat{\mathcal{H}}_J + \hat{\mathcal{H}}_Q, \quad (1)$$

where the subscripts denote the following interactions: Z, Zeeman; rf, radiofrequency; DD, direct dipolar; CS, chemical shielding; J, indirect spin-spin; and Q, quadrupolar. Presented now is a somewhat more rigorous description of each of these interactions. There are many treatments available that are more detailed and quite varied in approach, in particular this includes a comprehensive, though certainly not exhaustive, set of monographs by Abragam,<sup>4</sup> Haeberien,<sup>13</sup> Spiess,<sup>6</sup> Mehring,<sup>14</sup> Gerstein and Dybowski,<sup>15</sup> Ernst, Bodenhausen and Wokaun,<sup>16</sup> Slichter,<sup>7</sup> and Munowitz,<sup>17</sup> as well as reviews by Taylor, Baugher and Kriz,<sup>18</sup> Vaughan,<sup>19</sup> Duncan and Dybowski,<sup>20</sup> and Gerstein.<sup>21</sup>

### 2.2.1 The Zeeman Interaction

In the presence of a strong magnetic field, a nucleus possessing spin ( $I > 0$ ) will be in one of  $2I+1$  equally spaced energy levels. The energy difference between levels depends on the magnetic moment of the nucleus,  $\mu$ , and the external magnetic field,  $\mathbf{B}_0$ ,

$$\hat{\mathcal{H}}_Z = -\hbar^{-1} \boldsymbol{\mu} \cdot \mathbf{B}_0 = -\gamma_n \mathbf{B}_0 \cdot \mathbf{I}, \quad (2)$$

where  $\gamma_n$  is the characteristic magnetogyric ratio for a nuclear isotope,  $n$ , and  $\mathbf{I}$  is the nuclear spin. The magnetic field vector,  $\mathbf{B}_0$ , is usually chosen such that it lies along the  $z$  axis of the laboratory frame, *i.e.*,  $\mathbf{B}_0 = (0,0,B_0)$ . This allows one to express the

nuclear spin vector  $\mathbf{I}$  in terms of  $I_z$ , the component along its axis of quantization, the magnetic field. The frequency of a pure Zeeman single-quantum transition is called the Larmor frequency, and is given by

$$\nu_o = \frac{\gamma_n B_o}{2\pi}, \quad (3)$$

where  $\nu_o$  is in Hz. This is the basic interaction involved in the nmr experiment; perturbations of it by the other interactions described herein provide the information that is of interest to the chemist.

### 2.2.2 The Radiofrequency Interaction

Transitions between the Zeeman energy levels are usually induced by radiofrequency (rf) fields,  $B_{rf}$ , applied perpendicular to the magnetic field direction, taken as the x direction of the lab frame. It is a time-dependent field,

$$\mathbf{B}_{rf}(t) = (B_1(t) \cos \omega t, 0, 0), \quad (4)$$

where  $B_1$  is the amplitude of the rf field and  $\omega/2\pi$  is the carrier frequency. The nuclear spin interacts with the rf field as it does with the static magnetic field, *i.e.*,

$$\hat{\mathcal{H}}_{rf} = -\gamma_n \mathbf{B}_{rf} \cdot \mathbf{I}. \quad (5)$$

Time-dependent radiofrequency fields are used extensively in pulse Fourier-transform nmr to permit observation, and sometimes suppression, of the effects of the various internal Hamiltonians.

### 2.2.3 The Direct Dipolar Interaction

This is the through-space coupling of two nuclear spins I and S. It can be expressed as

$$\hat{\mathcal{H}}_{DD} = \frac{\gamma_I \gamma_S \hbar^2}{r_{IS}^3} \left[ \mathbf{I} \cdot \mathbf{S} - \frac{3(\mathbf{I} \cdot \mathbf{r}_{IS})(\mathbf{S} \cdot \mathbf{r}_{IS})}{r_{IS}^2} \right] \left( \frac{\mu_o}{4\pi} \right), \quad (6)$$

where  $\mathbf{I}$  and  $\mathbf{S}$  may be like or unlike spins and  $\mathbf{r}_{IS}$  is the I-S internuclear vector. This Hamiltonian may be expressed in polar coordinates as a sum of six terms, the so-called "dipolar alphabet",<sup>4</sup>

$$\hat{\mathcal{H}}_{DD} = \frac{\gamma_I \gamma_S \hbar^2}{r_{IS}^3} [A + B + C + D + E + F] \left( \frac{\mu_o}{4\pi} \right),$$

where

$$\begin{aligned} A &= -I_z S_z (3 \cos^2 \theta - 1), \\ B &= \frac{1}{4} [I_+ S_- + I_- S_+] (3 \cos^2 \theta - 1), \\ C &= -\frac{3}{2} [I_z S_+ + I_+ S_z] \sin \theta \cos \theta e^{-i\phi}, \\ D &= -\frac{3}{2} [I_z S_- + I_- S_z] \sin \theta \cos \theta e^{i\phi}, \\ E &= -\frac{3}{4} I_+ S_+ \sin^2 \theta e^{-2i\phi} \\ \text{and } F &= -\frac{3}{4} I_- S_- \sin^2 \theta e^{2i\phi}. \end{aligned} \quad (7)$$

For heteronuclear spin-pairs, normally only term A contributes to the observed spectra, while both terms A and B contribute to the spectra of homonuclear spin-pairs, due to the "flip-flop" operator in term B. Consequently, the equations describing the resonance frequencies for dipolar coupled spins are different for hetero- and homonuclear cases. For two isolated spin- $1/2$  nuclei, the dipolar interaction leads to an orientation dependent splitting,<sup>1</sup>

$$\Delta \nu_{DD}(\textit{hetero}) = R_{DD}(3 \cos^2\theta - 1), \quad (8)$$

$$\Delta \nu_{DD}(\textit{homo}) = \frac{3}{2} R_{DD}(3 \cos^2\theta - 1), \quad (9)$$

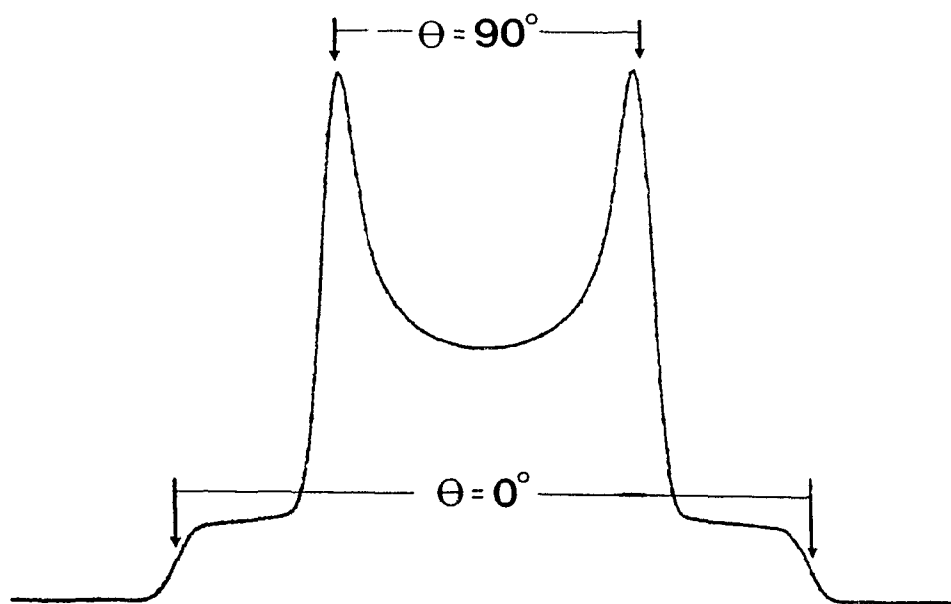
where  $\theta$  is the angle between the I-S internuclear vector  $r_{IS}$  and the magnetic field direction, and  $R_{DD}$  is the dipolar coupling constant, expressed in SI units as

$$R_{DD} = \frac{\gamma_I \gamma_S \hbar}{2\pi r_{IS}^3} \left( \frac{\mu_o}{4\pi} \right). \quad (10)$$

In a powder sample, the dipolar nmr spectrum of an isolated spin-pair will appear as a characteristic "Pake doublet" (Figure 1). For a heteronuclear spin-pair, the splitting between the discontinuities is  $R_{DD}$  ( $\theta = 90^\circ$ ) and between the outer shoulders is  $2R_{DD}$  ( $\theta = 0^\circ$ ). For homonuclear systems containing a magnetically equivalent spin-pair, the corresponding splittings are  $3R_{DD}/2$  and  $3R_{DD}$ , respectively. For an AB spin system, where the two coupled nuclei are "like" spins (*i.e.*,  $\nu_{\text{obs}}(A) \approx \nu_{\text{obs}}(B)$ ) but are not magnetically equivalent, the situation is more complex.<sup>22,23</sup> The four observed transitions are not split according to the limits given above, but are somewhere between the two, depending on the degree of mixing of the spin states of the two nuclei. Such mixing will occur whenever the difference in resonance frequencies for the two nuclei is of the order of, or smaller than, the strength of the coupling between them.

The dipolar interaction is directed along the internuclear vector,  $r_{IS}$ , and, in the absence of oriented librations,<sup>24</sup> is both axially symmetric ( $C_\infty$  symmetry) and traceless in the observed nmr spectrum. Therefore, the value of  $R_{DD}$  is sufficient to describe the

Figure 1. The characteristic "Pake pattern" that arises between two dipolar coupled nuclei.



dipolar coupling completely. Note that  $R_{DD}$  depends on the separation between the two nuclei; in principle, measurement of  $R_{DD}$  can provide internuclear distances. The observed dipolar coupling vanishes whenever the internuclear vector is undergoing rapid isotropic motion. Averaging of the dipolar interaction also can be accomplished in spin space.<sup>13</sup>

#### 2.2.4 The Chemical Shielding Interaction

The motion of electrons in a molecule generates magnetic fields that modify the applied field,  $B_o$ , felt by a nucleus. The induced fields are proportional to the strength of the external field and generally shield the nucleus from the applied field,

$$\hat{H}_{CS} = \gamma_n I \cdot \sigma \cdot B_o, \quad (11)$$

where  $\sigma$  is the chemical shielding tensor of the observed nucleus. This tensor describes the three-dimensional nature of the electronic "screening" of the nucleus, which in general will vary with the orientation of the molecule in the magnetic field. In practice, only the symmetric part of the shielding tensor contributes to the nmr spectrum.<sup>13</sup> In its principal axis system (PAS), the diagonalized tensor is described by three orthogonal principal components,  $\sigma_{11}$ ,  $\sigma_{22}$  and  $\sigma_{33}$ , designating the directions of least, intermediate and greatest shielding, respectively ( $\sigma_{11} \leq \sigma_{22} \leq \sigma_{33}$ ). The magnitudes of these shielding components are absolute values with respect to the bare nucleus. In nmr, it is common to observe signals with respect to that of a reference, where the difference between the sample and the reference signals is called the chemical shift, symbolized by  $\delta$  and expressed in field-independent units of parts per million (ppm) as

$$\delta_{\text{sample}} = \frac{\nu_{\text{sample}} - \nu_{\text{reference}}}{\nu_{\text{reference}}} \times 10^6 = (\sigma_{\text{reference}} - \sigma_{\text{sample}}) \times 10^6. \quad (12)$$

The principal components of  $\sigma$  also can be expressed as chemical shifts, with  $\delta_{11}$ ,  $\delta_{22}$  and  $\delta_{33}$  corresponding to  $\sigma_{11}$ ,  $\sigma_{22}$  and  $\sigma_{33}$ , respectively. As the scales for shielding and shift increase in opposite directions, the chemical shift scale is defined such that  $\delta_{11} \geq \delta_{22} \geq \delta_{33}$ . It is important to recognize the fundamental difference between absolute chemical shielding and relative chemical shift values; this distinction will be preserved in the thesis.

In a solid, the chemical shielding experienced by a particular nucleus varies with the orientation of the molecule in  $B_0$ , according to

$$\nu_{\sigma} = \nu_o [1 - (\sigma_{11} \sin^2\theta \cos^2\phi + \sigma_{22} \sin^2\theta \sin^2\phi + \sigma_{33} \cos^2\theta)], \quad (13)$$

where  $\theta$  and  $\phi$  are the polar and azimuthal angles, respectively, orienting the applied magnetic field direction in the principal axis system of the chemical shielding tensor, as shown in Figure 2. In a single crystal, this leads to a variation in the chemical shift of a nucleus as a function of orientation of the crystal in the magnetic field. In a powder, all possible orientations of the molecule contribute to the observed signal, and a powder line shape results, with limits marked by inflection points at  $\delta_{11}$  and  $\delta_{33}$ , and a discontinuity at  $\delta_{22}$ . Examples of axially symmetric and nonaxially symmetric chemical shift powder patterns are given in Figure 3. In high resolution nmr experiments, where the chemical shift tensor is often averaged by rapid magic-angle spinning (MAS), all anisotropic information is generally lost and only the isotropic average,  $\delta_{\text{iso}}$ , is measured. The breadth of the static chemical shielding powder line shape is defined by the chemical

Figure 2. The orientation of  $B_0$  in the principal axis system of the chemical shielding tensor is described by the angles  $\theta$  and  $\phi$ . Such axis systems for the other interactions are identical.

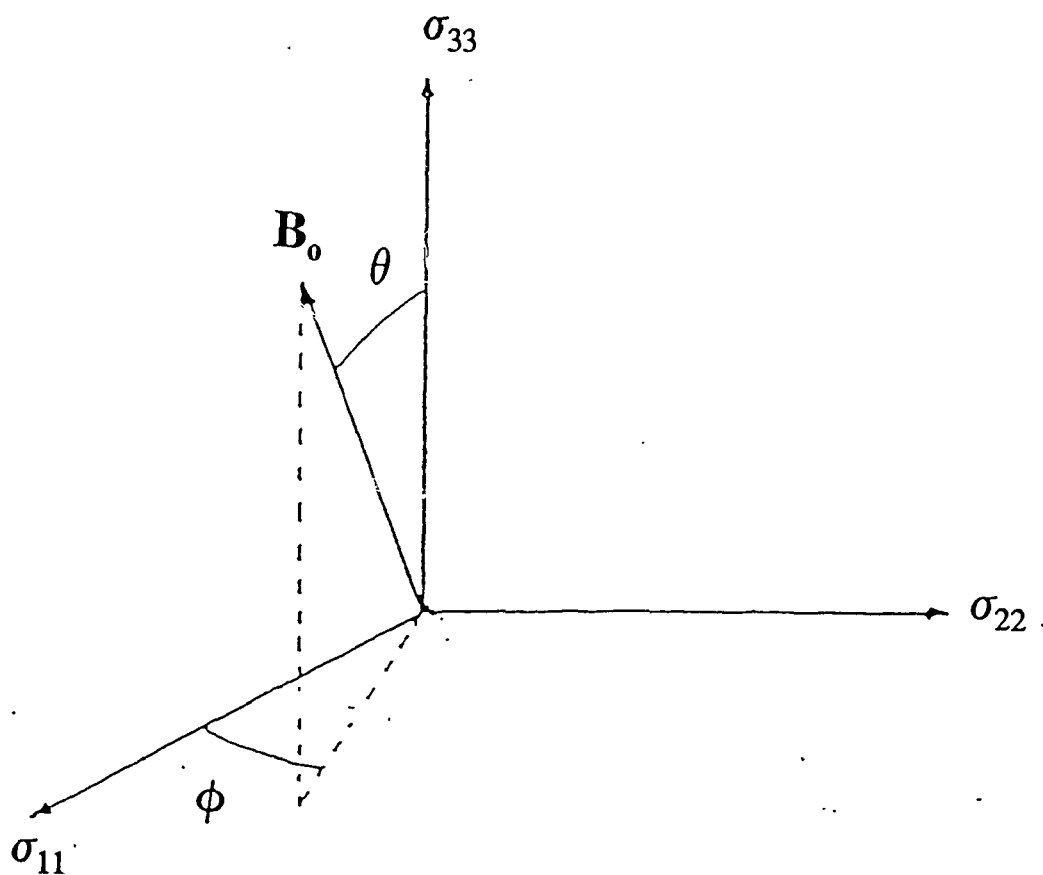
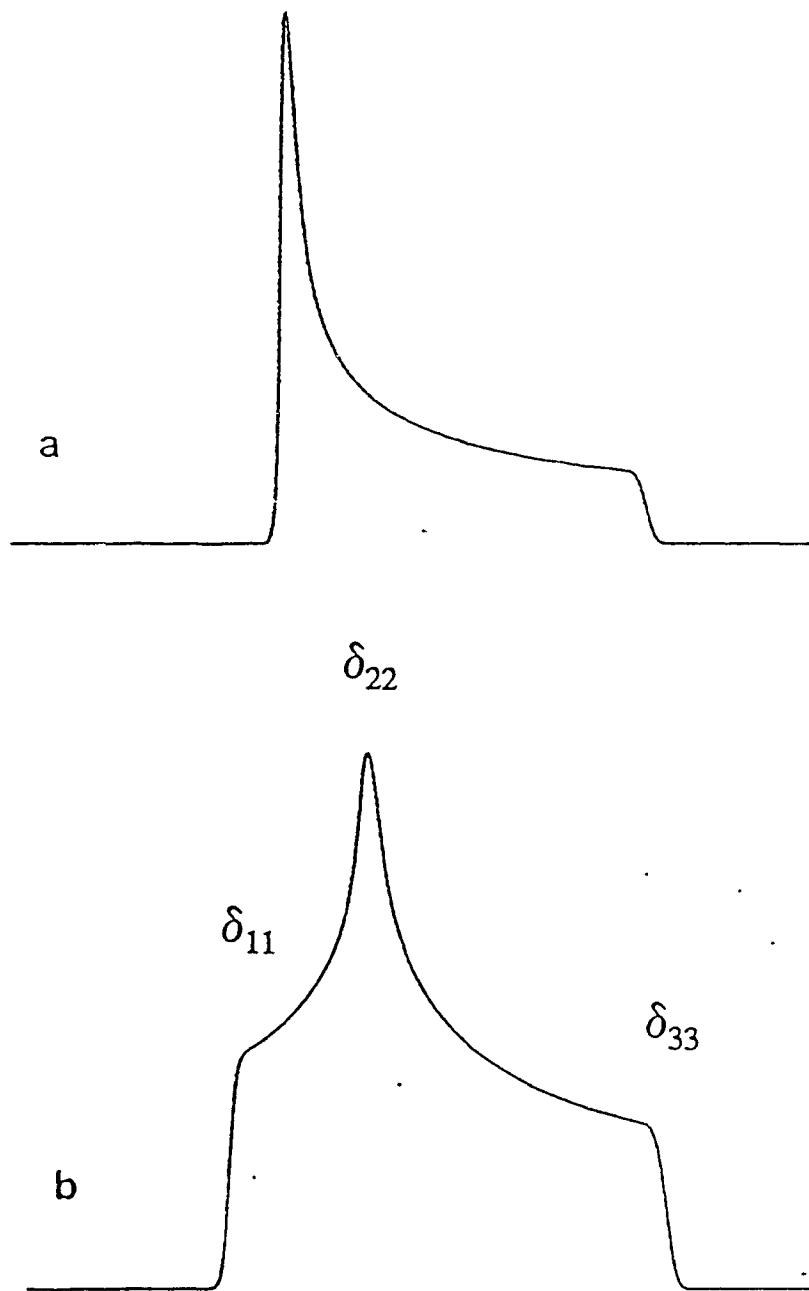


Figure 3. Calculated powder line shapes due to chemical shielding with (a) axial symmetry and (b) nonaxial symmetry.



shielding anisotropy,  $\Delta\sigma$ , while the asymmetry parameter,  $\eta_\sigma$ , denotes the departure from axial symmetry in a range from 0 to 1. These definitions are given below,

$$\delta_{iso} = \frac{1}{3}(\delta_{11} + \delta_{22} + \delta_{33});$$

$$\text{if } |\delta_{33} - \delta_{iso}| \geq |\delta_{iso} - \delta_{11}|, \text{ then}$$

$$\Delta\sigma = \frac{1}{2}(\delta_{11} + \delta_{22}) - \delta_{33} \quad \text{and} \quad \eta_\sigma = \frac{\delta_{22} - \delta_{11}}{\delta_{33} - \delta_{iso}}; \quad (14)$$

$$\text{if } |\delta_{33} - \delta_{iso}| \leq |\delta_{iso} - \delta_{11}|, \text{ then}$$

$$\Delta\sigma = \delta_{11} - \frac{1}{2}(\delta_{22} + \delta_{33}) \quad \text{and} \quad \eta_\sigma = \frac{\delta_{33} - \delta_{22}}{\delta_{iso} - \delta_{11}}.$$

### 2.2.5 The Indirect Spin-Spin Interaction

This involves a coupling between two nuclear spins I and S, mediated by the electronic environment between the nuclei, rather than behaving as a through-space interaction. It can be expressed as

$$\hat{\mathcal{H}}_J = \mathbf{I} \cdot \mathbf{J} \cdot \mathbf{S}, \quad (15)$$

where  $\mathbf{J}$  is the indirect spin-spin coupling tensor. This tensor describes the variation of the indirect spin-spin coupling with the orientation of the molecule in the magnetic field. In solution, only the isotropic average,  $J_{iso} = \frac{1}{3} \text{Tr}(\mathbf{J})$ , is observed. In principle, one can measure both the anisotropy and asymmetry of the  $\mathbf{J}$  tensor in rigid solids. However, the anisotropy,  $\Delta J$ , mathematically transforms similar to the direct dipolar coupling, thus, the two interactions cannot be easily separated *via* experiment. In practice, this leads to an effective dipolar coupling constant,  $R_{eff}$ ,

$$R_{eff} = R_{DD} - \frac{1}{3} \Delta J, \quad (16)$$

$$\Delta J = J_{\parallel} - J_{\perp}, \quad (17)$$

assuming that  $\mathbf{J}$  is axially symmetric, with  $J_{\parallel}$  designating the component oriented along the I-S internuclear vector and  $J_{\perp}$  the component that is perpendicular. This characteristic can complicate the interpretation of dipolar spectra, leading to erroneous results for internuclear separations derived from the observed dipolar splitting.<sup>25</sup> Reliable experimental values of  $\Delta J$  are scarce in the literature; however, for any given spin-pair, theoretical molecular orbital (MO) calculations indicate that the magnitude of  $\Delta J$  is of the same order of magnitude as, or smaller than, values for  $J_{iso}$ .<sup>10</sup> Also, on the basis of the MO calculations, the anisotropy in  $J$  is predicted to become more important for indirect couplings involving heavier nuclei.<sup>26</sup>

### 2.2.6 The Quadrupolar Interaction

This interaction is important for all nuclei possessing a nuclear quadrupole moment, *i.e.*, all nuclei with nuclear spin  $I > \frac{1}{2}$ . It is an electrostatic interaction between the quadrupole moment,  $eQ$ , and the electric field gradient (efg) at the nucleus, and is described by

$$\mathcal{H}_Q = \frac{eQ}{6I(2I-1)} \mathbf{I} \cdot \mathbf{V} \cdot \mathbf{I}, \quad (18)$$

where  $\mathbf{I}$  and  $\mathbf{V}$  are the nuclear spin vector and efg tensor, respectively. The principal components of  $\mathbf{V}$  ( $V_{ii} = eq_{ii}$ ,  $i = 1, 2, 3$ ) are defined such that  $|V_{33}| \geq |V_{11}| \geq |V_{22}|$ .

The efg tensor is traceless, therefore, the quadrupolar interaction is not observed directly in solution. The strength of this interaction is usually expressed (in Hz) in terms of the quadrupolar coupling constant,  $\chi$ , and the magnitudes of the minor components are expressed *via* the asymmetry parameter,  $\eta_Q$ , where

$$\chi = \frac{e^2 q_{33} Q}{h} \quad \text{and} \quad \eta_Q = \frac{V_{22} - V_{11}}{V_{33}}. \quad (19)$$

The quadrupolar interaction is only of interest in the final chapter of the thesis, and will be discussed in more detail at that point.

### 2.3 Tensors

The Hamiltonians for the interactions described in the previous section define the relationships between the nuclear spins and their surroundings *via* second-rank tensors, which characterize the orientational dependence of the interactions. A second-rank tensor is a  $3 \times 3$  matrix that relates two vectors, which may or may not be parallel.<sup>27,28</sup> In general, this tensor is composed of nine independent terms; however, it can be broken down into symmetric and antisymmetric parts. In most cases, the antisymmetric part has a negligible influence on nmr interactions up to a second-order perturbation approach, resulting in only six unique terms being required to fully define the tensor.<sup>13</sup>

It is most convenient to express these tensors in their principal axis system, or PAS. Here, the off-diagonal terms vanish and the three diagonal terms, *i.e.*,  $T_{11}$ ,  $T_{22}$  and  $T_{33}$  for a general tensor  $\mathbf{T}$ , define the principal components of the tensor and are oriented along three mutually orthogonal axes. In studying a powder sample, all three components can be determined and are usually defined sequentially across the spectrum, *i.e.*,  $T_{22}$  is always the intermediate component, while  $T_{11}$  and  $T_{33}$  are the extreme components. The order of increasing value may differ depending on the scale for the interaction being described, *e.g.*, chemical shielding *vs.* chemical shift. Three angles are required to unambiguously orient the tensor in its PAS with respect to the laboratory frame, the molecular frame or any other desired reference frame.

$$\begin{aligned}
\mathbf{T}_{general} & \Rightarrow \mathbf{T}'_{PAS}{}^{sym} + \mathbf{T}'_{PAS}{}^{anti} \\
\begin{pmatrix} T_{11} & T_{12} & T_{13} \\ T_{21} & T_{22} & T_{23} \\ T_{31} & T_{32} & T_{33} \end{pmatrix} & \xrightarrow{\text{transform to PAS}} \begin{pmatrix} T'_{11} & 0 & 0 \\ 0 & T'_{22} & 0 \\ 0 & 0 & T'_{33} \end{pmatrix} + \begin{pmatrix} 0 & T'_{12} & T'_{13} \\ -T'_{12} & 0 & T'_{23} \\ -T'_{13} & -T'_{23} & 0 \end{pmatrix} \quad (20)
\end{aligned}$$

Tensors are usually described in terms of three characteristic quantities (other than the values of the three principal components): the isotropic average, the anisotropy and the asymmetry.<sup>6,13,14</sup> The isotropic average,  $T_{iso}$ , is simply one-third of the trace of the tensor, where the trace is the sum of the diagonal elements.

$$T_{iso} = \frac{1}{3}Tr(\mathbf{T}) = \frac{1}{3}(T_{11} + T_{22} + T_{33}) \quad (21)$$

The anisotropy,  $\Delta T$ , depends on the position of  $T_{22}$  with respect to  $T_{iso}$ . If  $T_{11} \geq T_{22} \geq T_{33}$  in frequency units,  $\Delta T$  will be defined in this thesis as

$$\begin{aligned}
\Delta T &= \frac{1}{2}(T_{11} + T_{22}) - T_{33} \quad \text{if} \quad |T_{33} - T_{iso}| \geq |T_{11} - T_{iso}|; \\
\Delta T &= T_{11} - \frac{1}{2}(T_{22} + T_{33}) \quad \text{if} \quad |T_{33} - T_{iso}| \leq |T_{11} - T_{iso}|.
\end{aligned} \quad (22)$$

The asymmetry,  $\eta_T$ , also has two conditional definitions, given by

$$\begin{aligned}
\eta_T &= \frac{T_{22} - T_{11}}{T_{33} - T_{iso}} \quad \text{if} \quad |T_{33} - T_{iso}| \geq |T_{11} - T_{iso}|; \\
\eta_T &= \frac{T_{22} - T_{33}}{T_{11} - T_{iso}} \quad \text{if} \quad |T_{33} - T_{iso}| \leq |T_{11} - T_{iso}|.
\end{aligned} \quad (23)$$

The anisotropic part of a tensor has a particular orientation dependence with respect to the laboratory frame, which in nmr is usually denoted as the magnetic field

direction. This dependence is in the form of a  $(3\cos^2\theta - 1)$  term. Averaging of this term to zero will remove the influence of any anisotropy,<sup>13</sup> and can be accomplished in two ways. In solution or in an orientationally-disordered solid performing isotropic motion, a molecule undergoes rapid random tumbling where, on average, it samples all possible orientations with respect to the magnetic field. This results in the time average,  $\langle 3\cos^2\theta - 1 \rangle = 0$ . Another way to accomplish this averaging, most commonly for rigid solids, is to rotate the sample rapidly about a certain angle with respect to the magnetic field, the so-called "magic angle",  $\theta_m = 54.74^\circ$ , for which  $(3\cos^2\theta_m - 1) = 0$ .

## 2.4 Origin of Powder Line Shapes

In §2.2, only the frequency dependence of the various interactions was considered. This provides no explanation for the characteristic line shapes of nmr powder patterns, as given in Figure 3 for chemical shielding line shapes. These line shapes are due to the random orientation of the crystallites with respect to the laboratory frame which make up a powder sample. One single crystal yields a single nmr peak for each magnetically distinct nucleus, and the frequency of this line varies with the orientation of the crystal in the magnetic field. A powder pattern is simply a superposition of all of the possible signals, as the many tiny "crystals" which make up a powder sample generally will be randomly oriented in all possible directions. The spectral intensity over any frequency interval is proportional to the number of nuclei that resonate in that interval. Thus the orientation distribution of nuclei in a powder sample determines the intensity distribution of the nmr line shape.<sup>13</sup>

The orientation of the crystallites in the laboratory frame alternatively can be expressed as the orientation of the magnetic field vector in the principal axis system (PAS) of the dominant interaction for the observed nucleus. The orientation of  $\mathbf{B}_0$  in the PAS can be described in terms of the unit sphere. This is a sphere where all possible orientations of the magnetic field vector are defined by a vector from the centre of the sphere to any point on the surface. The symmetry properties of the unit sphere make it necessary to consider only one hemisphere of the sphere, which has as limits the three principal components of the relevant interaction tensor, *e.g.*, the chemical shielding tensor. Thus the intensity of the line shape can be obtained by the simple volume

integral,

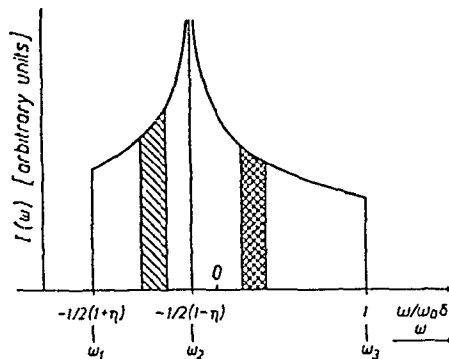
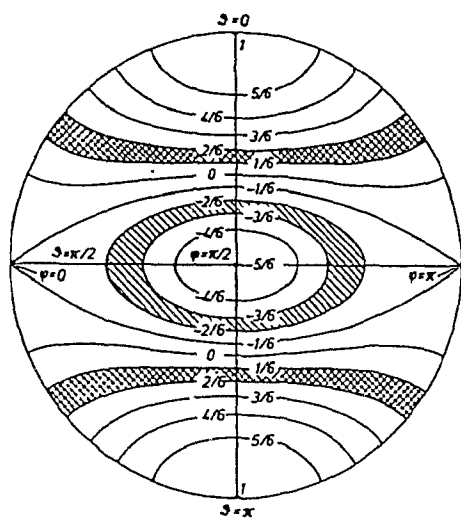
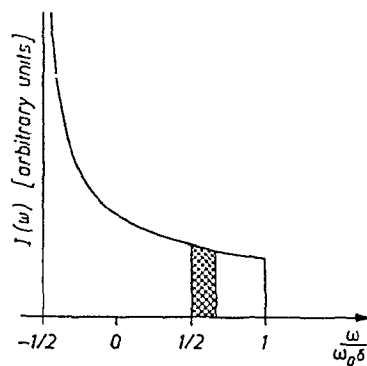
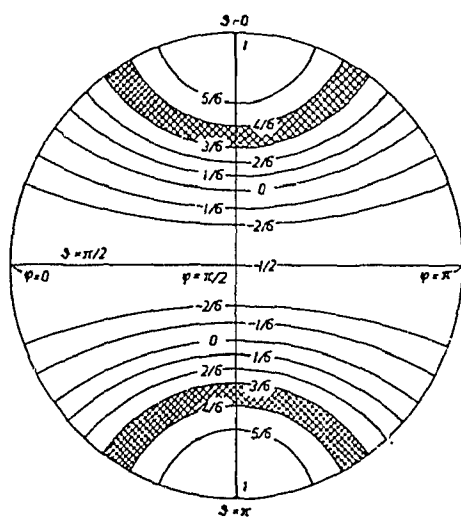
$$I(\nu) = \int_0^{\frac{\pi}{2}} \int_0^{2\pi} \delta(\nu - \nu(\theta, \phi)) \sin\theta d\theta d\phi, \quad (24)$$

where  $\nu(\theta, \phi)$  describes the orientation dependence of the particular interaction or interactions concerned, and  $\delta(\nu)$  is a delta function.

A pictorial representation can be accomplished using stereographic projections of the unit sphere.<sup>13</sup> These are given in Figure 4 for the case of axial symmetry ( $\eta_a = 0$ ) and non-axial symmetry ( $\eta_a > 0$ ) of the chemical shielding tensor. The contours indicate curves of constant frequency and are in one-sixth intervals of  $\nu_0\delta$ , where  $\delta = \sigma_{33} - \sigma_{iso}$ . There are only two extremes in (a), at the poles and along the circumference at the equator of the sphere. One important aspect of (a) is the much larger area between contours as  $\theta \rightarrow \frac{\pi}{2}$ . This gives rise to the large peak at  $\delta = -1/2$  in the line shape given to the right of the sphere. In (b) the non-axial symmetry changes the contours considerably in the centre of the projection, and three separate critical points can be identified; at the poles, and at the  $\phi = 0$  and  $\frac{\pi}{2}$  points on the equator. These correspond to the three discontinuities evident on the resulting line shape. The shaded areas in the projections correspond to the areas of spectral intensity in the accompanying line shapes.

The traditional way to simulate such line shapes has been to partition a sphere into intervals in the angles  $\theta$  and  $\phi$  of  $5^\circ$  or smaller. However, such calculations can be extremely time-consuming, as much time is spent calculating intensities for angles that contribute little to the overall intensity, such as intervals in  $\phi$  of  $1^\circ$  at values of  $\theta$  near  $0^\circ$ . An alternative method of line shape calculation has been developed by Alderman,

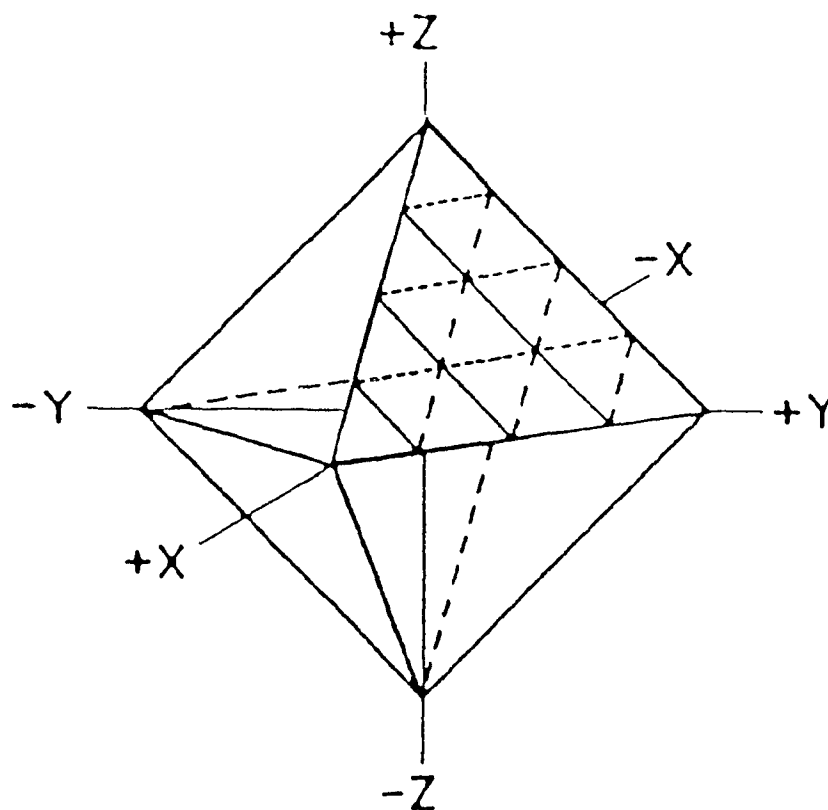
Figure 4. Stereographic representations of the unit sphere for chemical shielding line shapes (from Haeberlen<sup>13</sup>).



Solum and Grant that is called the POWDER simulation routine.<sup>29</sup> Their approach involves representing the unit sphere as an octahedron, then splitting one triangular face into much smaller triangles, as in Figure 5, the number depending on the resolution desired. A vector from the centre of the octahedron to the centre of each small triangle on the surface is used to represent the different orientations of a vector in the unit sphere, and the resulting intensities are interpolated between these points to provide a smooth line shape. This provides greatly reduced computational demands in the simulation of line shapes. All static powder simulation programs written in the course of the work described in this thesis have incorporated this routine.

In this thesis, the prime criterion for determining a "best fit" simulation between the theoretical and experimental line shapes has been the matching of frequencies for the characteristic features. These features may be either peaks or shoulders, and the important components of each are the maxima and the inflection points, respectively. Although some attempts have been made to introduce least-squares routines to the simulation of various solid-state static powder spectra,<sup>30,31</sup> powder line shapes are not amenable in general to such analyses. A least-squares-fitting of the entire line shape would be dominated by the overall intensity, which in general occurs at uninformative frequencies throughout the line shape. Also, in pulse Fourier-transform nmr, it is usually difficult to get intensities that are free of distortions, due to instrumental or relaxation effects. A simple visual fitting of the line shape can determine whether the characteristic frequencies are properly described in the calculated spectra, and has the advantage of fitting distorted spectra to the theoretical pattern better than any computer algorithm.

Figure 5. Octahedral model of the unit sphere used in the POWDER simulation routine  
(from Alderman, Solum and Grant<sup>29</sup>).



## 2.5 Multiple-Interaction Line Shapes

When faced with a system that contains more than one internal Hamiltonian that can contribute to the observed nmr spectrum, the nmr spectroscopist has two options in order to obtain the desired information: complicated experiments resulting in simplified spectra; or simplified experiments resulting in complicated spectra.<sup>17</sup> One can choose between using sophisticated pulse techniques to tailor the total Hamiltonian to include only the desired interactions, or one can develop a method of interpretation that will either correct for or fully characterize the other influences on the observed spectrum. In general, the latter option has been the one of choice for the work contained in this thesis, compelling at this point a consideration of the effects of multiple interactions on the nmr line shape. Two examples will be presented. The first, dipolar - chemical shift nmr, will provide a simple introduction to the concept of multiple interactions in a single nmr line shape, and is the framework upon which the second example is built. The second is more relevant to the thesis, describing the line shape theory essential to analyze the powder spectra of spin- $\frac{1}{2}$  nuclei that are adjacent to nuclei which have isotopes both with and without nuclear spin, and are also J-coupled, as well as dipolar coupled, to the nuclear isotopes with spin.

### 2.5.1 Dipolar - Chemical Shift NMR Line Shapes

In the solid state, the most common combination of interactions one encounters is that found in dipolar - chemical shift nmr experiments.<sup>32</sup> The line shapes of either nucleus result from the superposition of the chemical shielding of the observed nucleus,

as well as direct dipolar coupling to the other nucleus, in the absence of any indirect J coupling between the two nuclei. In order to interpret spectra of this type, the magnitudes of the two interactions must be determined, as well as their relative orientation. Because each of these interactions is anisotropic, their influence on the line shape will not be equivalent across the spectrum, but will vary in a specific way that can be used to evaluate the orientation of one with respect to the other. This characteristic has been used to great advantage in dipolar - chemical shift nmr to derive orientations of the chemical shift tensor in the molecular frame from powder spectra, negating the need for demanding single-crystal nmr measurements to obtain this same information.

The observed nmr line shape for nucleus I that is a member of an isolated pair of heteronuclear spin-1/2 nuclei with another nucleus S is given by,

$$\begin{aligned} \nu_{obs}(\theta, \phi, \vartheta) &= \nu_{\sigma}(\theta, \phi) \mp \nu_{DD}(\vartheta) \\ &= \nu_{\sigma} \left[ 1 - (\sigma_{11} \sin^2 \theta \cos^2 \phi + \sigma_{22} \sin^2 \theta \sin^2 \phi + \sigma_{33} \cos^2 \theta) \right] \\ &\quad \mp \frac{1}{2} R_{DD} (3 \cos^2 \vartheta - 1), \end{aligned} \quad (25)$$

where the parameters correspond to the definitions given in §2.2. Note that the angles relating the magnetic field vector,  $\mathbf{B}_0$ , to the chemical shielding tensor,  $\sigma$ , and the dipolar vector,  $\mathbf{r}_{IS}$ , are not equivalent; this is due to the possibility that these two interactions are not aligned. To relate one interaction to the other, a rotational transformation must be applied<sup>27</sup> so that the fixed difference in orientation can be removed and the two interactions can be represented in the volume integral (Equation 24) by one set of angles,  $(\theta, \phi)$ . The fixed difference in orientation is represented by the Euler angles,  $\alpha$  and  $\beta$ , resulting in the expression,

$$\begin{aligned}
v_{obs}(\theta, \phi) = v_o & \left[ 1 - (\sigma_{11} \sin^2 \theta \cos^2 \phi + \sigma_{22} \sin^2 \theta \sin^2 \phi + \sigma_{33} \cos^2 \theta) \right] \\
& \mp \frac{1}{2} R_{DD} \left[ 3 (\sin \beta \sin \theta \cos(\alpha - \phi) + \cos \beta \cos \theta)^2 - 1 \right],
\end{aligned}
\tag{26}$$

where the angles  $\theta$  and  $\phi$  now represent the orientation of the magnetic field vector in the reference frame of the chemical shielding tensor, and, through the Euler angles,  $\alpha$  and  $\beta$ , with respect to the dipolar vector as well, as illustrated in Figure 6. Estimates of these angles can be derived from the splittings apparent about each of the three regions of the spin-I line shape corresponding to  $\delta_{11}$ ,  $\delta_{22}$  and  $\delta_{33}$ ,

$$\begin{aligned}
\Delta v_{11} &= |R_{DD} (3 \sin^2 \beta \cos^2 \alpha - 1)|, \\
\Delta v_{22} &= |R_{DD} (3 \sin^2 \beta \sin^2 \alpha - 1)|, \\
\Delta v_{33} &= |R_{DD} (3 \cos^2 \beta - 1)|,
\end{aligned}
\tag{27}$$

where the splittings, shown in Figure 7, are absolute values as their relative signs cannot be determined from the nmr line shape. Consequently, there may be more than one choice of angles possible from the splittings, but only one set of values for  $\alpha$  and  $\beta$  will be consistent with all three splittings or with the resulting nmr line shape. These angles are fundamental properties of the chemical shift tensor, as they describe the orientation of this tensor in the molecular frame, *via* the dipolar vector,  $\mathbf{r}_{IS}$ ; if this vector is a bond, which is normally the case, the orientation of  $\sigma$  in the molecular frame has been derived. However, this derived orientation of  $\sigma$  is accurate only within an arbitrary rotation about  $\mathbf{r}_{IS}$ , as three angles are required to unambiguously orient the chemical shift tensor. In most instances, it is possible to identify the most likely orientation of  $\sigma$  within this rotation about the dipolar vector.

Figure 6. Definition of the Euler angles  $\alpha$  and  $\beta$ , relating  $\sigma$  and  $\mathbf{r}_{IS}$ , and the orientation angles  $\theta$  and  $\phi$ , relating  $\sigma$  and  $\mathbf{B}_0$ .

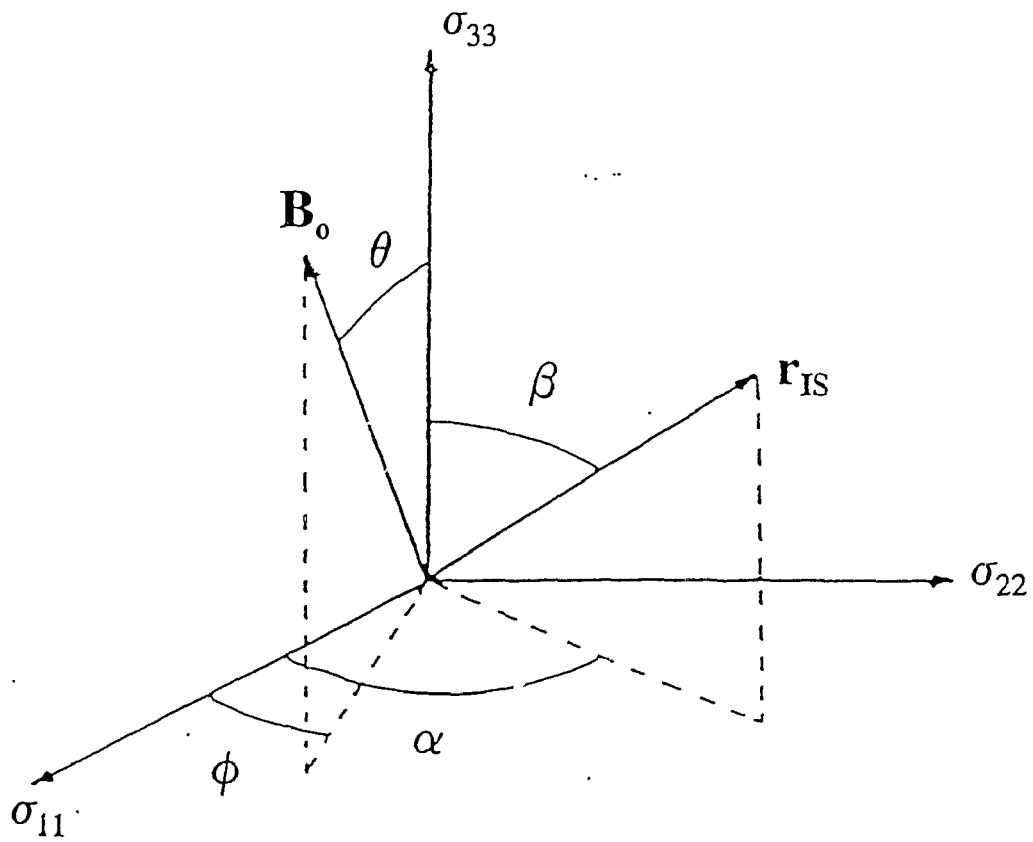
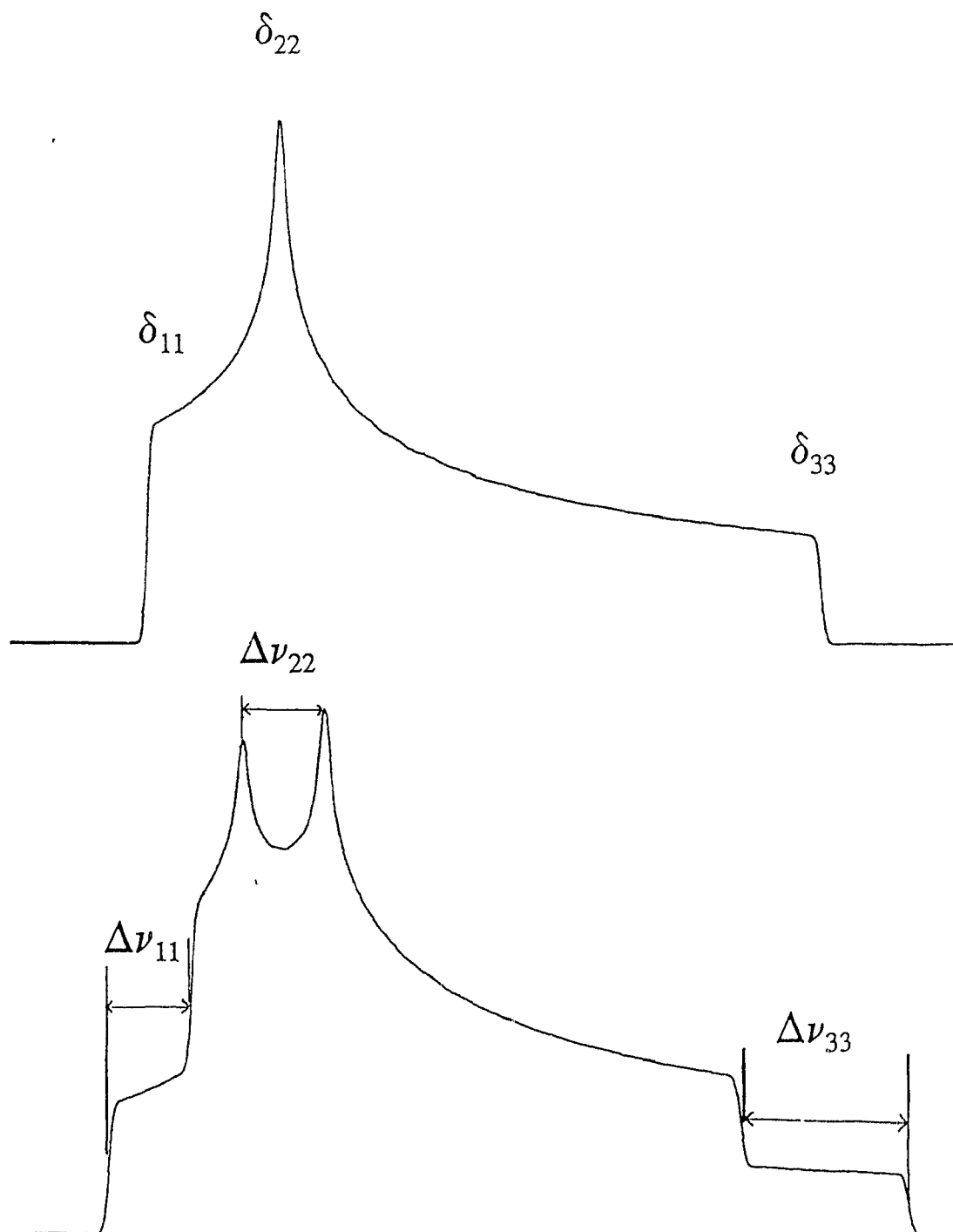


Figure 7. Calculated nmr line shapes for (a) chemical shielding alone and (b) chemical shielding with direct dipolar coupling, with splittings given by Equation 27.



### 2.5.2 Influence of Isotropic and Anisotropic Indirect Coupling

The nmr line shape for a nucleus I that is adjacent to another nucleus S will depend on the chemical shielding interaction, as well as any coupling that may exist to the adjacent isotopes of S possessing spin that may exist. Where both spin-active and inactive isotopes of S are present, the I spin line shape will consist of components with weighted intensities corresponding to the natural abundance of each of the magnetically active and inactive isotopes of S. The presence of a large isotropic J coupling constant simplifies this situation by separating the "satellites", the line shapes of the I nuclei which are adjacent to S nuclei with spin, from the uncoupled centre band, arising from I nuclei next to spin-inactive S isotopes. The uncoupled centre band will be determined exclusively by the I spin chemical shielding interaction. The satellite line shapes are sensitive to the chemical shielding, direct dipolar and indirect spin-spin interactions, as well as their relative orientations. This will influence the line shape in the manner described in §2.5.1 by incorporating the Euler angles  $\alpha$  and  $\beta$ , which orient the dipolar vector in the chemical shielding tensor (see Figure 6).<sup>23,25,32</sup> The overall spin-I powder line shape can be described by Equation 28,

$$\nu_{obs}(\theta, \phi) = \nu_o(\theta, \phi) - m_S [\nu_{DJ}(\theta, \phi) - {}^1J_{iso}(I, S)], \quad (28)$$

where

$$\nu_o(\theta, \phi) = \nu_o [1 - (\sigma_{11} \sin^2\theta \cos^2\phi + \sigma_{22} \sin^2\theta \sin^2\phi + \sigma_{33} \cos^2\theta)], \quad (29)$$

$$\nu_{DJ} = R_{eff} [3(\sin\beta \sin\theta \cos(\alpha - \phi) + \cos\beta \cos\theta)^2 - 1], \quad (30)$$

$$\nu_o = \frac{\gamma_I B_o}{2\pi}, \quad (31)$$

and

$$\begin{aligned} R_{eff} &= R_{DD} - \frac{1}{3} \Delta J(I,S) \\ &= \left( \frac{\gamma_I \gamma_S \hbar}{2\pi r_{IS}^3} \frac{\mu_o}{4\pi} - \frac{1}{3} (J_{\parallel} - J_{\perp}) \right). \end{aligned} \quad (32)$$

The spin state of nucleus S,  $m_s$ , will be zero for S isotopes without spin, and  $\pm 1/2$  for isotopes of S possessing spin- $1/2$ . Quadrupolar isotopes of S are not included in this analysis. The relative intensities of the satellites ( $m_s = \pm 1/2$ ) and the central feature ( $m_s = 0$ ) will be given by the ratio of their respective natural abundances, keeping in mind that the total satellite intensity will be split between two line shapes. The overlap of interactions is presented in Figure 8, for spectra arising from such an IS spin-pair outlined above with isotropic J coupling alone, with the addition of spin-I chemical shielding, and the total line shape once the effects of dipolar coupling and anisotropic J coupling are included. The splittings indicated in (c) result from the combined effects of  $J_{iso}$  and  $R_{eff}$ , as,

$$\begin{aligned} \Delta \nu_{11} &= |J_{iso} - R_{eff}(3 \sin^2 \beta \cos^2 \alpha - 1)|, \\ \Delta \nu_{22} &= |J_{iso} - R_{eff}(3 \sin^2 \beta \sin^2 \alpha - 1)|, \\ \Delta \nu_{33} &= |J_{iso} - R_{eff}(3 \cos^2 \beta - 1)|. \end{aligned} \quad (33)$$

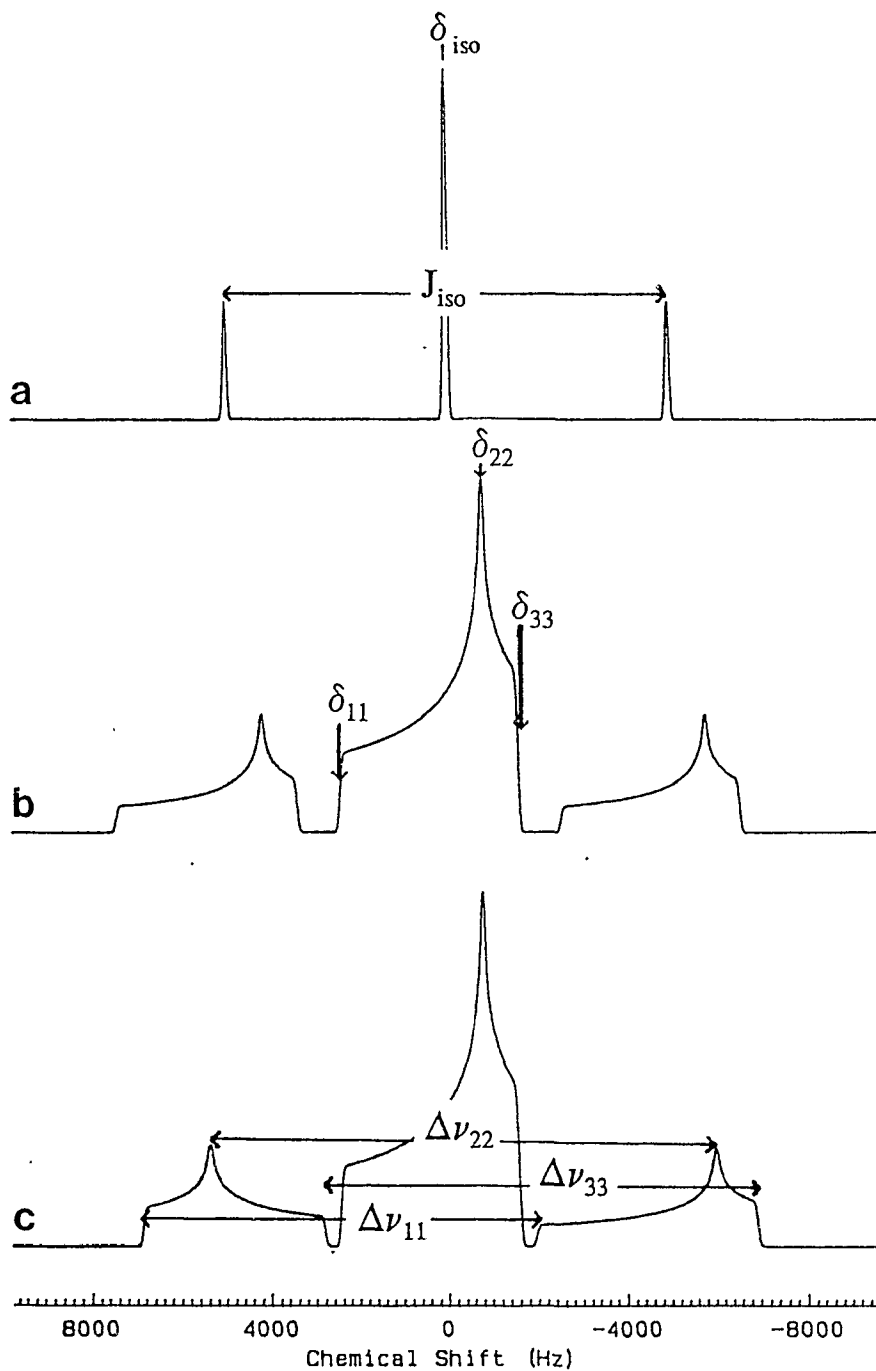
The principal components of the spin-I chemical shielding tensor,  $\sigma_{ii}$ ,  $i=1,2,3$ , are reported most commonly as chemical shifts,  $\delta_{ii}$ , with respect to a reference. The convention is maintained that  $\delta_{11}$  and  $\delta_{33}$  denote the shifts of the least shielded and most

shielded principal components, respectively. The equations above assume that  $\mathbf{J}$  is axially symmetric and that  $\mathbf{J}_{\parallel}$  lies along the I-S bond, which should be a good approximation for nuclei with approximately axial symmetry about the bond between them. The experimental static nmr line shapes can be simulated using Equation 28 to extract the relevant parameters describing each of the interactions.

A program based on Equation 28 was written to perform line shape calculations, and was used to generate all simulated spectra in Chapters 2 through 5. A complete listing of this program is included in the Appendix. This program has been rigorously tested against other simulation programs and compared to the results of explicit calculation of the frequencies for various features of the line shape. In all cases, this program has been found to provide accurate line shapes, with very modest computational demands. All calculations were performed on desktop microcomputers.

In conclusion, the important aspects of multiple-interaction line shapes include the construction of the proper expression regarding the joint effects of the relevant interactions on the observed nmr line shape using the equations given in §2.2, including the relative signs, and then transformation to a common reference frame so that differences in orientation of the interactions may be determined. In this fashion, theoretical expressions describing the line shapes from any combination of interactions may be constructed, and using them, experimental line shapes may be simulated to yield the desired information.

Figure 8. Calculated nmr spectra for a nucleus I of an IS heteronuclear spin-pair, including the interactions of (a) isotropic spin-I chemical shielding and  $J(I,S)$  coupling, (b) isotropic  $J$  coupling and anisotropic spin-I chemical shielding, and (c) isotropic  $J(I,S)$  coupling, anisotropic spin-I chemical shielding, and I-S direct dipolar and anisotropic  $J$  coupling.



## 2.6 Analysis of Spinning Sidebands in MAS Spectra

Analysis such as that outlined above becomes difficult whenever there is more than one crystallographically distinct nucleus that contributes to the observed nmr spectrum in a given sample. This may be due to the presence of lattice sites in the unit cell that are not related by symmetry, or to the fact that there is more than one type of crystal in the bulk powder sample. Whichever is the case, interpretation of the resulting powder spectra becomes difficult, as it may be unclear which spectral features correspond to which site. When such circumstances have arisen in this work, slow magic-angle spinning experiments have been applied to allow resolution of the spectral features of each site. A judicious choice of spinning speed will allow one to completely resolve the spinning sidebands of one site from the others. For spin- $1/2$  nuclei, the powder nmr spectrum due to each independent site can be reconstructed from the spinning sidebands using a technique developed by Herzfeld and Berger.<sup>33</sup> The critical frequencies of the reconstructed powder patterns are analyzed in exactly the same fashion as that outlined in §2.5. Once this has been performed for all the sites that are present in the nmr spectra, the overall multi-site powder nmr line shape can be calculated, using the parameters derived independently for each site from the slow-MAS spectra, as well as properly weighting their respective contributions to the nmr spectrum. Comparison of this calculated line shape to the original multi-site powder line shape provides a final check on the precision of both the Herzfeld-Berger fitting and the resulting nmr parameters derived for each site. While this approach may increase the error, it is often the only way to obtain this information when there are multiplicities in the nmr spectra.

The traditional method used in the Herzfeld-Berger fitting of MAS sidebands has been a graphical technique.<sup>33</sup> Contours derived from the relative intensities of the sidebands and isotropic peak are plotted together and their confluence indicates the anisotropy and asymmetry of the underlying powder line shape which would be obtained without magic-angle spinning. A more convenient approach, provided by Dr. A. Kentgens of the University of Nijmegen and used exclusively throughout this thesis, involves a SIMPLEX algorithm<sup>34</sup> to determine the minimum in parameter space for a given set of sideband values. This program uses previously-generated tables of theoretical sideband intensities to determine a "best fit" to the input experimental sideband intensities. These tables were produced at Dalhousie University using the original program described by Herzfeld and Berger,<sup>33</sup> which was developed and provided by Dr. A.E. Berger. A similar technique for fitting MAS sideband intensities has been described recently,<sup>35</sup> as has a different iterative procedure.<sup>36</sup> In general, it was found that the SIMPLEX sideband-fitting program would reproduce reliable values (within 2% of the total breadth of the spectrum) for the characteristic frequencies of a powder line shape from MAS spectra. This was tested using MAS spectra for samples of which high-quality powder line shapes were also obtained.

## Chapter 3

### Anisotropic Indirect Spin-Spin Coupling in Solid Mercury Phosphines, $[\text{HgPR}_3(\text{NO}_3)_2]_2$

#### 3.1 Introduction

Indirect spin-spin (J) couplings between  $^{31}\text{P}$  and various metal nuclei, such as  $^{109}\text{Ag}$ ,  $^{195}\text{Pt}$  and  $^{199}\text{Hg}$ , have been used to derive structural information of coordination compounds from solution nmr spectra over the last twenty years.<sup>37,38,39,40</sup> For a given class of compounds, the values of  $^1J(\text{M}, ^{31}\text{P})$  often have been found to correlate with a variety of properties, such as metal-phosphorus bond lengths, bond angles at the metal centre, electronegativity of *trans*-ligands, among others. Interpretations of these couplings have been based exclusively on the contact mechanism for electron-mediated communication between the two nuclear spins involved, which, following McConnell,<sup>41</sup> can be described by Equation 34,

$$^1J(\text{M}, ^{31}\text{P}) = \left(\frac{\mu_o}{3\pi}\right)^2 \mu_B^2 h \gamma_M \gamma_P (\Delta E)^{-1} |s_M(0)|^2 |s_P(0)|^2 P_{s_M s_P}^2, \quad (34)$$

where  $^3\Delta E$  is the average triplet excitation energy,  $s_M(0)$  and  $s_P(0)$  are the magnitudes of the *s*-orbitals precisely at the metal and phosphorus nuclei, respectively,  $P_{s_M s_P}$  is the molecular orbital (MO) bond order between the two nuclei, and all other terms are standard constants. This simple equation involves a number of approximations, as previously described by Pidcock,<sup>39</sup> not least of which is the assumption that the J coupling depends exclusively on the Fermi contact mechanism. The apparent success of

this equation in rationalizing various experimental trends in metal-phosphorus couplings has led to the belief that experimental values of  $J_{iso}$  provide a measure of the degree of  $s$ -orbital character in the bond between two nuclei. However, the original theoretical description of  $\mathbf{J}$  coupling provided by Ramsey<sup>42</sup> was more complex, and involved not only the Fermi contact mechanism, but several others as well. In his formulation, the overall indirect spin-spin coupling was made up of four terms,

$$\mathbf{J} = \mathbf{J}_{OB} + \mathbf{J}_{SD} + \mathbf{J}_{FC} + \mathbf{J}_{FC \times SD}, \quad (35)$$

where OB, SD and FC correspond to orbital, spin-dipolar and Fermi contact contributions, respectively. The final contribution arises from a cross-term in second-order perturbation theory between the Fermi contact and spin-dipolar mechanisms.

The orbital contribution to  $\mathbf{J}$  results from the interaction between the magnetic moments of the nuclei and the orbital angular momentum of the surrounding electrons. The spin-dipolar mechanism involves a coupling between the nuclear spins and electron spins which are at a finite distance from the nucleus. The Fermi contact is similar to the spin-dipolar term, except that it depends on electron density precisely at the nuclei involved. The similar origin of these latter two terms gives rise to the cross-term between them. Of the four contributions to the indirect spin-spin coupling, all except the contact - spin-dipolar cross-term contribute to the isotropic value of  $\mathbf{J}$  (*i.e.*, this latter term is traceless); conversely, only the Fermi contact term does not contribute to the anisotropy in  $\mathbf{J}$ , as its dependence on  $s$ -electron density at the nucleus precludes any orientation dependence. Thus, according to the theory of Ramsey, the anisotropy in  $\mathbf{J}$  should be precisely zero if the exclusive mechanism for spin-spin coupling is the Fermi

contact mechanism.<sup>43</sup>

Over the past fifteen years, a relativistic analogue to Ramsey's theory of spin-spin coupling has been developed by Pyykkö.<sup>26</sup> Relativistic effects have been found to be important in the theoretical treatment of any of the heavier elements, due to the high velocities of the electrons near the massive and highly charged nuclei.<sup>44</sup> The relativistic expression for indirect spin-spin coupling involves only one Hamiltonian; however, it is possible to extract terms which, at their non-relativistic limits, roughly correspond to Ramsey's expressions. Although the spin-dipolar and orbital analogues cannot be explicitly separated, residing together in Pyykkö's  $\mathbf{J}_{p-p}$  and  $\mathbf{J}_{\sigma-\pi}$  terms, a contact contribution,  $\mathbf{J}_{s-s}$ , does appear, which again depends on *s*-electron density at the nuclei involved, and is completely isotropic. Another relativistic term,  $\mathbf{J}_{s-p}$ , is traceless, but does contribute to the anisotropy in  $\mathbf{J}$ . Clearly, in relativistic theory, as in that of Ramsey, the presence of any anisotropy in  $\mathbf{J}$  indicates that the contact mechanism is not solely responsible for the observed indirect spin-spin coupling.

The theory for anisotropic  $\mathbf{J}$  coupling has been presented by Buckingham *et al.*,<sup>43</sup> and MO calculations were reported to illustrate the influence of the various mechanisms on the overall magnitude of  $\Delta\mathbf{J}$ . For couplings between first-row elements, the calculations suggested that the anisotropy in  $\mathbf{J}$  was dominated by the Fermi contact - spin-dipolar cross-term, for which the contribution to  $J_{iso}$  is precisely zero. This is significant, as it implies that the presence of  $\Delta\mathbf{J}$  in these couplings does not indicate a dominance of  $J_{iso}$  by terms other than the Fermi contact. However, for couplings involving heavier elements, the calculated contributions to  $\Delta\mathbf{J}$  by the orbital and spin-dipolar mechanisms

increased. Larger contributions to  $\Delta J$  were not, in general, accompanied by any trends in the contributions to  $J_{\text{iso}}$ . It should be noted that experimental values will not provide information on the source of  $\Delta J$ , but only its magnitude. Theoretical calculations are the only method by which such influences can be suggested. Unfortunately, the agreement between the calculated values provided by Buckingham and Love<sup>43(a)</sup> and experimental data existing at that time was poor. The calculations, now over 20 years old, involved substantial approximations, including the use of average excitation energies and the neglect of two-centre integrals and relativistic effects for the heavy nuclei. Interest in the calculation of nuclear spin-spin coupling constants using *ab initio* methods has waned recently, so improved calculations with more sophisticated theory and more powerful computers have not been forthcoming.

Reliable experimental determinations of the  $\mathbf{J}$  tensor, and more specifically anisotropies of  $\mathbf{J}$ , are scarce in the literature.<sup>10,45,46,47,48</sup> In general, this can be attributed to difficulties in measuring  $\Delta J$ . In isotropic phases, there are no manifestations of anisotropy in  $\mathbf{J}$  on observed nmr spectra because of rapid molecular tumbling. In ordered or anisotropic phases, such as liquid crystal systems or crystalline solids,  $\Delta J$  appears only in combination with the direct dipolar coupling,  $R_{\text{DD}}$ , resulting in an effective dipolar coupling constant,  $R_{\text{eff}}$ .<sup>25</sup>

One popular method used to determine  $\Delta J$  values has been to study the nmr spectra of solute molecules oriented in liquid crystal solvents.<sup>45,49</sup> In general, the analysis is complicated because the orientational order tensor,  $S^{\text{D}}$ , must be determined. Although only a single order parameter (one element of  $S^{\text{D}}$ ) is necessary to describe the

order in highly symmetric molecules, the degree of order is low and apparent coupling constants must be corrected for vibrational motions of the solute. In addition, one must account for the orientation-dependent deformations of the solute molecule induced by the anisotropic forces present in the liquid crystalline matrix.<sup>50,51</sup>

Reliable experimental data concerning anisotropy in  $J$  should be available from solid-state nmr. The greatest advantage of this technique is the precise knowledge of the compound's molecular structure that is provided by crystallographic data. Comparison of crystallographic and nmr spectroscopic data is justified when the nmr sample is in the same physical state, as opposed to cases where crystallographic data are assumed to be models of the solute structure in liquid crystalline solvents. The effects of motional averaging also should be eliminated or substantially attenuated in the solid state, which is a complication when performing measurements in liquid crystal solvents.

With these considerations, a study of the nature of the indirect spin-spin coupling between  $^{31}\text{P}$  and  $^{199}\text{Hg}$  has been performed, for a series of mercury phosphines<sup>52</sup> of the general form  $[\text{HgPR}_3(\text{NO}_3)_2]_2$ , where R is an alkyl or aryl group. Compounds of this latter type have been well characterized by both  $^{31}\text{P}$  solution nmr<sup>53</sup> and X-ray crystallography.<sup>54,55,56</sup> In the solid state, these compounds generally form centrosymmetric dimers or polymeric chains, containing bridging nitrate groups. In solution nmr studies, they have been found to possess very large isotropic  $^1J_{\text{iso}}(^{31}\text{P}, ^{199}\text{Hg})$  coupling constants, of the order of 10 kHz. The direct dipolar coupling constant between these two nuclei is small due to the relatively long P-Hg bond. The combination of a large  $J_{\text{iso}}$  and a small  $R_{\text{DD}}$  should permit reliable measurement of anisotropic  $J$  couplings.

### 3.2 Experimental

The 1:1 mercury(II) nitrate - phosphine complexes were prepared according to literature methods,<sup>53</sup> where equimolar amounts of  $\text{Hg}(\text{NO}_3)_2 \cdot \text{H}_2\text{O}$  (0.01 mol., 3.5 g) and the appropriate phosphine (0.01 mol., 2.7 g) were refluxed in ethanol for one to two hours. Products were recrystallized from dichloromethane by slow addition of diethyl ether. All compounds were characterized by their solution  $^{31}\text{P}$  nmr spectra. Solution-state  $^{31}\text{P}$  nmr spectra were obtained on a Nicolet NT360 nmr spectrometer at 146.1 MHz.

All solid-state  $^{31}\text{P}$  nmr spectra were obtained at 81.0 MHz on a Bruker MSL-200 nmr spectrometer under conditions of cross-polarization (CP) and high-power proton decoupling. Typical pulse widths were 4  $\mu\text{s}$ , with contact times for the cross-polarization sequence lasting 3 ms. Magic-angle spinning (MAS) spectra were obtained at spinning rates up to 4 kHz, using 7 mm o.d. zirconia rotors in a Bruker double-air-bearing MAS probe. Acquisition times for both static and spinning spectra were 65.54 ms, during which 8192 data points were collected. All spectra were obtained at 293 K and were referenced with respect to 85%  $\text{H}_3\text{PO}_4(\text{aq})$  at 0 ppm, using the  $^{31}\text{P}$  signal of external  $\text{NH}_4\text{H}_2\text{PO}_4(\text{s})$ , which occurs at +0.81 ppm.

### 3.3 Results

The  $^{31}\text{P}$  nmr spectra of all of the mercury phosphines consist of three main spectral features: an intense central feature arising from  $^{31}\text{P}$  nuclei which are bonded to Hg isotopes which do not possess nuclear spin  $I=1/2$ , and two satellites, each with approximately 10% of the intensity of the central feature, arising from  $^{31}\text{P}$  nuclei which are adjacent to  $^{199}\text{Hg}$  nuclei (16.84% natural abundance,  $I=1/2$ ). There was no evidence of coupling to  $^{201}\text{Hg}$  (13.22% natural abundance,  $I=3/2$ ); this may have been due to self-decoupling of this quadrupolar isotope or to extreme broadening of the  $^{31}\text{P}$  signals for phosphorus nuclei coupled to  $^{201}\text{Hg}$ . The satellites are displaced to either side of the central feature due to the large indirect spin-spin coupling (J coupling) between  $^{31}\text{P}$  and  $^{199}\text{Hg}$ . Spectra obtained under conditions of rapid magic-angle spinning (MAS), as portrayed in Figure 9(a) for  $[\text{HgP}(m\text{-tolyl})_3(\text{NO}_3)_2]_2$ , resemble what is observed in solution, with sharp peaks at frequencies corresponding to the  $^{31}\text{P}$  isotropic chemical shift,  $\delta_{\text{iso}}$ , and at  $\delta_{\text{iso}} \pm 1/2 J_{\text{iso}}$  for those  $^{31}\text{P}$  nuclei adjacent to  $^{199}\text{Hg}$  nuclei ( $m_{\text{Hg}} = \pm 1/2$ ). Thus isotropic values for the  $^{31}\text{P}$  chemical shift and the  $^{31}\text{P}$ - $^{199}\text{Hg}$  J coupling in the solid state are readily determined.

When spectra of the static powder samples are obtained, orientation-dependent signals, such as those shown in Figure 9(b), are observed, which depend on the anisotropic nature of the chemical shift for the central feature, and, for the satellites, on the combined anisotropic effects of the chemical shift and direct dipolar coupling, as well as any anisotropy in J which may be present.<sup>25</sup> The large values of  $^1J_{\text{iso}}(^{31}\text{P}, ^{199}\text{Hg})$  in the mercury phosphines permit unobscured observation of the central and satellite regions

Figure 9. Phosphorus-31 solid-state nmr spectra of  $[\text{HgP}(m\text{-tolyl})_3(\text{NO}_3)_2]_2$ , (a) with magic-angle spinning at 3.0 kHz, and (b) static, with the splittings about each of the principal components of the  $^{31}\text{P}$  chemical shift tensor indicated.

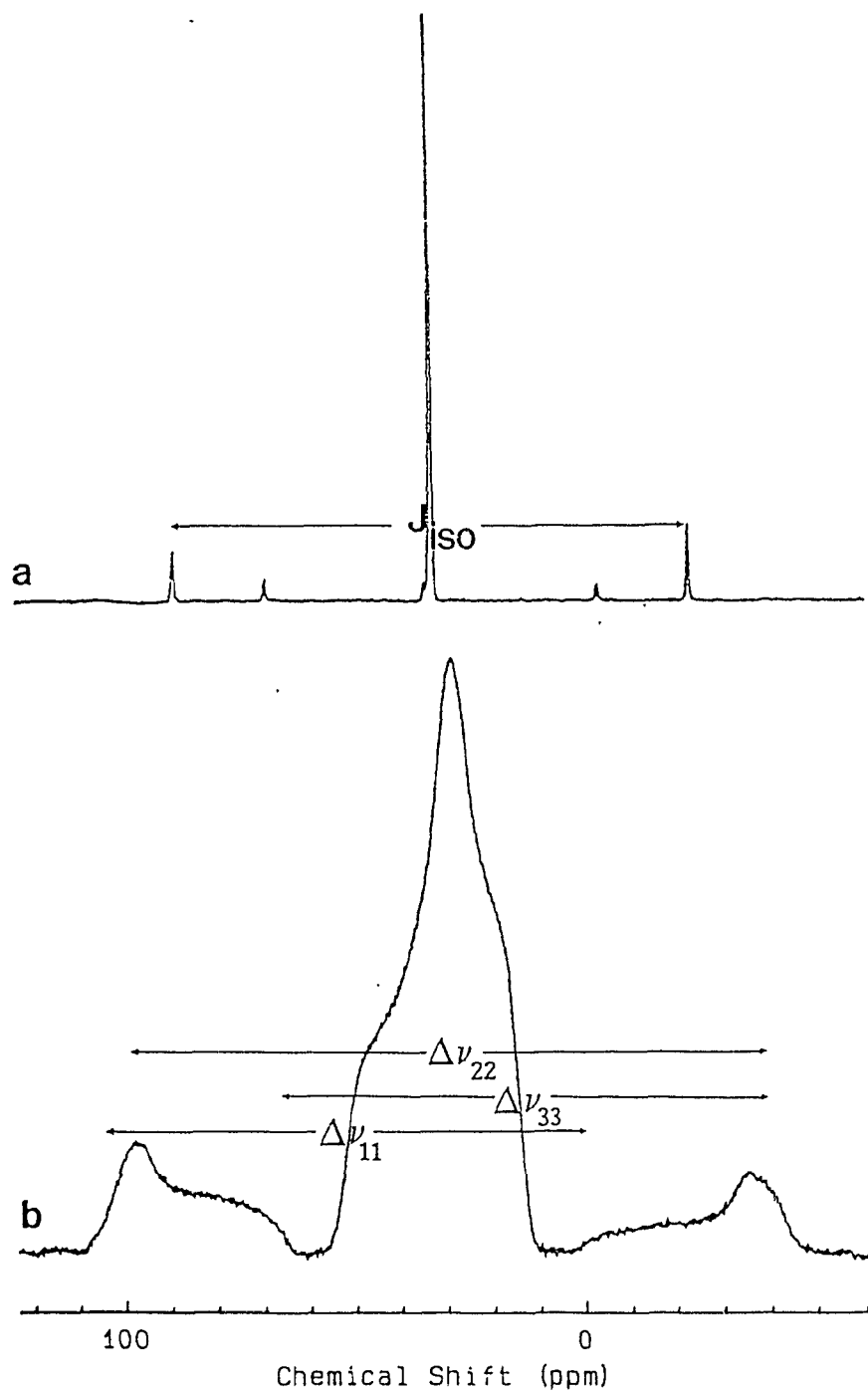


Table 1. Phosphorus-31 nmr parameters for solid  $[\text{HgPR}_3(\text{NO}_3)_2]_2$ .

R	$\delta_{\text{iso}}$	$\delta_{11}$	$\delta_{22}$	$\delta_{33}$	$^1J_{\text{iso}}(^{31}\text{P}, ^{199}\text{Hg})$	$\Delta J$
phenyl	32.2	44.2	34.6	<u>17.7</u>	9572	4550
<i>o</i> -tolyl <sup>a</sup>	3.6	<u>29.1</u>	-9.2	-9.2	9660	5200
<i>m</i> -tolyl	32.6	54.1	<u>28.4</u>	15.7	9165	5250
<i>p</i> -tolyl	40.3	72.8	27.1	<u>20.7</u>	9144	5450
mesityl <sup>b</sup>	3.2	<u>10.2</u>	4.4	-5.0	10468	5550
	1.9	<u>9.2</u>	2.1	-5.6	10566	5550
<i>p</i> -MeO-Ph <sup>b</sup>	42.2	68.3	40.8	<u>17.4</u>	9327	4750
	36.7	52.1	36.8	<u>21.1</u>	9309	3750
cyclohexyl	79.5	114.9	91.3	<u>32.5</u>	8008	5500

Chemical shifts are given in ppm from 85%  $\text{H}_3\text{PO}_4(\text{aq})$ , and J coupling parameters are expressed in Hz. The underline indicates the component of the  $^{31}\text{P}$  chemical shift tensor which lies along or closest to the P-Hg bond. In all cases, the values for  $\Delta J$  were determined assuming that the dipolar coupling constant between  $^{31}\text{P}$  and  $^{199}\text{Hg}$  was 645 Hz, which corresponds to a P-Hg bond length of 2.385 Å. Errors in  $\delta_{\text{iso}}$  and  $J_{\text{iso}}$  are  $\pm 0.2$  ppm and  $\pm 15$  Hz, respectively; the errors in  $\delta_{ii}$  ( $i = 1,2,3$ ) are less than 2.0 ppm. Errors in  $\Delta J$  are  $\pm 200$  Hz, except as otherwise noted in the text.

(a) From reference 52.

(b) Determined from analysis of slow-spinning MAS spectrum.

of the spectra, greatly facilitating their interpretation. The results of analysis performed based on the theory outlined in §2.5 are presented in Table 1.

The three principal components of the  $^{31}\text{P}$  chemical shift tensor can be determined directly from the central feature and used to interpret the satellite line shapes. The values determined for the three principal components of the  $^{31}\text{P}$  chemical shift tensor for each of the compounds are given in Table 1. The only remaining unknown parameters required to characterize the satellites are the orientation of the  $^{31}\text{P}$  chemical shielding tensor and the effective dipolar coupling constant, which include the effects of any anisotropy in  $\mathbf{J}$ . The orientation of the shielding tensor in the molecular frame is readily identified from these powder patterns. The splittings of the three singularities of the satellites about those of the central feature are due to the combined influence of  $J_{\text{iso}}$  and  $R_{\text{eff}}$ ; that of maximum splitting,  $|2 R_{\text{eff}} - J_{\text{iso}}|$ , corresponds to an orientation where that component of the shielding tensor is along the P-Hg bond, while the other two splittings, which should be equal to  $|R_{\text{eff}} + J_{\text{iso}}|$ , denote orientations of the shielding tensor perpendicular to the P-Hg bond.<sup>25</sup> If none of the principal components of the  $^{31}\text{P}$  chemical shielding tensor lie directly along the P-Hg bond, the values of these splittings are slightly modified. However, in all compounds discussed here, it was found that one component of the shielding tensor is along, or very close to, the P-Hg bond. For example, in  $[\text{HgP}(m\text{-tolyl})_3(\text{NO}_3)_2]_2$  (Figure 9(b)), it is clear that the direction of maximum splitting about each of the three principal components of the central line shape is  $\Delta\nu_{22}$ , corresponding to splitting about the intermediate shielding component,  $\delta_{22}$ , while the splittings about the other two components are approximately equal. The chemical

shift values underlined in Table 1 indicate the principal component of the  $^{31}\text{P}$  chemical shift tensor which was determined to lie along or close to the P-Hg bond in each compound.

Once values of  $R_{\text{eff}}$  are obtained from the satellite line shapes, estimates of the anisotropy in  $J$  ( $\Delta J$ ) are obtained using two further pieces of information: the absolute sign of  $^1J_{\text{iso}}(^{31}\text{P}, ^{199}\text{Hg})$  and values of the P-Hg bond length as determined by X-ray crystallography. The sign of the one-bond coupling between  $^{31}\text{P}$  and  $^{199}\text{Hg}$  in various mercury-phosphorus compounds has been determined to be positive.<sup>10,40,57,58</sup> The absolute sign of  $J_{\text{iso}}$  limits the possible values of  $\Delta J$  that are consistent with the observed line shape. The P-Hg bond length of 2.385 Å was used to derive the direct dipolar coupling constant,  $R_{\text{DD}} = 645$  Hz, in the absence of influences due to motional averaging. This value for  $r_{\text{P-Hg}}$  corresponds to an average bond length determined from three crystal structures for compounds of the general form  $[\text{HgPR}_3(\text{NO}_3)_2]_2$ , for  $\text{R} = \text{PPh}_3$  ( $r_{\text{P-Hg}} = 2.359$  Å)<sup>54</sup>,  $\text{R} = \text{PCy}_3$  (2.359 Å)<sup>55</sup> and  $\text{R} = \text{PMes}_3$  (2.395 Å and 2.418 Å).<sup>56</sup> Crystallographic data that exists for other similar compounds, with acetate<sup>59</sup> or thiocyanate<sup>60</sup> anions, reported P-Hg bond lengths which fall within the range for the above nitrate derivatives. Thus, the variation in  $r_{\text{P-Hg}}$  in these mercury phosphines is probably less than  $\pm 0.04$  Å, corresponding to a deviation in  $R_{\text{DD}}$  of  $\pm 33$  Hz. A reduction in  $R_{\text{DD}}$  of an equal amount due to libration of the P-Hg bond would require motion through a cone with a half-angle of  $10.4^\circ$  about the equilibrium position,<sup>23,61</sup> which would be an extremely large degree of motion for these heavy nuclei within a large molecule. The X-ray data discussed above do not provide evidence for motion of

this order in this class of compounds. Thus it is evident that the estimate for  $R_{DD}$  given here is quite robust with respect to the possible sources of error in its derivation.

The values of  $\Delta J$  given in Table 1 are the results determined within the bounds outlined above. It should be noted that any error in the estimate of  $R_{DD}$  will be multiplied by three in the derivation of  $\Delta J$  (see Equation 32); however, that source of error is limited to  $(\pm 33 \text{ Hz}) \times 3 = \pm 99 \text{ Hz}$ . Overall uncertainties in the values of  $\Delta J$  given in Table 1 are  $\pm 200 \text{ Hz}$ , except for  $[\text{HgP}(\text{phenyl})_3(\text{NO}_3)_2]_2$ , due to the presence of some impurities, including the 2:1 phosphine - mercury(II) nitrate complex. Also, larger errors in  $\Delta J$  are given for  $[\text{HgP}(p\text{-methoxyphenyl})_3(\text{NO}_3)_2]_2$  and  $[\text{HgP}(\text{mesityl})_3(\text{NO}_3)_2]_2$ , due to the presence of two nonequivalent  $^{31}\text{P}$  sites in powder samples of each. Errors in  $\Delta J$  for the *p*-methoxyphenyl compound are  $\pm 250 \text{ Hz}$  and  $\pm 375 \text{ Hz}$  for the two sites, respectively, and  $\pm 500 \text{ Hz}$  for  $[\text{HgPPh}_3(\text{NO}_3)_2]_2$  and for each site in  $[\text{HgP}(\text{mes})_3(\text{NO}_3)_2]_2$ . The two-component spectra of  $[\text{HgP}(p\text{-methoxyphenyl})_3(\text{NO}_3)_2]_2$  and  $[\text{HgP}(\text{mes})_3(\text{NO}_3)_2]_2$  were analyzed using Herzfeld-Berger fitting<sup>33</sup> of the  $^{31}\text{P}$  slow-MAS nmr spectra (*e.g.*, Figure 10). The values for  $\Delta J$  for the two sites in  $[\text{HgP}(\text{mes})_3(\text{NO}_3)_2]_2$  are identical within experimental error. Slow-spinning MAS experiments allows the spinning sidebands of each site to be resolved, then separately analyzed, which is not possible with the static spectra due to considerable overlap of the spectral features. The resulting parameters determined from the MAS spectra were used to generate a calculated spectrum of each static powder sample, which provided excellent fits to the experimental line shapes, an example of which is given in

Figure 10. Phosphorus-31 solid-state nmr spectra of  $[\text{HgP}(p\text{-methoxyphenyl})_3(\text{NO}_3)_2]_2$ , (a) with slow MAS ( $\nu_r = 862$  Hz), (b) static, and (c) calculated static, using parameters derived from fitting of the MAS sidebands.

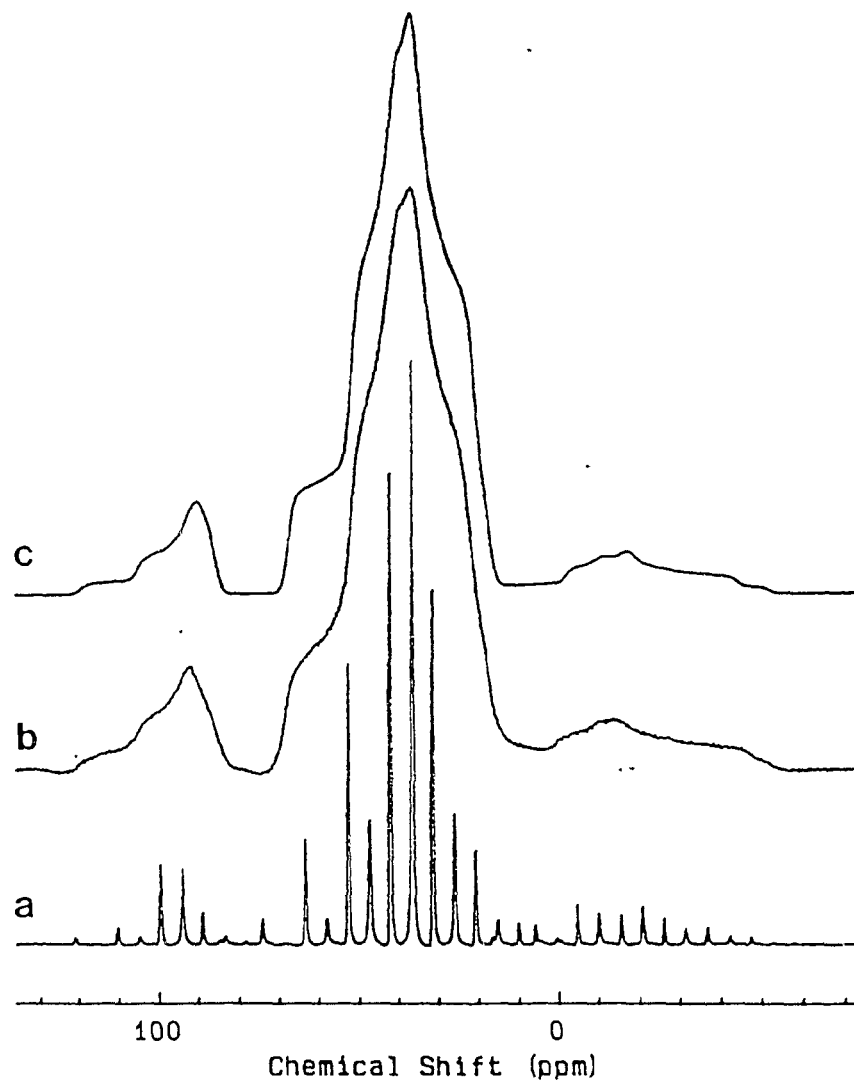
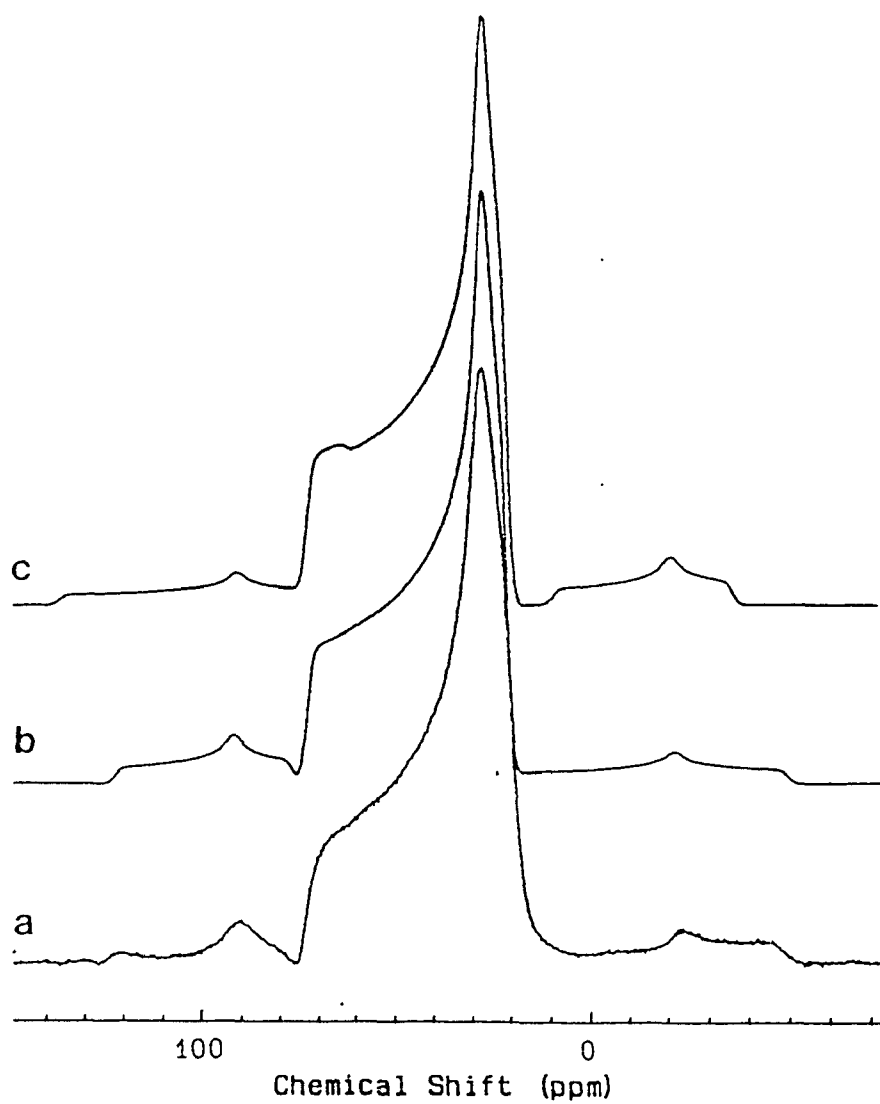


Figure 10. The X-ray crystal structure for  $[\text{HgP}(\text{mes})_3(\text{NO}_3)_2]_2$ <sup>56</sup> has reported the presence of two distinct centrosymmetric dimers in the unit cell, which is in agreement with the observation of two peaks of equal intensity in the  $^{31}\text{P}$  MAS nmr spectrum. It is unclear whether the presence of two signals in the  $^{31}\text{P}$  solid-state nmr spectra of the tri(*p*-methoxyphenyl)phosphine mercury(II) nitrate complex are due to two crystallographically-distinct sites within the unit cell, or two different types of crystals in the bulk powder sample. That the two signals are equally intense indicates that the former case is more likely, although crystallographic data would prove useful in distinguishing the proper choice for this compound.

Although there are two possible choices for  $\Delta J$  depending on the sign that one chooses for  $R_{\text{eff}}$ , only one of the choices is reasonable. Presented in Figure 11 are two calculated  $^{31}\text{P}$  nmr powder spectra for the tri(*p*-tolyl)phosphine derivative as well as the experimental line shape. Quite clearly, one calculated spectrum, corresponding to values of  $(J_{\text{iso}}, \Delta J)$  of  $(+9144 \text{ Hz}, +5450 \text{ Hz})$  or  $(-9144 \text{ Hz}, -1600 \text{ Hz})$ , fits the experimental better than the other,  $(+9144 \text{ Hz}, -1600 \text{ Hz})$  or  $(-9144 \text{ Hz}, +5450 \text{ Hz})$ . However, as this fixes only the relative signs of  $J_{\text{iso}}$  and  $\Delta J$ , further information is required to identify the proper choice for  $\Delta J$ . The previous experimental determination of the sign of  $^1J_{\text{iso}}(^{31}\text{P}, ^{199}\text{Hg})$  as positive<sup>57,58</sup> then allows the proper discrimination between the two possibilities. It was in this fashion that the values for  $\Delta J$  in Table 1 were determined.

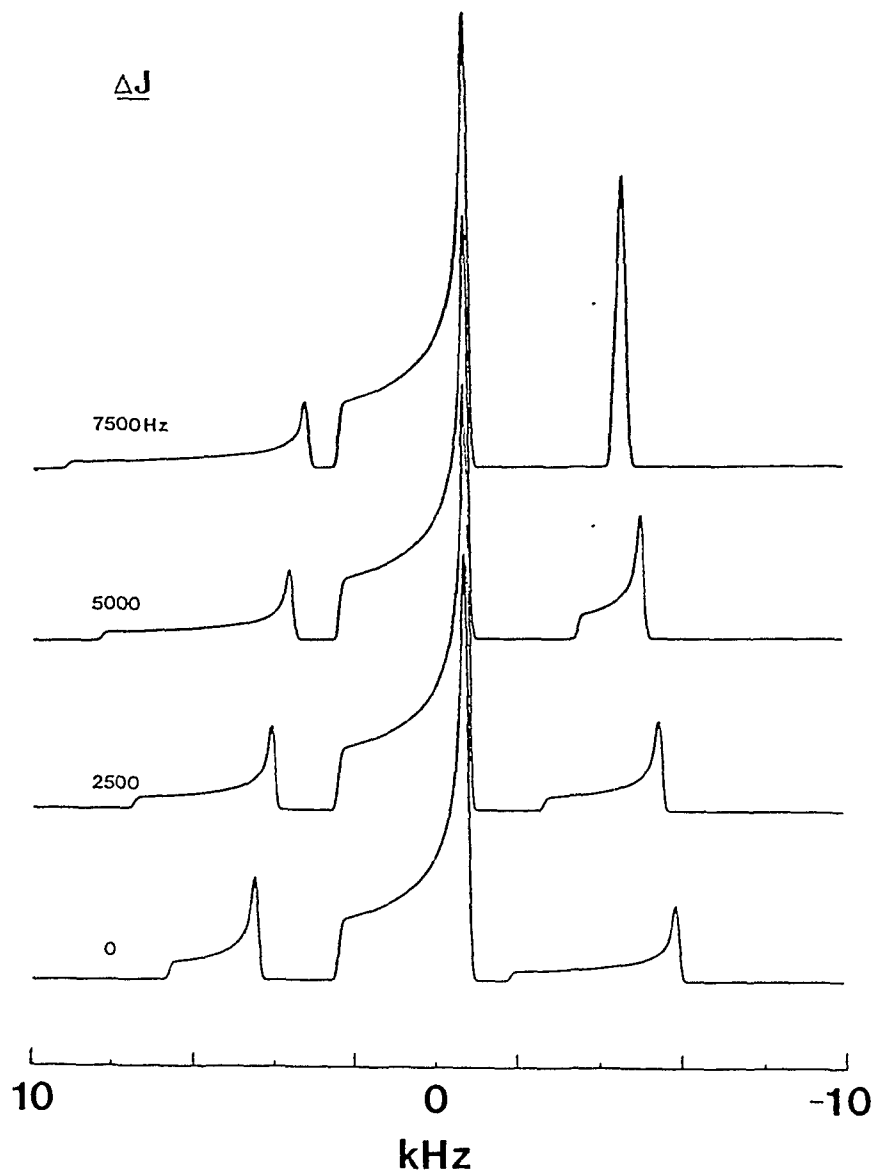
It should be noted that analysis of the values for  $R_{\text{eff}}$  obtained from the spectra for these mercury(II) phosphines assuming  $\Delta J = 0$  yielded values for  $r_{\text{P-Hg}}$  of approximately 1.95 Å and indicated that  $^1J_{\text{iso}}(^{31}\text{P}, ^{199}\text{Hg})$  was negative. Both of these conclusions are in

Figure 11. Phosphorus-31 solid-state nmr line shapes of  $[\text{HgP}(p\text{-tolyl})_3(\text{NO}_3)_2]_2$ , (a) experimental, and calculated spectra with  $(J_{\text{iso}}, \Delta J)$  values of (b) (+9144 Hz, +5450 Hz) or (-9144 Hz, -1600 Hz), and (c) (+9144 Hz, -1600 Hz) or (+9144 Hz, +5450 Hz).



complete disagreement with previous findings, demonstrating that anisotropy in  $\mathbf{J}$  must be present. In order to demonstrate how  $\Delta J$  influences the  $^{31}\text{P}$  nmr powder line shapes, Figure 12 illustrates the calculated spectra that are obtained for different values of  $\Delta J$ , using the parameters corresponding to the observations for the tri(*o*-tolyl)phosphine mercury(II) nitrate compound for the other variables in the calculation. This clearly shows the influence of the anisotropy in the indirect spin-spin coupling between  $^{31}\text{P}$  and  $^{199}\text{Hg}$  on the  $^{31}\text{P}$  nmr powder line shape for these compounds.

Figure 12. Calculated  $^{31}\text{P}$  nmr line shapes of  $[\text{HgP}(o\text{-tolyl})_3(\text{NO}_3)_2]_2$  for values for  $\Delta J$  of 0, 2500, 5000 and 7500 Hz, as indicated.



### 3.4 Discussion

The isotropic values of the  $^{31}\text{P}$  chemical shift and the  $^{31}\text{P}$ - $^{199}\text{Hg}$  indirect spin-spin coupling in the solid state for the mercury(II) phosphines are near the values obtained previously for these compounds in solution.<sup>53</sup> This indicates that there are probably no significant changes in the structure of these compounds in going from solution to the solid state. However, the solid-state nmr spectral data provide a more reliable basis upon which to make comparisons to crystallographic results, as well as giving a more detailed portrayal of the origin of the structural influences on chemical shielding and J coupling, by exhibiting the anisotropic nature of these interactions. The effects of ligand exchange in solution are also eliminated, although steric influences may be amplified in the solid state due to crystal-packing forces.

It is apparent from the data in Table 1 that the  $^{31}\text{P}$  chemical shielding parameters in these compounds are widely varied, as the principal components span a spectral range of approximately 125 ppm. The principal component of the  $^{31}\text{P}$  chemical shift tensor which was determined to lie along the P-Hg bond is relatively constant, only varying from 9.2 ppm to 32.5 ppm. This indicates that, in these compounds, the electronic environments about the  $^{31}\text{P}$  nuclei in the plane perpendicular to the P-Hg bond are similar, at least much more so than in the other directions. The variability in the  $^{31}\text{P}$  chemical shift for different phosphine ligands in the mercury phosphines is similar to that observed in the free phosphines themselves.<sup>62</sup> However, the orientations of the  $^{31}\text{P}$  chemical shift tensor in several free phosphines were based on symmetry arguments and could not be determined with certainty. The magnitude of the  $^{31}\text{P}$  coordination shift in

the solid state, which is the difference in isotropic chemical shifts of the free phosphine and the phosphine bonded to mercury, range from 35 to 72 ppm. The phosphines with aryl ligands have similar coordination shifts, with a range of only 35 to 57 ppm. A somewhat larger coordination shift of 72 ppm is observed for the tricyclohexylphosphine derivative.

The values for  $\Delta J$  are relatively constant,  $5400 \pm 200$  Hz, with the exception of the results for  $[\text{HgPPh}_3(\text{NO}_3)_2]_2$  and  $[\text{HgP}(p\text{-methoxyphenyl})_3(\text{NO}_3)_2]_2$ , while the isotropic indirect spin-spin coupling constants vary from 8008 to 10566 Hz. This result establishes the presence of substantial anisotropy in  $J$  involving  $^{31}\text{P}$  and  $^{199}\text{Hg}$ , in contrast with previous assumptions and calculations which proposed that the Fermi contact mechanism is responsible for at least 98% of the observed indirect spin-spin interaction.<sup>63</sup> It should be noted that Allman and Lenkinski were unsuccessful in establishing a correlation between parameters related to the Fermi contact interpretations and  $^1J_{\text{iso}}(^{31}\text{P}, ^{199}\text{Hg})$  in the  $\text{Hg}(\text{PR}_3)_2\text{X}_2$  series of compounds in the solid state.<sup>64</sup> One aspect of the data in Table 1 that remains unclear is the apparent uniformity of values for  $\Delta J$  in these compounds. Perhaps this reflects a dominance of the contact mechanism in variations of the observed  $J_{\text{iso}}(^{31}\text{P}, ^{199}\text{Hg})$ ; however, there is as yet insufficient data to draw definite conclusions. The values for  $[\text{HgP}(p\text{-methoxyphenyl})_3(\text{NO}_3)_2]_2$  and  $[\text{HgPPh}_3(\text{NO}_3)_2]_2$  do not appear to follow this trend. Clearly, theoretical calculations of  $^1J_{\text{iso}}(^{31}\text{P}, ^{199}\text{Hg})$  in these mercury-phosphorus compounds would be useful in indicating the extent of contact contributions to and the sources of the anisotropy in the indirect spin-spin coupling. Unfortunately, the complexity of these heavy-atom systems may preclude reliable theoretical calculations

of  $J$  couplings for some time.

Anisotropies in the indirect coupling between  $^{31}\text{P}$  and other nuclei have been previously reported in the literature. In  $^{31}\text{P}$  single-crystal nmr studies of two tetraalkyl diphosphine disulfides ( $\text{R}_2\text{P}(\text{S})\text{-P}(\text{S})\text{R}_2$ ,  $\text{R}=\text{ethyl, butyl}$ ), Tutunjian and Waugh<sup>65</sup> found that the  $^{31}\text{P}\text{-}^{31}\text{P}$  indirect spin-spin coupling was anisotropic, with values for  $\Delta J$  between 2.2 and 3.5 kHz. They also found that  $J$  was approximately axially symmetric, along the P-P bond. The  $^{31}\text{P}\text{-}^{31}\text{P}$   $J$  coupling in solid  $\text{Ag}_4\text{P}_2\text{O}_6$  was also reported to be significantly anisotropic, where  $\Delta J = +800$  Hz.<sup>66</sup> Anisotropies in  $J$  between  $^{31}\text{P}$  and  $^{19}\text{F}$  of approximately +3.0 kHz were determined for the  $\text{FPO}_3^{2-}$  group in several fluorophosphates from  $^{31}\text{P}$  static powder spectra.<sup>67</sup> A liquid crystal and X-ray diffraction study of  $(\text{CH}_3)_3\text{P}=\text{Se}$  determined an anisotropy in the  $^{31}\text{P}\text{-}^{77}\text{Se}$   $J$  coupling of -680 Hz,<sup>68</sup> possessing the same absolute sign as  $^1J_{\text{iso}}(^{31}\text{P}, ^{77}\text{Se})$ .

Anisotropies in  $J$  between  $^{199}\text{Hg}$  and other nuclei have also received some attention, such as the coupling between  $^{199}\text{Hg}$  and  $^{13}\text{C}$  in dimethylmercury.<sup>50(b)</sup> Although there was some variation with the solvent system used, this liquid crystal study has reported a value of 864 Hz for  $\Delta J(^{13}\text{C}, ^{199}\text{Hg})$ . Solid-state nmr spectra of the metal tellurides,  $\text{MTe}$ ,  $\text{M}=\text{Cd, Hg, Pb}$ , have indicated substantial anisotropies in  $J$ , ranging from -180 Hz for  $\Delta J(^{113}\text{Cd}, ^{125}\text{Te})$  to -4920 Hz for  $\Delta J(^{199}\text{Hg}, ^{125}\text{Te})$ .<sup>69</sup> However, Viste and coworkers<sup>70</sup> have questioned the choice of the sign of  $\Delta J$  in these compounds, as they found a much better correlation with their calculated values if the other choice was made. As mentioned previously, one must remember that the absolute sign of  $R_{\text{eff}}$  is not available from the solid-state nmr line shape alone, although other information, such as

the internuclear separation and absolute sign of  $J$ , can be used to limit the possible values for  $\Delta J$ .

In light of this work and the results available in the literature, from both experimental and theoretical investigations, it is clear that there are significant anisotropies in the indirect spin-spin coupling involving heavier elements of the periodic table. Such observations conclusively show that these couplings are not governed solely by contact terms, and that interpretations based upon this assumption need to be re-evaluated. It may be revealed, after further effort, that the trends in  $J$  couplings previously proposed from solution studies are indeed primarily due to variations in the contact terms, and that the traceless Fermi contact - spin-dipolar cross-term is the dominant contributor to the observed  $\Delta J$ . However, at present, there is no evidence to support this, due in part to the paucity of both theoretical and experimental data for  $\Delta J$ , and also to the inability to identify the contributing mechanisms *via* experiment. It is believed that the examples presented here provide unequivocal evidence for the magnitude of  $\Delta J$  in these compounds. Further investigations such as that performed here will be described in the two chapters that follow.

### 3.5 Conclusion

Anisotropies in the  $^{31}\text{P}$  chemical shift tensor and the  $^{31}\text{P}$ - $^{199}\text{Hg}$  indirect spin-spin coupling tensor for a series of mercury phosphines have been determined from their  $^{31}\text{P}$  solid-state nmr line shapes. The principal components of the  $^{31}\text{P}$  chemical shift tensor are found to vary over a total range of 125 ppm as the phosphine ligands are changed, but the component of the shift tensor that lies along or near the P-Hg bond is relatively invariant. The indirect spin-spin coupling tensor,  $\mathbf{J}(^{31}\text{P}, ^{199}\text{Hg})$ , exhibits considerable anisotropy, greater than 5 kHz in most cases. This result indicates that mechanisms other than the contact term are in part responsible for the transfer of nuclear-spin information between  $^{31}\text{P}$  and  $^{199}\text{Hg}$  in these compounds. This implies that previous interpretations of values of  $J_{\text{iso}}$  between  $^{31}\text{P}$  and metal nuclei in various metal-phosphine complexes using the assumption of contact-dominated couplings may be invalid.

## Chapter 4

### Solid-State $^{31}\text{P}$ NMR Studies of Mercury(II) Phosphonates.

#### Anisotropies of the $^{31}\text{P}$ Chemical Shift and the $^{31}\text{P}$ - $^{199}\text{Hg}$ Indirect Spin-Spin Coupling.

##### 4.1 Introduction

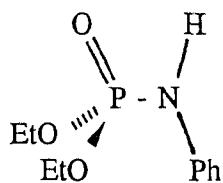
The isotropic values of chemical shifts and indirect spin-spin or J coupling constants have been used for many years to derive information concerning the molecular structure of transition-metal compounds from high resolution nmr spectra. Modern solid-state high-resolution nmr techniques,<sup>71</sup> using high-power proton decoupling, cross-polarization and magic-angle spinning, have been applied recently to metal complexes<sup>72,73,74</sup> to provide a more exact comparison between spectroscopic data and the molecular structure as determined by X-ray diffraction. It has become apparent from these nmr investigations, as well as nmr studies of many other compounds in solid or oriented phases, that substantially more information can be obtained from the three-dimensional nature of the various interactions which are manifested in the nmr spectrum.<sup>13,14,16,47,75</sup> In this fashion, various values of the chemical shift or the J coupling may be found to correspond with specific orientations of a molecule in the magnetic field, providing a more complete picture of the anisotropic nature of the molecule under investigation.

While numerous studies of this type have been performed to determine chemical shift anisotropies,<sup>76</sup> relatively little is known about the anisotropy in the indirect

spin-spin coupling. Although much theoretical effort has been placed on calculating anisotropies in J coupling ( $\Delta J$ ),<sup>10,26,77</sup> the experimental difficulties in measuring this parameter precisely have discouraged its study. In the solid state, the Hamiltonian containing the anisotropy in J is coupled mathematically with that of the direct dipolar coupling between two nuclei.<sup>10,25</sup> Thus, in practice, the two interactions cannot be measured independently. For light nuclei, there is usually some uncertainty in the magnitude of the direct dipolar coupling due to librational motion.<sup>61</sup> The propagation of this error into estimates of  $\Delta J$  has often lead to uncertainties on the order of, or even greater than, the actual magnitude of  $\Delta J$  quoted. Despite the difficulties in determining the anisotropy in J coupling, the importance of its measurement cannot be diminished, as has been shown in the preceding chapter, and will be further developed here.

In order to provide both experimental evidence for the existence of  $\Delta J$  and some idea of the magnitudes that can be expected, the study of a number of mercury-phosphorus compounds was initiated, and this chapter will concentrate on the mercury(II) phosphonates. These compounds have been well characterized by both solution nmr and X-ray diffraction.<sup>78</sup> Previous nmr studies have shown that the indirect spin-spin couplings between <sup>199</sup>Hg and <sup>31</sup>P in these compounds are some of the largest couplings yet measured.<sup>40</sup> The theoretical calculations also indicate that the anisotropic terms of the J coupling Hamiltonian contribute more for the heavier nuclei, due to relativistic effects.<sup>26</sup> The effects of any librational motion should be quite minimal for these large, heavy molecules, thus estimates of the <sup>199</sup>Hg-<sup>31</sup>P direct dipolar coupling based on Hg-P bond lengths determined by X-ray diffraction should be quite accurate. In the process

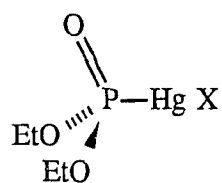
of this investigation, the orientation of the  $^{31}\text{P}$  chemical shift tensor for the phosphonate group in diethyl *N*-phenylphosphoramidate, **1**, has been determined, making it one of the few  $^{31}\text{P}$  chemical shift tensor orientations determined for  $\text{P}=\text{O}$  compounds which have not relied on symmetry arguments. The analysis of the  $^{31}\text{P}$  line shapes from a series of (diethyl phosphonato)mercury(II) complexes, **2a-e**, was then performed to establish the presence of any anisotropy in the  $^{31}\text{P}$ - $^{199}\text{Hg}$  indirect spin-spin coupling of these compounds.



1

a  $^{15}\text{N}$

b  $^{14}\text{N}$



2

a X =  $\text{CH}_3\text{COO}$

b SCN

c Cl

d Br

e I

## 4.2 Experimental

### Preparation of Compounds

(EtO)<sub>2</sub>P(O)<sup>14/15</sup>NHPh (**1**) : These compounds were prepared using literature methods,<sup>79</sup> by reacting diethyl phosphite (0.01 mol, 1.4 g) with aniline-<sup>15</sup>N (99%) (for **1a**) or aniline (for **1b**) (0.01 mol, 0.95 g), in the presence of triethylamine (0.01 mol, 1.04 g) and CCl<sub>4</sub> (0.02 mol, 3.1 g), to yield a yellow oil. White crystals were obtained by adding a small amount of ethanol to the oil, followed by cooling in an ice bath. The crystals were isolated by filtration and washed with H<sub>2</sub>O.

(EtO)<sub>2</sub>P(O)Hg Acetate (**2a**), and (EtO)<sub>2</sub>P(O)Hg Thiocyanate (**2b**) : Prepared as described by Fox and Venezky,<sup>80</sup> by mixing equimolar amounts of Hg(O<sub>2</sub>CCH<sub>3</sub>)<sub>2</sub> (0.05 mol, 15.9 g) and (EtO)<sub>2</sub>P(O)H (0.05 mol, 6.5 mL) in toluene (melting point: 104-106 °C). The thiocyanate complex was prepared by ligand exchange of the acetate complex (0.01 mol, 3.96 g) and aqueous NaSCN (0.01 mol, 0.8 g) in 50 mL H<sub>2</sub>O (melting point: 125-126 °C).

(EtO)<sub>2</sub>P(O)Hg Halides (**2c-e**) : Prepared as described by Fox and Venezky,<sup>80</sup> by mixing equimolar amounts of HgO (0.025 mol, 5.4 g) and the appropriate mercuric halide (0.025 mol) with a dimolar amount of (EtO)<sub>2</sub>P(O)H (0.05 mol, 6.44 mL) in benzene (100 mL) and refluxing for several hours in a Dean-Stark apparatus to remove water formed during the reaction. The products were recrystallized from a benzene-hexane mixture (melting points: chloride 102-104 °C, bromide 86-87 °C, iodide 99-100 °C). The iodide salt was found to turn yellow with the appearance of elemental Hg upon prolonged exposure to air and/or light.

## NMR Spectra

The purity of all of the compounds prepared was determined by  $^{31}\text{P}$  solution nmr at 146.3 MHz on a Nicolet NT360 nmr spectrometer, with the compounds dissolved in dichloromethane (0.4 M), except compound **2b**, which was dissolved in dimethylformamide (0.4 M). Solution spectra were obtained using acquisition times of 0.606 s at a temperature of 293 K. All solid-state  $^{31}\text{P}$  nmr spectra were obtained at 81.0 MHz on a Bruker MSL-200 nmr spectrometer under conditions of cross-polarization (CP) and high-power proton decoupling. Typical  $^1\text{H}$ - $^{31}\text{P}$  contact times for the CP sequence were 3 ms. The  $^1\text{H}$   $90^\circ$  pulse widths were 4  $\mu\text{s}$ , corresponding to a  $^1\text{H}$  decoupling field of 62.5 kHz (14.7 Gauss). Magic-angle spinning (MAS) spectra were obtained at spinning rates between 2 and 4 kHz in a Bruker double-air-bearing MAS probe. Acquisition times for the solid-state nmr experiments were 65.57 ms, during which 4096 data points were collected. The resulting free-induction decays were zero-filled to 8192 data points prior to Fourier-transformation. All spectra were obtained at 293 K and were referenced with respect to 85%  $\text{H}_3\text{PO}_4(\text{aq})$ ; for the solid-state nmr spectra, this was accomplished using  $\text{NH}_4\text{H}_2\text{PO}_4(\text{s})$ , which has a  $^{31}\text{P}$  chemical shift of +0.81 ppm with respect to 85%  $\text{H}_3\text{PO}_4(\text{aq})$ .

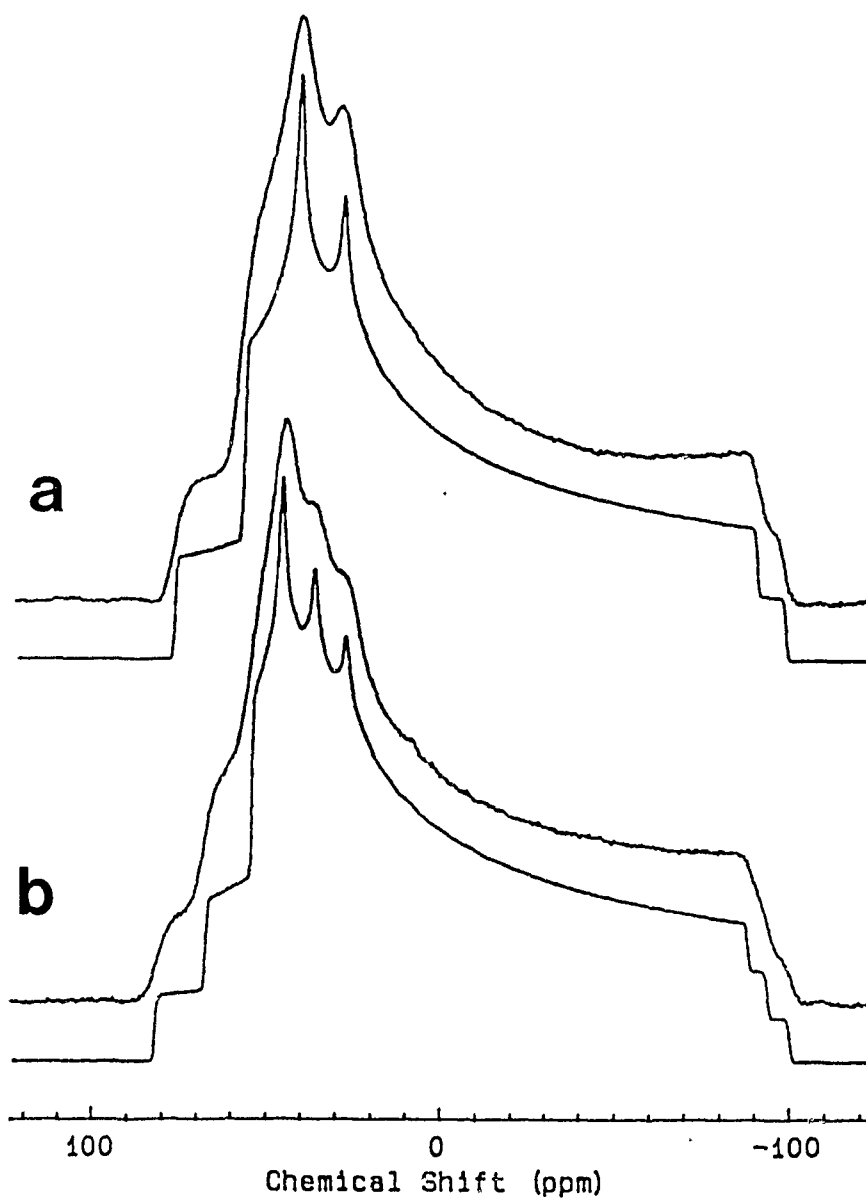
### 4.3 Results and Discussion

#### 4.3.1 (EtO)<sub>2</sub>P(O)<sup>14/15</sup>NHPh (1)

The <sup>31</sup>P static powder nmr spectra for compounds **1a** and **1b** are given in Figure 13. The detailed line shapes result from the orientation dependence of the <sup>31</sup>P chemical shift and <sup>31</sup>P-<sup>15</sup>N or <sup>31</sup>P-<sup>14</sup>N dipolar coupling. The dipolar coupling causes the anisotropic <sup>31</sup>P chemical shift powder pattern to be split into two and three subspectra for the <sup>15</sup>N ( $I=1/2$ ) and <sup>14</sup>N ( $I=1$ ) compounds, respectively.<sup>81</sup> The magnitude of the splittings at the shoulders and peaks of the <sup>31</sup>P spectra were analyzed to provide the orientation of the <sup>31</sup>P chemical shift tensor with respect to the dipolar vector,<sup>23,25,32</sup> which in this case is the P-N bond. For compound **1b**, the <sup>31</sup>P line shape was analyzed under the high-field approximation, where it is assumed that the quadrupolar interaction of the <sup>14</sup>N nucleus does not distort the <sup>31</sup>P-<sup>14</sup>N dipolar splittings.<sup>81(c)</sup> The parameters used to generate these best-fit line shapes shown in Figure 13 are given in the figure caption. The excellent agreement between the calculated <sup>31</sup>P powder nmr spectra for compound **1b**, using the parameters from the best-fit simulation for **1a** without adjustment, and the experimental line shape indicates that the high-field approximation is valid in this case.

The <sup>31</sup>P chemical shift tensor is quite anisotropic, with the overall line shape spanning a spectral width of over 160 ppm, or 13 kHz at 81.0 MHz, the Larmor frequency for <sup>31</sup>P at a magnetic field strength of 4.70 T. Using the convention outlined in Chapter 2 for chemical shielding parameters, the chemical shielding anisotropy,  $\Delta\sigma$ , is 145.5 ppm, with an asymmetry ( $\eta_\sigma$ ) or deviation from axial symmetry of 0.33. These values are typical for <sup>31</sup>P nuclei in phosphonates,<sup>76</sup> where, on average,  $\Delta\sigma = 168$  ppm

Figure 13. Experimental and calculated  $^{31}\text{P}$  CP static nmr spectra of  $(\text{EtO})_2\text{P}(\text{O})\text{NHPPh}$ , (a)  $^{15}\text{N}$ -enriched (compound **1a**) and (b)  $^{14}\text{N}$  (**1b**). The calculated spectra were generated using the following parameters;  $\delta_{11} = 67.9$  ppm,  $\delta_{22} = 36.1$  ppm,  $\delta_{33} = -93.5$  ppm,  $R_{\text{DD}}(^{31}\text{P}, ^{15}\text{N}) = -1010$  Hz,  $R_{\text{DD}}(^{31}\text{P}, ^{14}\text{N}) = +720$  Hz,  $^1J_{\text{iso}}(^{31}\text{P}, ^{15}\text{N}) = -42$  Hz,  $^1J_{\text{iso}}(^{31}\text{P}, ^{14}\text{N}) = +30$  Hz,  $\alpha = 0^\circ$ , and  $\beta = 110^\circ$ . The calculated spectra were convoluted with 100 Hz Gaussian broadening.

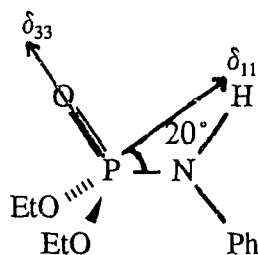


and  $\eta_\sigma = 0.47$ . The values obtained here also agree well with the results of Klose *et al.*<sup>82</sup> for a series of phosphonic acids and esters, especially for compounds that contain an alkoxy functionality in place of the anilino group in compound **1**.

The  $^{31}\text{P}$ - $^{15}\text{N}$  dipolar coupling constant,  $R_{\text{DD}} = 1010 \pm 30$  Hz for **1a**, is in good agreement with those reported for  $(\text{PhO})_2\text{P}(\text{O})^{15}\text{NHMe}$  (950 Hz and 1100 Hz) by Griffin *et al.*<sup>83</sup> using two separate MAS experiments that are sensitive to dipolar coupling. This value for the  $^{31}\text{P}$ - $^{15}\text{N}$  dipolar coupling constant ( $1010 \pm 30$  Hz) corresponds to a P-N bond length of  $1.70 \pm 0.02$  Å, somewhat longer than the X-ray diffraction value of 1.62 Å reported for a similar compound,  $(\text{MeO})_2\text{P}(\text{O})\text{NHPPh}$ .<sup>84</sup> This difference is not surprising as librational motion about the P-N bond will reduce the observed magnitude of  $R_{\text{DD}}$  obtained from the nmr spectrum.<sup>61</sup> Molecular motion causes bond lengths derived from dipolar nmr studies to be longer, in general, than those determined by X-ray diffraction, and can be expected to occur in molecules containing relatively light nuclei. This difference between X-ray diffraction and nmr-derived bond lengths is not expected to introduce substantial errors, and should not influence the results of the analysis performed here. It is unlikely that this difference in bond lengths determined by X-ray diffraction and nmr is due to anisotropy in  $\mathbf{J}$ , as such effects should be extremely minimal for indirect coupling between relatively light nuclei.<sup>43</sup>

The Euler angles,  $\alpha$  and  $\beta$ , orient the principal components of the  $^{31}\text{P}$  chemical shift tensor with respect to the P-N bond (dipolar vector), where  $\beta$  describes the angle between the most shielded component of the  $^{31}\text{P}$  chemical shift tensor,  $\delta_{33}$ , and the P-N vector, and  $\alpha$  is the angle between the projection of the P-N vector onto the  $\delta_{11}$ - $\delta_{22}$  plane

and  $\delta_{11}$  itself (see Figure 6 and §2.5). While generating calculated spectra, these angles are varied to match the splittings observed at the regions of the singularities of the  $^{31}\text{P}$  nmr powder pattern, and the ones quoted here are those that provided a best-fit simulation of the experimental line shapes. The X-ray crystal structure for  $(\text{MeO})_2\text{P}(\text{O})\text{NHPH}$  indicates that the  $\text{N}-\text{P}=\text{O}$  angle is approximately  $111 \pm 1^\circ$ .<sup>84</sup> The optimum values for  $\alpha$  and  $\beta$  of  $0 \pm 5^\circ$  and  $110 \pm 2^\circ$  (or equivalently,  $70 \pm 2^\circ$ ), respectively, places  $\delta_{33}$ , the most shielded component, along the  $\text{P}=\text{O}$  bond, as indicated.



This is in accord with  $^{31}\text{P}$  chemical shift tensor orientations derived for other phosphorus(V) compounds containing the  $\text{P}=\text{O}$  moiety based on symmetry considerations,<sup>82,85,86</sup> single-crystal nmr results<sup>87,88</sup> and theoretical calculations,<sup>89</sup> although it differs from the orientation determined for the fluorophosphates.<sup>67</sup> The values of  $\alpha$  and  $\beta$  for **1** place  $\delta_{22}$  perpendicular to the  $\text{N}-\text{P}=\text{O}$  plane. It is anticipated that the orientation of the  $^{31}\text{P}$  chemical shift tensor will be similar in all phosphonates.

The  $^{31}\text{P}$  nmr powder pattern for **1a** cannot be accurately simulated without including the indirect spin-spin coupling between  $^{31}\text{P}$  and  $^{15}\text{N}$ . The  $^{31}\text{P}$  CPMAS nmr spectra of compound **1a** shows a distinct splitting of the isotropic  $^{31}\text{P}$  signal that corresponds to  $J_{\text{iso}}(^{31}\text{P}, ^{15}\text{N}) = 42 \text{ Hz}$ , in excellent agreement with the solution value of

41.5 Hz. Simulations of the  $^{31}\text{P}$  nmr powder pattern of **1a** also indicate that the sign of  $J_{\text{iso}}$  is the same as that of  $R_{\text{DD}}$ , *i.e.*,  $J_{\text{iso}}(^{31}\text{P}, ^{15}\text{N})$  is negative, in accord with a previous study.<sup>79</sup> The isotropic  $^{31}\text{P}$  chemical shift in the solid-state of 3.6 ppm agrees with the value obtained in solution, 3.1 ppm.

### 4.3.2 (EtO)<sub>2</sub>P(O)HgX Complexes (2a-e)

The  $^{31}\text{P}$  CPMAS nmr spectrum of (EtO)<sub>2</sub>P(O)HgAc, **2a**, shows three separate signals independent of the rotor frequency; one major peak at 69.4 ppm and two minor peaks at  $\pm 6662$  Hz relative to the major one (151.6 ppm and -12.9 ppm), all three of which are flanked by spinning sidebands (see Figure 14(a)). The major  $^{31}\text{P}$  signal is due to  $^{31}\text{P}$  nuclei that are bonded to Hg nuclei which do not possess nuclear magnetic moments. Thus the observed frequency for these  $^{31}\text{P}$  nuclei is determined solely by the chemical shift interaction. The two minor components present on either side of the major peak arise from  $^{31}\text{P}$  nuclei that are adjacent to  $^{199}\text{Hg}$  nuclei ( $I=1/2$ , natural abundance 16.84%). Their signals are split to either side of the  $^{31}\text{P}$  isotropic shift by indirect spin-spin coupling, or J coupling, between  $^{31}\text{P}$  and  $^{199}\text{Hg}$ , and are referred to as  $^{199}\text{Hg}$  satellites of the  $^{31}\text{P}$  signal. These couplings are extremely large, *e.g.*, for **2a**,  $J_{\text{iso}}(^{31}\text{P}, ^{199}\text{Hg}) = 13324$  Hz, leading to the wide frequency range of the spectrum (over 25 kHz). There is no evidence of coupling to  $^{201}\text{Hg}$  ( $I=3/2$ , 13.22% natural abundance) in the  $^{31}\text{P}$  nmr spectra of compounds **2a-e**;  $^{31}\text{P}$  nuclei adjacent to  $^{201}\text{Hg}$  may not have been

Figure 14. Phosphorus-31 CPMAS spectra of two mercury phosphonate compounds, (a) acetate salt, **2a**, and (b) chloride salt, **2c**. The regions of the  $^{31}\text{P}$  isotropic chemical shifts are expanded on the right, and splittings due to J coupling with  $^{199}\text{Hg}$  nuclei are indicated in the full spectra.

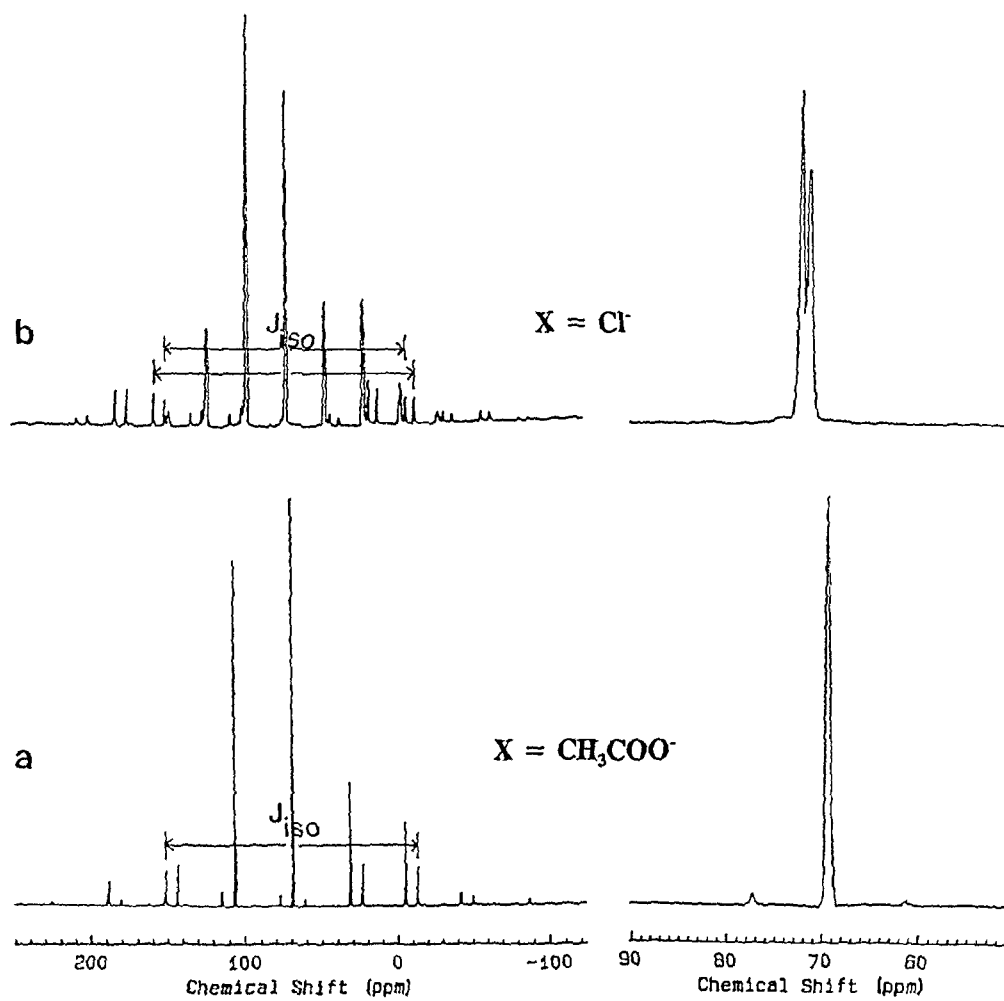


Table 2. Isotropic  $^{31}\text{P}$  chemical shifts (in ppm) and  $^{31}\text{P}$ - $^{199}\text{Hg}$  indirect spin-spin coupling constants (in Hz) for the mercury phosphonates,  $(\text{EtO})_2\text{P}(\text{O})\text{HgX}$  (**2a-e**), in dichloromethane solution and in the solid state, as determined by  $^{31}\text{P}$  solution nmr and  $^{31}\text{P}$  CPMAS nmr, respectively. All shifts are given with respect to external 85%  $\text{H}_3\text{PO}_4(\text{aq})$ .

Anion, $\text{X}^-$	solution		solid	
	$\delta_{\text{iso}}(^{31}\text{P})$	$^1J_{\text{iso}}(^{31}\text{P}, ^{199}\text{Hg})$	$\delta_{\text{iso}}(^{31}\text{P})$	$^1J_{\text{iso}}(^{31}\text{P}, ^{199}\text{Hg})$
$\text{CH}_3\text{COO}$ ( <b>2a</b> )	58.63	12868	69.4	13324
$\text{SCN}^{\text{a}}$ ( <b>2b</b> )	69.86	11948	76.9	12119
$\text{Cl}$ ( <b>2c</b> )	65.19	12665	72.2 71.3	13784 12708
$\text{Br}$ ( <b>2d</b> )	68.64	11989	87.4	13496
$\text{I}$ ( <b>2e</b> )	75.31	11085	88.9	12623

Uncertainties in the  $^{31}\text{P}$  chemical shifts are  $\pm 0.02$  ppm in solution and  $\pm 0.2$  ppm in the solid-state values. Uncertainties in the indirect spin-spin coupling constants are  $\pm 2$  Hz in solution and  $\pm 15$  Hz in the solid-state.

a) dissolved in dimethylformamide

observed due to dipolar coupling to this isotope, which has a large quadrupole moment.

The  $^{31}\text{P}$  CPMAS nmr spectra for compounds **2a-e** allow determination of the isotropic values of the  $^{31}\text{P}$  chemical shift and the  $^{31}\text{P}$ - $^{199}\text{Hg}$  indirect spin-spin coupling in the solid state. These values are given in Table 2 along with the values obtained for these compounds in dichloromethane solution, which agree with previous results.<sup>78,90</sup> The general trends in the  $^{31}\text{P}$  chemical shift and  $^{31}\text{P}$ - $^{199}\text{Hg}$  J coupling constants are the same in the solid state as in solution for this group of compounds. However, in all cases, the  $^{31}\text{P}$  chemical shift in the solid occurs to high frequency of the value obtained in solution. The isotropic J coupling also increases in the solid state, *e.g.*, in the case of the bromide (**2d**) and iodide (**2e**) complexes,  $J_{\text{iso}}(^{31}\text{P}, ^{199}\text{Hg})$  is over 1500 Hz larger in the solid than in solution. One possible explanation for this could be a difference in the solution and solid-state structures. In solution, these compounds exist predominantly as dimers,<sup>91</sup> whereas, in the solid, the crystal structure for the chloride salt, **2c**,<sup>78</sup> reported that the molecules were not associated in a dimeric fashion. Crystal structures for the other salts, as yet not available in the literature, would prove interesting for comparison of the solution and solid isotropic chemical shift and J coupling values, and the underlying structural influences on these parameters that they would imply. However, as these differences in isotropic chemical shift and coupling constants generally are small in relation to the total magnitudes of these parameters, it appears that there are no gross differences in the P-Hg-X framework between the solution and solid structures.

One interesting feature of the  $^{31}\text{P}$  CPMAS spectrum of the chloride, **2c**, is the presence of two distinct phosphorus sites in the crystal, giving rise to two signals

separated by approximately 70 Hz (see Figure 14(b) and Table 2). The isotropic J values for the two sites differ by over 1000 Hz. However, the crystal structure determined by X-ray diffraction<sup>78</sup> indicates that there are four crystallographically distinct molecules in the unit cell. Two of these molecules contain Hg atoms in a distorted trigonal-bipyramid environment, and in the remaining two molecules, the Hg atoms are in a distorted octahedral environment. On the basis of this crystal structure, one expects to observe four distinct <sup>31</sup>P signals in the <sup>31</sup>P CPMAS spectrum for **2c**. It would be extremely coincidental that both the isotropic chemical shifts and  $J(^{31}\text{P}, ^{199}\text{Hg})$  couplings are identical in two separate cases in one crystal. Re-investigation of the X-ray diffraction results may be necessary in light of the solid-state <sup>31</sup>P CPMAS nmr spectrum.

The <sup>31</sup>P static powder nmr spectra of the mercury phosphonates are dominated by the effects of <sup>31</sup>P anisotropic chemical shift; for the satellites, this is combined with both <sup>31</sup>P-<sup>199</sup>Hg indirect J coupling and direct dipolar coupling. The experimental <sup>31</sup>P nmr powder pattern for **2a**, given in Figures 15 and 16, illustrates that, although the satellites overlap extensively with the central line shape, the three singularities of each pattern can be discerned. Unobscured observation of the central line shape allows direct determination of the principal components of the <sup>31</sup>P chemical shift tensor. This was performed for compounds **2a-e**, with the results listed in Table 3. Relative to the shift tensor components obtained for the phosphoramidate, **1**, each of the components is shifted, on average, 77 ppm to high frequency. It is anticipated that the orientations of the <sup>31</sup>P chemical shift tensors in compounds **2a-e** are similar to what was determined for **1**, and has been observed for all other phosphonates, as mentioned previously.

Table 3. Phosphorus-31 chemical shift tensor components (in ppm with respect to 85%  $\text{H}_3\text{PO}_4(\text{aq})$ ) and anisotropies in  $^{31}\text{P}$ - $^{199}\text{Hg}$  indirect spin-spin coupling (in Hz) for the mercury phosphonates (**2a-e**), as determined from the  $^{31}\text{P}$  CP static powder nmr spectra. The chemical shift tensor data for **1** is included for comparison.

Anion, X	$\delta_{11}$	$\delta_{22}$	$\delta_{33}$	$\Delta\sigma$	$\eta_\sigma$	$\Delta J$
$\text{CH}_3\text{COO}$ ( <b>2a</b> )	125.5	109.7	-27.0	144.6	0.16	2700
SCN ( <b>2b</b> )	147.5	105.7	-22.5	149.1	0.42	1600
Cl ( <b>2c</b> )	121.6	110.1	-13.6	129.5	0.13	-
Br ( <b>2d</b> )	143.7	122.6	4.2	129.0	0.25	-
I ( <b>2e</b> )	144.9	116.1	7.2	123.3	0.35	1500
Compound <b>1</b>	67.9	36.1	-93.5	145.5	0.33	0

Uncertainties in the chemical shift tensor components are  $\pm 1$  ppm, and in the values for  $\Delta J$  are  $\pm 250$  Hz.

The line shapes for the satellites, shifted from the isotropic  $^{31}\text{P}$  chemical shift by  $\frac{1}{2}J_{\text{iso}}$  in each direction, are analyzed in terms of the  $^{31}\text{P}$  anisotropic chemical shift,  $^{31}\text{P}$ - $^{199}\text{Hg}$  direct dipolar coupling and any anisotropy that may exist in the  $^{31}\text{P}$ - $^{199}\text{Hg}$  indirect spin-spin coupling ( $\Delta J$ ). Two of these three parameters can be evaluated independently of the  $^{31}\text{P}$  satellite line shapes. The three principal components of the  $^{31}\text{P}$  chemical shift tensor are available from the central line shape. The  $^{31}\text{P}$ - $^{199}\text{Hg}$  direct dipolar coupling constant,  $R_{\text{DD}}$ , is calculated to be  $677 \pm 43$  Hz using the known range of the Hg-P bond lengths for compound **2c**,  $2.36 \pm 0.04$  Å, as determined by X-ray diffraction.<sup>78</sup> Although the  $^{31}\text{P}$  MAS results for **2c** are not in agreement with the expectations based on this diffraction study in terms of the number of signals, it is expected that the Hg-P bond lengths do not differ by more than  $\pm 0.04$  Å. The orientation of the principal components of the  $^{31}\text{P}$  chemical shift tensor relative to the P-Hg bond are assumed to be similar (within  $10^\circ$ ) to that determined with respect to the P-N bond in **1**. Any further influences on the  $^{31}\text{P}$  satellite line shapes must arise from the effects of anisotropy in the J coupling.<sup>52</sup>

Simulations of the  $^{31}\text{P}$  nmr line shape for **2a** are given with the experimental spectrum in Figure 15. The simulations correspond to the spectra anticipated for  $\Delta J = 0, 1000, 2000$  and  $3000$  Hz, with all other parameters held at their independently-determined values. The vertical lines extending down from the experimental spectrum correspond to its critical frequencies, *i.e.*, those frequencies, three for each of the two spin-states of  $^{199}\text{Hg}$  ( $m_I = +\frac{1}{2}, -\frac{1}{2}$ ), that denote inflection points or peaks in the satellite line shapes. Clearly, a value for  $\Delta J$  between  $2000$  and  $3000$  Hz provides a calculated

Figure 15. Phosphorus-31 static nmr spectra of  $(\text{EtO})_2\text{P}(\text{O})\text{HgO}_2\text{CCH}_3$ , **2a**. At the top is the experimental spectrum, with vertical lines extending down from the critical frequencies of the satellite line shapes. The remaining four spectra were calculated using values of  $\Delta J$  which vary from 0 to 3000 Hz, as indicated. All other parameters were held constant as discussed in the text.

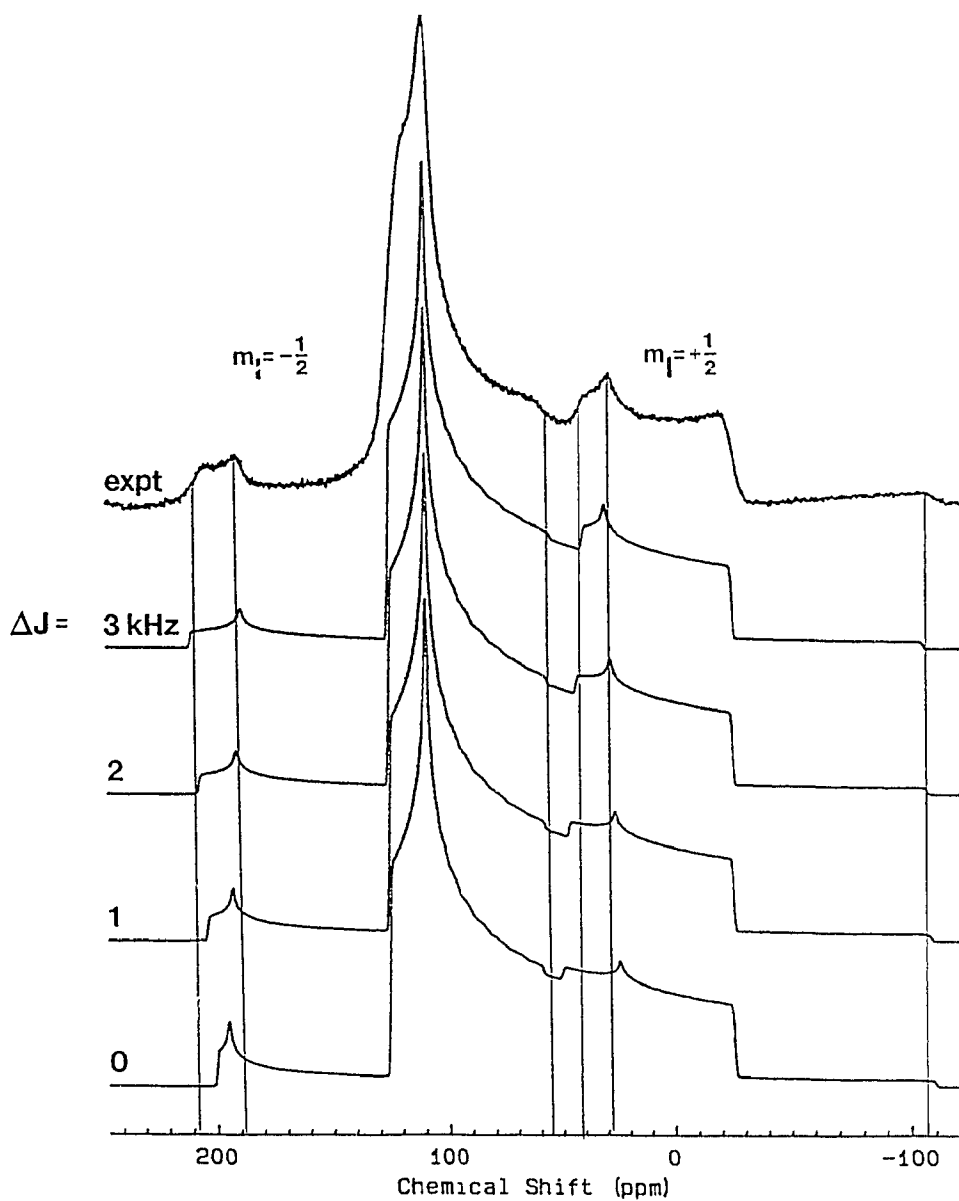
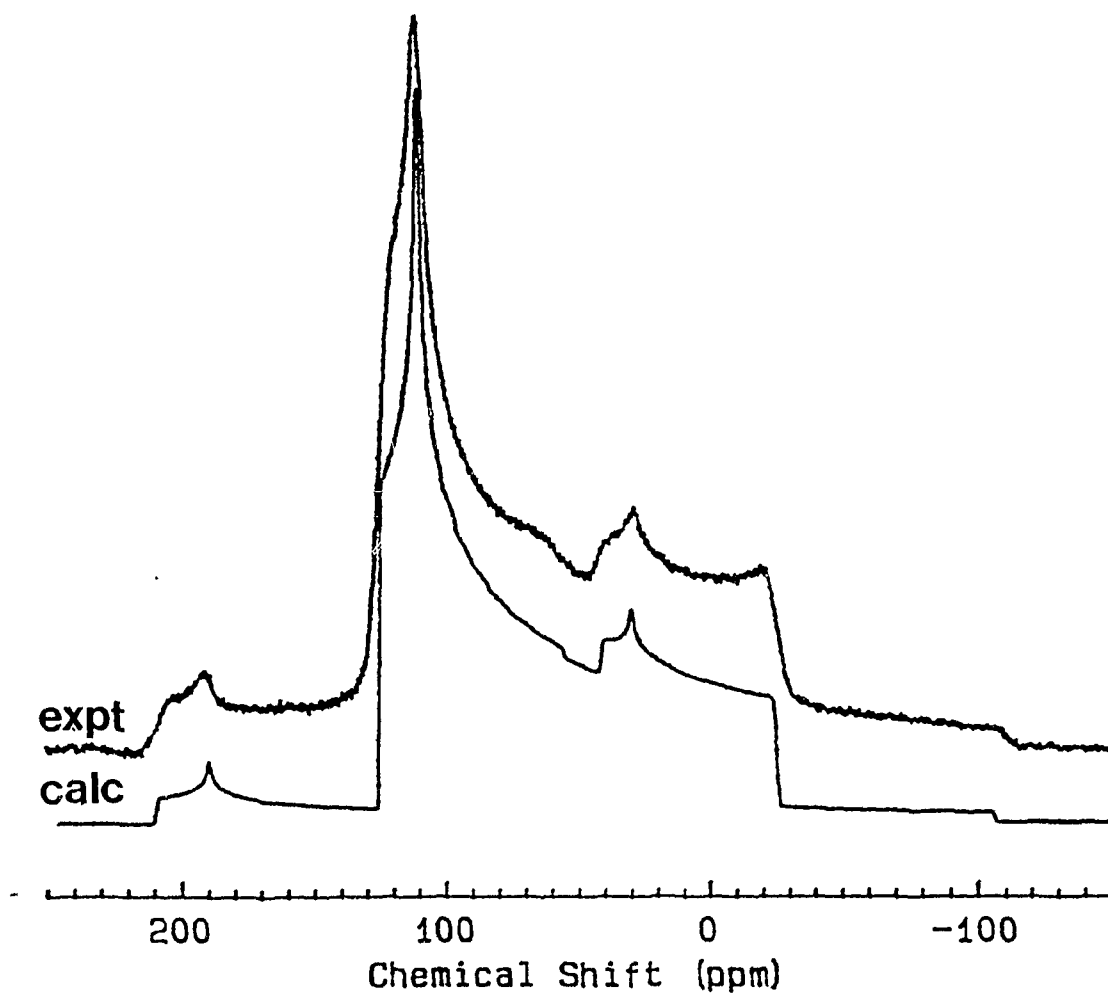


Figure 16. Phosphorus-31 CP static nmr spectrum of  $(\text{EtO})_2\text{P}(\text{O})\text{HgO}_2\text{CCH}_3$ , **2a**, and the best-fit calculated spectrum, corresponding to a value of  $\Delta J = 2700$  Hz.



spectrum that best fits the one observed experimentally. The best-fit simulation was obtained for  $\Delta J = 2700$  Hz, and this calculated spectrum is given with the experimental spectrum in Figure 16. It should be noted that an identical calculated line shape is obtained for  $\Delta J = 1300$  Hz, if the absolute sign of  $J_{\text{iso}}(^{31}\text{P}, ^{199}\text{Hg})$  is taken to be negative. This arises because absolute sign information is not available from the solid-state nmr spectrum; only the relative signs of the isotropic J coupling constant and the "effective" dipolar coupling constant,  $R_{\text{eff}} = R_{\text{DD}} - \Delta J/3$ , can be determined. However, a negative sign for  $^1J_{\text{iso}}(^{31}\text{P}, ^{199}\text{Hg})$  would be contrary to all double-resonance nmr investigations of this coupling, as they have shown that the sign of this coupling constant is positive.<sup>10,57,58</sup>

In such a fashion, the  $^{31}\text{P}$  nmr spectra for compounds **2a**, **2b** and **2e** have been analyzed, and the results are presented in Table 3. The values of  $\Delta J$  for **2b** and **2e** correspond to the case where  $^1J_{\text{iso}}(^{31}\text{P}, ^{199}\text{Hg})$  is positive; identical line shapes can be obtained for a negative  $J_{\text{iso}}$  if  $\Delta J = 2400$  and  $2500$  Hz for **2b** and **2e**, respectively. Due to excessive line broadening introduced by the quadrupolar chlorine and bromine nuclei, the spectra of **2c** and **2d** were not sufficiently defined to allow determination of  $\Delta J$ . Also, the presence of two distinct  $^{31}\text{P}$  nuclei in the  $^{31}\text{P}$  nmr spectrum of the chloride salt, as indicated by the MAS results, further complicates any attempt to analyze its line shape. The error quoted for  $\Delta J$  in Table 3 of  $\pm 250$  Hz is based on the sensitivity of the simulations to changes in its value, as well as to changes of  $R_{\text{DD}}$  ( $\pm 43$  Hz) and the angles  $\alpha$  and  $\beta$  ( $\pm 10^\circ$ ).

The quoted values for  $\Delta J$  assume that the indirect spin-spin coupling tensor,  $\mathbf{J}$ , is axially symmetric. This should be a reasonable assumption if the Hg-P bond has

approximately  $C_3$  or higher symmetry about it. Phosphorus-31 single-crystal nmr studies of two tetraalkyl diphosphine disulfides indicated that  $J(^{31}\text{P}, ^{31}\text{P})$  was axially symmetric along the P-P bond.<sup>65</sup> From the crystal structure for **2c**,<sup>78</sup> there appears to be fairly regular axial symmetry about the Hg-P bond. From the simulations, it is also evident that there are no substantial differences in the observed and calculated values of the splittings about the three principal components of the  $^{31}\text{P}$  chemical shift tensor. Such distortions may be expected to influence the line shape if the asymmetry in  $J$  is significantly different from zero, and can be clearly recognized as they should result in different asymmetries for the central and satellite line shapes.

It is quite clear that there is substantial anisotropy in the  $^{31}\text{P}$ - $^{199}\text{Hg}$   $J$  coupling, *i.e.*, that mechanisms other than the Fermi contact contribute to the transmission of nuclear spin information *via* the electrons between the two nuclei. The values for  $\Delta J$  determined here indicate that 10 to 20% of the total observed coupling is anisotropic in the mercury phosphonates; it appears that the Fermi contact still dominates the indirect spin-spin coupling. Significantly, the value of  $\Delta J$  determined in this study is much smaller than the anisotropy in  $J(^{31}\text{P}, ^{199}\text{Hg})$  of  $5170 \pm 250$  Hz observed for a mercury phosphine,  $[\text{HgP}(o\text{-tolyl})_3(\text{NO}_3)_2]_2$ .<sup>52</sup> The  $^{31}\text{P}$  powder nmr line shapes of a number of other mercury phosphines have also been studied, as presented in Chapter 3, which indicate that anisotropies in  $J$  of the order of 5-6 kHz are present. Apparently, the greater electron-donating ability of the phosphine ligand compared to that of the phosphonate may influence the contributions of mechanisms other than the Fermi contact to the overall indirect spin-spin coupling.

Anisotropy in the indirect spin-spin coupling between  $^{199}\text{Hg}$  and  $^{13}\text{C}$  in dimethylmercury has been recently determined by Pulkkinen *et al.*<sup>50(b)</sup> The isotropic  $J(^{13}\text{C}, ^{199}\text{Hg})$  coupling constant was 692.5 Hz, for which a value for  $\Delta J = 864 \pm 15$  Hz was obtained for this compound dissolved in various liquid crystals. It has been suggested recently by Olivieri<sup>92</sup> that substantial anisotropies exist in the indirect spin-spin coupling between  $^{119}\text{Sn}$  and  $^{35}\text{Cl}$  and between  $^{31}\text{P}$  and  $^{63}\text{Cu}$ . As will be shown in the next chapter, the coupling between  $^{31}\text{P}$  and  $^{195}\text{Pt}$  is also anisotropic. It is anticipated that such influences are present in many transition-metal complexes or compounds containing the heavier elements of the periodic table. Further study of J couplings in the solid state will be necessary before a complete understanding of the importance of the various mechanisms, and a precise interpretation of metal-phosphorus J couplings, among others, is available.

#### 4.4 Conclusions

Phosphorus-31 powder nmr line shapes of solid diethyl *N*-phenylphosphoramidate were analyzed to obtain the magnitudes and orientation of the  $^{31}\text{P}$  chemical shift tensor. The most shielded component of this tensor was found to lie along the  $\text{P}=\text{O}$  bond, without resorting to symmetry arguments. It is believed that this orientation is relatively constant for  $^{31}\text{P}$  nuclei in all phosphonates. The orientation derived for the phosphoramidate was used to interpret the  $^{31}\text{P}$  powder nmr line shapes of a series of mercury phosphonate complexes. In the solid, the isotropic values of the  $^{31}\text{P}$  chemical shift and the  $^{31}\text{P}$ - $^{199}\text{Hg}$  indirect spin-spin coupling were observed to increase compared to those in solution, presumably because of slight structural changes. The  $^{31}\text{P}$  nmr line shapes reveal substantial anisotropies in the  $J$  coupling between  $^{31}\text{P}$  and  $^{199}\text{Hg}$ , which indicates that mechanisms for  $J$  coupling other than the Fermi contact are important. It is anticipated that these mechanisms make significant contributions in mercury-phosphorus compounds, and possibly other metal-phosphorus complexes. Such observations may compel re-evaluation of interpretations of metal-phosphorus  $J$  couplings based on Fermi contact explanations and the  $s$ -character of the bonding orbitals around the nuclei involved.

## Chapter 5

### Anisotropies of the $^{31}\text{P}$ Chemical Shift and

### $^{31}\text{P}$ - $^{195}\text{Pt}$ Indirect Spin-Spin Coupling in Platinum Phosphines

#### 5.1 Introduction

Since the first applications of nmr, and specifically  $^{31}\text{P}$  nmr, to the field of inorganic chemistry, much interest has been placed on the possibility that this technique could identify very fundamental features of structure and bonding in metal complexes.<sup>37</sup> It was quickly recognized that the magnitude of coupling constants among  $^{31}\text{P}$  nuclei, and between  $^{31}\text{P}$  and metal nuclei, provided a quick and effective probe of the stereochemistry of these compounds. The classic example of this was the difference in  $^1J_{\text{iso}}(^{31}\text{P}, ^{195}\text{Pt})$  in square-planar platinum(II) bisphosphine complexes, where *cis* geometry led to a value of about 3500 Hz for this coupling, and *trans* geometry resulted in  $J_{\text{iso}}$  being approximately 1000 Hz smaller. The ease and reliability of  $^{31}\text{P}$  nmr in providing data to assign structure made it the first practical alternative to crystallography in structure determination, and has had much to do with the advances in inorganic chemistry over the last 25 years. Many examples exist in the literature today where the only evidence of structure comes from nmr spectral data, without resorting to diffraction techniques.

Another contribution to inorganic chemistry has been realized with solid-state nmr techniques, which can supply information complementary to the results of diffraction experiments.<sup>71,93</sup> Ambiguities in symmetry elements, and hence space groups, in the crystal lattice often occur in the solution of a crystal diffraction pattern. If the

corresponding sample is available for a solid-state nmr experiment, these ambiguities frequently can be resolved, by comparing the number of isotropic signals observed in a CPMAS experiment with the number expected based on the crystal structure results.<sup>13</sup> Where isochronous signals occur in the MAS experiment, it may be possible to identify differences in the overall chemical shift tensor from static spectra.<sup>94</sup> Increased access to solid-state nmr facilities in recent years has allowed researchers to correlate crystallographic features to those of solid-state nmr spectra, especially the isotropic chemical shift and the chemical shift tensor.

The large differences in  $J_{iso}$  values for different geometries mentioned above sparked the interest of many who wished to determine the interactions of various orbitals on the metal and phosphorus centres.<sup>37</sup> It was believed that the values of the indirect spin-spin coupling constants between these nuclei was a measure of such interactions. A theoretical justification for this was provided by Pople and Santry in 1964,<sup>95</sup> who used molecular orbital (MO) theory to describe the interaction between coupled nuclei and the electrons surrounding them. Although their original theory included all four of the terms introduced by Ramsey,<sup>42</sup> *i.e.*, the Fermi contact, orbital, spin-dipolar and the cross term between the contact and spin-dipolar Hamiltonians, much of the subsequent work assumed the dominance of the Fermi contact interaction. This interaction involves the nuclear spins, A and B, and electron spins in *s*-orbitals only. The indirect spin-spin coupling between the two directly-bonded nuclei,  $^1J_{A-B}$ , was expressed as,

$${}^1J_{A-B} = -\gamma_A \gamma_B \cdot \frac{\hbar}{2\pi} \cdot \frac{256\pi^2}{9} \beta^2 |s_A(0)|^2 |s_B(0)|^2 \sum_i^{\text{occ}} \sum_j^{\text{unocc}} {}^3\Delta E_{i \rightarrow j}^{-1} c_{is_A} c_{js_A} c_{js_B} c_{is_B}. \quad (36)$$

The magnetogyric ratios of the two nuclei were given by  $\gamma_n$  ( $n=A,B$ ),  $\beta$  was the Bohr magneton,  $s_n(0)$  was the magnitude of the valence  $s$  orbital at nucleus  $n$ ,  ${}^3\Delta E_{i \rightarrow j}$  was the triplet excitation energy between occupied ( $i$ ) and unoccupied ( $j$ ) molecular orbitals, and the coefficients  $c$  described the contributions of the  $s$  atomic orbitals of the two nuclei to the occupied and unoccupied molecular orbitals. The summation was carried out over all occupied and unoccupied molecular orbitals. This formulation assumed that  ${}^1J_{A-B}$  depended only on the Fermi contact mechanism; the contributions from other mechanisms were taken to be zero.

Using this and similar theoretical descriptions,<sup>10</sup> many interpretations of the magnitudes and trends of  $J_{\text{iso}}$  values in metal-phosphorus compounds were made, describing the variations in terms of changes in the  $s$ -character of the bond between the two nuclei. The current consensus<sup>40</sup> appears to be that the differences in  ${}^1J_{\text{iso}}({}^{31}\text{P}, {}^{195}\text{Pt})$  for *cis* and *trans* isomers in  $\text{Pt}(\text{PR}_3)_2\text{Cl}_2$  complexes parallel the trends in Pt-P bond lengths. Phosphine ligands that are *trans* to a chlorine possess shorter Pt-P bond lengths, in general, than phosphines that are *trans* to other phosphines.<sup>39</sup> The shorter Pt-P internuclear distance in the *cis*-bisphosphine complexes, where both phosphines are *trans* to chlorine atoms, is thought to be an indication of greater  $s$ -character in the Pt-P bond, which in turn results in larger isotropic J coupling constants.<sup>38</sup> This characteristic often is referred to as the *trans* influence.<sup>96</sup>

In this chapter, the classic examples of geometry-dependent J couplings, the

platinum(II) bisphosphines, were examined using solid-state nmr. These compounds have been investigated previously by  $^{31}\text{P}$  MAS nmr,<sup>72,85</sup> but only in terms of the isotropic values of the  $^{31}\text{P}$  chemical shift and  $^{31}\text{P}$ ,  $^{195}\text{Pt}$  J coupling in the solid state. Static and rotating-sample nmr spectra have been analyzed to characterize the  $^{31}\text{P}$  chemical shift tensors in these complexes, and to identify the presence of anisotropy in J, and quantify it accurately when found.

## 5.2 Experimental

All compounds were obtained from Aldrich Chemical Company, with the exception of the *cis* and *trans* complexes of  $\text{Pt}(\text{PCy}_3)_2\text{Cl}_2$ , which were kindly provided by Dr. A.M. Nicholas. These compounds proved pure upon initial acquisition of their spectra, so no further purification was performed, except where noted otherwise in the next section.

All  $^{31}\text{P}$  solution nmr spectra were obtained at 293 K at a frequency of 146.1 MHz on a Nicolet NT360 nmr spectrometer and referenced with respect to external 85%  $\text{H}_3\text{PO}_4(\text{aq})$ . Phosphorus-31  $90^\circ$  pulse widths were 25  $\mu\text{s}$ , with acquisition times of 106.5 ms, during which 16384 data points were collected.

All  $^{31}\text{P}$  solid-state nmr spectra were obtained at 293 K on a Bruker MSL-200 nmr spectrometer, operating at 81.033 MHz for  $^{31}\text{P}$ . Cross-polarization was used in the acquisition of all spectra, with  $^1\text{H}$   $90^\circ$  pulses of 3.6-4.0  $\mu\text{s}$ . Contact times for polarization transfer were typically 3 ms, except for *trans*- $\text{Pt}(\text{PEt}_3)_2\text{Cl}_2$ , for which it was 300  $\mu\text{s}$ . Contact times were optimized on spinning samples. Recycle delays of 10-20 s were used. Acquisition times for static and spinning samples were 41 ms, during which 4096 data points were collected. Zero-filling to twice this amount of data points was applied prior to Fourier-transformation. Magic-angle spinning was performed in a Bruker double-air-bearing MAS probe using zirconia rotors, with spinning rates up to 6 kHz. All spectra were referenced with respect to 85%  $\text{H}_3\text{PO}_4(\text{aq})$  at 0 ppm; this was accomplished using an external sample of  $\text{NH}_4\text{H}_2\text{PO}_4(\text{s})$ , which has a shift of +0.81 ppm with respect to the reference.

## 5.3 Results

### 5.3.1 MAS Spectra

The results of the analysis of  $^{31}\text{P}$  MAS nmr spectra of the platinum phosphines are given in Table 4. The isotropic values of the  $^{31}\text{P}$  chemical shift ( $\delta_{\text{iso}}$ ) and the  $^{31}\text{P}$ ,  $^{195}\text{Pt}$  indirect spin-spin coupling ( $^1J_{\text{iso}}(^{31}\text{P}, ^{195}\text{Pt})$ ) for the *cis* and *trans* complexes follow the trends noted previously from solution nmr spectra, most notably in the values of  $J_{\text{iso}}$ .<sup>37,39,40</sup> In general,  $J_{\text{iso}}$  is near 3500 Hz in the *cis* complexes, and approximately 2500 Hz in the *trans* complexes. One aspect of the solid-state nmr study that was not possible to observe in solution nmr studies was the correspondence of crystallographic symmetry to the number of signals observed in the  $^{31}\text{P}$  MAS spectra.<sup>71</sup> This is especially apparent in the *cis* complexes, where, in general, the crystal symmetry for the two phosphine ligands of one complex renders each crystallographically distinct. As a consequence, more than one signal is observed in MAS spectra while only one signal would be observed in solution for a given *cis* complex. However, in the *trans* complexes, the crystal symmetry generally places the platinum at a centre of symmetry, which makes the two phosphorus nuclei equivalent in the solid, as well as in solution due to random tumbling of the molecule and/or chemical exchange. Such features have been noted previously,<sup>93</sup> although for some compounds there has been substantial variation in the results available in the literature.

One example is the  $^{31}\text{P}$  MAS spectra observed for *trans*-Pt(PPh<sub>3</sub>)<sub>2</sub>Cl<sub>2</sub>. Previously, two closely spaced  $^{31}\text{P}$  signals were observed for this complex in the  $^{31}\text{P}$  MAS spectra of a mixture of *trans* and *cis* isomers, with isotropic shifts of 20.9 and 19.0 ppm assigned

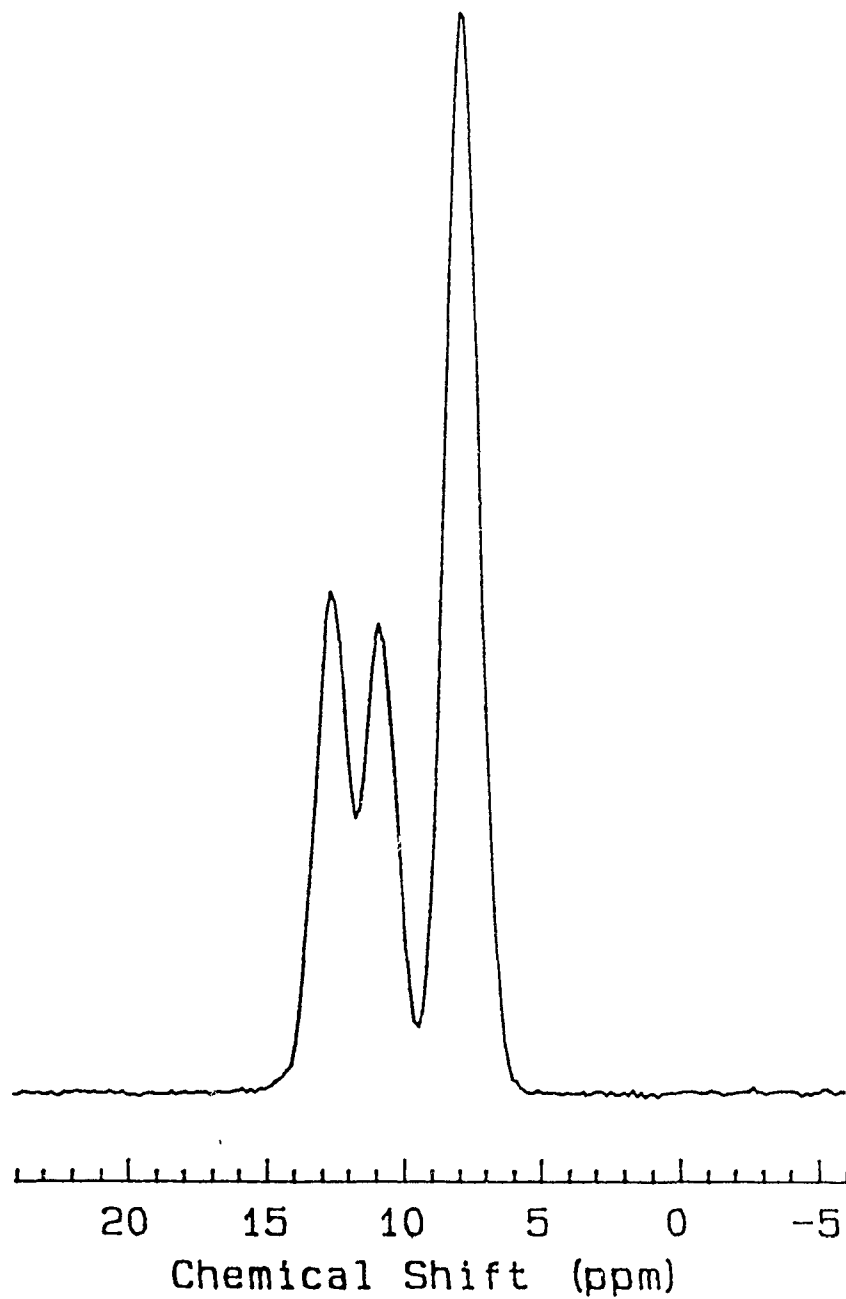
Table 4. Phosphorus-31 solid-state nmr spectral parameters for the platinum phosphines from  $^{31}\text{P}$  MAS spectra. Errors in  $\delta_{\text{iso}}$  are  $\pm 0.3$  ppm and in  $J_{\text{iso}}$  are  $\pm 25$  Hz

Compound	$\delta_{\text{iso}}$	$^1J_{\text{iso}}(^{31}\text{P}, ^{195}\text{Pt})$
<i>trans</i> -Pt(PPh <sub>3</sub> ) <sub>2</sub> Cl <sub>2</sub>	21.6	2624
<i>trans</i> -Pt(PCy <sub>3</sub> ) <sub>2</sub> Cl <sub>2</sub>	14.6	2420
<i>trans</i> -Pt(PEt <sub>3</sub> ) <sub>2</sub> Cl <sub>2</sub>	13.2	2392
<i>cis</i> -Pt(PPh <sub>3</sub> ) <sub>2</sub> Cl <sub>2</sub>	12.7	3727
	10.9	3910
<i>cis</i> -Pt(PCy <sub>3</sub> ) <sub>2</sub> Cl <sub>2</sub>	7.8	3596
	14.8	3565
<i>cis</i> -Pt(PEt <sub>3</sub> ) <sub>2</sub> Cl <sub>2</sub>	10.1	3432
	8.5	3464

to the *trans* complex.<sup>85</sup> However, in the spectra obtained here, only one signal is observed, at 21.6 ppm, with a line-width of less than 80 Hz (1.0 ppm). One possible explanation for this difference is the presence of different crystal forms in the two samples that were studied. If the structure of this complex follows the trend of other *trans*-bisphosphine platinum(II) complexes, one expects that the two phosphorus centres will be equivalent, and only one <sup>31</sup>P signal will be observed. Unfortunately, no crystal structure has been reported for this compound, so this discrepancy cannot be resolved.

Another case is that of *cis*-Pt(PPh<sub>3</sub>)<sub>2</sub>Cl<sub>2</sub>, which has been reported to have two components, but with much different isotropic shifts, of 12.9 and 8.6 ppm,<sup>85</sup> 12.6 and 7.8 ppm,<sup>97</sup> and 7.9 and -4.1 ppm,<sup>72</sup> in each of the three studies. A commercial sample of this compound yields a <sup>31</sup>P MAS spectrum with three distinct signals, at 12.7, 10.9 and 7.8 ppm, with relative intensities of 1:1:2 (see Figure 17). The peak with double intensity possesses satellites which are also of double intensity and have approximately the same line width as the satellites for the other two signals. Such an equivalence of both  $\delta_{\text{iso}}$  and  $J_{\text{iso}}$  probably indicates that the peak with double intensity is due to two crystallographically equivalent <sup>31</sup>P sites in the crystal. This is the first observation of three <sup>31</sup>P signals for this compound. The <sup>31</sup>P solution nmr spectrum of this compound in dichloromethane contains only a single <sup>31</sup>P signal with <sup>195</sup>Pt satellites, with  $\delta_{\text{iso}} = 14.5$  ppm and  $J_{\text{iso}} = 3679$  Hz, in excellent agreement with previous solution data,<sup>85</sup> indicating that the multiple signals in the solid-state spectrum are due to crystallographic effects. Recrystallization of the complex from dichloromethane solution yields an identical three-component solid-state spectrum. The crystal structure for this compound,<sup>98</sup> where

Figure 17. Phosphorus-31 CPMAS spectrum of *cis*-Pt(PPh<sub>3</sub>)<sub>2</sub>Cl<sub>2</sub> at a spinning rate of 4.0 kHz. Note the presence of three isotropic signals at 12.7, 10.9 and 7.8 ppm.



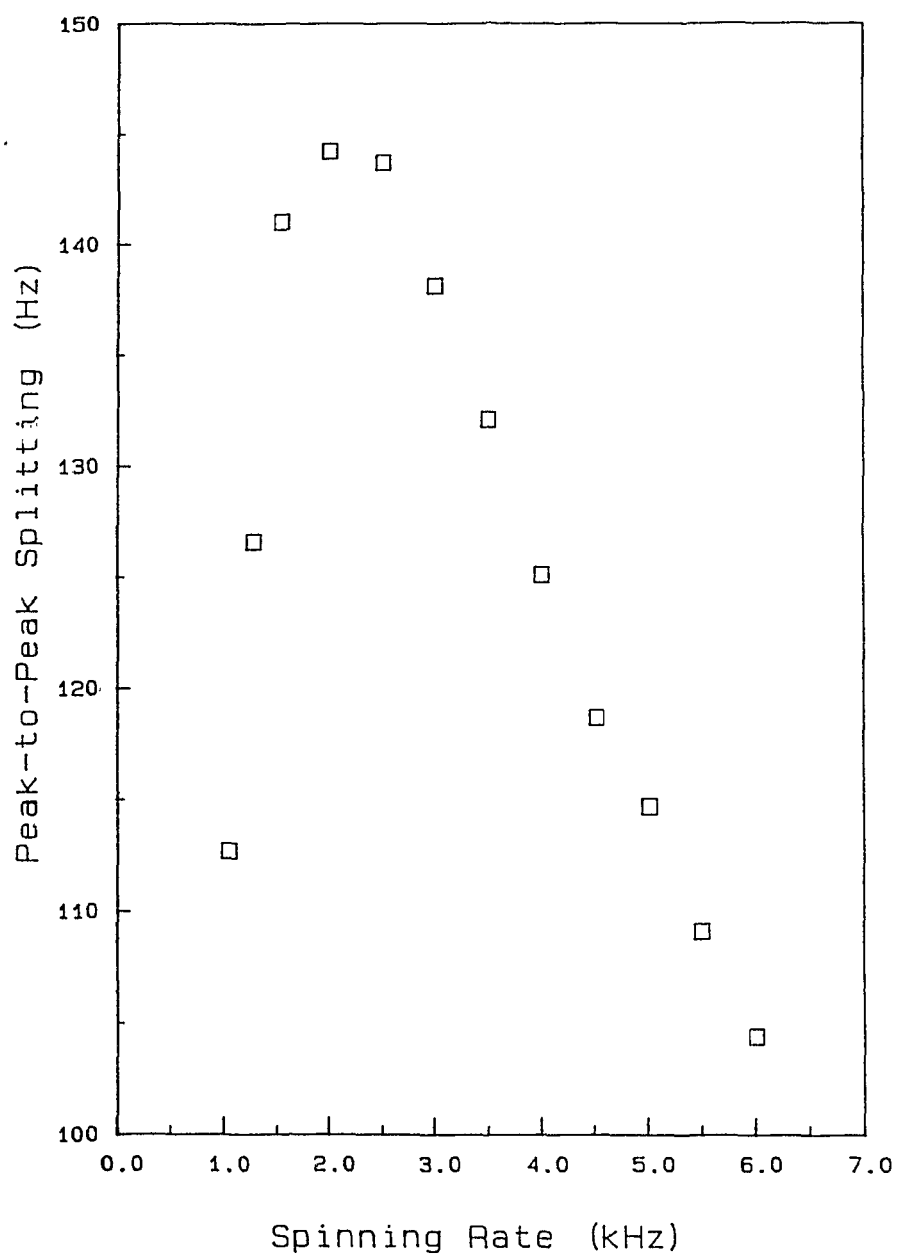
it was isolated from an acetone reaction mixture, shows that the crystal lattice contains a molecule of acetone as solvate for each platinum complex, and indicates that only two  $^{31}\text{P}$  signals should be observed. Recrystallization of this sample from acetone was not possible due to its insolubility in that solvent, so direct comparison of the nmr spectral results to the crystal structure could not be obtained. The differences between the results reported here and the previous literature could have various explanations. The sample used in this study may be a different polymorph from the samples used previously. Also, the two higher-frequency signals, at 12.7 and 10.9 ppm, may not have been resolved in the earlier work, due to spinning instabilities of the older MAS probes,<sup>85</sup> or to overlap in the two-dimensional spectra analyzed by Allman.<sup>97</sup> The reason for the large disagreement with the most recent work is less obvious, as the shift reported for one site (-4.1 ppm) in that report<sup>72</sup> is substantially different from all other  $^{31}\text{P}$  chemical shifts attributed to this compound. That sample, like all others discussed here, was retrieved from dichloromethane solution. However, the  $^{31}\text{P}$  solution nmr data for that sample<sup>72</sup> does not correspond to the accepted values available in the literature,<sup>85,99</sup> indicating that it may not have been *cis*-Pt(PPh<sub>3</sub>)<sub>2</sub>Cl<sub>2</sub>.

In many *cis* complexes, two closely-spaced signals commonly are observed, their shifts differing by only 2-3 ppm.<sup>93</sup> In *cis*-Pt(PCy<sub>3</sub>)<sub>2</sub>Cl<sub>2</sub>, no splitting is observed, although the  $^{31}\text{P}$  MAS isotropic peak is quite broad, with a line-width of 170 Hz. Two signals are anticipated based on the crystallographic results.<sup>100</sup> This splitting is apparent in the spectrum of *cis*-Pt(PEt<sub>3</sub>)<sub>2</sub>Cl<sub>2</sub>, in agreement with the results of the crystal structure determination,<sup>101</sup> and the two  $^{31}\text{P}$  signals are separated by 1.6 ppm (145 Hz).

However, the splitting was observed to vary with the spinning speed, a phenomenon that was first characterized in  $^{31}\text{P}$  MAS spectra of  $\text{Na}_4\text{P}_2\text{O}_7 \cdot 10\text{H}_2\text{O}$  by Kubo and McDowell.<sup>102</sup> They attributed this spinning-rate-dependent splitting to a difference in the orientation of the chemical shielding tensors of two otherwise equivalent  $^{31}\text{P}$  nuclei which are dipolar coupled. In *cis*- $\text{Pt}(\text{PEt}_3)_2\text{Cl}_2$ , the peak-to-peak splitting varies from 105 to 145 Hz, the maximum splitting being observed at moderate spinning rates, 2.9-2.5 kHz, as evident in Figure 18. The variation observed in this compound is much less than the rate-dependent splittings that were reported by Kubo and McDowell. This may be due to two factors, the much smaller  $^{31}\text{P}$ - $^{31}\text{P}$  homonuclear dipolar coupling in *cis*- $\text{Pt}(\text{PEt}_3)_2\text{Cl}_2$  (approximately 400 Hz compared to about 800 Hz in the  $\text{P}_2\text{O}_7^{4-}$  ion), or to a more significant difference in the  $^{31}\text{P}$  chemical shielding tensors of the two phosphorus nuclei in the platinum complex (*i.e.*, the isotropic shift difference may be small but not zero). Similar effects have been noticed in the  $^{31}\text{P}$  CPMAS nmr spectra of  $(\text{OC})_4\text{W}(\text{dppp})$  (dppp = 1,3-bis(diphenylphosphino)propane) and similar complexes.<sup>103</sup>

An interesting experimental aspect of the  $^{31}\text{P}$  solid-state nmr spectra of *trans*- $\text{Pt}(\text{PEt}_3)_2\text{Cl}_2$  was the extremely short contact time for cross-polarization necessary to obtain them. Whereas all other samples were obtained with contact times of 3 ms, comparable sensitivity for this complex could only be realized with a considerably shorter contact time of 300  $\mu\text{s}$ . Polarization transfer is a competing process between an increasing exponential due to the transfer of magnetization from protons to  $^{31}\text{P}$  nuclei, and a decreasing exponential due to the relaxation of the  $^1\text{H}$  magnetization in the rotating frame.<sup>14</sup> This latter exponential is governed by  $T_{1\rho}(^1\text{H})$ , the proton spin-lattice relaxation

Figure 18. Variation of the peak-to-peak splitting with spinning rate of the two isotropic signals of *cis*-Pt(PEt<sub>3</sub>)<sub>2</sub>Cl<sub>2</sub>.



time in the rotating frame. The remarkably short  $^1\text{H}$   $T_{1\rho}$  probably indicates that the rotation of the methyl groups in this compound occurs at about the same frequency as the  $^1\text{H}$  rf field.

### 5.3.2 Static Spectra

More detailed information about these platinum phosphine complexes can be obtained from the anisotropic information obtained from either static spectra or recovered from MAS spectra using Herzfeld-Berger analysis.<sup>33</sup> The data obtained by such analysis for the platinum(II) bisphosphine complexes is given in Table 5. The chemical shielding anisotropy,  $\Delta\sigma$ , and the asymmetry in the chemical shielding,  $\eta_\sigma$ , provide a description of the local symmetry about the phosphorus nuclei in these compounds. In all of the platinum phosphine complexes, the chemical shielding anisotropy is roughly equivalent, within 25 ppm of 100 ppm. If one considers the total breadth of the  $^{31}\text{P}$  powder pattern ( $\delta_{11} - \delta_{33}$ ), the range of the  $^{31}\text{P}$  chemical shielding in these compounds is much wider, ranging from 95 ppm to 154 ppm. In *trans*-Pt(PPh<sub>3</sub>)<sub>2</sub>Cl<sub>2</sub>, the asymmetry in the  $^{31}\text{P}$  chemical shielding of close to zero indicates that there is near-axial symmetry about the phosphorus nuclei. However, the unique component is not the one which lies along the P-Pt bond (*vide infra*). This example shows the danger of orienting a chemical shielding tensor based on local symmetry arguments. Although they may be useful in identifying the directions one may expect the principal axes to lie, such arguments may not be the proper means to discriminate which direction corresponds to which element of the chemical shift tensor. Unfortunately, no crystal structure has been reported for *trans*-

Table 5. Phosphorus-31 solid-state anisotropic nmr spectral parameters for the platinum phosphines. Errors in the  $\delta_{ii}$  ( $i = 1,2,3$ ) are  $\pm 1$  ppm for the *trans* complexes and  $\pm 2$  ppm for the *cis* complexes, in  $R_{\text{eff}}$  are  $\pm 80$  Hz (*trans*) and  $\pm 160$  Hz (*cis*), and in  $\Delta J$  are  $\pm 250$  Hz (*trans*) and  $\pm 500$  Hz (*cis*).

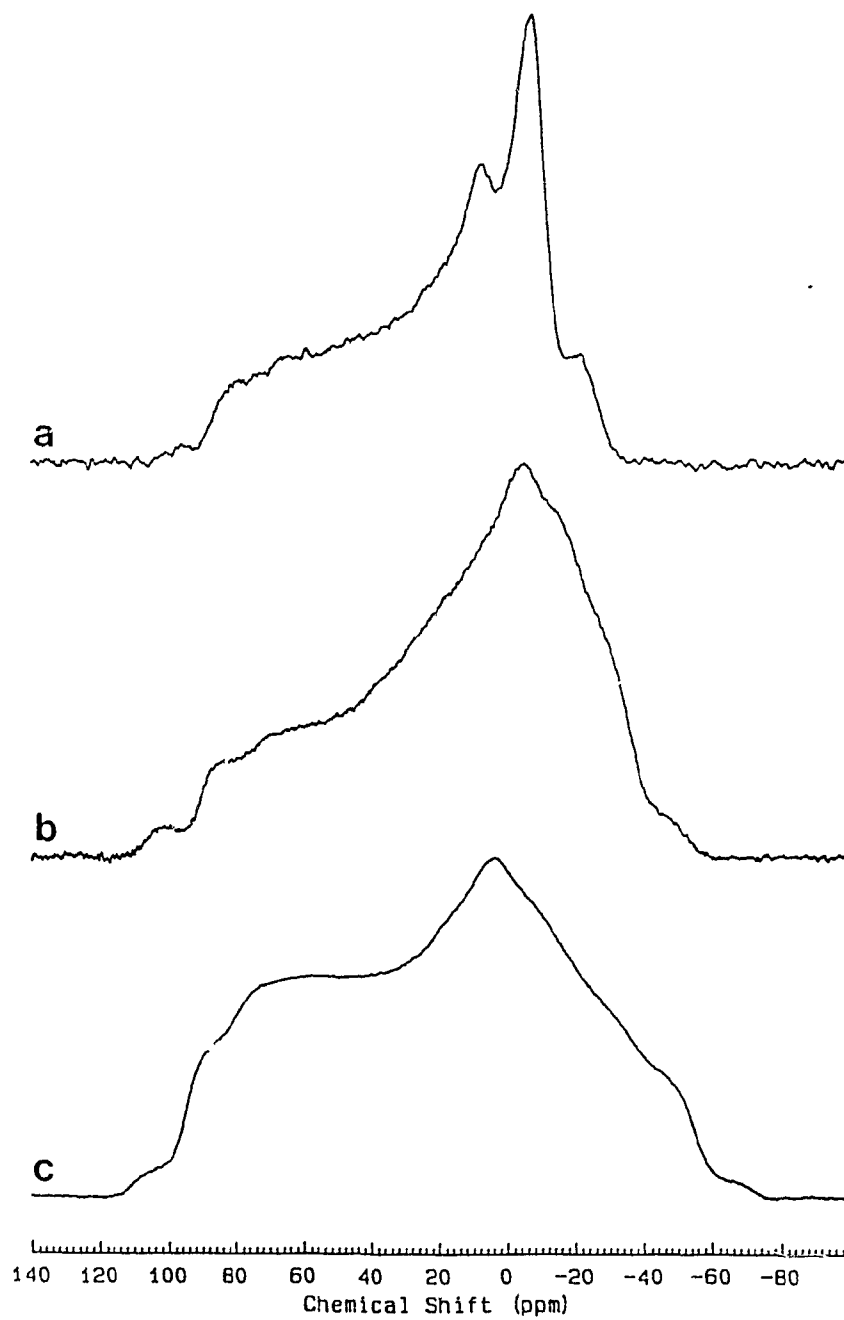
Compound	$\delta_{11}$	$\delta_{22}$	$\delta_{33}$	$\Delta\sigma$	$\eta^\sigma$	$R_{\text{eff}}$	$\Delta J$
<i>trans</i> -Pt(PPh <sub>3</sub> ) <sub>2</sub> Cl <sub>2</sub>	85	-7	-13	95	0.09	240	1850
<i>trans</i> -Pt(PCy <sub>3</sub> ) <sub>2</sub> Cl <sub>2</sub>	90	-6	-40	113	0.45	290	1600
<i>trans</i> -Pt(PEt <sub>3</sub> ) <sub>2</sub> Cl <sub>2</sub>	96	1	-58	125	0.71	350	1550
<i>cis</i> -Pt(PPh <sub>3</sub> ) <sub>2</sub> Cl <sub>2</sub>	89	-10	-41	115	0.41	180	2200 or 3300
	86	-18	-35	113	0.23	260	1950 or 3500
	58	3	-37	75	0.80	230	2050 or 3450
<i>cis</i> -Pt(PCy <sub>3</sub> ) <sub>2</sub> Cl <sub>2</sub>	78	-11	-23	95	0.19	--	--
<i>cis</i> -Pt(PEt <sub>3</sub> ) <sub>2</sub> Cl <sub>2</sub>	73	-6	-37	95	0.49	360	1650 or 3800
	78	-20	-33	105	0.19	560	1050 or 4400

$$\Delta\sigma = \delta_{11} - \frac{1}{2}(\delta_{22} + \delta_{33}), \quad \eta^\sigma = (\delta_{22} - \delta_{33})/(\delta_{11} - \delta_{\text{iso}}).$$

Pt(PPh<sub>3</sub>)<sub>2</sub>Cl<sub>2</sub> to provide a clear picture of the environment about the phosphorus ligands in this complex. In both *trans*-Pt(PCy<sub>3</sub>)<sub>2</sub>Cl<sub>2</sub> and *trans*-Pt(PEt<sub>3</sub>)<sub>2</sub>Cl<sub>2</sub>, there is a large departure from axial symmetry in the <sup>31</sup>P chemical shielding,  $\eta_\sigma = 0.45$  and  $0.71$ , respectively. This is in accord with the results from the X-ray diffraction studies for the two compounds,<sup>104,105</sup> which indicate that there is at most *m* (C<sub>s</sub>) symmetry at the phosphorus sites. The differences in the three *trans* complexes are also reflected in the total breadth of the <sup>31</sup>P powder patterns, which are 98 ppm for the triphenylphosphine complex, and 130 and 154 ppm in the tricyclohexylphosphine and triethylphosphine complexes, respectively. The static spectra of these compounds are shown in Figure 19.

In the previous studies of anisotropies in J coupling between Hg and P (Chapters 3 and 4), the large magnitudes of the isotropic indirect spin-spin coupling constant relative to the direct dipolar coupling and chemical shielding anisotropy simplified analysis of the solid-state nmr line shapes by providing complete or near-complete resolution of the central and satellite line shapes. The smaller values of  $J_{\text{iso}}(^{31}\text{P}, ^{195}\text{Pt})$  lead to considerable overlap of the central and satellite features of the <sup>31</sup>P line shape for the platinum phosphines. The central uncoupled <sup>31</sup>P line shape, accounting for 66.2% of the <sup>31</sup>P spectral intensity, contains information concerning only the phosphorus chemical shielding. From this feature, the three components of the <sup>31</sup>P chemical shift tensor can be determined. The two satellite line shapes, comprising 33.8% of the <sup>31</sup>P intensity (or 16.9% each), are sensitive to the combined effects of phosphorus chemical shielding, <sup>31</sup>P-<sup>195</sup>Pt direct dipolar and indirect spin-spin coupling, as well as the relative orientations of these tensorial interactions. Using estimates for the magnitudes and orientations of

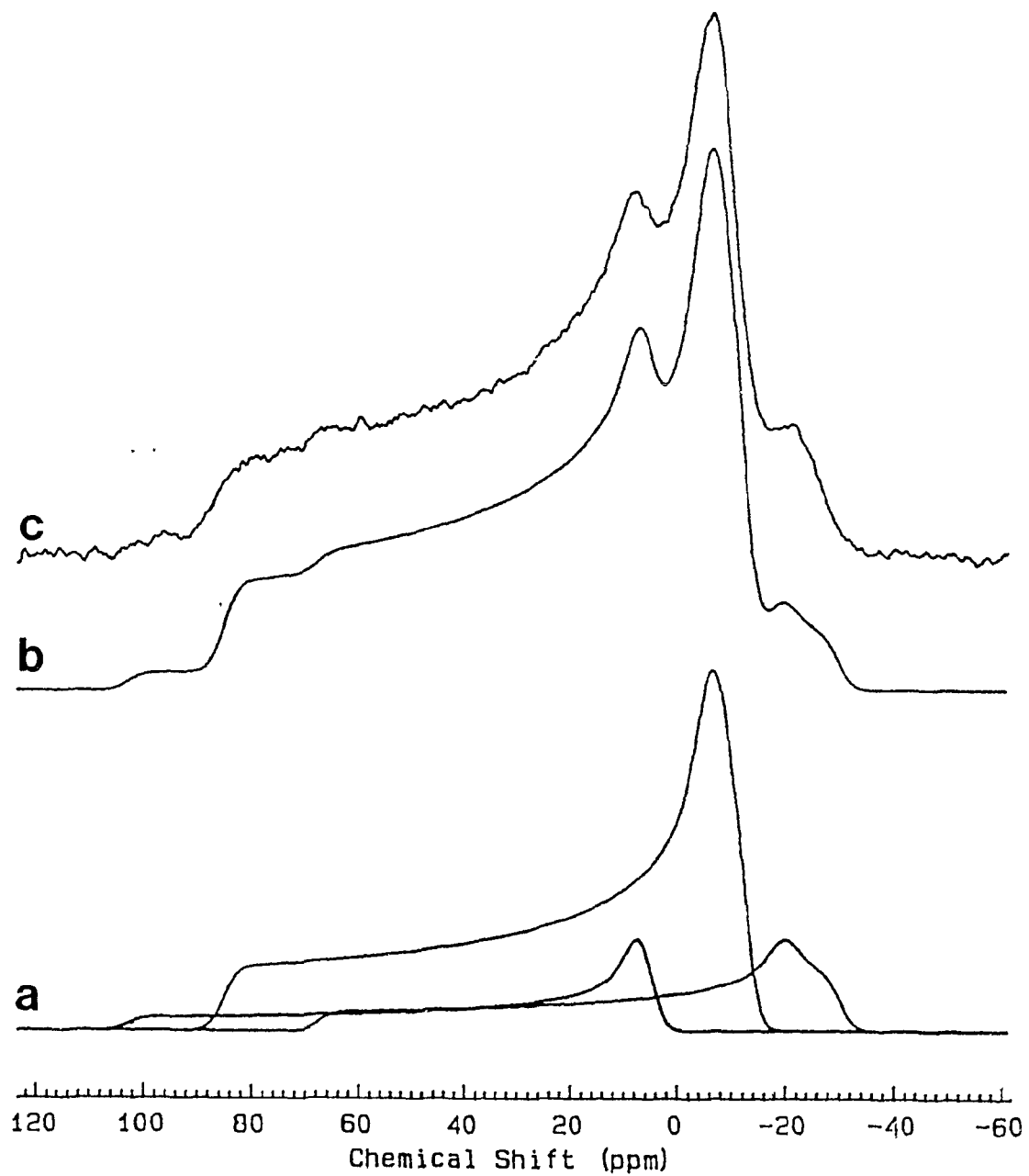
Figure 19. Phosphorus-31 static nmr spectra of the *trans* isomers of (a)  $\text{Pt}(\text{PPh}_3)_2\text{Cl}_2$ , (b)  $\text{Pt}(\text{PCy}_3)_2\text{Cl}_2$  and (c)  $\text{Pt}(\text{PEt}_3)_2\text{Cl}_2$ .



these interactions, each of the three subspectra of the  $^{31}\text{P}$  line shape were calculated separately, then summed with the appropriate relative intensities to yield an overall line shape that could be compared to the experimental spectrum. This process is presented in Figure 20 for *trans*-Pt(PPh<sub>3</sub>)<sub>2</sub>Cl<sub>2</sub>. When the overlap of spectral features prevented a clear distinction of each of the subspectra, slow-spinning MAS spectra were used to either indicate the spectral envelopes of each component, or to reconstruct the complete powder spectrum from resolved spinning sideband patterns using the Herzfeld-Berger technique.<sup>33</sup> One interesting aspect of the spectra examined here is the interplay of the effective dipolar coupling and the isotropic J coupling constant. On first examination, it appears in most cases that the direction of maximum splitting is along the least shielded component,  $\delta_{11}$ . This is usually the best resolved region of the static spectrum, enhancing this effect. This belief could be strengthened by expectations based on the symmetry of the spectrum and local symmetry arguments, as mentioned previously. However, upon careful analysis, the true situation becomes evident. The magnitude of the J coupling between  $^{31}\text{P}$  and  $^{195}\text{Pt}$  has to be removed from the magnitudes of the splittings at the different regions of the spectrum before assignment of the orientation of the  $^{31}\text{P}$  chemical shift tensor can be made. In all cases, it was found that  $\delta_{22}$  lies along or close to the Pt-P bond. Based on the results for *cis*-chelate ring systems involving platinum with phosphorus ligands,<sup>103</sup> where components with  $^{31}\text{P}$  chemical shifts close to 0 ppm were oriented along the Pt-P bond, one would expect a similar behaviour in the platinum(II) bisphosphine complexes.

The most striking feature of the data in Table 5 is the observation of substantial

Figure 20. Phosphorus-31 powder nmr line shapes for *trans*-Pt(PPh<sub>3</sub>)<sub>2</sub>Cl<sub>2</sub>. (a) Individual calculated subspectra corresponding to the uncoupled centreband and two satellite line shapes, (b) summed calculated line shape, and (c) experimental line shape.



anisotropies in the indirect spin-spin coupling between  $^{31}\text{P}$  and  $^{195}\text{Pt}$ . These values were derived under the assumption that the direct dipolar coupling between these two nuclei corresponds to the internuclear separations determined by X-ray crystallography. The reported bond lengths and calculated dipolar coupling constants are: *trans*-Pt(PCy<sub>3</sub>)<sub>2</sub>Cl<sub>2</sub>,  $r_{\text{PtP}} = 2.337 \text{ \AA}$ ,<sup>104</sup>  $R_{\text{DD}} = 822 \text{ Hz}$ ; *trans*-Pt(PEt<sub>3</sub>)<sub>2</sub>Cl<sub>2</sub>,  $2.298 \text{ \AA}$ ,<sup>105</sup>  $865 \text{ Hz}$ ; *cis*-Pt(PPh<sub>3</sub>)<sub>2</sub>Cl<sub>2</sub>,  $2.258 \text{ \AA}$ ,<sup>98</sup>  $911 \text{ Hz}$ ; *cis*-Pt(PCy<sub>3</sub>)<sub>2</sub>Cl<sub>2</sub>,  $2.294 \text{ \AA}$ ,<sup>100</sup>  $869 \text{ Hz}$ ; *cis*-Pt(PEt<sub>3</sub>)<sub>2</sub>Cl<sub>2</sub>,  $2.259 \text{ \AA}$ ,<sup>101</sup>  $910 \text{ Hz}$ . As the crystal structure for *trans*-Pt(PPh<sub>3</sub>)<sub>2</sub>Cl<sub>2</sub> has not been reported in the literature, an average value of  $2.302 \text{ \AA}$  (corresponding to  $R_{\text{DD}} = 860 \text{ Hz}$ ) was used. This average value was the reported weighted average of Pt-P bond lengths in 22 *trans* complexes of platinum(II) phosphines.<sup>106</sup> Direct dipolar coupling and anisotropy in  $J$  affect the solid-state nmr line shape in the same fashion, resulting in an "effective" dipolar coupling constant, as described in detail in both §2.2 and §2.5. It is sufficient at this point to remark again that, as the internuclear separations between P and Pt are quite large (between 2.25 and 2.35 Å), resulting in relatively small  $R_{\text{DD}}$  values, the estimates of  $\Delta J$  are quite robust with respect to any errors in the assumed values of the direct dipolar coupling constant. Librational motion about a cone of half-angle of  $10^\circ$ , which would be large-amplitude motion for these heavy nuclei in a large molecule, would reduce the observed magnitude of the dipolar coupling constant by only approximately 40 Hz. The values for  $R_{\text{eff}}$  given in Table 5 are substantially smaller than the values for  $R_{\text{DD}}$  anticipated from the X-ray values for the Pt-P separation. For example, if the reduction in the calculated  $R_{\text{DD}}$  for *trans*-Pt(PCy<sub>3</sub>)<sub>2</sub>Cl<sub>2</sub> to the observed  $R_{\text{eff}}$  is due only to librational motion, this indicates that the Pt-P bond is librating through a cone with a

half-angle of  $41^\circ$ . Anisotropy in  $J$  must be present to account for the enormous reduction of the dipolar coupling in the observed nmr spectra.

The presence of two values for  $\Delta J$  for the *cis* complexes in Table 5 results from a difficulty in assignment of the relative signs of  $R_{\text{eff}}$  and  $J_{\text{iso}}$  due to the presence of substantial spectral overlap and line broadening, especially in the case of the *cis* complexes. In the analysis of the *trans* complexes, only one value for  $\Delta J$  provides a proper simulation of the experimental line shape, as the absolute sign of  $J_{\text{iso}}(^{31}\text{P}, ^{195}\text{Pt})$  was determined previously to be positive by McFarlane.<sup>107</sup> As discussed in the previous two chapters, the relative signs of  $J_{\text{iso}}$  and  $R_{\text{eff}}$  usually can be discerned from the solid state nmr line shape. The proximity of two  $^{31}\text{P}$  nuclei in the *cis* complexes introduces additional line broadening to the  $^{31}\text{P}$  nmr line shapes of these compounds due to homonuclear  $^{31}\text{P}$ - $^{31}\text{P}$  dipolar coupling. Based on the separation of the  $^{31}\text{P}$  nuclei determined by X-ray diffraction, the strength of this  $^{31}\text{P}$ - $^{31}\text{P}$  coupling is estimated to be of the order of 400 Hz. While this coupling is probably not strong enough to change the frequencies of the distinct features of the  $^{31}\text{P}$  line shape, it makes analysis of the satellites considerably more difficult, thus precluding the relative sign determination.

#### 5.4 Discussion

The principal components of the  $^{31}\text{P}$  chemical shift tensor vary little through the six complexes that have been characterized, regardless of ligand or geometry. This indicates that the environments immediately surrounding the phosphorus nuclei are relatively similar, and there are no gross distortions from a regular phosphine structure in any one complex. One component of the  $^{31}\text{P}$  chemical shift tensor,  $\delta_{22}$ , lies along the Pt-P bond, and the range of values for this component is less than 25 ppm. This is similar to what was observed for the mercury(II) phosphines (Chapter 3), although it appears that the component along the mercury-phosphorus bond in those complexes is about 29 ppm less shielded. The method used to orient the  $^{31}\text{P}$  chemical shift tensor in this study does not permit the assignment of particular directions to the other two principal components,  $\delta_{11}$  and  $\delta_{33}$ , other than placing them in the plane perpendicular to the Pt-P bond. They, as well, do not differ greatly in magnitude among the different platinum(II) bisphosphine complexes. There is an approximate mirror plane at the phosphorus site in these complexes, containing the P-Pt bond and perpendicular to the plane of the complex. This restricts the orientation of the principal components of the  $^{31}\text{P}$  chemical shift tensor such that one component is perpendicular to this mirror plane. In a series of cyclic platinum(II) bisphosphine complexes, principal components of the  $^{31}\text{P}$  chemical shift tensors with shifts between 61 and 111 ppm (mean value of 83 ppm) were assigned to an orientation in the molecular plane and perpendicular to the Pt-P bond. This is similar in magnitude to the values of  $\delta_{11}$  reported in Table 5. On this basis, it seems reasonable to expect  $\delta_{11}$  to have a similar orientation in the  $\text{Pt}(\text{FR}_3)_2\text{Cl}_2$

complexes. The remaining component,  $\delta_{33}$ , is oriented perpendicular to the plane of the molecule. The shift of  $\delta_{11}$  of the  $^{31}\text{P}$  chemical shift tensor upon coordination to the platinum leads to an overall deshielding of the  $^{31}\text{P}$  isotropic shift. It is interesting that the entire coordination shift appears to be limited to one component of the  $^{31}\text{P}$  chemical shift tensor.

Although some ambiguities remain in the possible values of  $\Delta J$ , it is clear that substantial anisotropies exist in the indirect spin-spin coupling between  $^{195}\text{Pt}$  and  $^{31}\text{P}$  in these complexes. Their values are at least 1000 Hz, and may be as large as 4400 Hz. This observation conclusively shows that  $J(^{31}\text{P}, ^{195}\text{Pt})$  is sensitive to much more than Fermi contact parameters, *i.e.*, that factors other than the *s*-character of the bond between the two nuclei determine its value. It appears that  $\Delta J$  is at least marginally larger in the *cis* complexes, in parallel to the trend in  $J_{\text{iso}}$  values. If the greater value for  $\Delta J$  was determined to be the proper choice, it indicates substantial differences in the coupling mechanisms for the two complexes. However, it is not possible to draw such conclusions from the data presented here. More effort using both experiment and theory will be needed before the full extent of the contributions by the various mechanisms of  $J$  will be known. It is evident that mechanisms other than the Fermi contact are making significant contributions to the indirect spin-spin coupling tensor,  $J$ , between  $^{31}\text{P}$  and  $^{195}\text{Pt}$  in both *trans* and *cis* isomers of the platinum(II) bisphosphine complexes.

It would not be proper to compare the results for anisotropies in  $J$  for the mercury and platinum compounds directly, as no account would be made for the differences in the magnetic moments of the  $^{199}\text{Hg}$  and  $^{195}\text{Pt}$  nuclei. To account for this difference, one

must use reduced coupling constants,  $K$ , where the dependence on the magnetic moments of the nuclei is removed.<sup>95</sup> This is performed using the relation,

$$K_{A-B} = \frac{4 \pi^2 J_{A-B}}{h \gamma_A \gamma_B}, \quad (37)$$

where  $K_{A-B}$  is in units of  $10^{20} \text{ kg m}^{-2} \text{ s}^{-2} \text{ A}^{-2}$ . An equivalent expression can be used to convert  $\Delta J$  to  $\Delta K$ . This conversion has been performed for the compounds discussed in this thesis in Table 6.

Santos *et al.*<sup>108</sup> have reported an anisotropy of -450 Hz for the J coupling between  $^{15}\text{N}$  and  $^{195}\text{Pt}$  in a *cis*-platin complex, *cis*-di(ammine- $^{15}\text{N}$ )bis(thiocyanato-S)platinum(II), where the isotropic J coupling constant was -275 Hz. Although this is much smaller than the isotropic and anisotropic values of the J coupling determined in this study, it is not proper to compare them before converting to reduced coupling units. Applying Equation 37 results in  $K_{\text{iso}}$  and  $\Delta K$  values of 105 and 171, respectively (in units of  $10^{20} \text{ kg m}^{-2} \text{ s}^{-2} \text{ A}^{-2}$ ). The value for  $\Delta K$  is remarkably close to the values given in Table 6 for the platinum(II) phosphines.

The anisotropies in the indirect spin-spin coupling ( $\Delta K$ ) in Table 6 are quite large, especially for the mercury(II) phosphines, which are close to double, if not more, than the values for the other compounds. This is not surprising, considering the qualitative differences expected based on the different coordination of the platinum and mercury centres. The anisotropies in  $K$  for the mercury(II) phosphonates are similar to those for the platinum phosphines of both geometries. There also may be little difference in  $\Delta K$  for *cis* and *trans* isomers (if the lesser of two choices for the *cis* complexes is chosen).

Table 6. Average isotropic and anisotropic values of the observed (J) and reduced (K) indirect spin-spin coupling tensors for the mercury(II) phosphines, mercury(II) phosphonates and the platinum(II) phosphines. Values of J are in Hz, while values of K are in units of  $10^{20} \text{ kg m}^{-2} \text{ s}^{-2} \text{ A}^{-2}$ .

Compound	$J_{\text{iso}}$	$\Delta J$	$K_{\text{iso}}$	$\Delta K$
$[\text{HgPR}_3(\text{NO}_3)_2]_2$	9469	5067	1081	578
$\text{HgP}(\text{O})(\text{OEt})_2\text{X}$	13009	1933	1485	221
<i>trans</i> - $\text{Pt}(\text{PR}_3)_2\text{Cl}_2$	2479	1668	236	159
<i>cis</i> - $\text{Pt}(\text{PR}_3)_2\text{Cl}_2$	3616	1781 or 3683	345	170 or 351

R = alkyl or aryl group    X = halide, thiocyanate, acetate

The results that have been presented here conclusively show that substantial anisotropies are present in the indirect spin-spin coupling between  $^{31}\text{P}$  and  $^{195}\text{Pt}$ . The implication is that mechanisms other than the Fermi contact are making significant contributions to the transmission of information between the coupled nuclei. In light of these results, it is clear that interpretations of the values of  $J_{\text{iso}}$  based solely on Fermi contact arguments and Equation 36 are tenuous. For example, the values of  $\Delta J$  for the *trans* complexes in Table 5 follow the trend in the values of  $J_{\text{iso}}$  in these compounds, but this certainly does not indicate that  $\Delta J$  is a measure of *s*-character. Although arguments based on the contribution of *s* orbitals may be a useful tool, it is evident that widespread application of this proposal may be a oversimplification.

## 5.5 Conclusion

A series of *cis* and *trans* platinum(II) bisphosphine complexes have been investigated using  $^{31}\text{P}$  solid state nmr. One component of the  $^{31}\text{P}$  shift tensor,  $\delta_{22}$ , is found to lie along the Pt-P bond in all complexes, and its value varies little, between 3 and -20 ppm. The  $^{31}\text{P}$  chemical shift anisotropies are dominated by a high-frequency shift in one component of the  $^{31}\text{P}$  chemical shift tensor. This shift is also the major contributor to the "coordination shift" of the  $^{31}\text{P}$  signal of the phosphine. It is proposed that this component lies in the plane of the complex, perpendicular to the Pt-P bond.

Significant anisotropies in  $J$  are observed indirectly in the  $^{31}\text{P}$  nmr spectra, through their influence on the observed dipolar coupling,  $R_{\text{eff}}$ . Using estimates for the direct dipolar coupling constant based on Pt-P bond lengths determined by X-ray diffraction, values of  $\Delta J$  in the range from 1500 to 1900 Hz have been unambiguously determined for the *trans* complexes, while estimates of 1000 to 2200 or 3300 to 4400 Hz have been derived for the *cis* complexes. Although the sign of  $R_{\text{eff}}$  cannot be assigned relative to the sign of  $J_{\text{iso}}$  for compounds of the latter geometry, it is still possible to show that there are substantial contributions to the overall indirect spin-spin coupling tensor,  $J(^{31}\text{P}, ^{195}\text{Pt})$ , from mechanisms other than the Fermi contact. This mechanism has been assumed to dominate these couplings in all previous interpretations of the trends in  $J_{\text{iso}}$  values for complexes of this type. While it is not possible to identify the source of the anisotropy in  $J$  in these experiments, conclusions based exclusively on Fermi contact descriptions have been placed in doubt and should be re-examined.

## Chapter 6

# Simulation of NMR Powder Line Shapes of Quadrupolar Nuclei with Half-Integer Spin at Low-Symmetry Sites

### 6.1 Introduction

The study of quadrupolar nuclei by nuclear magnetic resonance has long been used to provide information on the structural and electronic characteristics of various inorganic solids.<sup>109,110,111,112,113</sup> Much of this work has dealt with the effects of both the nuclear quadrupolar coupling and the chemical shielding interactions on the observed spectrum. This work has included single crystal studies,<sup>114,115</sup> as well as analyses of static<sup>116,117,118,119,120</sup> and rotating<sup>121,122,123,124,125,126</sup> samples of polycrystalline and amorphous materials. Single crystal studies provide unambiguous information on the orientation and magnitude of the various interactions, but they are often time-consuming and depend on the availability of a suitably sized single crystal. It is usually much easier from an experimental point of view to study powders or glasses, but this technique suffers from the fact that simulation is usually required to extract the parameters of interest. Analysis of nmr powder patterns arising from quadrupolar nuclei by spectral simulation is complicated because, in general, the line shape will depend on both the magnitudes and relative orientation of the nuclear quadrupolar (Q) and chemical shielding (CS) interactions (*vide infra*). If both interactions are present in the sample under study, the site symmetry of the nucleus of interest in the crystal lattice will determine whether these interactions have the same or

different orientation dependence. The latter case is obviously the most general and the focus of this chapter.

There have been earlier studies on the effects of both nuclear quadrupolar coupling and chemical shielding on the nmr line shapes of powder samples. However, earlier experimental studies were often carried out at low applied magnetic fields where the chemical shielding interaction caused only a minor or negligible perturbation on the observed spectrum. Jones, Graham and Barnes<sup>109</sup> were the first to describe the nature of this line shape under conditions where both the quadrupolar and chemical shielding interactions were axially symmetric and had the same orientation dependence, *i.e.*, the principal components of **Q** and **CS** could be defined in the same axis system. Such situations occur for nuclei at trigonal or higher symmetry point group sites in the crystal, as these sites possess an  $n$ -fold axis of rotation where  $n > 2$ .

A more general treatment was provided by Baugher, Taylor, Oja and Bray.<sup>110</sup> They described the nmr powder pattern for systems involving both chemical shielding and quadrupolar coupling, where both interactions were non-axially symmetric. They were still constrained to have the same principal axis system, however. This extended the work of Jones, Graham and Barnes<sup>109</sup> to apply also to nuclei at orthorhombic sites, since the symmetry at these sites requires that the principal axes of the **Q** and **CS** tensors be coincident.

This, until recently, was as far as the theory had developed in the literature since 1969, providing no method of line shape analysis for quadrupolar nuclei occurring at monoclinic (point symmetry  $C_{2h}$ ,  $C_s$  or  $C_2$ ) or triclinic ( $C_i$  or  $C_1$ ) crystal sites.<sup>127</sup>

Although it was mentioned over 20 years ago<sup>110</sup> that the assumption that the **Q** and **CS** tensors are coincident could introduce errors into the analyses of the powder patterns of quadrupolar nuclei, and an example of this situation was provided by <sup>51</sup>V single-crystal nmr of V<sub>2</sub>O<sub>5</sub>,<sup>114</sup> it has been only within the last two years that researchers have begun to consider the influence of such non-coincidence on the observed nmr powder line shape. Chu and Gerstein<sup>128</sup> have developed complex formulae to extract magnitude and orientation information for the **Q** and **CS** tensors from the field dependence of the characteristic frequencies of the nmr line shapes. Cheng, Edwards and Ellis<sup>31</sup> have developed an iterative method to extract such information from the nmr powder line shapes of the central transitions ( $\frac{1}{2} \longleftrightarrow -\frac{1}{2}$ ) of half-integer spin quadrupolar nuclei with strong nuclear quadrupole moments, *e.g.*, <sup>87</sup>Rb. France<sup>129</sup> has also proposed a method of analysis for spectra in derivative mode.

Two recent developments have aided in the analysis of nmr powder line shapes arising from non-coincident quadrupolar and shielding interactions. The first of these was the widespread application of dipolar - chemical shielding nmr spectroscopy, which was used to determine the orientation of chemical shielding tensors from powder samples.<sup>32</sup> In such studies an isolated spin pair interacts *via* dipolar coupling, which is directed along the vector between the two nuclei. Since dipolar coupling is anisotropic in oriented phases, this provides an internal reference frame about which the chemical shielding tensor can be oriented. Two Euler angles describe the orientation of the chemical shielding tensor with respect to the dipolar vector, whose orientation is known from the molecular structure. Many recent examples of such studies are now available

in the literature (*e.g.*, see reference 32).

One problem in determining the orientation of the shielding tensor in static powder samples using the dipolar interaction is that the dipolar coupling tensor is axially symmetric,<sup>4</sup> thus the derived orientation is only accurate to within an arbitrary rotation about the dipolar vector. To provide an unambiguous orientation of the chemical shielding tensor, a third Euler angle is required, and this can only be obtained when both interactions observed are non-axially symmetric. In general, both the quadrupolar and chemical shielding tensors satisfy this condition. The intent of this project was to extend the techniques used in dipolar - chemical shielding nmr to the quadrupolar - chemical shielding systems.

The second development was the introduction of the POWDER simulation package by Alderman, Solum and Grant.<sup>29</sup> This package provides rapid and reliable simulation of nmr powder patterns, at computational speeds orders of magnitude faster than previously possible. When complete orientation independence of the two interactions is allowed, the computer time required to obtain simulated spectra of suitable resolution and accuracy by conventional iterative methods is prohibitive. The application of the POWDER technique has reduced the computational demands to routine dimensions. This routine has also been applied to the simulation of line shapes in Zeeman-perturbed nqr spectroscopy of powder samples.<sup>130</sup>

The system that is the focus of this analysis is cesium chromate. The <sup>133</sup>Cs nucleus is an attractive one for study as it has a relatively small quadrupole moment and a moderate chemical shift range.<sup>131</sup> A single crystal nmr study has established the

characteristics of the cesium nuclei in this compound (see Appendix 1). There are two crystallographically distinct cesium sites in the unit cell,<sup>132,133</sup> each of which has different orientation dependencies for both interactions. Consequently the powder spectrum of this salt is very complex, and has proved impossible to simulate by a conventional program<sup>134</sup> that assumes coincidence of the principal axis systems of the Q and CS interactions.

## 6.2 Theory

The total Hamiltonian,  $\hat{\mathcal{H}}$ , for a dilute quadrupolar ( $I \geq 1$ ) nucleus in a static magnetic field stems from three main contributions:

$$\hat{\mathcal{H}} = \hat{\mathcal{H}}_Z + \hat{\mathcal{H}}_Q + \hat{\mathcal{H}}_{CS}, \quad (38)$$

where **Z**, **Q** and **CS** denote the Zeeman, quadrupolar and chemical shielding interactions, respectively. Two different situations within the high field limit will be considered, depending on the strength of the quadrupolar perturbation with respect to the dominant Zeeman interaction. The simplest is that of a first-order quadrupolar effect on the nmr line shape, and will be dealt with first. This will be followed by a brief consideration of second-order quadrupolar effects.

Following the treatment of Baugher *et al.*,<sup>110</sup> where the quadrupolar and chemical shielding interactions are described in the same principal axis system, the powder line shape,  $I(\nu)$ , to first-order, is given by:

$$I(\nu) = \sum_{m=-I+1}^{+I} \rho(m) \int_0^\pi \int_0^{2\pi} g \left\{ \nu - \left[ \nu_o \left[ 1 - \sigma_{iso} - \sigma_{ax} (3\cos^2\theta - 1) - \sigma_{aniso} \sin^2\theta \cos 2\phi \right] \right. \right. \quad (39)$$

$$\left. \left. - \nu_Q \left[ \frac{1}{2} (3\cos^2\theta - 1) - \frac{\eta_Q}{2} \sin^2\theta \cos 2\phi \right] \left( m - \frac{1}{2} \right) \right] \right\} \sin\theta d\theta d\phi,$$

where

$$\nu_o = \frac{\gamma B_o}{2\pi}, \quad (40)$$

$$\sigma_{iso} = \frac{1}{3} (\sigma_{11} + \sigma_{22} + \sigma_{33}), \quad (41)$$

$$\sigma_{ax} = \frac{1}{6}(2\sigma_{33} - \sigma_{11} - \sigma_{22}), \quad (42)$$

$$\sigma_{aniso} = \frac{1}{2}(\sigma_{22} - \sigma_{11}), \quad (43)$$

$$\nu_Q = \frac{3e^2q_{33}Q}{2I(2I-1)\hbar} = \frac{3\chi}{2I(2I-1)}, \quad (44)$$

$$\text{and } \eta_Q = \frac{V_{22} - V_{11}}{V_{33}}, \quad |V_{33}| \geq |V_{11}| \geq |V_{22}|, \quad V_{ii} = eq_{ii}. \quad (45)$$

The probability of the ( $m \leftrightarrow m-1$ ) transition is  $\rho(m)$ ,<sup>4,135</sup> and  $g(\nu)$  is the Gaussian broadening function. The parameter  $\chi$  is the quadrupolar coupling constant, and  $V$  represents the electric field gradient tensor. The angles  $\theta$  and  $\phi$  are the polar and azimuthal angles, respectively, that orient the direction of the applied magnetic field,  $\mathbf{B}_0$ , in the  $\mathbf{Q}$  tensor reference frame since the  $\mathbf{Q}$  and  $\mathbf{CS}$  tensors are assumed to be coincident. Using the approach from dipolar - chemical shift methods,<sup>32</sup> Equation 39 can also be expressed as:

$$I(\nu) = \sum_{m=-I+1}^{+I} \rho(m) \int_0^\pi \int_0^{2\pi} g\left\{ \nu - \left[ \nu_o \left( 1 - [\sigma_{11} \sin^2\theta \cos^2\phi + \sigma_{22} \sin^2\theta \sin^2\phi + \sigma_{33} \cos^2\theta] \right) \right. \right. \\ \left. \left. - \left( \frac{\nu_Q}{2} \right) [(3 \cos^2\theta - 1) - \eta_Q \sin^2\theta \cos 2\phi] \left( m - \frac{1}{2} \right) \right] \right\} \sin\theta d\theta d\phi, \quad (46)$$

where  $\sigma_{ii}$  are the principal components of the chemical shielding tensor in units of ppm, such that  $\sigma_{11} \leq \sigma_{22} \leq \sigma_{33}$ . These may be expressed as chemical shifts in ppm from a suitable reference signal, such that  $\delta_{11} \geq \delta_{22} \geq \delta_{33}$ . In Equation 46, the isotropic shift is not explicitly removed from the orientation dependence, as in Equation 39. This does

not imply that the isotropic shift is orientation dependent; rather, since the trace of a tensor is invariant under rotation, it need not be factored out.

If the principal axis system of the quadrupolar tensor and the chemical shielding tensor are not coincident, it is necessary to define two new angles  $\vartheta$  and  $\varphi$  which specify the orientation of  $B_o$  in the CS tensor (see Figure 21). Equation 46 then becomes:

$$I(\nu) = \sum_{m=-I+1}^{+I} \rho(m) \int_0^{\pi} \int_0^{2\pi} g\left\{ \nu - \left[ \nu_o \left( 1 - [\sigma_{11} \sin^2 \vartheta \cos^2 \varphi + \sigma_{22} \sin^2 \vartheta \sin^2 \varphi + \sigma_{33} \cos^2 \vartheta] \right) \right. \right. \\ \left. \left. - \left( \frac{\nu_Q}{2} \right) [(3 \cos^2 \theta - 1) - \eta_Q \sin^2 \theta \cos 2\phi] \left( m - \frac{1}{2} \right) \right] \right\} \sin \theta d\theta d\phi. \quad (47)$$

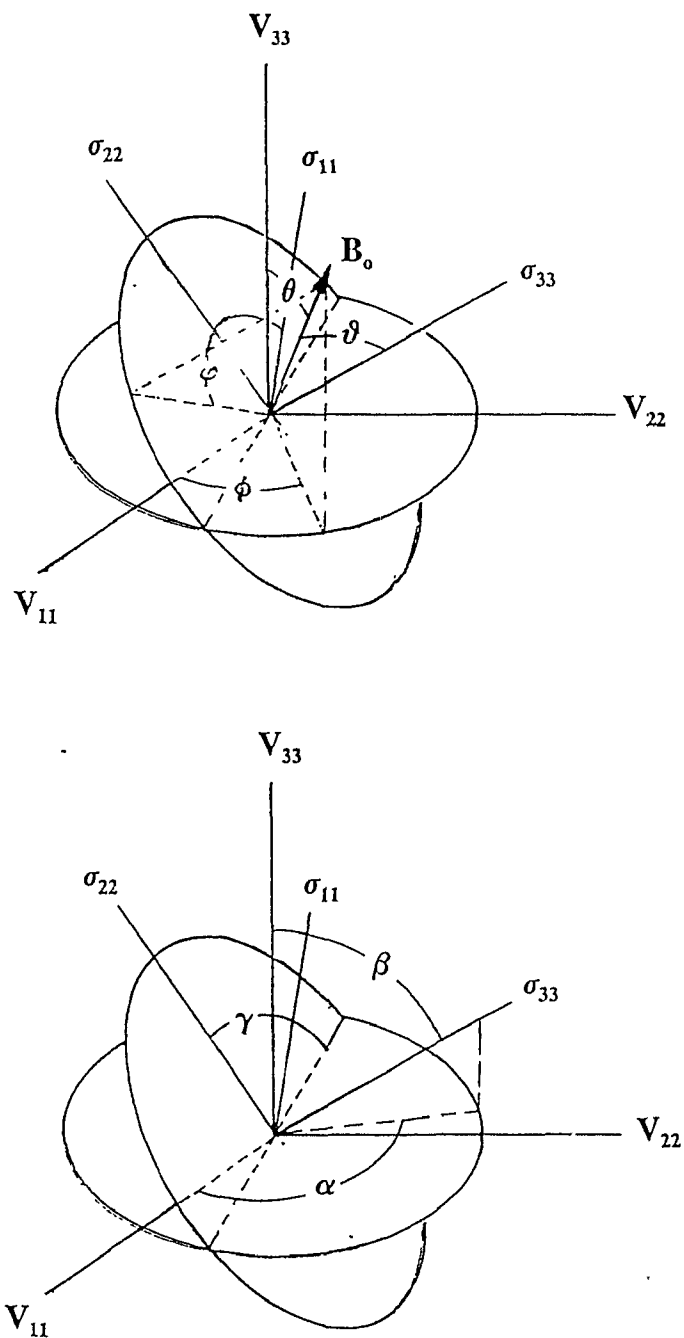
The orientation of the CS tensor in the quadrupolar frame of reference is defined by the Euler angles  $(\alpha, \beta, \gamma)$  illustrated in Figure 21. The expressions given in Equation 48,

$$\begin{aligned} \sin \vartheta \cos \varphi &= \cos \gamma \cos \beta \sin \theta \cos(\phi - \alpha) + \sin \gamma \sin \theta \sin(\phi - \alpha) - \cos \gamma \sin \beta \cos \theta, \\ \sin \vartheta \sin \varphi &= -\sin \gamma \cos \beta \sin \theta \cos(\phi - \alpha) + \cos \gamma \sin \theta \sin(\phi - \alpha) + \sin \gamma \sin \beta \cos \theta, \\ \cos \vartheta &= \sin \beta \sin \theta \cos(\phi - \alpha) + \cos \beta \cos \theta, \end{aligned} \quad (48)$$

were determined using a rotational transformation matrix,  $\mathbf{R}(\alpha\beta\gamma) = \mathbf{R}_z(\gamma)\mathbf{R}_y(\beta)\mathbf{R}_z(\alpha)$ .<sup>27</sup> This substitution can be made for either interaction; the relative orientations expressed with respect to either the quadrupolar tensor or the chemical shielding tensor yield identical line shapes, although, in practice, it is easier to orient the chemical shielding tensor in the quadrupolar principal axis system when considering second-order quadrupolar effects.

One interesting feature of the nmr spectra of half-integer spin quadrupolar nuclei is the fact that the central transition is not influenced by the quadrupolar interaction to first order. This is very important as it allows one to obtain isotropic chemical shifts

Figure 21. The magnetic field vector,  $B_0$ , is oriented in the quadrupolar tensor by the angles  $(\theta, \phi)$  and in the chemical shielding tensor by  $(\vartheta, \varphi)$ . The angles  $\alpha$ ,  $\beta$  and  $\gamma$  orient the chemical shielding tensor in the reference frame of the quadrupolar tensor via the expressions given in Equation 48.



from MAS<sup>122,123,124</sup> or nutation<sup>136,137,138,139</sup> experiments.

When quadrupolar effects become large, *i.e.*,  $(\nu_Q^2[I(I+1)-3/4]/144\nu_o) > 10$ , the powder line shape of the central transition ( $1/2 \leftrightarrow -1/2$ ) is known to depend not only on the chemical shielding anisotropy ( $\Delta\sigma$ ) but also on the magnitude of the quadrupolar coupling constant,  $\chi$ , and its asymmetry,  $\eta_Q$ ,<sup>110</sup> and is given by,

$$\nu_{\frac{1}{2} \leftrightarrow -\frac{1}{2}} = \nu_o \left( 1 - [\sigma_{11} \sin^2 \vartheta \cos^2 \varphi + \sigma_{22} \sin^2 \vartheta \sin^2 \varphi + \sigma_{33} \cos^2 \vartheta] \right) - \left( \frac{Q_2}{6\nu_o} \right) [A(\phi) \cos^4 \theta + B(\phi) \cos^2 \theta + C(\phi)], \quad (49)$$

$$Q_2 = \left( \frac{3\chi}{2I(2I-1)} \right)^2 \left[ I(I+1) - \frac{3}{4} \right], \quad (50)$$

$$A(\phi) = -\frac{27}{8} - \frac{9}{4} \eta_Q \cos 2\phi - \frac{3}{8} \eta_Q^2 \cos^2 2\phi, \quad (51)$$

$$B(\phi) = \frac{30}{8} - \frac{1}{2} \eta_Q^2 + 2 \eta_Q \cos 2\phi + \frac{3}{4} \eta_Q^2 \cos^2 2\phi, \quad (52)$$

$$C(\phi) = -\frac{3}{8} + \frac{1}{3} \eta_Q^2 + \frac{1}{4} \eta_Q \cos 2\phi - \frac{3}{8} \eta_Q^2 \cos^2 2\phi. \quad (53)$$

The satellites are also shifted by the second-order quadrupolar effect, although the splitting between any pair of satellite transitions remains unchanged. In order to calculate the powder line shape of the central transition allowing for non-coincidence of the Q and CS tensors, the only modifications needed are the relevant substitutions (*i.e.*, Equation 48) for the chemical shielding effects, as described for first-order spectra. Otherwise the expressions in reference 110 may be used without further changes.

### 6.3 Experimental

Cesium chromate was purchased from Alfa Products and used without further purification. Samples were packed in 10 mm thin-walled glass tubes. Cesium-133 nmr spectra were obtained on various Bruker spectrometers: MSL-200 (4.7 T, 26.247 MHz for  $^{133}\text{Cs}$ ), MSL-300 and AM-300WB (7.0 T, 39.359 MHz), and AM-500 and MSL-500 (11.75 T, 65.599 MHz); and a Varian spectrometer, Unity-400 (9.4 T, 52.47 MHz). All spectra were acquired with CYCLOPS, a pulse program where pulses are cycled through the four quadrature phases, collecting between 2048 and 4096 real data points after each pulse. Zero-filling to twice the original file size was applied in some cases. A small flip angle (approx.  $20^\circ$ ) was used to minimize distortions,<sup>135</sup> with a relaxation delay of 30 to 60 s between pulses. Typically 1000 to 2000 scans were recorded. A sweep width of 200 kHz was used on the MSL-200 and Unity-400; this was limited to 125 kHz on the 7.0 T and 11.75 T instruments. All chemical shifts were referenced with respect to a 0.5 molar solution of CsCl at 0 ppm.

Simulation programs were written based on the theoretical description, incorporating the POWDER simulation package<sup>29</sup> to reduce computation time to under 10 seconds on a VAX 8800 computer or under 2 minutes on an 80286/287 microcomputer; all calculations were performed on these two systems, and a complete Fortran-77 listing of the programs are given in Appendix 2. The conventional method of integrating in  $1^\circ$  intervals over  $\theta$  and  $\phi$ , which yielded identical line shapes, required approximately 12 hours of CPU time per spectrum on a VAX 8800 computer when axial symmetry is assumed for both the quadrupolar and chemical shielding interaction.

## 6.4 Results and Discussion

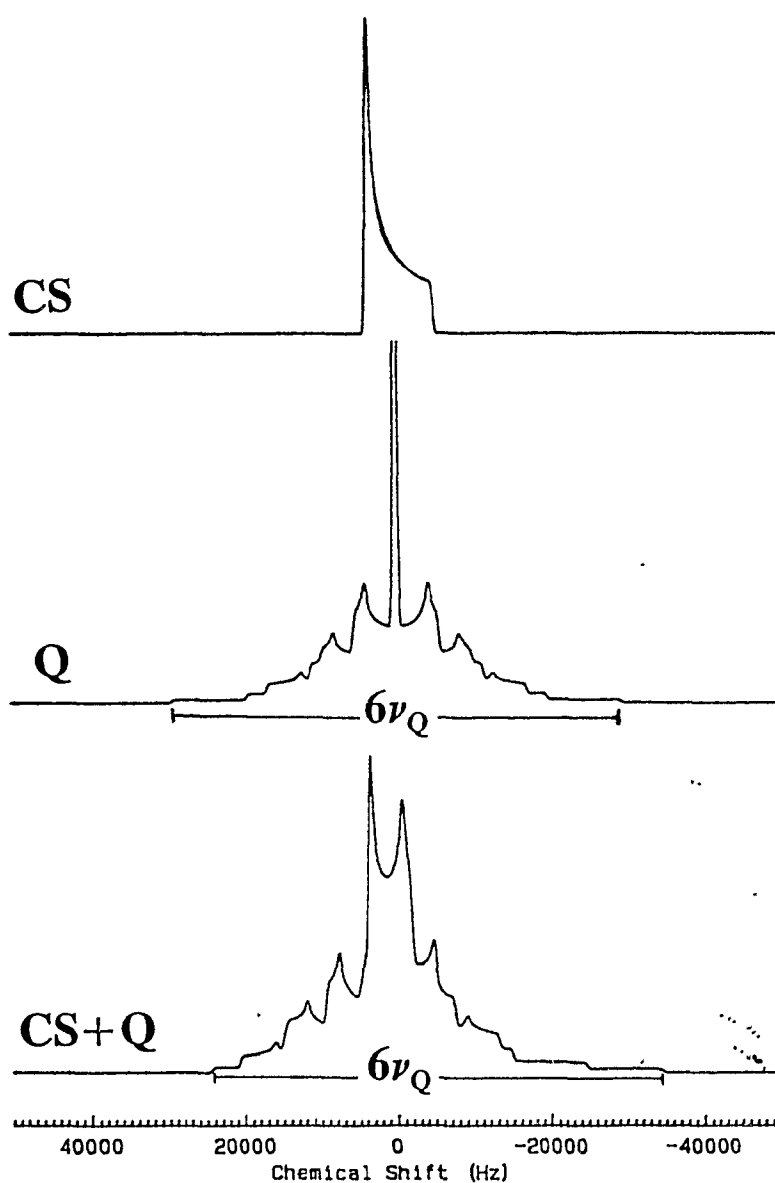
This chapter is mainly concerned with the line shape for a spin  $I=7/2$  nucleus, in particular  $^{133}\text{Cs}$ , which has a relatively small nuclear quadrupole moment, comparable to that of deuterium. Consequently, in the first part of the discussion, second-order quadrupolar effects are neglected; these are addressed in the final section.

### 6.4.1 First-Order Quadrupolar - Chemical Shielding Line Shapes

This, the simplest case to consider when both interactions are present, arises when  $\nu_Q \ll \nu_o$ . Under these conditions the anisotropy of the central ( $1/2 \leftrightarrow -1/2$ ) transition is a result of chemical shielding effects alone.<sup>118,4</sup> The satellites contained contributions from both chemical shielding and quadrupolar coupling. This is illustrated in Figure 22, where the introduction of anisotropic chemical shielding onto the quadrupolar powder pattern results in much more complicated spectrum. The small quadrupolar coupling constant leads to spectral overlap of the central transition by the satellites. The satellites are affected equally by the chemical shielding resulting in no change in the splitting of the various transitions (*e.g.*, the splitting of the outermost shoulders remained constant at  $6\nu_Q$ , regardless of the asymmetry of the chemical shielding). The breadth of the satellites are weighted more to one side or the other of the central features, as shown in Figure 22, depending on the form of the chemical shielding anisotropy.

The effect of varying the relative orientations of the **Q** and **CS** tensors about a single axis is illustrated in Figure 23. These simulations were generated using the parameters for the  $^{133}\text{Cs}$  site 1 in  $\text{Cs}_2\text{CrO}_4$  (see Figure 24), which is discussed in more

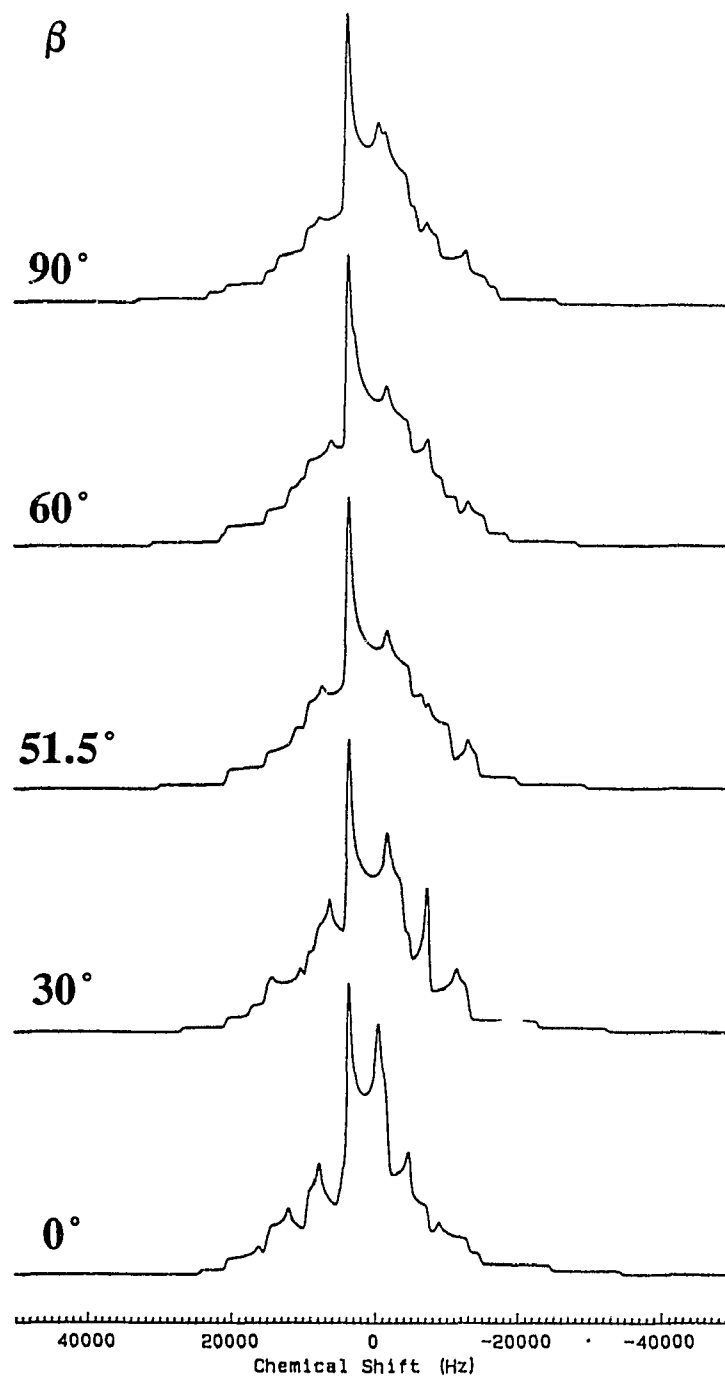
Figure 22. Chemical shielding, quadrupolar, and chemical shielding with quadrupolar calculated nmr spectra for a  $^{133}\text{Cs}$  ( $I = 7/2$ ) nucleus. Note that the outermost quadrupolar splitting remained the same after the introduction of chemical shielding. The parameters used were:  $B_0 = 4.7 \text{ T}$  ( $\nu_0 = 26.247 \text{ MHz}$ ),  $\delta_{11} = 142 \text{ ppm}$ ,  $\delta_{22} = 134 \text{ ppm}$ ,  $\delta_{33} = -195 \text{ ppm}$ ,  $\chi = 138 \text{ kHz}$ ,  $\eta_Q = 0.15$ . The principal axis systems for the two interactions were coincident in this example.



detail later. The angle  $\beta$  between the principal component of the efg tensor,  $V_{33}$ , and the most shielded component of the chemical shift tensor,  $\delta_{33}$ , was varied from  $0^\circ$  to  $90^\circ$ . The angles  $\alpha$  and  $\gamma$  were held at  $0^\circ$ . The central transition, arising solely from chemical shielding, is clearly visible in all the simulations as the invariant peak and shoulder at  $+3$  and  $-5$  kHz, respectively. All other features are due to the combined influence of quadrupolar coupling and chemical shielding. As the angle  $\beta$  between the two tensors deviated from  $0^\circ$ , one expects to observe influences on the line shape due to the two tensors having divergences at different crystallite orientations with respect to the magnetic field. This is indeed the case, as evident in Figure 23. The pattern of peaks and shoulders clearly shifts as  $\beta$  is increased in these simulated spectra. In most cases, all six satellite peaks are distinguishable; where they are not, their approximate positions can be estimated from the trends visible in the series. The peaks on the high frequency side move to lower frequency as  $\beta$  is increased. The shoulders also redistribute, the outermost shoulder changing from the low frequency to the high frequency side of the central transition. The magnitude of the separation between the outermost shoulders on each side of the spectrum remains constant at  $6\nu_Q$ . The contradirectional motion of the peaks and shoulders maintains the centre of mass of the line shape at the isotropic shift, as required by rotations about a fixed origin. This also verifies that the entire chemical shift tensor can be rotated, as opposed to just the traceless part, since the trace itself is invariant to rotation.

A completely general treatment, which allows non-coincidence of the **Q** and **CS** tensors, increases the number of parameters that must be determined to eight; the nuclear

Figure 23. Effect on the calculated  $^{133}\text{Cs}$  nmr line shape of varying the angle  $\beta$  between the Q and CS tensors. The parameters used are those for  $^{133}\text{Cs}$  site 1 of  $\text{Cs}_2\text{CrO}_4$ ; the  $\beta = 51.5^\circ$  pattern is the one experimentally observed. The rotation was about the  $V_{11} - \delta_{11}$  axis.



quadrupolar coupling constant and its asymmetry parameter, the three components of the chemical shift tensor, and the three Euler angles that describe the relative orientation of the two tensors. It is possible to determine several of these directly from experimental spectra obtained at two or more different magnetic field strengths. The central transition is easily identified by those features that maintain the same chemical shift in ppm at all fields, giving three of the unknown parameters. The quadrupolar coupling constant is determined from the splitting of the outermost shoulders, as indicated in Figure 22. Of the remaining four parameters, the site symmetry of the observed nucleus in the lattice aids by limiting the possible choices. In particular, a mirror plane forces one axis of each tensor to lie perpendicular to the mirror, and hence coincident, leaving undetermined only one angle,  $\beta$ , between the different tensors' axes in the plane. Under these conditions,  $\alpha = \gamma = 0^\circ$  and the expressions in Equation 48 simplify to:

$$\begin{aligned} \sin\vartheta \cos\phi &= \cos\beta \sin\theta \cos\phi - \sin\beta \cos\theta, \\ \sin\vartheta \sin\phi &= \sin\theta \sin\phi, \\ \cos\vartheta &= \sin\beta \sin\theta \cos\phi + \cos\beta \cos\theta. \end{aligned} \quad (54)$$

However, computer simulation is the only method by which reliable estimates of the relevant parameters for the experimental spectra can be obtained. In the case of no symmetry in the Q and CS interactions, many combinations of the Euler angles may be possible, which can lead to numerous simulations being performed in order to find the proper values. A stepwise approach to the possible combinations of  $\alpha$ ,  $\beta$  and  $\gamma$ , *e.g.*, in  $30^\circ$  intervals, should indicate the range where the best-fit values of these angles can be found. It is clear that the effects of non-coincident interactions should be considered whenever a quadrupolar nucleus is located in the lattice at a position that does not require

the two principal axis systems to be coincident, *i.e.*, at monoclinic or triclinic sites.

Such non-coincidence between the **Q** and **CS** tensors is a physical property of the observed nucleus in a particular chemical system. In spite of the fact that a powder spectrum has contributions from all possible orientations of the nuclei with respect to the magnetic field, the difference in the orientations of the two tensors is NOT averaged to bring them into coincidence, though one recent work<sup>140</sup> has claimed otherwise. The relative combinations of the quadrupolar tensor and chemical shielding tensor orientations do not vary, but are fixed by the particular electronic environment around the nucleus. This invariance in relative orientation is contained in the fixed Euler angles  $\alpha$ ,  $\beta$  and  $\gamma$ , which are constants as important and unique as the magnitudes of the interactions for any particular crystal.

#### 6.4.2 Cesium-133 NMR Powder Spectrum of $\text{Cs}_2\text{CrO}_4$

The system that stimulated consideration of non-coincident **Q** and **CS** interactions was cesium chromate. This salt has an orthorhombic structure, **Pnma**, with  $Z = 4$ .<sup>132,133</sup> There are two crystallographically distinct cesium sites in the unit cell, each of which is located on a mirror plane ( $C_s$  symmetry, monoclinic point group). A previous  $^{133}\text{Cs}$  nmr study<sup>141</sup> had interpreted the  $^{133}\text{Cs}$  nmr powder spectrum of  $\text{Cs}_2\text{CrO}_4$  in terms of only a single site. However, a single crystal nmr study (see Appendix 1) recently established the quadrupolar and chemical shielding parameters for the two nonequivalent cesium nuclei, and also indicated that at both sites, the quadrupolar tensor was not coincident with the chemical shift tensor in the mirror plane. One axis of each tensor is constrained

by the site symmetry to be perpendicular to the mirror plane, and thus they are collinear, as discussed in §6.4.1. The single crystal results are illustrated in Figure 24. The designation of "Site 1" and "Site 2" is strictly arbitrary and is not an assignment of one nmr-characterized nucleus to either crystallographic site.

The differences between the two sites are clearly evident in the  $^{133}\text{Cs}$  nmr powder spectrum obtained with magic-angle spinning of the sample, given in Figure 25. Because the width of the powder pattern is much larger than the spinning rate in frequency units, spinning sidebands are observed at integer multiples of the spinning rate from the isotropic shift.<sup>142</sup> If a spinning rate is chosen such that these sidebands arising from each site do not overlap, it is possible to obtain some idea of the contribution each site makes to the overall line shape. The isotropic peaks for each site are the two most intense near the centre of the spectrum, with chemical shifts of 27 and -100 ppm for sites 1 and 2, respectively. These isotropic shift values are within 1 ppm of the values determined by single crystal nmr. It is clear that the site 2 sidebands extend further across the spectral window, which is probably due to its larger quadrupolar coupling constant. Conversely, most of the intensity towards the centre of the spectrum arises from nuclei at site 1 in the crystal. This is exactly what one would expect on the basis of the single crystal nmr work. It is interesting to note that the MAS sideband pattern depends on the satellite intensities as well as that of the central transition, evident from the wide spectral window the sideband pattern occupies.

The  $^{133}\text{Cs}$  nmr powder spectrum of this compound is a superposition of the line shapes due to nuclei at each site, leading to a complicated line shape (see Figure 26).

Figure 24. Parameters for the two  $^{133}\text{Cs}$  sites in  $\text{Cs}_2\text{CrO}_4$ . Errors are  $\pm 5$  kHz in  $\chi$ ,  $\pm 0.05$  in  $\eta_Q$ ,  $\pm 5$  ppm in the  $\delta_{ii}$ 's and  $\pm 2^\circ$  in the angles.

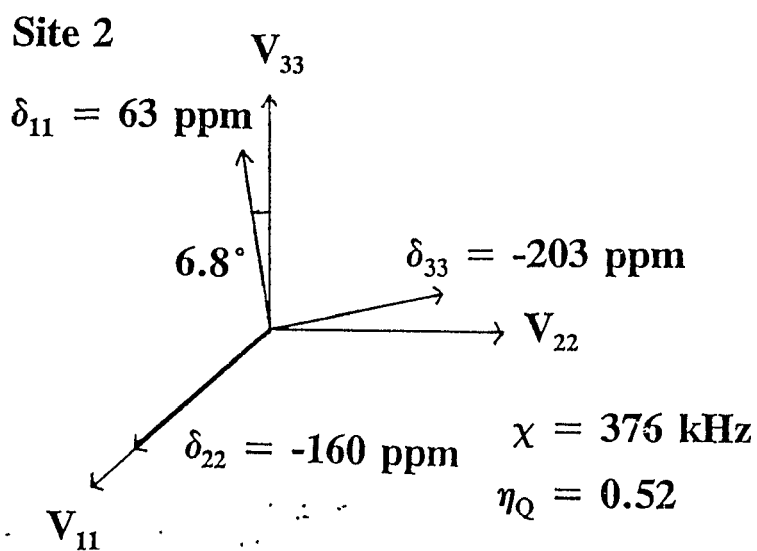
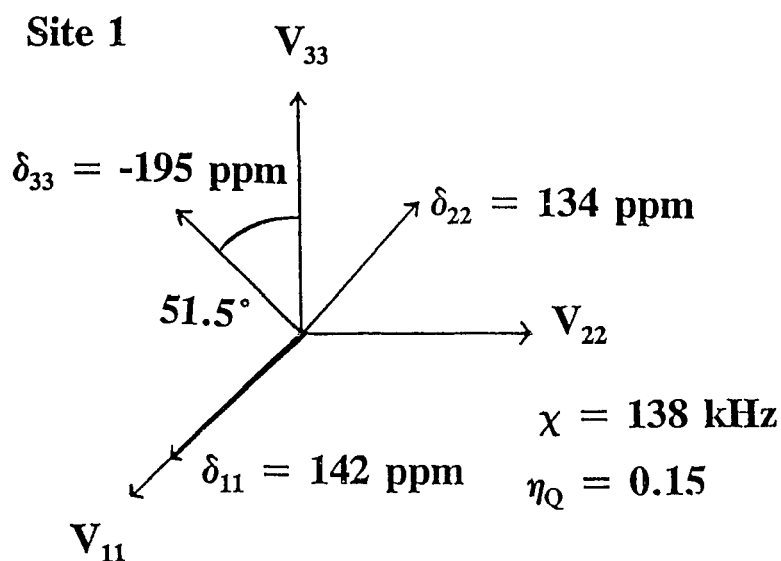
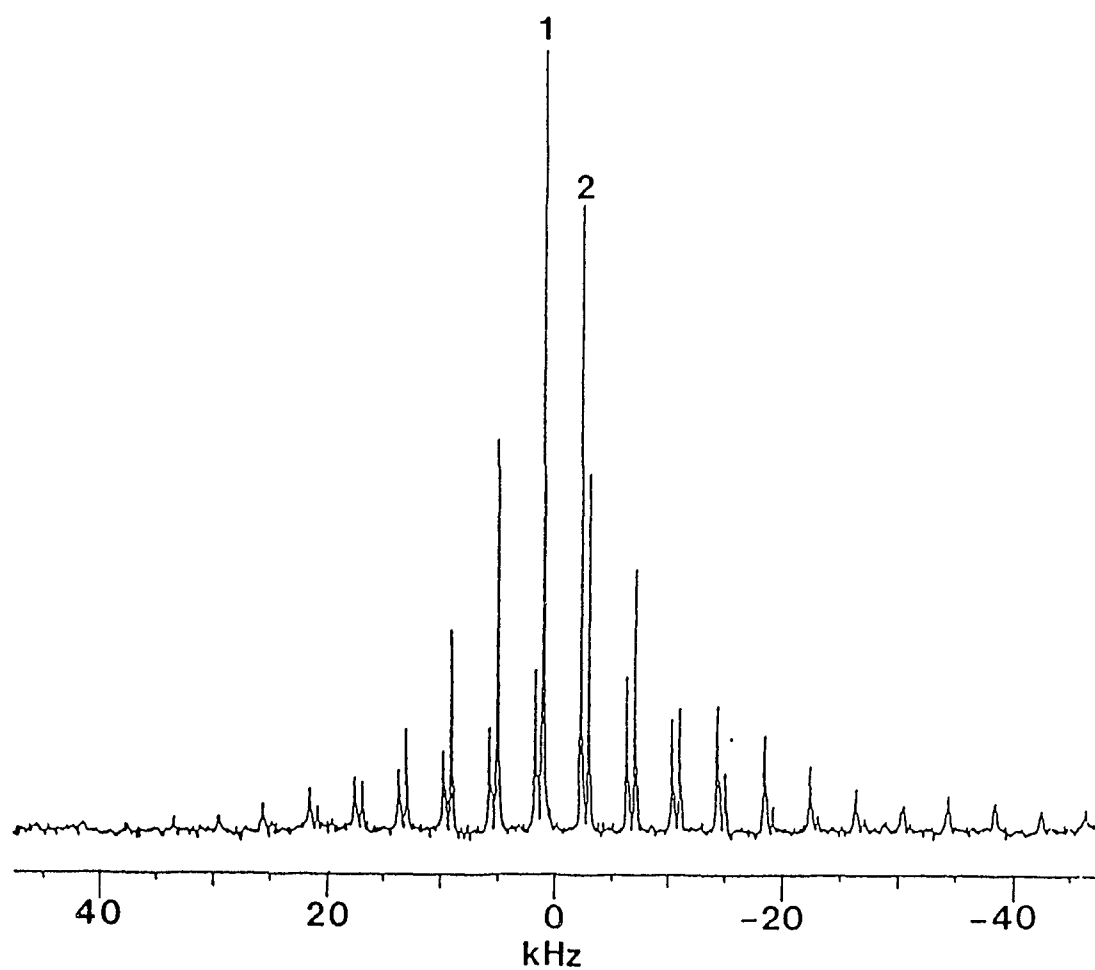


Figure 25.  $^{133}\text{Cs}$  nmr powder spectrum obtained with magic-angle spinning at 4 kHz. The isotropic shifts for nuclei at the two crystallographic sites are the two most intense peaks at the centre of the spectrum, with  $\delta_{\text{iso}}(1) = 27$  ppm and  $\delta_{\text{iso}}(2) = -100$  ppm with respect to a 0.5 molal CsCl solution.



Attempts to simulate this spectrum using a routine that assumes coincidence of the principal components of the **Q** and **CS** tensors<sup>134</sup> proved unsuccessful. Applying the approach introduced in the theory section and further discussed in §6.4.1, the single crystal results were used to simulate the powder spectrum. The presence of two nonequivalent nuclei requires that each site be simulated separately then summed before comparison with the experimental spectrum. This is illustrated in Figure 26, where the simulation for each site is given along with their sum and the observed line shape at 4.7 T. This allows particular features of the spectrum to be assigned to each site. The error estimates for the values given in Figure 24 are based on the sensitivity of the line shape to changes in those parameters; the single crystal results were found to provide the best fit to the experimental spectrum under these variations. Although there is considerable distortion in the experimental spectrum, particularly in the regions of the shoulders to either side of the central ( $1/2 \leftrightarrow -1/2$ ) transition, each feature matches that of the simulation, both in the frequency at which it occurs (see Table 7), and in its relative intensity. The outermost limits of the spectra for each site are related to  $\chi$ , the quadrupolar coupling constant. Values for  $\chi$  derived from the  $^{133}\text{Cs}$  nmr powder spectrum in Figure 26 are 371 and 145 kHz, within experimental error of 376 and 138 kHz from the single crystal data. The distorted spectrum arises from the non-uniform power of the excitation pulse across the total frequency bandwidth (approximately 160 kHz), and also from the loss of the first few points of the free induction decay due to the finite deadtime between the end of the excitation pulse and the beginning of acquisition. Attempts to circumvent this difficulty using an echo sequence were unsuccessful.

Figure 26. Calculated  $^{133}\text{Cs}$  nmr of each site, their sum, and the experimental  $^{133}\text{Cs}$  nmr spectrum of  $\text{Cs}_2\text{CrO}_4$  powder at 26.247 MHz ( $B_0 = 4.7$  T).

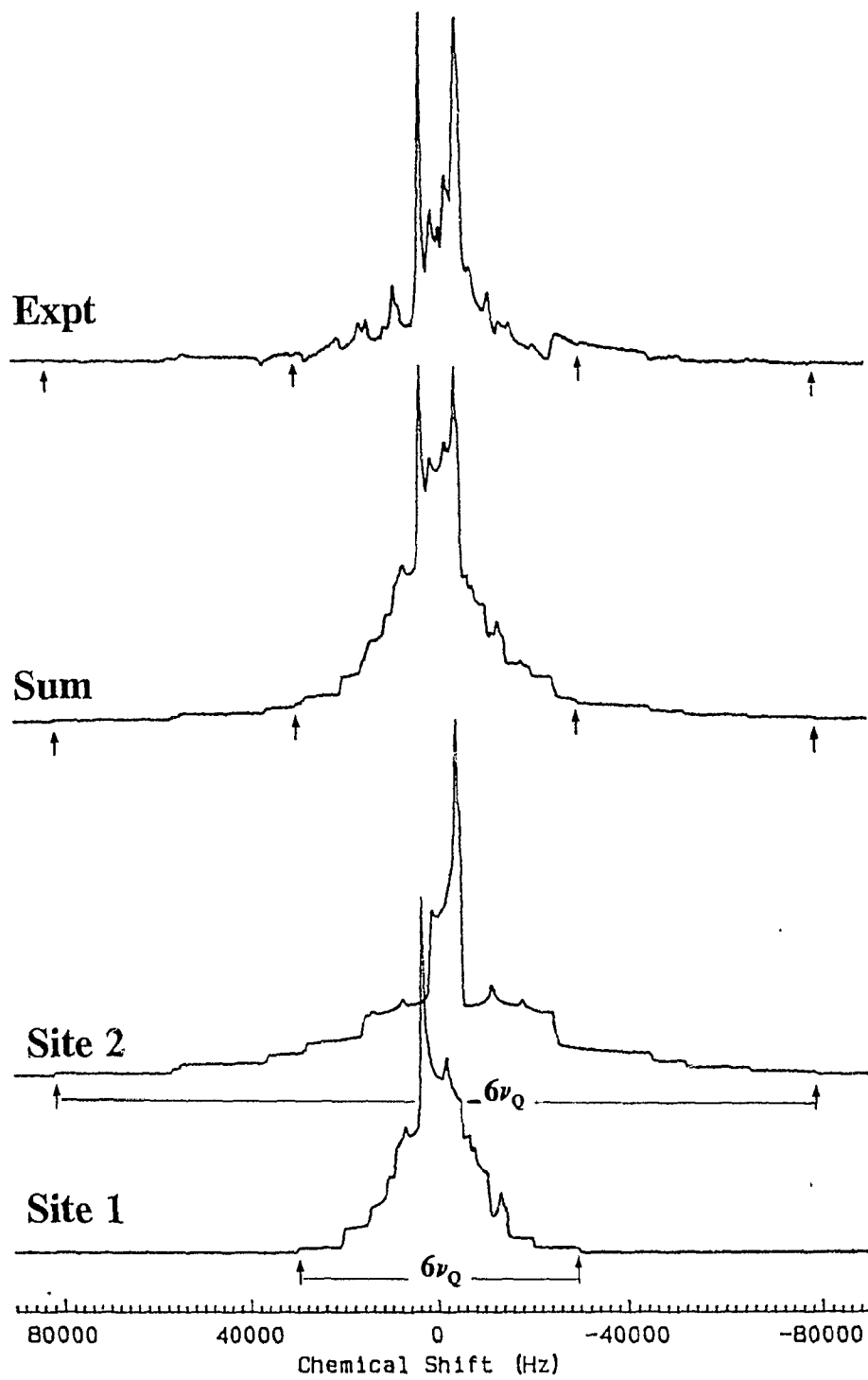
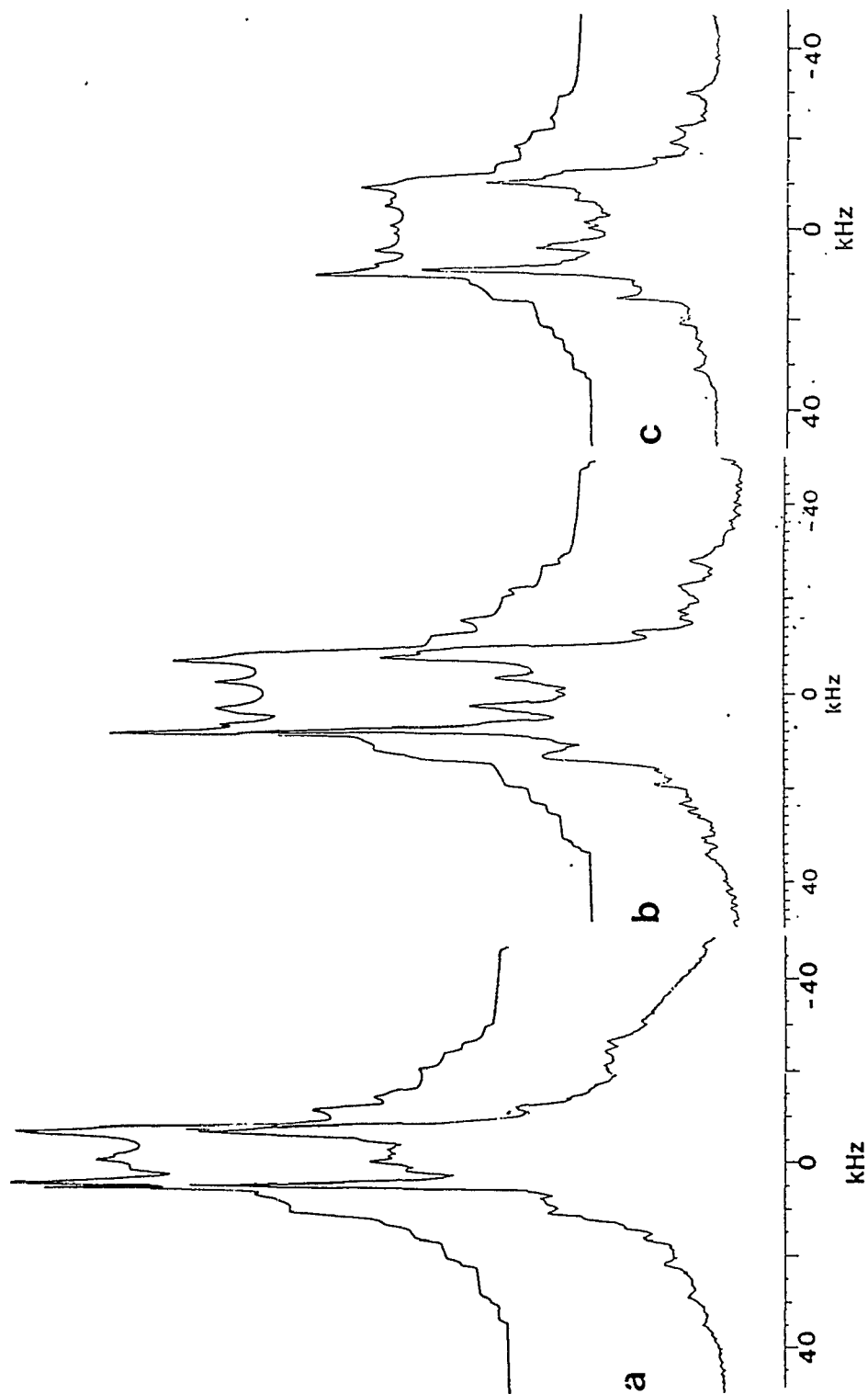




Figure 27. Calculated and experimental  $^{133}\text{Cs}$  nmr spectra of  $\text{Cs}_2\text{CrO}_4$  powder at (a) 39.366 MHz (7.0 T), (b) 52.47 MHz (9.4 T) and (c) 65.613 MHz (11.75 T).



In order to verify the 4.7 T simulation, spectra were also obtained at 7.0, 9.4 and 11.75 T and simulated using the same parameters. These are given in Figure 27, demonstrating that the accuracy of the simulation is satisfactory. Although variation in the parameters used was permitted to ensure the best fit to the experimental spectra, it was found again that the single crystal results provide the highest quality simulations. As the field strength is increased, the central feature increasingly dominates the spectrum, from the increased influence of the chemical shielding. In both of the 7.0 T and 11.75 T spectra, the maximum sweep width available on the spectrometers was 125 kHz, limiting observation to roughly  $\pm 50$  kHz to either side of the central region. However, the fit is of sufficient quality that any errors which result from not observing the full powder pattern should be negligible.

The relative magnitudes of the quadrupolar and chemical shielding interactions determine the sensitivity of the line shape to differences in their relative orientation. The line shape is most sensitive when the Q and CS interactions are of comparable magnitude. This situation can be controlled to some extent by choice of an appropriate field strength, as this determines the influence of the chemical shielding. The relevant ratio is that of the chemical shielding anisotropy,  $\Delta\sigma$ , expressed in Hz, to the magnitude of the quadrupolar interaction,  $\nu_Q$ . The maximum influence of the relative orientation of the two tensors should be observed when this ratio is close to unity. Similar results have been reported for dipolar - chemical shielding experiments.<sup>145</sup>

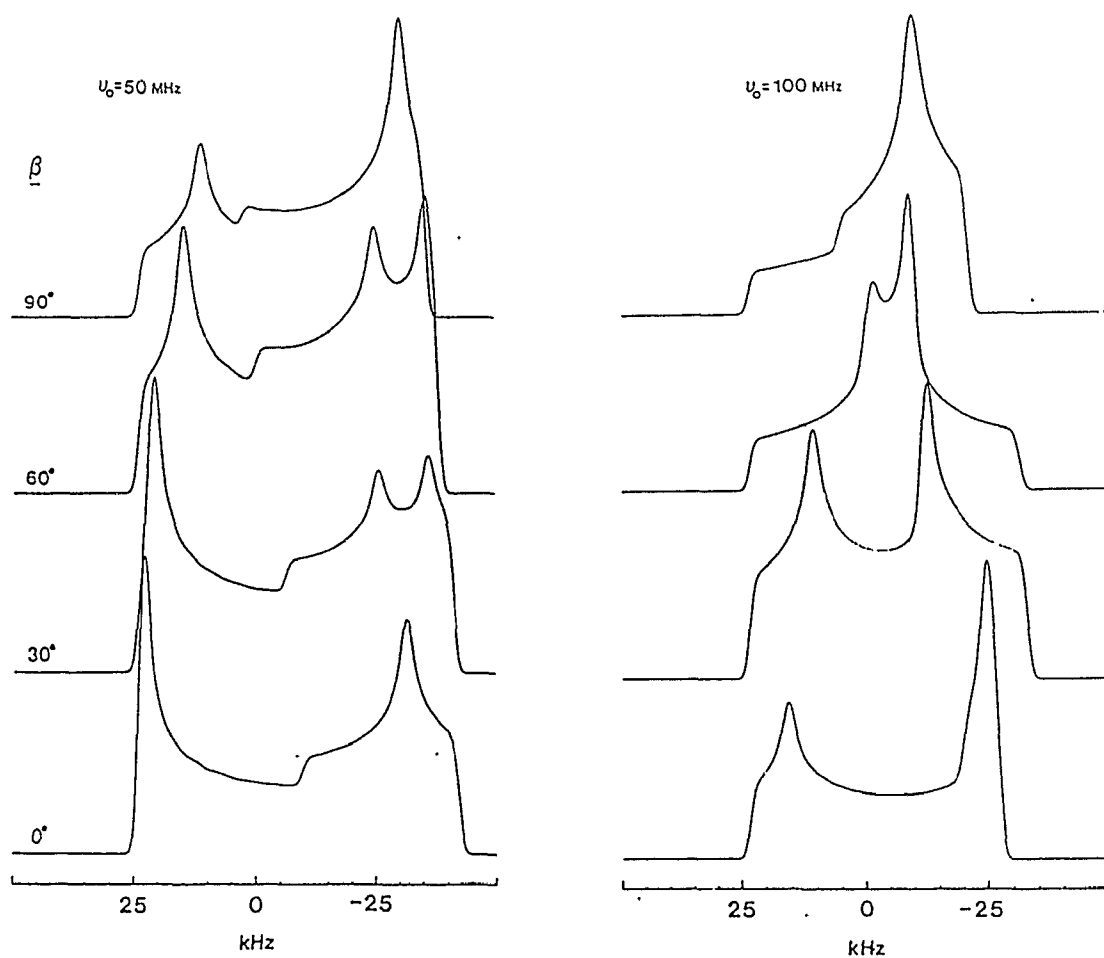
### 6.4.3 Second-Order Quadrupolar - Chemical Shielding Effects on the Central Transition

When the quadrupolar coupling constant of a particular half-integer spin nucleus is large enough, second-order quadrupolar effects must be considered. However, as only the central transition is usually observed for such nuclei, the satellites need not be considered, the large value of  $\nu_Q$  ensuring that they have a negligible influence on the observed powder pattern. In principle, they still are affected by the relative orientation of the two tensors, as in the case of first-order effects. The second-order spectrum that results, arising mainly from the central transition, is then a combination of the second-order quadrupolar and chemical shielding interactions only. The consequences of non-coincidence of these interactions on the central transition nmr line shape has recently been discussed by Cheng, Edwards and Ellis.<sup>31</sup>

The effects of varying the relative orientations of the two tensors about a single axis are illustrated in Figure 28, using the angle relations given in §6.4.1 as Equation 54. It should be noted that the parameters chosen are strictly for illustrative purposes, and do not necessarily conform to any experimental situation. The  $\beta = 0^\circ$  simulations were checked against an accepted routine<sup>134</sup> for their accuracy, which was found to be excellent. Simulations at two different field strengths are given to demonstrate the increasing influence of chemical shielding on the line shape.

The change in the central transition with the angle  $\beta$  between the two tensors is quite substantial, as was found for the satellites in §6.4.1. For the lower field simulations, new peaks appear and eventually merge, giving a  $\beta = 90^\circ$  spectrum that

Figure 28. Calculated nmr powder line shapes of the central transition as the angle  $\beta$  is increased from  $0^\circ$  to  $90^\circ$  for nuclei with Larmor frequencies of (a) 50 MHz and (b) 100 MHz. The parameters for simulation were:  $I = 7/2$ ,  $\delta_{11} = 150$  ppm,  $\delta_{22} = 50$  ppm,  $\delta_{33} = -200$  ppm,  $\chi = 14$  MHz and  $\eta_Q = 0.20$ .



resembles the mirror image of the  $\beta = 0^\circ$ , save for the position and unchanged orientation of the discontinuity in the centre of the pattern. This discontinuity appears to move evenly across the line shape as the angle  $\beta$  is increased. In the higher field simulations, where chemical shielding has a much greater influence on the line shape, the effects are different although just as pronounced. The peaks move across the line shape with increasing angle, eventually merging into a single peak at  $\beta = 90^\circ$ , with little similarity to the original spectrum. The one unchanging feature in both sets of simulations is the position of the high frequency limit of the line shape at approximately 25 kHz. This is a result of the rotation being along the coincident  $\delta_{11}$  and  $V_{11}$  axes, which should not change the contribution of these elements to the spectrum with any variation of the angle  $\beta$ .

In a recent  $^{59}\text{Co}$  nmr study of several octahedral cobalt complexes, it has been remarked that, with experiments being carried out at higher field strengths, some discrepancies between previously reported data and the high field spectra are becoming evident.<sup>120</sup> This has been attributed to various causes, including breakdown of the accepted theory of Baugher *et al.*<sup>110</sup> at high field<sup>120</sup> and inhomogeneous broadening.<sup>144</sup> The effects illustrated in this study provide another explanation. When the site symmetry of these nuclei that have been studied is low, the effect of any difference in the relative orientation of the chemical shielding and efg tensors should become magnified as these two interactions become comparable in magnitude, which in most cases will be at the higher field strengths now available. In this case, the relevant ratio is that of the chemical shielding anisotropy,  $\Delta\sigma$ , to the second-order quadrupolar factor,  $(Q_2/6\nu_0)$ ,

where  $Q_2 = \nu_Q^2 [I(I+1)]^{-3/4}$ . As for first-order quadrupolar - chemical shielding effects, the line shape will be most sensitive when this ratio is on the order of unity.

## 6.5 Conclusion

It has been found that changes in the relative orientation of the quadrupolar and chemical shielding tensors have considerable influence on the nmr powder line shapes of half-integer spin quadrupolar nuclei. Changes of only a few degrees between the principal components of the two tensors lead to movement of the spectral features across the powder pattern. This is found to be of importance in the analysis of powder spectra from nuclei at lattice sites where symmetry does not require the two tensors to be aligned, *i.e.*, at monoclinic and triclinic sites, especially when the two interactions are comparable in magnitude. The  $^{133}\text{Cs}$  nmr spectra of polycrystalline  $\text{Cs}_2\text{CrO}_4$  illustrate this effect, as they cannot be simulated without accounting for the non-coincidence of the two interactions. When second-order quadrupolar effects are present, the central transition shows a pronounced dependence on the relative orientation of the two tensors. This may be an important consideration in the analysis of some commonly studied quadrupolar nuclei, such as  $^{17}\text{O}$ ,  $^{51}\text{V}$ ,  $^{59}\text{Co}$  and  $^{63}\text{Cu}$ .

## Chapter 7

### Concluding Remarks

This thesis has attempted to establish two features involving multiple-interaction nmr line shapes; that non-contact contributions to the indirect spin-spin coupling are present and significant; and that the nmr powder line shapes of quadrupolar nuclei are sensitive to the relative orientations, as well as magnitudes, of the quadrupolar and chemical shielding interactions. In general, these attempts have been successful. The implications of these results are clear. The observation of  $\Delta J$  for couplings involving  $^{31}\text{P}$  and metal nuclei calls into question the *s*-character arguments previously proposed to explain various trends, as such interpretations appear to be too simplistic. The possibility of simulating nmr line shapes for quadrupolar nuclei with non-coincident interactions should increase the applicability of solid-state nmr studies to a wider range of chemical systems, or resolve discrepancies evident at higher magnetic fields using the older theory.

Possible extensions of this work can also be recognized. Single crystal  $^{31}\text{P}$  nmr studies of the metal phosphine systems would be of interest for several reasons. This would allow unambiguous assignment of the orientation of the  $^{31}\text{P}$  chemical shift tensor in the molecular frame. Such information would be of greatest interest in the platinum(II) phosphines, as it would indicate the orientation of the principal component responsible for the bulk of the coordination shift. Single crystal measurements would also not require the assumption that  $\mathbf{J}$ , the indirect spin-spin coupling tensor, was axially symmetric. Only two types of metal coordination have been examined in this thesis,

linear Hg(II) and square-planar Pt(II). Investigations to find  $\Delta J$  using other metal centres with different coordination numbers may prove useful in understanding the factors that influence the indirect spin-spin coupling. Ligands other than phosphorus-containing ones should also be examined, and, of these, carbon monoxide- $^{13}\text{C}$  may be the most convenient. It would be interesting to examine the metal- $^{13}\text{C}$  couplings in these systems, as multiple bonding should increase the participation of the anisotropic paramagnetic orbital and spin-dipolar mechanisms in the observed indirect coupling.

The influence of non-coincident interactions on the nmr powder line shape clearly has been established. The challenge remains to make the identification of such influences more readily apparent. This may be possible using MAS, echo or two-dimensional techniques to separate the interactions, yet maintain their correlations such that their relative orientations can be discerned. This has been accomplished for experiments involving dipolar and chemical shift correlations; its extension to the quadrupolar systems, though not straightforward, would be of great utility.

More exciting potential exists for this area in its application to systems of general interest, such as semi-conducting thin films, zeolites and catalytic surfaces. As the majority of nuclei possessing spin are quadrupolar, it is hoped that the basic line shape theory presented here assists in making systems involving quadrupolar nuclei more amenable to characterization by nmr. Of particular interest is the ability of such nmr investigations to identify sites of different site symmetries while also characterizing the local electronic environment. These factors may be important for the study of materials which undergo phase transitions, *e.g.*, to a superconducting phase.

## Appendix 1

### $^{133}\text{Cs}$ Single Crystal NMR Results for $\text{Cs}_2\text{CrO}_4$

#### A.1.1 Introduction

The most precise way to obtain information on both the magnitudes and orientations of the various nmr interactions is to perform a single crystal nmr experiment. The frequency of the nmr signal is tracked as a function of the orientation of the crystal in the magnetic field, then the orientation dependence of the signal is matched to the crystallographic features of the crystal. However, these experiments are extremely time-consuming, in both the data collection and data analysis parts of the overall experiment. Much of the work described in the body of the thesis, deriving magnitude and orientation information from a single powder spectrum, has been designed to provide an alternative to this demanding technique.

A practical guide to preparing and performing a single crystal nmr experiment will be outlined in this first part of this appendix. The system studied was the  $^{133}\text{Cs}$  nmr of  $\text{Cs}_2\text{CrO}_4$ , previously discussed in Chapter 6. Although this system has been characterized before,<sup>145</sup> the acquisition of an automatic single crystal rotation probe from Doty Scientific and the importance of the single crystal nmr data to the powder nmr studies described in Chapter 6 made it desirable to repeat the  $^{133}\text{Cs}$  single crystal nmr measurements. The  $^{133}\text{Cs}$  nmr spectrum is dominated by chemical shielding and first-order quadrupolar coupling. Cesium chromate provides an example of the analysis of chemical shielding and quadrupolar coupling interactions that are not aligned, where each

can be characterized separately. Similar operations to those performed here would be used for the single crystal analysis of dipolar-coupled spin- $\frac{1}{2}$  nuclei. Much of the work described in this section has been more rigorously described by Kennedy and Ellis<sup>146</sup> for chemical shielding influences, and by Volkoff, Petch and Smellie<sup>147</sup> for first-order quadrupolar effects. Volkoff<sup>148</sup> and Liechti and co-workers<sup>149</sup> have also presented the analysis needed for crystals exhibiting second-order quadrupolar effects, which will not be dealt with here.

#### A.1.2 Experimental Preparation and Operation

The first and primary requirement of a single crystal nmr experiment is a crystal of suitable size and quality. The size requirements of the apparatus used in this study is a cube approximately 4 mm on each edge. The crystal of  $\text{Cs}_2\text{CrO}_4$  used in this study was grown from aqueous solution, and cut to a 4 mm cube. It may be possible to use crystals smaller than this when studying the more sensitive or more abundant nuclei, such as  $^{31}\text{P}$ . The quality requirements of the crystal are primarily concerned with the absence of twinning in the crystal and the ability to limit any degradation of the crystal during the experiment. This may present insurmountable difficulties for air-sensitive compounds, unless they can be protected from the environment in some fashion.

Once a suitable crystal is obtained, it is mounted for the nmr experiment and its crystallographic features are defined with respect to this mounting. These two steps may be performed in either order. Where crystallographic data already exists for the compound in question, it may be easier to mount the crystal first, then identify its crystal

axes with respect to the axis system of the mount or goniometer. For the apparatus used in this study, the mount consists of a three-sided hollow alumina cube to which the crystal is fixed with glue. The directions perpendicular to the three sides of the cube represents the cube axes, labelled X, Y and Z. These three directions are defined in a right-handed fashion. The crystal in its mount is then placed on a diffractometer, and its crystal axes,  $a$ ,  $b$  and  $c$ , are identified and related to the cube axes. Where the crystal has not been characterized previously by X-ray diffraction, or where the crystal is known to contain rather high symmetry, it may be desirable to define the crystal axes before mounting the crystal, so that any symmetry elements may be placed along one of the cube axes. Symmetry in the single crystal nmr experiment often provides simplified analysis.

The crystal structure of  $\text{Cs}_2\text{CrO}_4$  was first solved by X-ray diffraction in 1938<sup>132</sup> and the space group was reported in non-standard orthorhombic form,  $\text{Pm}cn$ , with four molecules in the unit cell ( $Z = 4$ ). A more recent crystal determination using neutron diffraction<sup>133</sup> used the standard form,  $\text{Pnma}$ . The dimensions of the unit cell from the neutron diffraction study are:  $a = 8.427(4) \text{ \AA}$ ,  $b = 6.300(2) \text{ \AA}$ ,  $c = 11.200(6) \text{ \AA}$ . The plane perpendicular to  $b$  is a mirror plane. For the  $^{133}\text{Cs}$  single crystal nmr study of  $\text{Cs}_2\text{CrO}_4$ , the crystal was aligned such that the crystal  $b$  axis and the cube Y axis were almost collinear, to take advantage of the crystal symmetry.

The acquisition of the nmr data is then begun. This is performed most commonly by collecting spectra at equal intervals in  $180^\circ$  rotations about the three orthogonal axes of the cube, as the interactions have  $\pi$ -periodicity in the single crystal nmr experiment.

The rotations occur about an axis perpendicular to the applied field. In the apparatus used for  $\text{Cs}_2\text{CrO}_4$ , the interval was set most conveniently to  $9^\circ$ . Twenty-one spectra over  $180^\circ$  degrees of rotation were collected. It is important to begin and end the rotations with one cube axis along the magnetic field direction. The rotations should occur in a right-handed fashion, *e.g.*, for the X rotation, the experiment should begin with the Y axis along the field, rotating through Z along the field, until Y is once again along the field, although antiparallel to the field. (It should be noted that the "normal" direction for automatic operation in the Doty Scientific apparatus gives a left-handed rotation; the automation should be set for "reverse" rotation.) For Y rotations, the progression should be from Z to X to Z, and for Z rotations, this should be X to Y to X. It is important to have this continuity in the rotations to ensure that the data blend easily from one rotation into the next. This correspondence may be checked, as the  $90^\circ$  spectrum in the X rotation should correspond to the  $0^\circ$  spectrum in the Y rotation, and equivalently for the other end-points. As a check, it is also useful to collect independent spectra with the field aligned along each of the cube axes.

### A.1.3 Idiosyncrasies of the Bruker MSL-200 at Dalhousie

Most of the spectra presented in this thesis were obtained on the Bruker MSL-200 nmr spectrometer, which is part of the Atlantic Region Magnetic Resonance Centre. It was one of the first of these instruments supplied to Canada, and because it was an early edition, it possesses several strange characteristics that present difficulties and frustration in some operations, if they are not understood. Difficulties encountered in the course

of this research will be presented here for the sake of those left behind in the lab.

Most of the problems are associated with the high-speed digitizer in the Aspect 3000 computer, which is needed for acquisition of spectra with sweep widths of over 125 kHz. Although the literature accompanying the MSL-200 specifies that the maximum number of time-domain (TD) points that can be used at these large sweep widths is 8192 (8 kB), in practice this maximum is only 4096 (4 kB), with zero-filling up to twice this size permitted. If attempts are made to acquire spectra with TD set to a value too large for the digitizer, two spectra will be acquired for every one counted internally by the computer.

Another problem involves the filter widths for sweep widths of greater than 125 kHz. The two filters, 500 kHz and 2 MHz, were connected backwards, so computer defaults to one of these values actually initiates the other. Whenever the sweep width is adjusted at values greater than 125 kHz, this should be checked. For sweep widths between 125 and 500 kHz, the filter width (FW) should be set to 2000000; for sweep widths of 500 kHz or larger, FW should be set to 500000.

A misconnection is also present on the input of the imaginary channels of the receiver to the fast digitizer. When using CYCLOPS, one normally will choose the quadrature phase cycling (QPN). This works well for sweep widths of 125 kHz or below. This does not work for larger sweep widths. A receiver phase cycling (RPN) with a receiver phase list (RLS) has been used to overcome this problem; however, this phase cycle reverses the spectrum, *i.e.*, high and low frequency regions with respect to the transmitter are interchanged about the transmitter frequency.

One final point concerns the "SWEEP OFF" button on the SCM panel adjacent to the keyboard on the MSL console. This button on the top row should always have its light on, to ensure the field is not sweeping. This is a feature used for the  $^2\text{H}$  lock in solution nmr, which is not present in the Dalhousie MSL-200. However, if this light is not illuminated, cross-polarization will be impossible to achieve, and most spectra will appear distorted or have multiple signals, due to the fluctuations in the applied magnetic field strength.

#### A.1.4 Data Analysis

Once the data are acquired, the signals pertaining to the relevant interactions are identified and any necessary manipulation of the frequencies are performed. For chemical shielding information, no manipulation is required, as it alone determines the absolute frequency of the central transition of  $^{133}\text{Cs}$ . To obtain information on the quadrupolar interaction, the variation in the splitting of the satellite signals are needed. Although the absolute frequency of a satellite line depends on both chemical shielding and quadrupolar coupling, the splitting between any two corresponding satellite lines, *e.g.*,  $\nu(7/2 \leftrightarrow 5/2)$  and  $\nu(-5/2 \leftrightarrow -7/2)$ , depends on the quadrupolar interaction alone, as described in Chapter 6. For the  $^{133}\text{Cs}$  nmr data of  $\text{Cs}_2\text{CrO}_4$ , the "average" outer quadrupolar splitting  $\Delta\nu(7/2)$  was used, where

$$\overline{\Delta\nu\left(\frac{7}{2}\right)} = \frac{1}{6} \left[ 6 \Delta\nu\left(\frac{3}{2}\right) + 3 \Delta\nu\left(\frac{5}{2}\right) + 2 \Delta\nu\left(\frac{7}{2}\right) \right]. \quad (55)$$

When there is more than one distinct nucleus in the unit cell, it is essential that

the signals for each site be distinguished in the rotation patterns. This is performed readily if the entire data set is first plotted in a frequency vs. rotation angle plot. As the interactions have  $\pi$ -periodicity, it is possible to distinguish the sinusoidal pattern made by each site in these plots. At this point it is also useful to check the matching of the  $0^\circ$  and  $90^\circ$  values of the frequencies for the three sets of data. As remarked before, the rotation about X by  $90^\circ$  should result in the  $0^\circ$  values for the Y rotation, and likewise for the  $Y \rightarrow Z$  and  $Z \rightarrow X$  limits. Where there may be slight differences in the frequencies at these points, small phase angles (commonly labelled  $\delta$ ) are added to improve the match. These angles indicate the error in attempting to align one axis along the magnetic field direction at the beginning of each rotation. Examples of the plots for  $^{133}\text{Cs}$  in  $\text{Cs}_2\text{CrO}_4$  are given in Figures 29 to 34. The phase angles for these plots were:  $\delta_x = 1^\circ$ ,  $\delta_y = 2.5^\circ$ ,  $\delta_z = 5^\circ$ .

Once the rotation plots are prepared and the sites are assigned, the actual analysis may begin. This is performed by a least-squares fitting of the rotation data to the equation,

$$\nu_i \text{ (or } \Delta \nu_i) = A_i + B_i \cos 2\psi + C_i \sin 2\psi, \quad (56)$$

where  $\psi$  is the rotation angle,  $i$  is the axis about which the rotation occurs, and A, B and C are the parameters from the least-squares fit of the data. This equation is used for both the chemical shielding (central transition) analysis and the quadrupolar coupling (satellite splitting) analysis, hence the option of  $\nu$  (absolute frequency) or  $\Delta\nu$  (frequency difference).

The parameters A, B and C are then used to construct the interaction tensors in

the cube axis system. For the central transition, one may use the expressions of Kennedy and Ellis<sup>146</sup> with one small correction, as a negative sign was omitted in their equations. The correct expressions for the chemical shielding tensor in the cube frame are given here,

$$\begin{aligned}
 \sigma_{XX} &= \frac{1}{2}(A_Y - B_Y + A_Z + B_Z), \\
 \sigma_{YY} &= \frac{1}{2}(A_Z - B_Z + A_X + B_X), \\
 \sigma_{ZZ} &= \frac{1}{2}(A_X - B_X + A_Y + B_Y), \\
 \sigma_{XY} &= \sigma_{YX} = -C_Z, \\
 \sigma_{XZ} &= \sigma_{ZX} = -C_Y, \\
 \sigma_{YZ} &= \sigma_{ZY} = -C_X.
 \end{aligned} \tag{57}$$

The quadrupolar tensor in the cube frame derived from the quadrupolar splittings is constructed similarly, using from Volkoff *et al.*,<sup>147</sup>

$$\begin{aligned}
 V_{XX} &= \frac{1}{3}(-2A_X + A_Y - B_Y + A_Z + B_Z), \\
 V_{YY} &= \frac{1}{3}(-2A_Y + A_Z - B_Z + A_X + B_X), \\
 V_{ZZ} &= \frac{1}{3}(-2A_Z + A_X - B_X + A_Y + B_Y), \\
 V_{XY} &= V_{YX} = -C_Z, \\
 V_{XZ} &= V_{ZX} = -C_Y, \\
 V_{YZ} &= V_{ZY} = -C_X.
 \end{aligned} \tag{58}$$

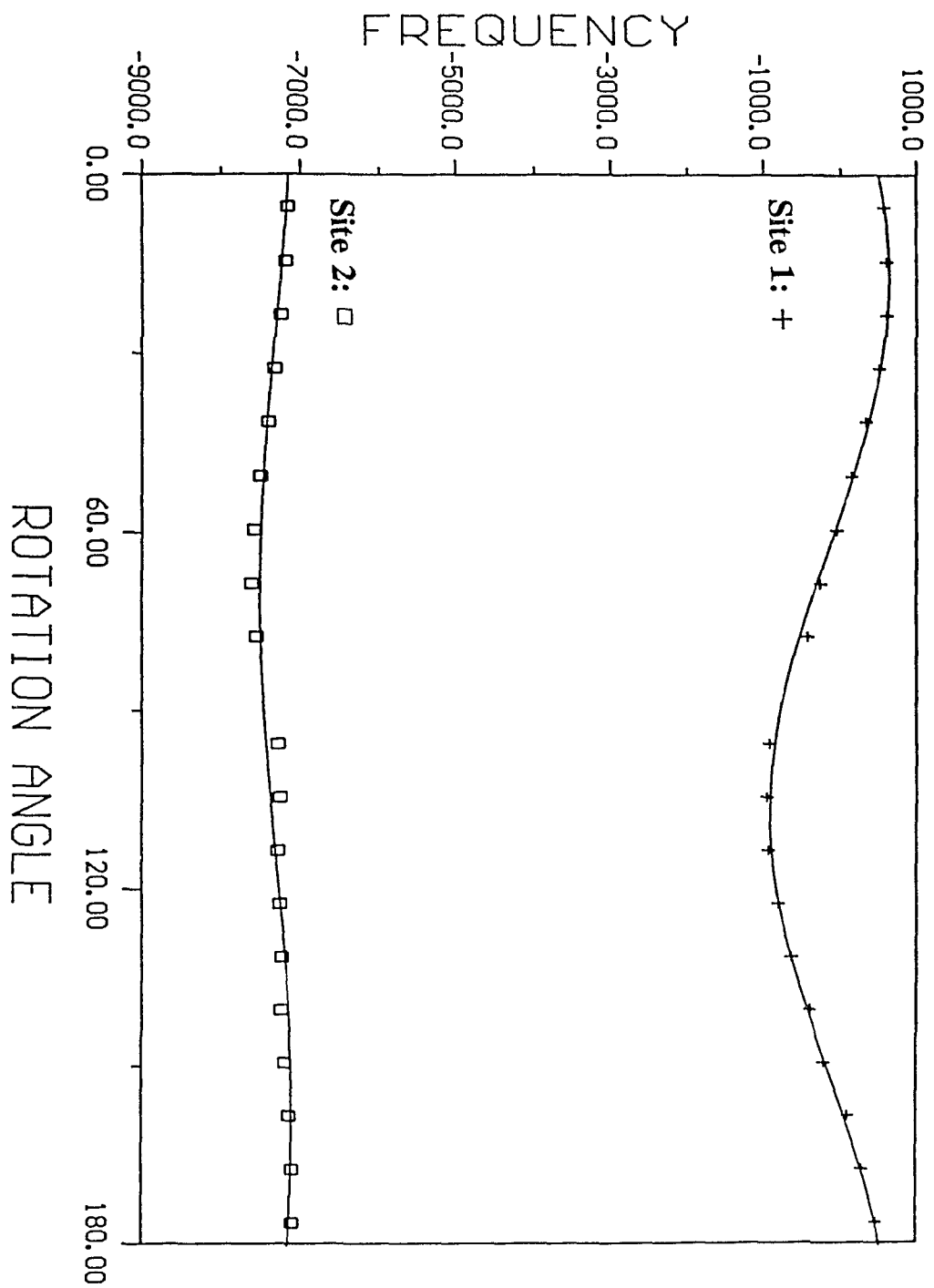
The tensor  $\mathbf{V}$  does not correspond exactly to the electric field gradient tensor, as it is constructed on the basis of the  $(7/2 \leftrightarrow -7/2)$  splitting. It is, in fact,  $3/7$  of the quadrupolar coupling tensor, but will be called  $\mathbf{V}$  for convenience. The fraction  $3/7$  is related to the outermost splitting of a spin- $7/2$  nucleus being  $6\nu_Q$ , as discussed in Chapter 6. For  $I = 7/2$ ,  $\nu_Q = \chi/14$ , thus  $\Delta\nu(7/2) = 3\chi/7$ .

The tensors that are constructed in the cube frame are diagonalized to obtain the

principal components and the direction cosines. It is the direction cosines that provide the most precious information from a single crystal experiment. While the magnitudes of the principal components may be determined with ease from nmr powder line shapes, the orientation of these components with respect to the molecule or crystal lattice cannot be determined. The direction cosines relate the orientation of the principal components to the cube axis system, from which it is possible to assign their orientation in the crystallographic axis system.

#### A.1.5 Chemical Shielding Parameters

The variation of the  $^{133}\text{Cs}$  nmr frequency of the central transition as a function of the orientation of the  $\text{Cs}_2\text{CrO}_4$  crystal in the magnetic field provides the information that is necessary to characterize the  $^{133}\text{Cs}$  chemical shielding tensor. This was performed, and the rotation plots of the data are given in Figures 29, 30 and 31. Least-squares fitting of the data yields the parameters given in Table 8. From these parameters, it is possible to construct the  $^{133}\text{Cs}$  chemical shielding tensors in the cube frame for each crystallographic-distinct site. The assignment of Site 1 and 2 is arbitrary and not an assignment of a particular crystallographic designation to either nucleus characterized in the nmr experiment.



$(\frac{1}{2} \leftrightarrow -\frac{1}{2})$  transition of  $\text{Cs}_2\text{CrO}_4$  for rotations about the X cube axis.

Figure 29. Cesium-133 single crystal nmr data and least-squares curves for the central

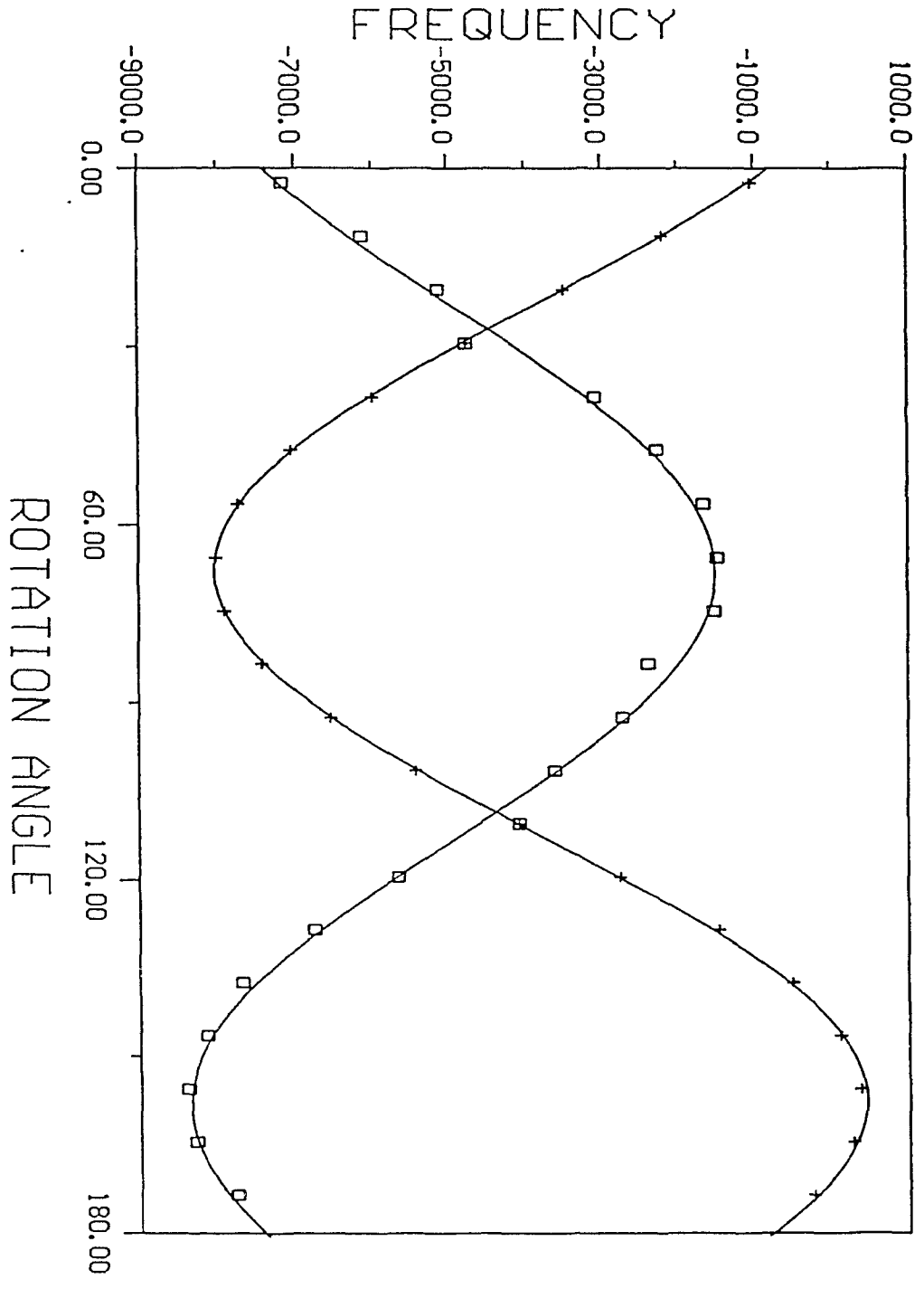
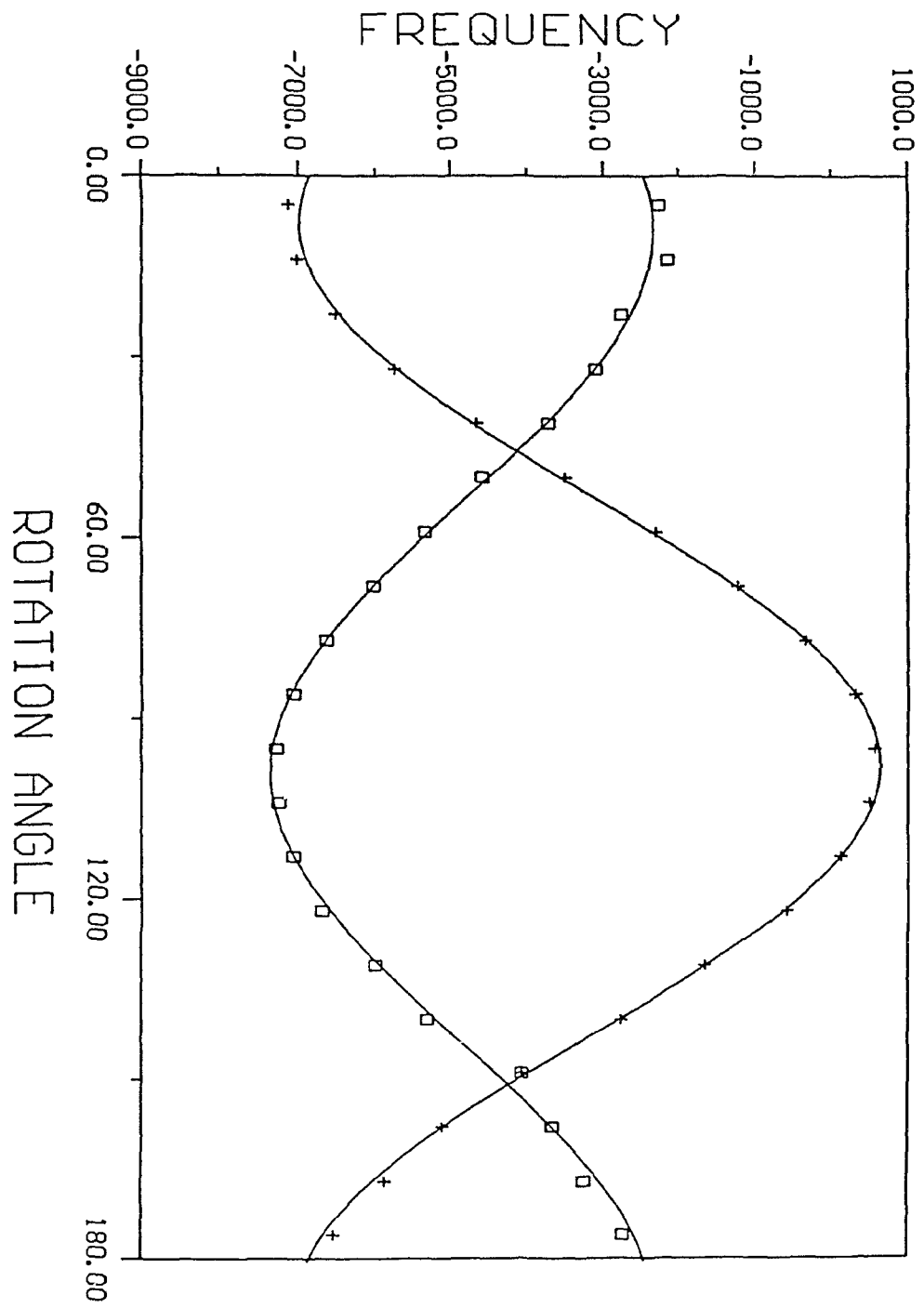


Figure 30. Cesium-133 single crystal nmr data and least-squares curves for the central  $1/2 \leftrightarrow -1/2$  transition of  $\text{Cs}_2\text{CrO}_4$  for rotations about the Y cube axis.



( $\frac{1}{2} \leftrightarrow -\frac{1}{2}$ ) transition of  $\text{Cs}_2\text{CrO}_4$  for rotations about the Z cube axis.

Figure 31. Cesium-133 single crystal nmr data and least-squares curves for the central

Table 8. Cesium-133 chemical shielding (central transition) parameters from the least-squares fits of the rotation plots for the two sites in  $\text{Cs}_2\text{CrO}_4$ . The parameters are in Hz from the spectrometer frequency of 26.244097 MHz. The numbers in parentheses are the standard deviations of the corresponding parameters.

	Site 1	Site 2
$A_x$	-132 (10)	-7301 (17)
$B_x$	648 (14)	153 (25)
$C_x$	435 (13)	-132 (23)
$A_y$	-3791 (9)	-4933 (52)
$B_y$	3003 (13)	-2478 (74)
$C_y$	-2984 (13)	2362 (74)
$A_z$	-3176 (18)	-4848 (30)
$B_z$	-3677 (26)	2379 (42)
$C_z$	-1036 (26)	768 (42)

<sup>133</sup>Cs Chemical Shielding Tensors in the Cube Frame.

Site 1	Site 2
$\begin{pmatrix} -6824 & 1036 & 2984 \\ 1036 & 509 & -435 \\ 2984 & -435 & -784 \end{pmatrix}$	$\begin{pmatrix} -2464 & -768 & -2362 \\ -768 & -7188 & 132 \\ -2364 & 132 & -7433 \end{pmatrix}$

Diagonalization of these tensors provides the principal components of the <sup>133</sup>Cs chemical shift tensor in its principal axis system; the accompanying direction cosines relate the orientation of the chemical shift tensor principal axis system to the cube axis system.

Site 1			Site 2		
654	441	-8195	-1420	-7265	-8400
0.10277	0.38456	0.91736	0.92176	0.06770	0.38181
0.99094	0.04059	-0.12803	-0.13107	0.98108	0.14249
-0.08648	0.92221	-0.37691	-0.36494	-0.18138	0.91319

These values are in Hz with respect to the spectrometer frequency of 26.244097 MHz. A convenient reference for solid-state <sup>133</sup>Cs nmr is the cubic salt CsCl, which has a shift of 223.2 ppm with respect to the standard reference, 0.5 m CsCl(aq). In the single-crystal experiment above, <sup>133</sup>CsCl produced a signal at 26.246878 MHz. This places the "0 Hz" point for the above shielding values at +3076 Hz with respect to 0.5 m CsCl(aq) (*i.e.*,  $\nu_0 = 26.241021$  MHz). The resulting corrected values for the <sup>133</sup>Cs chemical shielding tensors are,

Site 1:  $\delta_{11} = 142$  ppm (*b*),  $\delta_{22} = 134$  ppm (*c*),  $\delta_{33} = -195$  ppm (*a*),  $\delta_{\text{iso}} = 27$  ppm.

Site 2:  $\delta_{11} = 63$  ppm (*a*),  $\delta_{22} = -160$  ppm (*b*),  $\delta_{33} = -203$  ppm (*c*),  $\delta_{\text{iso}} = -100$  ppm.

As the orientation of the crystallographic axes with respect to the cube axes is determined prior to the single crystal nmr experiment, it is possible to orient the chemical shift tensor with respect to the  $a$ ,  $b$  and  $c$  axes. For both sites, the principal components of the chemical shift tensor were found to lie along the crystallographic axes. These orientations have been indicated in parentheses following each component.

#### A.1.6 Quadrupolar Parameters

The  $^{133}\text{Cs}$  quadrupolar splittings within the pair of satellites vary with the orientation of the  $\text{Cs}_2\text{CrO}_4$  crystal in the magnetic field, providing information on the magnitude and orientation of the quadrupolar interaction. The data has been presented in rotation plots in Figure 32, 33 and 34; the least-squares fitting of the data provides the parameters given in Table 9. The parameters are then used to construct a reduced quadrupolar coupling tensor, reduced due to the  $3/7$  factor discussed in §A.1.4. Because of the Cs atom site symmetry in the crystal of  $\text{Cs}_2\text{CrO}_4$ , two sets of quadrupolar splittings are observed, which are crystallographically equivalent yet magnetically distinct in the single crystal nmr experiment. The designation of Site 1 and Site 2 is consistent with that used for the chemical shielding parameters; however, this is not an assignment of one crystallographic site to the characteristics of either nuclear site in the nmr experiment.

Using the parameters in Table 9, it is possible to construct the quadrupolar splitting tensor in the cube frame for each of the two patterns for each site.

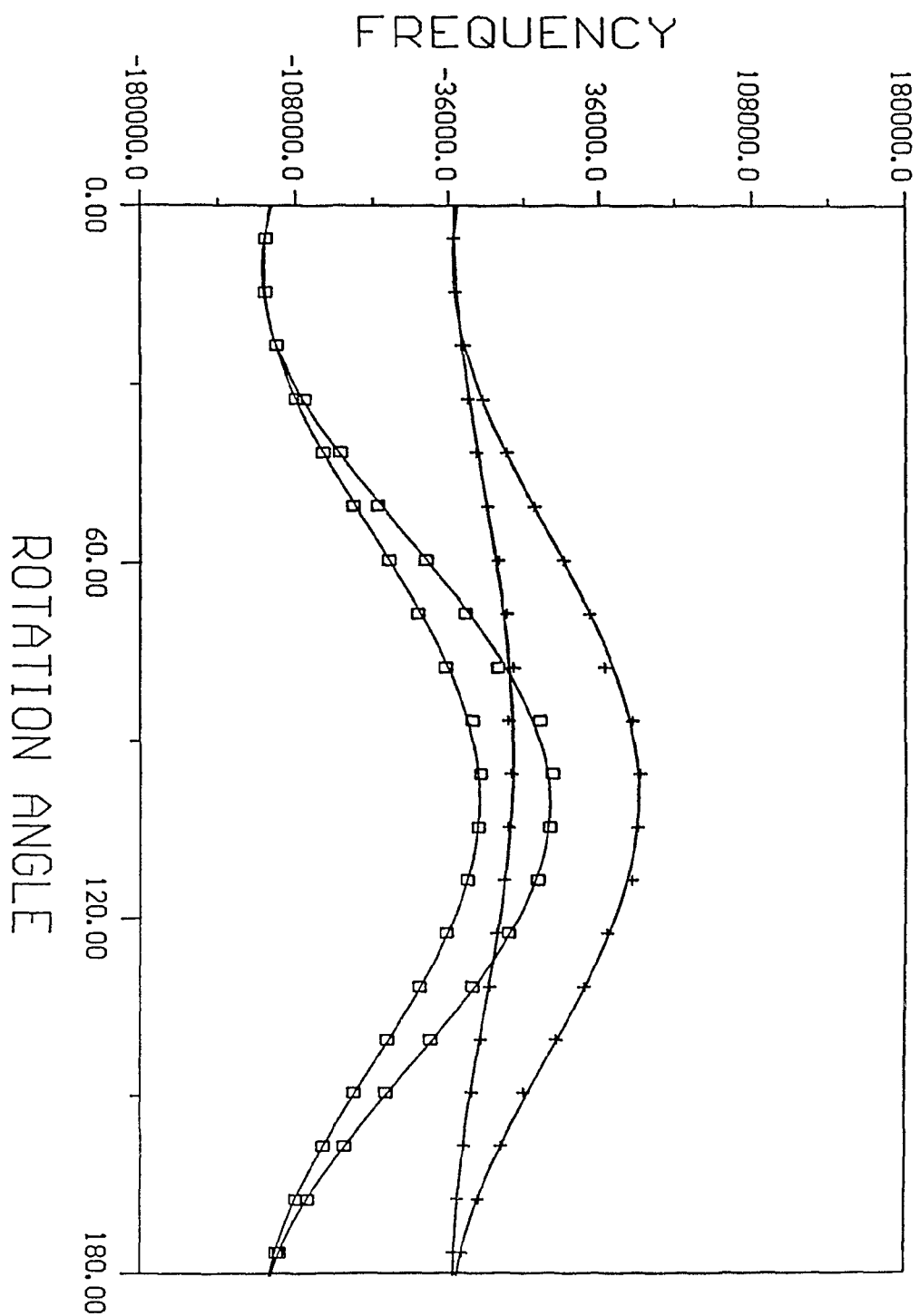


Figure 32. Cesium-133 single crystal nmr data and least-squares curves for the average  $(7/2 \leftrightarrow -7/2)$  quadrupolar splittings of  $\text{Cs}_2\text{CrO}_4$  for rotations about the X cube axis.

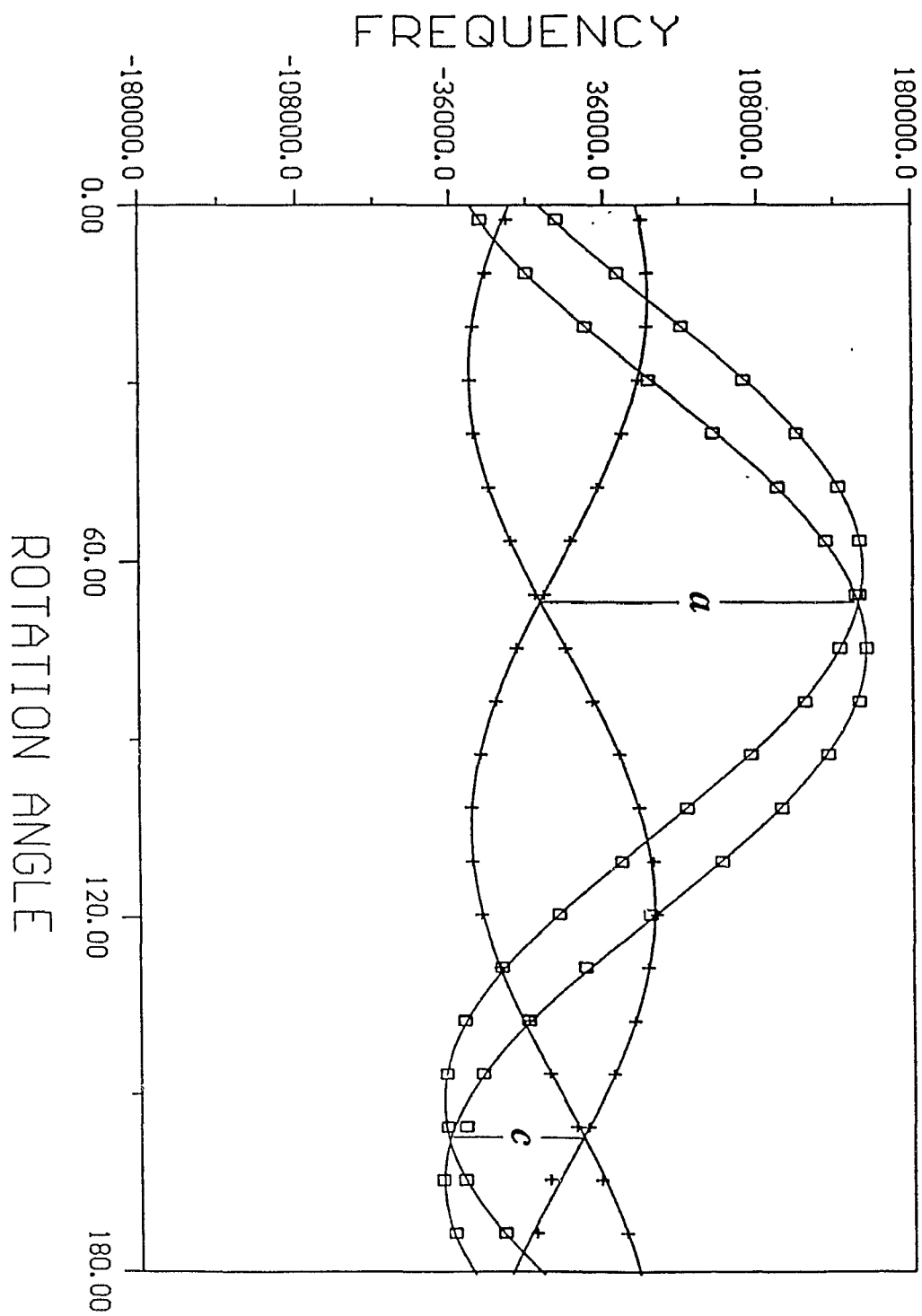


Figure 33. Cesium-133 single crystal nmr data and least-squares curves for the average (7/2  $\leftrightarrow$  -7/2) quadrupolar splittings of  $\text{Cs}_2\text{CrO}_4$  for rotations about the Y cube axis.

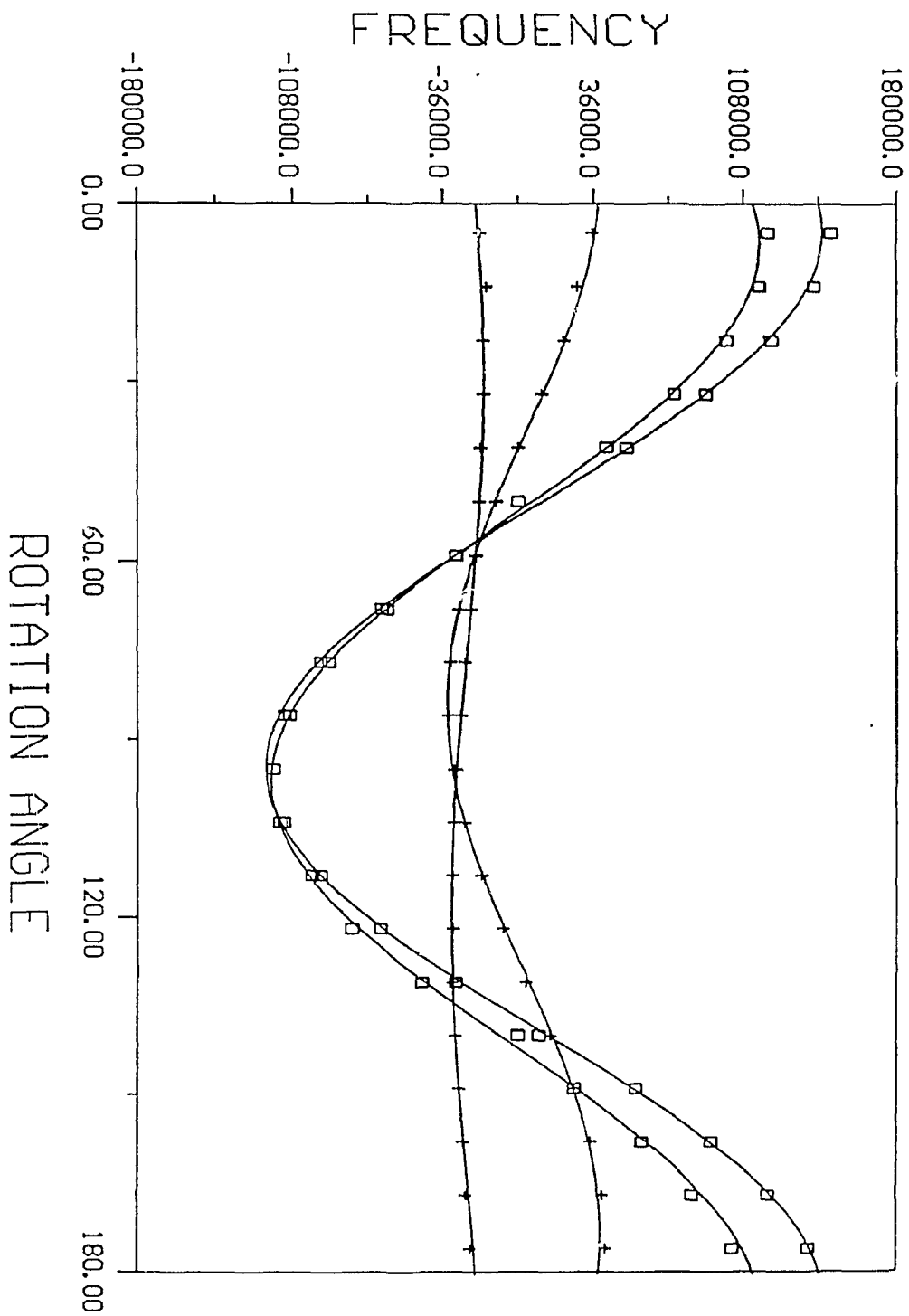


Figure 34. Cesium-133 single crystal nmr data and least-squares curves for the average  $(7/2 \leftrightarrow -7/2)$  quadrupolar splittings of  $\text{Cs}_2\text{CrO}_4$  for rotations about the Z cube axis.

Table 9. Cesium-133 quadrupolar ( $\Delta\nu(7/2)$  splitting) parameters (in Hz) from the least-squares fits of the rotation plots for the two sites (two for each site) in  $\text{Cs}_2\text{CrO}_4$ . The numbers in parentheses are the standard deviations of the corresponding parameters.

	Site 1		Site 2	
$A_x$	-19490 (205)	10230 (300)	-72318 (202)	-55779 (369)
$B_x$	-14136 (290)	-42123 (424)	-47609 (286)	-63315 (522)
$C_x$	-1046 (290)	-13954 (424)	-17426 (286)	-24840 (522)
$A_y$	16093 (306)	15362 (186)	59108 (393)	58301 (164)
$B_y$	-23668 (433)	36134 (264)	-85483 (555)	-52865 (232)
$C_y$	-36027 (433)	21145 (264)	50618 (555)	83125 (232)
$A_z$	2695 (279)	-24110 (185)	12644 (782)	-1117 (817)
$B_z$	35811 (394)	4017 (262)	131258 (1106)	113435 (1155)
$C_z$	-7546 (394)	6530 (262)	21652 (1106)	27671 (1155)

Reduced Quadrupolar Tensors in the Cube Frame.

$$\text{Site 1.} \quad \begin{pmatrix} 39082 & 7546 & 36027 \\ 7546 & -32976 & 1046 \\ 36027 & 1046 & -6106 \end{pmatrix} \quad \begin{pmatrix} -20442 & -6530 & -21145 \\ -6530 & -30248 & 13954 \\ -21145 & 13954 & 50690 \end{pmatrix}$$

$$\text{Site 2.} \quad \begin{pmatrix} 144376 & -21652 & -50618 \\ -21652 & -118919 & 17426 \\ -50618 & 17426 & -25457 \end{pmatrix} \quad \begin{pmatrix} 111681 & -27671 & -83125 \\ -27671 & -116750 & 24840 \\ -83125 & 24840 & 5069 \end{pmatrix}$$

Diagonalization of the tensors in the cube frame yields the principal components of the reduced quadrupolar tensors in their principal axis system and the direction cosines which orient the principal axis system with respect to cube axis system.

$$\begin{array}{l} \text{Site 1.} \\ 59560 \quad -25148 \quad -34412 \quad 59085 \quad -25275 \quad -33710 \\ \\ 0.87362 \quad -0.43743 \quad -0.21316 \quad -0.25616 \quad 0.89618 \quad 0.35500 \\ 0.07667 \quad -0.30884 \quad 0.94802 \quad 0.16773 \quad -0.31961 \quad 0.93259 \\ 0.48052 \quad 0.84456 \quad 0.23627 \quad 0.94922 \quad 0.30776 \quad -0.06525 \end{array}$$

$$\begin{array}{l} \text{Site 2.} \\ 160649 \quad -37950 \quad -122699 \quad 161832 \quad -39508 \quad -122324 \\ \\ 0.95875 \quad 0.27954 \quad 0.05160 \quad 0.86749 \quad 0.49346 \quad 0.06290 \\ -0.09104 \quad 0.12998 \quad 0.98733 \quad -0.12900 \quad 0.10104 \quad 0.98648 \\ -0.26929 \quad 0.95130 \quad -0.15007 \quad -0.48044 \quad 0.86388 \quad -0.15131 \end{array}$$

The quadrupolar splitting data provide no information on the sign of the quadrupolar coupling constant,  $\chi$ . The data has been presented such that this parameter possessed a

positive sign. Taking the average values for each site, and multiplying by 7/3, resulted in the nuclear quadrupolar coupling parameters for the  $^{133}\text{Cs}$  nuclei, as well as the orientation of the principal components given by the direction cosines.

Site 1:  $\chi = 138$  kHz,  $\eta_Q = 0.15$ .      Site 2:  $\chi = 376$  kHz,  $\eta_Q = 0.52$ .

The principal components of the electric field gradient tensors can be oriented with respect to the crystallographic axes. For both sites, it was found that  $V_{11}$  is perpendicular to the mirror plane, *i.e.*, along  $b$ . The other two components are in the mirror plane, but not along either of the two remaining crystallographic axes. For site 1,  $V_{33}$  is  $\pm 51.5^\circ$  from  $a$ , while for site 2,  $V_{33}$  is  $\pm 6.8^\circ$  from  $a$ . This offset from the crystal axes is best displayed in Figure 33 for the quadrupolar splittings as a function of rotation about the  $Y$  cube axis. The rotations were approximately along the crystallographic  $b$  axis, which was perpendicular to the mirror plane. The two patterns for each site cross at the crystallographic  $a$  and  $c$  axes, and these positions have been indicated in Figure 33.

## Appendix 2

### Complete FORTRAN-77 Listings of NMR Line Shape Simulation Programs

Included here are the complete listings of the simulation programs developed and used during the course of the research described in the thesis, all of which make use of the POWDER simulation routine of Alderman, Solum and Grant.<sup>29</sup> The first, called DIPCHEM, was used to simulate the nmr line shapes described in Chapters 3, 4 and 5. They can also be used to simulate the nmr powder line shapes resulting from any pair of spin- $\frac{1}{2}$  nuclei, homonuclear or heteronuclear (but not AB-type spectra), including the effects of anisotropic chemical shift, direct dipolar coupling and anisotropic J coupling. The only assumptions inherent in this program are that **J**, the indirect spin-spin coupling tensor, is axially symmetric and lies along the vector between the two coupled nuclei.

The next two programs simulate the powder line shapes of quadrupolar nuclei with anisotropic chemical shift and nuclear quadrupolar coupling. The first of these, QUADPOW, simulates line shapes where the quadrupolar coupling constant is not strong enough to introduce second-order quadrupolar effects to the observed line shape. This influence is incorporated into the second program, SECQUAD. In this latter program, one has the option to simulate the central transition alone or to also include the satellite transitions. Both these programs allow complete non-coincidence of the chemical shielding and electric field gradient tensors, and were used to generate all calculated spectra given in Chapter 6.

## PROGRAM DIPCHEM

```
C
C POWDER SIMULATION OF A SPIN-1/2 DIPOLAR COUPLED TO ANOTHER
C SPIN-1/2 NUCLEUS, INCORPORATING THE "POWDER" SIMULATION
C ROUTINE OF ALDERMAN, SOLUM AND GRANT. FOR FURTHER DETAILS,
C PLEASE REFER TO: D. W. ALDERMAN, M. S. SOLUM AND D. M. GRANT,
C           J. CHEM. PHYS. 84, 3717 (1986).
C
C PROGRAM WRITTEN BY BILL POWER (BITNET: BPOWER @ AC.DAL.CA)
C SOLID-STATE NMR LAB
C DEPT. OF CHEMISTRY
C DALHOUSIE UNIVERSITY
C HALIFAX, N.S. CANADA
C
C PLEASE ADDRESS ANY QUESTIONS OR COMMENTS TO:
C PROF. R.E. WASYLISHEN
C DEPT. OF CHEMISTRY
C DALHOUSIE UNIVERSITY
C HALIFAX, N.S. B3H 4J3 CANADA
C
C PROGRAM UPDATED 08/01/91
C
C   IMPLICIT REAL*4(A-H,O-Z)
C VARIABLES
C   REAL*4 SPEC(0:1023),FSTART,FWIDTH,MAXIMUM,SPIN,PROB
C   REAL*4 FEND,HW,PNA,PNAD2
C   INTEGER*4 NPOINTS,NP
C   CHARACTER*20 FILEN,FILEP
C   COMMON/TRIG/PI,COSB,SINB,COSA,SINA
C   COMMON/PARAM/S11,S22,S33,FNEW,D,BETA,ALFA,CJ,PF,DELJ
C   COMMON/FILES/FILEN,FILEP
C
C FIRST EXECUTABLE STATEMENT
C
C   PI=3.1415926
C   WRITE(6,*) ' OUTPUT FILENAMES?'
C   WRITE(6,*) ' DATAFILE = ?'
C   READ(*,3) FILEN
3  FORMAT(A20)
C   OPEN(UNIT=7,FILE=FILEN,STATUS='NEW')
C   WRITE(7,*)
C   WRITE(7,*) FILEN
C   WRITE(6,*) ' PLOTFILE = ?'
C   READ(*,3) FILEP
C   WRITE(6,*) ' NUMBER OF SITES?'
C   READ(*,*) NSITE
C   WRITE(7,*)
```

```

WRITE(7,*) ' NUMBER OF SITES = ',NSITE
NPOINTS=1024
WRITE(6,*) ' LARMOR FREQUENCY OF OBSERVED NUCLEUS (IN MHz)?'
READ(*,*) FNEW
WRITE(7,*)
WRITE(7,*) ' LARMOR FREQUENCY OF OBSERVED NUCLEUS = ',FNEW,'
+ MHz'
WRITE(6,*) ' UPPER AND LOWER FREQUENCY LIMITS OF SIMULATION',
+ ' (IN kHz)?'
READ(*,*) FEND,FSTART
WRITE(7,*)
WRITE(7,*) ' SPECTRAL WIDTH EXTENDS FROM ',FEND,' kHz TO
+ ',FSTART,' kHz'
FWIDTH=(FEND-FSTART)*1000.
FSTART=FSTART*1000.
WRITE(6,*) ' LINE BROADENING (IN Hz)?'
READ(*,*) HW
WRITE(7,*)
WRITE(7,*) ' THE CALCULATED SPECTRUM WILL BE BROADENED BY
+ ',HW,' Hz'
WRITE(6,*) ' NATURAL ABUNDANCE OF COUPLED NUCLEUS (IN % UNITS)?'
READ(*,*) PNA
WRITE(7,*)
WRITE(7,*) ' NATURAL ABUNDANCE OF COUPLED NUCLEUS IS ',PNA,'% '
PNAD2=PNA/200.
C CLEAR SPECTRUM TABLE
DO 5 NP=0,NPOINTS-1
  SPEC(NP)=0.
5 CONTINUE
DO 6 I=1,NSITE
  CALL INPUT(I)
C INVOKE "POWDER"
  WRITE(6,*)
  WRITE(6,*) ' CALCULATING THE POWDER PATTERN...'
  PROB=PNAD2
  SPIN=0.5
  CALL POWDER(SPEC,NPOINTS,FSTART,FWIDTH,SPIN,PROB)
  SPIN=-0.5
  CALL POWDER(SPEC,NPOINTS,FSTART,FWIDTH,SPIN,PROB)
  PROB=1.-(2*pnad2)
  SPIN=0.0
  CALL POWDER(SPEC,NPOINTS,FSTART,FWIDTH,SPIN,PROB)
6 CONTINUE
  CLOSE(UNIT=7)
C GAUSSIAN BROADEN THE SPECTRUM (IF DESIRED) AND
C FIND VALUE OF LARGEST POINT IN SPECTRUM
  IF (HW.EQ.0.) GO TO 8

```

```

WRITE(6,*) ' BROADENING THE SPECTRUM...'
CALL BROADEN(SPEC,NPOINTS,FWIDTH,HW)
8  CONTINUE
   MAXIMUM=0.
   DO 10 NP=0,NPOINTS-1
     IF (SPEC(NP).GT.MAXIMUM) MAXIMUM=SPEC(NP)
10  CONTINUE
C NORMALIZE SPECTRUM
   DO 20 NP=0,NPOINTS-1
20  SPEC(NP)=SPEC(NP)/MAXIMUM
C OUTPUT THE RESULT INTO A PLOTTING FILE
   WRITE(6,*) ' WRITING THE OUTPUT FILES...'
   CALL SHOW(SPEC,NPOINTS,FSTART,FWIDTH)
   WRITE(6,*) ' SIMULATION COMPLETED'
   WRITE(6,*) ' OUTPUT FILES ARE NAMED ',FILEN,' AND ',FILEP
   STOP
   END
C
C SUBROUTINE INPUT(NS)
C
C INTEGER*4 KPF
COMMON/TRIG/PI,COSB,SINB,COSA,SINA
COMMON/PARAM/S11,S22,S33,FNEW,D,BETA,ALFA,CJ,PF,DELJ
C
C WRITE(6,*) ' INPUT PARAMETERS FOR SITE ',NS
WRITE(7,*)
WRITE(7,*) ' INPUT PARAMETERS FOR SITE ',NS
WRITE(7,*)
WRITE(6,*) ' HOMONUCLEAR (1) OR HETERONUCLEAR (2) SPIN-PAIR?'
READ(*,*) KPF
IF(KPF.EQ.1) THEN
  PF=1.5
  WRITE(7,*) ' HOMONUCLEAR SPIN-PAIR'
ELSE
  PF=1.0
  WRITE(7,*) ' HETERONUCLEAR SPIN-PAIR'
ENDIF
WRITE(6,*) ' CHEMICAL SHIFT COMPONENTS (IN PPM): S11,S22,S33'
READ(*,*) S11,S22,S33
WRITE(7,*)
WRITE(7,*) ' CHEMICAL SHIFT COMPONENTS:'
WRITE(7,*) ' DELTA-11 = ',S11,' PPM'
WRITE(7,*) ' DELTA-22 = ',S22,' PPM'
WRITE(7,*) ' DELTA-33 = ',S33,' PPM'
WRITE(6,*) ' DIPOLAR COUPLING CONSTANT (IN Hz): D'
READ(*,*) D
WRITE(7,*)

```

```

WRITE(7,*) ' DIPOLAR COUPLING CONSTANT (IN Hz): ',D
WRITE(6,*) ' EULER ANGLES ORIENTING THE TWO TENSORS',
+ ' (IN DEGREES): ALFA,BETA'
READ(*,*) ALFA,BETA
WRITE(7,*)
WRITE(7,*) ' EULER ANGLES ORIENTING THE TWO TENSORS',
+ ' (IN DEGREES): '
WRITE(7,*) ' ALPHA = ',ALFA
WRITE(7,*) ' BETA = ',BETA
WRITE(7,*)
ALFA=ALFA*PI/180.0
BETA=BETA*PI/180.0
COSB=COS(BETA)
SINB=SIN(BETA)
COSA=COS(ALFA)
SINA=SIN(ALFA)
IF(KPF.EQ.1) GOTO 10
WRITE(6,*) ' ISOTROPIC J COUPLING CONSTANT (IN Hz): J'
READ(*,*) CJ
WRITE(7,*) ' ISOTROPIC J COUPLING CONSTANT (IN Hz): ',CJ
WRITE(6,*) ' ANISOTROPY IN J COUPLING (IN Hz): DELJ'
READ(*,*) DELJ
WRITE(7,*) ' ANISOTROPY IN J COUPLING (IN Hz): ',DELJ
DELJ=DELJ/3.
10 CONTINUE
RETURN
END

C
SUBROUTINE POWDER(SPEC,NPOINTS,FSTART,FWIDTH,SPIN,PROB)
C
C DONALD W. ALDERMAN
C DEPARTMENT OF CHEMISTRY
C UNIVERSITY OF UTAH
C SALT LAKE CITY, UTAH 84112
C
C VERSION: JANUARY 7, 1986
C
C IMPLICIT REAL*4(A-H,O-Z)
C VARIABLES (EXTERNAL)
INTEGER*4 NPOINTS
REAL*4 SPEC(0:NPOINTS-1),FSTART,FWIDTH,SPIN,PROB
C VARIABLES (INTERNAL)
C THE LIMITS FOR THESE ARRAYS ARE (NT,2*NT)
REAL*4 FREQ(0:32,0:64),AMP(0:32,0:64)
INTEGER*4 I,J,NT
REAL*4 X,Y,Z,R,FINC
COMMON/TRIG/PI,COSB,SINB,COSA,SINA

```

```

COMMON/PARAM/S11,S22,S33,FNEW,D,BETA,ALFA,CJ,PF,DELJ
C
C FIRST EXECUTABLE STATEMENT
C
C CHECK ARGUMENT VALUES
  NT=32
  IF (NPOINTS.GE.3.AND.FWIDTH.GT.0) GO TO 10
  WRITE(*,*) 'NPOINTS less than 3 or FWIDTH not positive,
+ POWDER aborting'
  CALL EXIT
C COMPUTE FREQUENCIES AND AMPLITUDES AT TRIANGULAR GRID
C INTERSECTIONS ON FACES OF OCTAHEDRON
10  DO 40 J=0,NT-1
    DO 20 I=0,NT-J
      X=NT-I-J
      Y=I
      Z=J
      R=SQRT(X*X+Y*Y+Z*Z)
      CALL LINE(X/R,Y/R,Z/R,FREQ(I,J),AMP(I,J),SPIN,PROB)
      AMP(I,J)=AMP(I,J)/R/R/R
20  CONTINUE
    DO 30 I=NT-J+1,NT
      X=NT-I-J
      Y=NT-J
      Z=NT-I
      R=SQRT(X*X+Y*Y+Z*Z)
      CALL LINE(X/R,Y/R,Z/R,FREQ(I,J),AMP(I,J),SPIN,PROB)
      AMP(I,J)=AMP(I,J)/R/R/R
30  CONTINUE
40  CONTINUE
    DO 70 J=NT,2*NT-1
      DO 50 I=J-NT+1,NT-1
        X=-NT-I+J
        Y=NT-J
        Z=NT-I
        R=SQRT(X*X+Y*Y+Z*Z)
        CALL LINE(X/R,Y/R,Z/R,FREQ(I,J),AMP(I,J),SPIN,PROB)
        AMP(I,J)=AMP(I,J)/R/R/R
50  CONTINUE
      DO 60 I=1,J-NT
        X=-NT-I+J
        Y=-I
        Z=2*NT-J
        R=SQRT(X*X+Y*Y+Z*Z)
        CALL LINE(X/R,Y/R,Z/R,FREQ(I,J),AMP(I,J),SPIN,PROB)
        AMP(I,J)=AMP(I,J)/R/R/R
60  CONTINUE

```

```

70  CONTINUE
    CALL LINE(0.,0.,1.,FREQ(0,NT),AMP(0,NT),SPIN,PROB)
    AMP(0,NT)=AMP(0,NT)/NT/NT/NT
    DO 80 J=0,NT-1
        FREQ(0,2*NT-J)=FREQ(0,J)
        AMP(0,2*NT-J)=AMP(0,J)
80  CONTINUE
    DO 90 I=0,NT
        FREQ(NT,NT+I)=FREQ(I,0)
        AMP(NT,NT+I)=AMP(I,0)
90  CONTINUE
    DO 100 J=1,NT-1
        FREQ(NT-J,2*NT)=FREQ(NT,J)
        AMP(NT-J,2*NT)=AMP(NT,J)
100 CONTINUE
C FORM SPECTRUM FROM FREQUENCIES AND AMPLITUDES AT TRIANGULAR GRID
C INTERSECTIONS ON FACES OF OCTAHEDRON BY ADDING "TENTS" TO
C SPECTRUM
    FINC=FWIDTH/FLOAT(NPOINTS)
    DO 130 I=0,NT-1
        DO 110 J=0,NT-1
            CALL TENT(FREQ(I+1,J),FREQ(I,J+1),FREQ(I,J),
+ AMP(I+1,J)+AMP(I,J+1)+AMP(I,J),SPEC,NPOINTS,FSTART,FINC)
            CALL TENT(FREQ(I+1,J),FREQ(I,J+1),FREQ(I+1,J+1),AMP(I+1,J)+
+ AMP(I,J+1)+AMP(I+1,J+1),SPEC,NPOINTS,FSTART,FINC)
110 CONTINUE
        DO 120 J=NT,2*NT-1
            CALL TENT(FREQ(I,J),FREQ(I+1,J+1),FREQ(I+1,J),
+ AMP(I,J)+AMP(I+1,J+1)+AMP(I+1,J),SPEC,NPOINTS,FSTART,FINC)
            CALL TENT(FREQ(I,J),FREQ(I+1,J+1),FREQ(I,J+1),
+ AMP(I,J)+AMP(I+1,J+1)+AMP(I,J+1),SPEC,NPOINTS,FSTART,FINC)
120 CONTINUE
130 CONTINUE
    RETURN
    END
C
    SUBROUTINE TENT(FREQ1,FREQ2,FREQ3,AMP,SPEC,NPOINTS,FSTART
+ ,FINC)
C
C CALLED FROM "POWDER". ADDS TO SPECTRUM THE "TENT" WHICH
C REPRESENTS THE CONTRIBUTION FROM A TRIANGLE ON THE VERTICES OF
C WHICH THE FREQUENCIES ARE FREQ1, FREQ2, AND FREQ3.
C
    IMPLICIT REAL*4(A-H,O-Z)
C VARIABLES (EXTERNAL)
    REAL*4 FREQ1,FREQ2,FREQ3,AMP
    INTEGER*4 NPOINTS

```

```

      REAL*4 SPEC(0:NPOINTS-1),FSTART,FINC
C VARIABLES (INTERNAL)
      REAL*4 FMIN,FMID,FMAX,F1,F2,TOP
      INTEGER*4 NP,NPMID,NPMAX
C
C FIRST EXECUTABLE STATEMENT
C
C SORT FREQUENCIES
      FMIN=AMIN1(FREQ1,FREQ2,FREQ3)
      FMID=AMIN1(AMAX1(FREQ1,FREQ2),AMAX1(FREQ2,FREQ3),AMAX1(FREQ3,
+ FREQ1))
      FMAX=AMAX1(FREQ1,FREQ2,FREQ3)
C COMPUTE HEIGHT OF "TENT"
      TOP=AMP*2./(FMAX-FMIN)
C COMPUTE INDICES OF TENT EDGES AND TOP
      NP=NINT((FMIN-FSTART)/FINC)
      NPMID=NINT((FMID-FSTART)/FINC)
      NPMAX=NINT((FMAX-FSTART)/FINC)
C LOOK FOR CONTRIBUTIONS OUTSIDE OF SPECTRUM
      IF (NPMAX.LT.NPOINTS.AND.NP.GE.0) GO TO 5
      WRITE(*,*) 'Frequency beyond limits of spectrum, POWDER
+ aborting'
      CALL EXIT
C ERECT "TENT" BY EXAMINING VARIOUS CASES
5   IF (NP.NE.NPMID) GO TO 10
      SPEC(NP)=SPEC(NP)+(FMID-FMIN)*TOP/2.
      GO TO 40
10  F2=FINC*FLOAT(NP+1)+FSTART
      SPEC(NP)=SPEC(NP)+(F2-FMIN)*(F2-FMIN)*TOP/2./(FMID-FMIN)
20  NP=NP+1
      F1=F2
      IF (NP.EQ.NPMID) GO TO 30
      F2=FINC*FLOAT(NP+1)+FSTART
      SPEC(NP)=SPEC(NP)+FINC*((F2-FMIN)+(F1-FMIN))*TOP/2./
+ (FMID-FMIN)
      GO TO 20
30  SPEC(NP)=SPEC(NP)+(FMID-F1)*((FMID-FMIN)+(F1-FMIN))*TOP/2./
+ (FMID-FMIN)
40  IF (NP.NE.NPMAX) GO TO 50
      SPEC(NP)=SPEC(NP)+(FMAX-FMID)*TOP/2.
      GO TO 80
50  F2=FINC*FLOAT(NPMID+1)+FSTART
      SPEC(NP)=SPEC(NP)+(F2-FMID)*((FMAX-F2)+(FMAX-FMID))*TOP/2./
+ (FMAX-FMID)
60  NP=NP+1
      F1=F2
      IF (NP.EQ.NPMAX) GO TO 70

```

```

      F2=FINC*FLOAT(NP+1)+FSTART
      SPEC(NP)=SPEC(NP)+FINC*((FMAX-F1)+(FMAX-F2))*TOP/2./
      + (FMAX-FMID)
      GO TO 60
70    SPEC(NP)=SPEC(NP)+(FMAX-F1)*(FMAX-F1)*TOP/2./(FMAX-FMID)
80    CONTINUE
      RETURN
      END
C
      SUBROUTINE LINE(COSX,COSY,COSZ,FREQ,AMP,SPIN,PROB)
C
C CALLED FROM "POWDER". COMPUTES LINE POSITION AND AMPLITUDE
C FOR A SPIN 1/2 NUCLEUS DIPOLE-COUPLED TO ANOTHER SPIN 1/2
C NUCLEUS.
C
      IMPLICIT REAL*4(A-H,O-Z)
C VARIABLES (EXTERNAL)
      REAL*4 COSX,COSY,COSZ,FREQ,AMP,SPIN
C
      COMMON/TRIG/PI,COSB,SINB,COSA,SINA
      COMMON/PARAM/S11,S22,S33,FNEW,D,BETA,ALFA,CJ,PF,DELJ
C
C FIRST EXECUTABLE STATEMENT
C
C COMPUTE FREQUENCY AND CONSTANT INTENSITY
C FREQ IS THE EQUATION GIVING THE LINESHAPE
      FREQ=FNEW*(COSX*S11*COSX+COSY*S22*COSY+COSZ*S33*COSZ)+
      + PF*SPIN*(D-DELJ)*(3*(SINB*COSA*COSX+SINB*SINA*COSY+
      + COSB*COSZ)**2-1.)-SPIN*CJ
      AMP=1.*PROB
      RETURN
      END
C
      SUBROUTINE BROADEN(SPEC,NPTS,FWIDTH,HW)
C
C VERSION: MAY 10, 1990
C
C PARAMETER DESCRIPTION:
C HW : LINE BROADENING DESIRED.
C XK : COMPUTED LINE BROADENING FACTOR
C
      IMPLICIT REAL*4(A-H,O-Z)
      DIMENSION SPEC(1024),BROD(1024)
      REAL*4 HW,XK,RJ,RESOL,INTEN,IMIN,FWIDTH
      REAL*4 SPEC,BROD
      INTEGER*4 NPTS,I,J,M,N
C

```

```

RESOL=(FWIDTH)/FLOAT(NPTS-1)
IF (ABS(HW).LT.ABS(0.5*RESOL)) GO TO 61
IMIN=0.00001
DO 20 I=1,NPTS
20  BROD(I)=0.0
C GAUSSIAN BROADENING
  XK=-2.7726/(HW*HW)
  DO 60 I=1,NPTS
    BROD(I)=BROD(I)+SPEC(I)
    J=1
    INTEN=IMIN+0.00001
50    IF (INTEN.LT.IMIN) GO TO 60
      RJ=J*RESOL
      INTEN=SPEC(I)*EXP(XK*RJ*RJ)
      M=I-J
      N=I+J
      IF (M.GT.0) BROD(M)=BROD(M)+INTEN
      IF (N.LE.NPTS) BROD(N)=BROD(N)+INTEN
      J=J+1
      GO TO 50
60    CONTINUE
61    CONTINUE
  DO 62 I=1,NPTS
62    SPEC(I)=BROD(I)
  RETURN
END
C
  SUBROUTINE SHOW(SPEC,NPOINTS,FSTART,FWIDTH)
C
C THIS SUBROUTINE SHOULD BE TAILORED TO THE SPECIFIC
C NEEDS OF THE USER. AS EXPRESSED HERE, THE OUTPUT
C FILE STARTS WITH ONE LINE DESIGNATING THE NUMBER
C OF POINTS, THEN A LIST OF FREQUENCY (IN kHz) VS.
C INTENSITY DATA POINTS. THE INTENSITIES ARE SCALED
C TO A MAXIMUM OF ONE. THE FILE IS THEN PLOTTED USING
C OTHER SOFTWARE, DRIVING EITHER GRAPHICS TERMINAL OR
C A PLOTTER.
C
  IMPLICIT REAL*4(A-H,O-Z)
C
  INTEGER*4 NPOINTS,NP
  REAL*4 SPEC(0:1023),FSTART,FWIDTH,FX,FSTEP
  CHARACTER*20 FILEN,FILEP
  COMMON/FILES/FILEN,FILEP
C
  FSTEP=(FWIDTH)/FLOAT(NPOINTS-1)
  OPEN(UNIT=8,FILE=FILEP,STATUS='NEW')

```

```
FSTEP=(FWIDTH)/FLOAT(NPOINTS-1)
WRITE (8,5) NPOINTS
5  FORMAT(1X,I4)
   DO 10 NP=0,NPOINTS-1
     FX=(FSTEP*NP+FSTART)/1000.
10  WRITE (8,20) FX,SPEC(NP)
20  FORMAT(1X,F10.4,2X,F10.6)
   RETURN
   END
C
  SUBROUTINE EXIT
  STOP
  END
```

## PROGRAM QUADPOW

```
C
C "POWDER" SIMULATION OF FIRST-ORDER QUADRUPOLAR CSA PATTERNS
C (E.G., CESIUM-133) INCORPORATING POWDER SIMULATION ROUTINE
C OF ALDERMAN, SOLUM AND GRANT. FOR FURTHER DETAILS,
C PLEASE REFER TO: D. W. ALDERMAN, M. S. SOLUM AND D. M. GRANT,
C           J. CHEM. PHYS. 84, 3717 (1986).
C
C PROGRAM WRITTEN BY BILL POWER (BITNET: BPOWER @ AC.DAL.CA)
C
C ADDRESS CORRESPONDENCE TO: DR. R.E. WASYLISHEN
C           DEPT. OF CHEMISTRY
C           DALHOUSIE UNIVERSITY
C           HALIFAX, N.S. B3H 4J3
C           CANADA
C
C THIS PROGRAM HAS BEEN TESTED TO THE BEST OF THE PROGRAMMER'S
C ABILITY. HOWEVER, SOME ERRORS MAY BECOME APPARENT AFTER DETAILED
C USE ON THE WIDE VARIETY OF CHEMICAL SYSTEMS. IF SUCH ERRORS ARE
C NOTICED, PLEASE NOTIFY BILL POWER OR ROD WASYLISHEN, AT THE ABOVE
C ADDRESS OR VIA BITNET, OF YOUR PROBLEMS, AND THE PRESCRIBED OR
C SUGGESTED CORRECTIONS, SO THAT OTHERS MAY BENEFIT FROM THE
C IMPROVED CODE.
C
C           THANK YOU,
C           BILL POWER      20/6/90
C
C PROGRAM UPDATED 14/5/90
C
C   IMPLICIT REAL*4(A-H,O-Z)
C VARIABLES
C   REAL*4 SPEC(0:1023),FSTART,FWIDTH,MAXIMUM,SPIN,HW
C   REAL*4 PROB,FEND,S11,S22,S33,SNEW,SNUC,CHI,ETA,ALFA
C   REAL*4 BETA,GAMMA,COSB,SINB,COSA,SINA,COSG,SING
C   INTEGER*4 NPOINTS,NP,NTRANS
C   CHARACTER*20 FILEN,FILEP
C   COMMON/TRIG/PI,COSB,SINB,COSA,SINA,COSG,SING
C   COMMON/PARAM/S11,S22,S33,SNEW,SNUC,CHI,ETA,BETA,ALFA,GAMMA
C   COMMON/FILES/FILEN,FILEP
C
C FIRST EXECUTABLE STATEMENT
C
C   PI=3.1415926
C   WRITE(6,*) ' OUTPUT FILENAME'
C   WRITE(6,*) ' DATAFILE = ?'
C   READ(*,3) FILEN
3  FORMAT(A20)
C   OPEN(UNIT=7,FILE=FILEN,STATUS='NEW')
```

```

WRITE(7,*) ' ',FILEN
WRITE(7,*)
WRITE(6,*) ' PLOTFILE = ?'
READ(*,3) FILEP
WRITE(6,*) ' NUMBER OF SITES?'
READ(*,*) NSITE
WRITE(7,*) ' THE NUMBER OF SITES IS ',NSITE
WRITE(7,*)
NPOINTS=1024
WRITE(6,*) ' LARMOR FREQUENCY OF OBSERVED NUCLEUS (IN MHz)?'
READ(*,*) SNEW
WRITE(7,*) ' LARMOR FREQUENCY OF THE OBSERVED NUCLEUS IS ',
+ SNEW,' MHz'
WRITE(6,*) ' NUCLEAR SPIN OF OBSERVED NUCLEUS?'
READ(*,*) SNUC
NTRANS=NINT(2*SNUC)
WRITE(7,*) ' WHICH HAS A NUCLEAR SPIN OF ',SNUC
WRITE(7,*) ' RESULTING IN ',NTRANS,' TRANSITIONS'
WRITE(7,*)
WRITE(6,*) ' UPPER AND LOWER FREQUENCY LIMITS OF SIMULATION',
+ ' (IN kHz)?'
READ(*,*) FEND,FSTART
WRITE(7,*) ' THE SPECTRAL WIDTH OF THE SIMULATION RUNS FROM'
WRITE(7,*) FEND,' kHz TO ',FSTART,' kHz'
WRITE(7,*)
FWIDTH=(FEND-FSTART)*1000.
FSTART=FSTART*1000.
WRITE(6,*) ' LINE BROADENING (IN Hz)?'
READ(*,*) HW
WRITE(7,*) ' THE LINE BROADENING WILL BE ',HW,' Hz'
WRITE(7,*)
C CLEAR SPECTRUM TABLE
DO 5 NP=0,NPOINTS-1
SPEC(NP)=0.
5 CONTINUE
DO 6 I=1,NSITE
CALL INPUT(I)
C INVOKE "POWDER"
C
C PROBABILITIES OF THE DIFFERENT TRANSITIONS IS TAKEN FROM
C FUKUSHIMA AND ROEDER, 'EXPERIMENTAL PULSE NMR', ADDISON-WESLEY,
C READING, MASS, 1981: PP. 106-112.
C
SPIN=1.-SNUC
DO 7 J=1,NTRANS
PROB=SQRT(SNUC*(SNUC+1.)-SPIN*(SPIN-1.))
WRITE(6,*) ' CALCULATING TRANSITION #',J,' FOR SITE '

```

```

+      ,I,...'
      CALL POWDER(SPEC,NPOINTS,FSTART,FWIDTH,SPIN,PROB)
      SPIN=SPIN+1.
7      CONTINUE
      WRITE(6,*)
6      CONTINUE
      CLOSE(7)
C GAUSSIAN BROADEN THE SPECTRUM (IF DESIRED) AND
C FIND VALUE OF LARGEST POINT IN SPECTRUM
      IF (HW.EQ.0) GO TO 8
      CALL BROADEN(SPEC,NPOINTS,FWIDTH,HW)
8      CONTINUE
      MAXIMUM=0.
      DO 10 NP=0,NPOINTS-1
      IF (SPEC(NP).GT.MAXIMUM) MAXIMUM=SPEC(NP)
10     CONTINUE
C NORMALIZE SPECTRUM
      DO 20 NP=0,NPOINTS-1
20     SPEC(NP)=SPEC(NP)/MAXIMUM
C OUTPUT THE RESULT INTO A PLOTTING FILE
      WRITE(6,*) ' WRITING THE OUTPUT FILES...'
      CALL SHOW(SPEC,NPOINTS,FSTART,FWIDTH)
      WRITE(6,*)
      WRITE(6,*) ' FIRST-ORDER QUADRUPOLEAR - CHEMICAL SHIELDING LINE'
      WRITE(6,*) ' SHAPE CALCULATION COMPLETE. THE OUTPUT FILES ARE '
      WRITE(6,*) FILEN,' AND ',FILEP
      STOP
      END

C
      SUBROUTINE INPUT(NS)
      REAL*4 COSB,SINB,COSA,SINA,COSG,SING
      REAL*4 S11,S22,S33,SNEW,SNUC,CHI,ETA,BETA,ALFA,GAMMA

C
      COMMON/TRIG/PI,COSB,SINB,COSA,SINA,COSG,SING
      COMMON/PARAM/S11,S22,S33,SNEW,SNUC,CHI,ETA,BETA,ALFA,GAMMA

C
      WRITE(6,*) ' INPUT PARAMETERS FOR SITE ',NS
      WRITE(7,*) ' PARAMETERS FOR SITE ',NS
      WRITE(6,*) ' CHEMICAL SHIELDING COMPONENTS (IN PPM) S11,S22,S33'
      READ(*,*) S11,S22,S33
      WRITE(7,*) ' CHEMICAL SHIELDING COMPONENTS (IN PPM)'
      WRITE(7,*) ' SIGMA-11 = ',S11
      WRITE(7,*) ' SIGMA-22 = ',S22
      WRITE(7,*) ' SIGMA-33 = ',S33
      WRITE(6,*) ' QUADRUPOLEAR COUPLING CONSTANT (IN Hz)',
+      ' AND ASYMMETRY: CHI,ETA'
      READ(*,*) CHI,ETA

```

```

WRITE(7,*) ' QUADRUPOLEAR COUPLING CONSTANT (CHI) = ',CHI,' Hz'
WRITE(7,*) ' WITH ASYMMETRY PARAMETER (ETA) = ',ETA
WRITE(6,*) ' EULER ANGLES ORIENTING THE TWO TENSORS',
+      ' (IN DEGREES): ALPHA,BETA,GAMMA'
READ(*,*) ALFA,BETA,GAMMA
WRITE(7,*) ' EULER ANGLES ORIENTING THE TWO TENSORS ARE'
WRITE(7,*) ' ALPHA = ',ALFA
WRITE(7,*) ' BETA = ',BETA
WRITE(7,*) ' GAMMA = ',GAMMA
WRITE(7,*)
ALFA=ALFA*PI/180.0
BETA=BETA*PI/180.0
GAMMA=GAMMA*PI/180.0
COSB=COS(BETA)
SINB=SIN(BETA)
COSA=COS(ALFA)
SINA=SIN(ALFA)
COSG=COS(GAMMA)
SING=SIN(GAMMA)
RETURN
END
C
SUBROUTINE POWDER(SPEC,NPOINTS,FSTART,FWIDTH,SPIN,PROB)
C
C DONALD W. ALDERMAN
C DEPARTMENT OF CHEMISTRY
C UNIVERSITY OF UTAH
C SALT LAKE CITY, UTAH 84112
C
C VERSION: JANUARY 7, 1986
C
C IMPLICIT REAL*4(A-H,O-Z)
C VARIABLES (EXTERNAL)
INTEGER*4 NPOINTS
REAL*4 SPEC(0:NPOINTS-1),FSTART,FWIDTH,SPIN,PROB
C VARIABLES (INTERNAL)
C THE LIMITS FOR THESE ARRAYS ARE NT,2*NT
REAL*4 FREQ(0:32,0:64),AMP(0:32,0:64)
INTEGER*4 I,J
REAL*4 X,Y,Z,R,FINC
REAL*4 COSB,SINB,COSA,SINA,COSG,SING
REAL*4 S11,S22,S33,SNEW,SNUC,CHI,ETA
COMMON/TRIG/PI,COSB,SINB,COSA,SINA,COSG,SING
COMMON/PARAM/S11,S22,S33,SNEW,SNUC,CHI,ETA,BETA,ALFA,GAMMA
C
C FIRST EXECUTABLE STATEMENT
C

```

```

C CHECK ARGUMENT VALUES
  NT=32
  IF (NPOINTS.GE.3.AND.FWIDTH.GT.0) GO TO 10
  WRITE(6,*) 'NPOINTS less than 3 or FWIDTH not positive, POWDER
+ aborting'
  CALL EXIT
C COMPUTE FREQUENCIES AND AMPLITUDES AT TRIANGULAR GRID
C INTERSECTIONS ON FACES OF OCTAHEDRON
10  DO 40 J=0,NT-1
    DO 20 I=0,NT-J
      X=NT-I-J
      Y=I
      Z=J
      R=SQRT(X*X+Y*Y+Z*Z)
      CALL LINE(X/R,Y/R,Z/R,FREQ(I,J),AMP(I,J),SPIN,PROB)
      AMP(I,J)=AMP(I,J)/R/R/R
20  CONTINUE
    DO 30 I=NT-J+1,NT
      X=NT-I-J
      Y=NT-J
      Z=NT-I
      R=SQRT(X*X+Y*Y+Z*Z)
      CALL LINE(X/R,Y/R,Z/R,FREQ(I,J),AMP(I,J),SPIN,PROB)
      AMP(I,J)=AMP(I,J)/R/R/R
30  CONTINUE
40  CONTINUE
    DO 70 J=NT,2*NT-1
      DO 50 I=J-NT+1,NT-1
        X=-NT-I+J
        Y=NT-J
        Z=NT-I
        R=SQRT(X*X+Y*Y+Z*Z)
        CALL LINE(X/R,Y/R,Z/R,FREQ(I,J),AMP(I,J),SPIN,PROB)
        AMP(I,J)=AMP(I,J)/R/R/R
50  CONTINUE
      DO 60 I=1,J-NT
        X=-NT-I+J
        Y=-I
        Z=2*NT-J
        R=SQRT(X*X+Y*Y+Z*Z)
        CALL LINE(X/R,Y/R,Z/R,FREQ(I,J),AMP(I,J),SPIN,PROB)
        AMP(I,J)=AMP(I,J)/R/R/R
60  CONTINUE
70  CONTINUE
    CALL LINE(0.,0.,1.,FREQ(0,NT),AMP(0,NT),SPIN,PROB)
    AMP(0,NT)=AMP(0,NT)/NT/NT/NT
    DO 80 J=0,NT-1

```

```

      FREQ(0,2*NT-J)=FREQ(0,J)
      AMP(0,2*NT-J)=AMP(0,J)
80  CONTINUE
      DO 90 I=0,NT
      FREQ(NT,NT+I)=FREQ(I,0)
      AMP(NT,NT+I)=AMP(I,0)
90  CONTINUE
      DO 100 J=1,NT-1
      FREQ(NT-J,2*NT)=FREQ(NT,J)
      AMP(NT-J,2*NT)=AMP(NT,J)
100 CONTINUE
C FORM SPECTRUM FROM FREQUENCIES AND AMPLITUDES AT TRIANGULAR GRID
C INTERSECTIONS ON FACES OF OCTAHEDRON BY ADDING "TENTS" TO
C SPECTRUM
      FINC=FWIDTH/FLOAT(NPOINTS)
      DO 130 I=0,NT-1
      DO 110 J=0,NT-1
      CALL TENT(FREQ(I+1,J),FREQ(I,J+1),FREQ(I,J),
+ AMP(I+1,J)+AMP(I,J+1)+AMP(I,J),SPEC,NPOINTS,FSTART,FINC)
      CALL TENT(FREQ(I+1,J),FREQ(I,J+1),FREQ(I+1,J+1),AMP(I+1,J)+
+ AMP(I,J+1)+AMP(I+1,J+1),SPEC,NPOINTS,FSTART,FINC)
110 CONTINUE
      DO 120 J=NT,2*NT-1
      CALL TENT(FREQ(I,J),FREQ(I+1,J+1),FREQ(I+1,J),
+ AMP(I,J)+AMP(I+1,J+1)+AMP(I+1,J),SPEC,NPOINTS,FSTART,FINC)
      CALL TENT(FREQ(I,J),FREQ(I+1,J+1),FREQ(I,J+1),
+ AMP(I,J)+AMP(I+1,J+1)+AMP(I,J+1),SPEC,NPOINTS,FSTART,FINC)
120 CONTINUE
130 CONTINUE
      RETURN
      END
C
      SUBROUTINE TENT(FREQ1,FREQ2,FREQ3,AMP,SPEC,NPOINTS,FSTART,
+ FINC)
C
C CALLED FROM "POWDER". ADDS TO SPECTRUM THE "TENT" WHICH
C REPRESENTS THE CONTRIBUTION FROM A TRIANGLE ON THE VERTICES OF
C WHICH THE FREQUENCIES ARE FREQ1, FREQ2, AND FREQ3.
C
      IMPLICIT REAL*4(A-H,O-Z)
C VARIABLES (EXTERNAL)
      REAL*4 FREQ1,FREQ2,FREQ3,AMP
      INTEGER*4 NPOINTS
      REAL*4 SPEC(0:NPOINTS-1),FSTART,FINC
C VARIABLES (INTERNAL)
      REAL*4 FMIN,FMID,FMAX,F1,F2,TOP
      INTEGER*4 NP,NPMID,NPMAX

```

```

C
C FIRST EXECUTABLE STATEMENT
C
C SORT FREQUENCIES
  FMIN=AMIN1(FREQ1,FREQ2,FREQ3)
  FMID=AMIN1(AMAX1(FREQ1,FREQ2),AMAX1(FREQ2,FREQ3),AMAX1(FREQ3,
+ FREQ1))
  FMAX=AMAX1(FREQ1,FREQ2,FREQ3)
C COMPUTE HEIGHT OF "TENT"
  TOP=AMP*2./(FMAX-FMIN)
C COMPUTE INDICES OF TENT EDGES AND TOP
  NP=NINT((FMIN-FSTART)/FINC)
  NPMID=NINT((FMID-FSTART)/FINC)
  NPMAX=NINT((FMAX-FSTART)/FINC)
C LOOK FOR CONTRIBUTIONS OUTSIDE OF SPECTRUM
  IF (NPMAX.LT.NPOINTS.AND.NP.GE.0) GO TO 5
  WRITE(6,*) 'Frequency beyond limits of spectrum, POWDER aborting'
  CALL EXIT
C ERCT "TENT" BY EXAMINING VARIOUS CASES
5  IF (NP.NE.NPMID) GO TO 10
  SPEC(NP)=SPEC(NP)+(FMID-FMIN)*TOP/2.
  GO TO 40
10  F2=FINC*FLOAT(NP+1)+FSTART
  SPEC(NP)=SPEC(NP)+(F2-FMIN)*(F2-FMIN)*TOP/2./(FMID-FMIN)
20  NP=NP+1
  F1=F2
  IF (NP.EQ.NPMID) GO TO 30
  F2=FINC*FLOAT(NP+1)+FSTART
  SPEC(NP)=SPEC(NP)+FINC*((F2-FMIN)+(F1-FMIN))*TOP/2./(FMID-FMIN)
  GO TO 20
30  SPEC(NP)=SPEC(NP)+(FMID-F1)*((FMID-FMIN)+(F1-FMIN))*TOP/2./
+ (FMID-FMIN)
40  IF (NP.NE.NPMAX) GO TO 50
  SPEC(NP)=SPEC(NP)+(FMAX-FMID)*TOP/2.
  GO TO 80
50  F2=FINC*FLOAT(NPMID+1)+FSTART
  SPEC(NP)=SPEC(NP)+(F2-FMID)*((FMAX-F2)+(FMAX-FMID))*TOP/2./
+ (FMAX-FMID)
60  NP=NP+1
  F1=F2
  IF (NP.EQ.NPMAX) GO TO 70
  F2=FINC*FLOAT(NP+1)+FSTART
  SPEC(NP)=SPEC(NP)+FINC*((FMAX-F1)+(FMAX-F2))*TOP/2./(FMAX-FMID)
  GO TO 60
70  SPEC(NP)=SPEC(NP)+(FMAX-F1)*(FMAX-F1)*TOP/2./(FMAX-FMID)
80  CONTINUE
  RETURN

```

```

      END
C
      SUBROUTINE LINE(COSX,COSY,COSZ,FREQ,AMP,SPIN,PROB)
C
C CALLED FROM "POWDER". COMPUTES LINE POSITION AND AMPLITUDE
C * PLEASE NOTE THAT THE ROTATION CONVENTION IN THIS PROGRAM      *
C * CORRESPONDS TO THE ANGLES ALPHA, BETA AND GAMMA WHICH ARE    *
C * SUCCESSIVE ROTATIONS ABOUT THE Z-AXIS, Y'-AXIS AND Z"-AXIS.  *
C
      IMPLICIT REAL*4(A-H,O-Z)
C VARIABLES (EXTERNAL)
      REAL*4 COSX,COSY,COSZ,FREQ,AMP,SPIN,PROB,QNU,CHI,ETA
      REAL*4 SNUC,SNEW,S11,S22,S33,BETA,ALFA,GAMMA
      REAL*4 COSB,SINB,COSA,SINA,COSG,SING
C
      COMMON/TRIG/PI,COSB,SINB,COSA,SINA,COSG,SING
      COMMON/PARAM/S11,S22,S33,SNEW,SNUC,CHI,ETA,BETA,ALFA,GAMMA
C
C FIRST EXECUTABLE STATEMENT
C
C COMPUTE FREQUENCY AND TRANSITION INTENSITY
      QNU=3.*CHI/(2.*SNUC*(2.*SNUC-1.))
      PSI1=COSX*COSA+COSY*SINA
      PSI2=COSY*COSA-COSX*SINA
      CSX=COSG*COSB*PSI1+SING*PSI2-COSG*SINB*COSZ
      CSY=-SING*COSB*PSI1+COSG*PSI2+SING*SINB*COSZ
      CSZ=SINB*PSI1+COSB*COSZ
      FREQ= SNEW*(CSX*S11*CSX+CSY*S22*CSY+CSZ*S33*CSZ)-
      + 0.5*(SPIN-0.5)*QNU*((3*COSZ*COSZ-1)-
      + ETA*(COSX*COSX-COSY*COSY))
      AMP=PROB
      RETURN
      END
C
      SUBROUTINE BROADEN(SPEC,NPTS,FWIDTH,HW)
C
C VERSION: MAY 10, 1990
C
      DIMENSION SPEC(1024),BROD(1024)
      REAL*4 HW,XK,RJ,RESOL,INTEN,IMIN,FWIDTH
      REAL*4 SPEC,BROD
      INTEGER NPTS,I,J,M,N
C
      RESOL=(FWIDTH)/FLOAT(NPTS-1)
      IF (ABS(HW).LT.ABS(0.5*RESOL)) GO TO 61
      IMIN=0.00001
      DO 20 I=1,NPTS

```

```

20  BROD(I)=0.0
C
C GAUSSIAN BROADENING
C
      XK=-2.7726/(HW*HW)
      DO 60 I=1,NPTS
        BROD(I)=BROD(I)+SPEC(I)
        J=1
        INTEN=IMIN+0.00001
50    IF (INTEN.LT.IMIN) GO TO 60
        RJ=J*RESOL
        INTEN=SPEC(I)*EXP(XK*RJ*RJ)
        M=I-J
        N=I+J
        IF (M.GT.0) BROD(M)=BROD(M)+INTEN
        IF (N.LE.NPTS) BROD(N)=BROD(N)+INTEN
        J=J+1
      GO TO 50
60    CONTINUE
61    CONTINUE
      DO 62 I=1,NPTS
62    SPEC(I)=BROD(I)
      RETURN
      END
C
      SUBROUTINE SHOW(SPEC,NPOINTS,FSTART,FWIDTH)
C
      IMPLICIT REAL*4(A-H,O-Z)
C
      INTEGER*4 NPOINTS,NP
      REAL*4 SPEC(0:1023),FSTART,FWIDTH,FX,FSTEP
      CHARACTER*20 FILEN,FILEP
      COMMON/FILES/FILEN,FILEP
C
      FSTEP=(FWIDTH)/FLOAT(NPOINTS-1)
      OPEN(UNIT=8,FILE=FILEP,STATUS='NEW')
      FSTEP=(FWIDTH)/FLOAT(NPOINTS-1)
      WRITE (8,5) NPOINTS
5    FORMAT(1X,I4)
      DO 10 NP=0,NPOINTS-1
        FX=(FSTEP*NP+FSTART)/1000.
10    WRITE (8,20) FX,SPEC(NP)
20    FORMAT(1X,F10.4,2X,F10.6)
      CLOSE(8)
      RETURN
      END
C

```

SUBROUTINE EXIT  
STOP  
END

## PROGRAM SECQUAD

```
C
C "POWDER" SIMULATION OF SECOND-ORDER QUADRUPOLEAR CSA PATTERNS
C (E.G., OXYGEN-17) INCORPORATING POWDER SIMULATION ROUTINE
C OF ALDERMAN, SOLUM AND GRANT. FOR FURTHER DETAILS,
C PLEASE REFER TO: D. W. ALDERMAN, M. S. SOLUM AND D. M. GRANT,
C           J. CHEM. PHYS. 84, 3717 (1986).
C
C PROGRAM WRITTEN BY BILL POWER (BITNET: BPOWER @ AC.DAL.CA)
C
C ADDRESS CORRESPONDENCE TO: DR. R.E. WASYLISHEN
C           DEPT. OF CHEMISTRY
C           DALHOUSIE UNIVERSITY
C           HALIFAX, N.S. B3H 4J3
C           CANADA
C
C THIS PROGRAM HAS BEEN TESTED TO THE BEST OF THE PROGRAMMER'S
C ABILITY. HOWEVER, SOME ERRORS MAY BECOME APPARENT AFTER DETAILED
C USE ON THE WIDE VARIETY OF CHEMICAL SYSTEMS. IF SUCH ERRORS ARE
C NOTICED, PLEASE NOTIFY BILL POWER OR ROD WASYLISHEN AT THE ABOVE
C ADDRESS OR VIA BITNET OF YOUR PROBLEMS, AND PRESCRIBED OR
C SUGGESTED CORRECTIONS, SO THAT OTHERS MAY BENEFIT FROM THE
C IMPROVED CODE.
C
C           THANK YOU,
C           BILL POWER 20/6/90
C
C PROGRAM UPDATED 14/5/90
C
C   IMPLICIT REAL*4(A-H,O-Z)
C VARIABLES
C   REAL*4 SPEC(0:1023),FSTART,FWIDTH,MAXIMUM,SPIN,HW
C   REAL*4 PROB,FEND
C   INTEGER*4 NPCINTS,NP,NTRANS
C   CHARACTER*20 FILEN,FILEP
C   COMMON/TRIG/PI,COSB,SINB,COSA,SINA,COSG,SING
C   COMMON/PARAM/S11,S22,S33,SNEW,SNUC,CHI,ETA,BETA,ALFA,GAMMA
C   COMMON/FILES/FILEN,FILEP
C
C FIRST EXECUTABLE STATEMENT
C
C   PI=3.1415926
C   WRITE(6,*) ' OUTPUT FILENAMES'
C   WRITE(6,*) ' DATAFILE = ?'
C   READ(*,3) FILEN
3   FORMAT(A20)
C   OPEN(UNIT=7,FILE=FILEN,STATUS='NEW')
C   WRITE(7,*) FILEN
```

```

WRITE(7,*)
WRITE(6,*) ' PLOTFILE = ?'
READ(*,3) FILEP
WRITE(6,*) ' NUMBER OF SITES?'
READ(*,*) NSITE
NPOINTS=1024
WRITE(6,*) ' LARMOR FREQUENCY OF OBSERVED NUCLEUS (IN MHz)?'
READ(*,*) SNEW
WRITE(7,*) ' LARMOR FREQUENCY OF OBSERVED NUCLEUS IS ',SNEW,' MHz'
WRITE(7,*)
WRITE(6,*) ' NUCLEAR SPIN OF OBSERVED NUCLEUS?'
READ(*,*) SNUC
NTRANS=NINT(2*SNUC)
WRITE(7,*) ' THE NUCLEAR SPIN OF THE OBSERVED NUCLEUS IS ',SNUC
WRITE(7,*) ' RESULTING IN ',NTRANS,' TRANSITIONS'
WRITE(7,*)
WRITE(6,*) ' UPPER AND LOWER FREQUENCY LIMITS OF SIMULATION',
+ ' (IN kHz)?'
READ(*,*) FEND,FSTART
WRITE(7,*) ' THE SIMULATION WILL EXTEND FROM ',FEND,' kHz TO'
WRITE(7,*) FSTART,' kHz'
WRITE(7,*)
FWIDTH=(FEND-FSTART)*1000.
FSTART=FSTART*1000.
WRITE(6,*) ' LINE BROADENING (IN Hz)?'
READ(*,*) HW
WRITE(7,*) ' LINE BROADENING OF ',HW,' Hz WILL BE APPLIED'
WRITE(7,*)
WRITE(6,*) ' FOR CENTRAL TRANSITION SIMULATION ONLY, TYPE "1"'
WRITE(6,*) ' OTHERWISE, TYPE "0"'
READ(*,*) LST
C CLEAR SPECTRUM TABLE
DO 5 NP=0,NPOINTS-1
SPEC(NP)=0.
5 CONTINUE
DO 6 I=1,NSITE
CALL INPUT(I)
C INVOKE "POWDER"
C
C PROBABILITIES OF THE DIFFERENT TRANSITIONS IS TAKEN FROM
C FUKUSHIMA AND ROEDER, 'EXPERIMENTAL PULSE NMR', ADDISON-WESLEY,
C READING, MASS, 1981: PP. 106-112.
C
IF (LST.EQ.1) THEN
WRITE(6,*) ' CALCULATING THE CENTRAL TRANSITION FOR SITE '
+ ',I,...'
WRITE(7,*) ' SIMULATION OF CENTRAL TRANSITION ONLY'

```

```

        WRITE(7,*)
        SPIN=0.5
        PROB=1.0
        CALL POWDER(SPEC,NPOINTS,FSTART,FWIDTH,SPIN,PROB)
    ELSE
        WRITE(7,*) ' SIMULATION OF FULL POWDER PATTERN'
        WRITE(7,*)
        SPIN=1.-SNUC
        DO 7 J=1,NTRANS
            PROB=SQRT(SNUC*(SNUC+1)-SPIN*(SPIN-1))
            WRITE(6,*) ' CALCULATING TRANSITION # ',J,' FOR SITE '
+           ,I,'...'
            CALL POWDER(SPEC,NPOINTS,FSTART,FWIDTH,SPIN,PROB)
            SPIN=SPIN+1.
7        CONTINUE
        WRITE(7,*)
        WRITE(6,*)
    ENDIF
6    CONTINUE
C GAUSSIAN BROADEN THE SPECTRUM (IF DESIRED) AND
C FIND VALUE OF LARGEST POINT IN SPECTRUM
    IF (HW.EQ.0) GO TO 8
    CALL BROADEN(SPEC,NPOINTS,FWIDTH,HW)
8    CONTINUE
    MAXIMUM=0.
    DO 10 NP=0,NPOINTS-1
        IF (SPEC(NP).GT.MAXIMUM) MAXIMUM=SPEC(NP)
10   CONTINUE
C NORMALIZE SPECTRUM
    DO 20 NP=0,NPOINTS-1
20   SPEC(NP)=SPEC(NP)/MAXIMUM
C OUTPUT THE RESULT INTO A PLOTTING FILE
    WRITE(6,*) ' WRITING THE OUTPUT FILES...'
    WRITE(6,*)
    CALL SHOW(SPEC,NPOINTS,FSTART,FWIDTH)
    WRITE(6,*) ' SECOND-ORDER QUADRUPOLEAR - CHEMICAL SHIELDING LINE'
    WRITE(6,*) ' SHAPE CALCULATION COMPLETE. THE OUTPUT FILES ARE'
    WRITE(6,*) ' FILEN,' AND ',FILEP
    STOP
    END
C
C SUBROUTINE INPUT(NS)
C
COMMON/TRIG/PI,COSB,SINB,COSA,SINA,COSG,SING
COMMON/PARAM/S11,S22,S33,SNEW,SNUC,CHI,ETA,BETA,ALFA,GAMMA
C
WRITE(6,*) ' INPUT PARAMETERS FOR SITE ',NS

```

```

WRITE(7,*) ' PARAMETERS FOR SITE ',NS
WRITE(7,*)
WRITE(6,*) ' CHEMICAL SHIELDING COMPONENTS (IN PPM): S11,S22,S33'
READ(*,*) S11,S22,S33
WRITE(7,*) ' CHEMICAL SHIELDING TENSOR COMPONENTS (IN PPM)'
WRITE(7,*) ' SIGMA-11 = ',S11
WRITE(7,*) ' SIGMA-22 = ',S22
WRITE(7,*) ' SIGMA-33 = ',S33
WRITE(7,*)
WRITE(6,*) ' QUADRUPOLEAR COUPLING CONSTANT (IN Hz)',
+ ' AND ASYMMETRY: CHI,ETA'
READ(*,*) CHI,ETA
WRITE(7,*) ' THE QUADRUPOLEAR COUPLING CONSTANT IS ',CHI,' Hz'
WRITE(7,*) ' WITH ASYMMETRY OF ',ETA
WRITE(7,*)
WRITE(6,*) ' EULER ANGLES ORIENTING THE TWO TENSORS'.
+ ' (IN DEGREES): ALPHA,BETA,GAMMA'
READ(*,*) ALFA,BETA,GAMMA
WRITE(7,*) ' EULER ANGLES ORIENTING THE TWO TENSORS'
WRITE(7,*) ' ALPHA = ',ALFA
WRITE(7,*) ' BETA = ',BETA
WRITE(7,*) ' GAMMA = ',GAMMA
WRITE(7,*)
ALFA=ALFA*PI/180.0
BETA=BETA*PI/180.0
GAMMA=GAMMA*PI/180.0
COSB=COS(BETA)
SINB=SIN(BETA)
COSA=COS(ALFA)
SINA=SIN(ALFA)
COSG=COS(GAMMA)
SING=SIN(GAMMA)
RETURN
END
C
SUBROUTINE POWDER(SPEC,NPOINTS,FSTART,FWIDTH,SPIN,PROB)
C
C DONALD W. ALDERMAN
C DEPARTMENT OF CHEMISTRY
C UNIVERSITY OF UTAH
C SALT LAKE CITY, UTAH 84112
C
C VERSION: JANUARY 7, 1986
C
IMPLICIT REAL*4(A-H,O-Z)
C VARIABLES (EXTERNAL)
INTEGER*4 NPOINTS

```

```

      REAL*4 SPEC(0:NPOINTS-1),FSTART,FWIDTH,SPIN,PROB
C VARIABLES (INTERNAL)
C THE LIMITS FOR THESE ARRAYS ARE NT,2*NT
      REAL*4 FREQ(0:32,0:64),AMP(0:32,0:64)
      INTEGER*4 I,J
      REAL*4 X,Y,Z,R,FINC
      COMMON/TRIG/PI,COSB,SINB,COSA,SINA,COSG,SING
      COMMON/PARAM/S11,S22,S33,SNEW,SNUC,CHI,ETA,BETA,ALFA,GAMMA
C
C FIRST EXECUTABLE STATEMENT
C
C CHECK ARGUMENT VALUES
      NT=32
      IF (NPOINTS.GE.3.AND.FWIDTH.GT.0) GO TO 10
      WRITE(6,*) 'NPOINTS less than 3 or FWIDTH not positive, POWDER
+ aborting'
      CALL EXIT
C COMPUTE FREQUENCIES AND AMPLITUDES AT TRIANGULAR GRID
C INTERSECTIONS ON FACES OF OCTAHEDRON
10  DO 40 J=0,NT-1
      DO 20 I=0,NT-J
          X=NT-I-J
          Y=I
          Z=J
          R=SQRT(X*X+Y*Y+Z*Z)
          CALL LINE(X/R,Y/R,Z/R,FREQ(I,J),AMP(I,J),SPIN,PROB)
          AMP(I,J)=AMP(I,J)/R/R/R
20  CONTINUE
      DO 30 I=NT-J+1,NT
          X=NT-I-J
          Y=NT-J
          Z=NT-I
          R=SQRT(X*X+Y*Y+Z*Z)
          CALL LINE(X/R,Y/R,Z/R,FREQ(I,J),AMP(I,J),SPIN,PROB)
          AMP(I,J)=AMP(I,J)/R/R/R
30  CONTINUE
40  CONTINUE
      DO 70 J=NT,2*NT-1
          DO 50 I=J-NT+1,NT-1
              X=-NT-I+J
              Y=NT-J
              Z=NT-I
              R=SQRT(X*X+Y*Y+Z*Z)
              CALL LINE(X/R,Y/R,Z/R,FREQ(I,J),AMP(I,J),SPIN,PROB)
              AMP(I,J)=AMP(I,J)/R/R/R
50  CONTINUE
      DO 60 I=1,J-NT

```

```

X=-NT-I+J
Y=-I
Z=2*NT-J
R=SQRT(X*X+Y*Y+Z*Z)
CALL LINE(X/R,Y/R,Z/R,FREQ(I,J),AMP(I,J),SPIN,PROB)
AMP(I,J)=AMP(I,J)/R/R/R
60 CONTINUE
70 CONTINUE
CALL LINE(0.,0.,1.,FREQ(0,NT),AMP(0,NT),SPIN,PROB)
AMP(0,NT)=AMP(0,NT)/NT/NT/NT
DO 80 J=0,NT-1
FREQ(0,2*NT-J)=FREQ(0,J)
AMP(0,2*NT-J)=AMP(0,J)
80 CONTINUE
DO 90 I=0,NT
FREQ(NT,NT+I)=FREQ(I,0)
AMP(NT,NT+I)=AMP(I,0)
90 CONTINUE
DO 100 J=1,NT-1
FREQ(NT-J,2*NT)=FREQ(NT,J)
AMP(NT-J,2*NT)=AMP(NT,J)
100 CONTINUE
C FORM SPECTRUM FROM FREQUENCIES AND AMPLITUDES AT TRIANGULAR GRID
C INTERSECTIONS ON FACES OF OCTAHEDRON BY ADDING "TENTS" TO
C SPECTRUM
FINC=FWIDTH/FLOAT(NPOINTS)
DO 130 I=0,NT-1
DO 110 J=0,NT-1
CALL TENT(FREQ(I+1,J),FREQ(I,J+1),FREQ(I,J),
+ AMP(I+1,J)+AMP(I,J+1)+AMP(I,J),SPEC,NPOINTS,FSTART,FINC)
CALL TENT(FREQ(I+1,J),FREQ(I,J+1),FREQ(I+1,J+1),AMP(I+1,J)+
+ AMP(I,J+1)+AMP(I+1,J+1),SPEC,NPOINTS,FSTART,FINC)
110 CONTINUE
DO 120 J=NT,2*NT-1
CALL TENT(FREQ(I,J),FREQ(I+1,J+1),FREQ(I+1,J),
+ AMP(I,J)+AMP(I+1,J+1)+AMP(I+1,J),SPEC,NPOINTS,FSTART,FINC)
CALL TENT(FREQ(I,J),FREQ(I+1,J+1),FREQ(I,J+1),
+ AMP(I,J)+AMP(I+1,J+1)+AMP(I,J+1),SPEC,NPOINTS,FSTART,FINC)
120 CONTINUE
130 CONTINUE
RETURN
END
C
SUBROUTINE TENT(FREQ1,FREQ2,FREQ3,AMP,SPEC,NPOINTS,FSTART,FINC)
C
C CALLED FROM "POWDER". ADDS TO SPECTRUM THE "TENT" WHICH
C REPRESENTS THE CONTRIBUTION FROM A TRIANGLE ON THE VERTICES OF

```

```

C WHICH THE FREQUENCIES ARE FREQ1, FREQ2, AND FREQ3.
C
  IMPLICIT REAL*4(A-H,O-Z)
C VARIABLES (EXTERNAL)
  REAL*4 FREQ1,FREQ2,FREQ3,AMP
  INTEGER*4 NPOINTS
  REAL*4 SPEC(0:NPOINTS-1),FSTART,FINC
C VARIABLES (INTERNAL)
  REAL*4 FMIN,FMID,FMAX,F1,F2, TOP
  INTEGER*4 NP,NPMID,NPMAX
C
C FIRST EXECUTABLE STATEMENT
C
C SORT FREQUENCIES
  FMIN= AMIN1(FREQ1,FREQ2,FREQ3)
  FMID= AMIN1(AMAX1(FREQ1,FREQ2),AMAX1(FREQ2,FREQ3),AMAX1(FREQ3,
+ FREQ1))
  FMAX= AMAX1(FREQ1,FREQ2,FREQ3)
C COMPUTE HEIGHT OF "TENT"
  TOP= AMP*2./(FMAX-FMIN)
C COMPUTE INDICES OF TENT EDGES AND TOP
  NP= NINT((FMIN-FSTART)/FINC)
  NPMID= NINT((FMID-FSTART)/FINC)
  NPMAX= NINT((FMAX-FSTART)/FINC)
C LOOK FOR CONTRIBUTIONS OUTSIDE OF SPECTRUM
  IF (NPMAX.LT.NPOINTS.AND.NP.GE.0) GO TO 5
  WRITE(6,*) 'Frequency beyond limits of spectrum, POWDER aborting'
  CALL EXIT
C ERECT "TENT" BY EXAMINING VARIOUS CASES
5  IF (NP.NE.NPMID) GO TO 10
  SPEC(NP)=SPEC(NP)+(FMID-FMIN)*TOP/2.
  GO TO 40
10  F2=FINC*FLOAT(NP+1)+FSTART
  SPEC(NP)=SPEC(NP)+(F2-FMIN)*(F2-FMIN)*TOP/2./(FMID-FMIN)
20  NP=NP+1
  F1=F2
  IF (NP.EQ.NPMID) GO TO 30
  F2=FINC*FLOAT(NP+1)+FSTART
  SPEC(NP)=SPEC(NP)+FINC*((F2-FMIN)+(F1-FMIN))*TOP/2./(FMID-FMIN)
  GO TO 20
30  SPEC(NP)=SPEC(NP)+(FMID-F1)*((FMID-FMIN)+(F1-FMIN))*TOP/2./
+ (FMID-FMIN)
40  IF (NP.NE.NPMAX) GO TO 50
  SPEC(NP)=SPEC(NP)+(FMAX-FMID)*TOP/2.
  GO TO 80
50  F2=FINC*FLOAT(NPMID+1)+FSTART
  SPEC(NP)=SPEC(NP)+(F2-FMID)*((FMAX-F2)+(FMAX-FMID))*TOP/2./

```

```

+ (FMAX-FMID)
60 NP=NP+1
   F1=F2
   IF (NP.EQ.NPMAX) GO TO 70
   F2=FINC*FLOAT(NP+1)+FSTART
   SPEC(NP)=SPEC(NP)+FINC*((FMAX-F1)+(FMAX-F2))*TOP/2./(FMAX-FMID)
   GO TO 60
70 SPEC(NP)=SPEC(NP)+(FMAX-F1)*(FMAX-F1)*TOP/2./(FMAX-FMID)
80 CONTINUE
   RETURN
   END

```

```

C
C SUBROUTINE LINE(COSX,COSY,COSZ,FREQ,AMP,SPIN,PROB)
C
C CALLED FROM "POWDER". COMPUTES LINE POSITION AND AMPLITUDE
C * PLEASE NOTE THAT THE ROTATION CONVENTION IN THIS PROGRAM *
C * CORRESPONDS TO THE ANGLES ALPHA, BETA AND GAMMA WHICH ARE *
C * SUCCESSIVE ROTATIONS ABOUT THE Z-AXIS, Y'-AXIS AND Z"-AXIS. *

```

```

C
C IMPLICIT REAL*4(A-H,O-Z)
C VARIABLES (EXTERNAL)
   REAL*4 COSX,COSY,COSZ,FREQ,AMP,SPIN,PROB,RQ,QNU
   REAL*4 APhi,BPhi,CPhi,COS2PH,PSI1,PSI2,CSX,CSY,CSZ
C
C COMMON/TRIG/PI,COSB,SINB,COSA,SINA,COSG,SING
C COMMON/PARAM/S11,S22,S33,SNEW,SNUC,CHI,ETA,BETA,ALFA,GAMMA

```

```

C
C FIRST EXECUTABLE STATEMENT
C
C COMPUTE FREQUENCY AND TRANSITION INTENSITY
   QNU=3.*CHI/(2.*SNUC*(2.*SNUC-1.))
   PSI1=COSX*COSA+COSY*SINA
   PSI2=COSY*COSA-COSX*SINA
   CSX=COSG*COSB*PSI1+SING*PSI2-COSG*SINB*COSZ
   CSY=-SING*COSB*PSI1+COSG*PSI2+SING*SINB*COSZ
   CSZ=SINB*PSI1+COSB*COSZ
   IF (COSZ.LT.1.0) THEN
       COS2PH=(COSX*COSX-COSY*COSY)/(1.-COSZ*COSZ)
   ELSE
       COS2PH=0.000000000
   ENDIF
   APhi=-3.375-2.25*ETA*COS2PH-0.375*ETA*ETA*COS2PH*COS2PH
   BPhi=3.75-0.5*ETA*ETA+2.*ETA*COS2PH+0.75*ETA*ETA*COS2PH*
+ COS2PH
   CPhi=-0.375+(ETA*ETA)/3.+0.25*ETA*COS2PH-0.375*ETA*ETA*
+ COS2PH*COS2PH

```

```

RQ=QNU*QNU*(SNUC*(SNUC+1)-0.75)
FREQ=SNEW*(CSX*S11*CSX+CSY*S22*CSY+CSZ*S33*CSZ)-
+ 0.5*(SPIN-0.5)*QNU*(3*COSZ*COSZ-1-ETA*(COSX*COSX-COSY*COSY))
+ -(RQ/(6*SNEW*1.0E06))*(APHI*COSZ**4+BPHI*COSZ*COSZ+CPHI)
AMP=PROB
RETURN
END
C
SUBROUTINE BROADEN(SPEC,NPTS,FWIDTH,HW)
C
C VERSION: MAY 10, 1990
C
C PARAMETER DESCRIPTION:
C HW : LINE BROADENING DESIRED.
C XK   : COMPUTED LINE BROADENING FACTOR
C
IMPLICIT REAL*4(A-H,O-Z)
DIMENSION SPEC(1024),BROD(1024)
REAL*4 HW,XK,RJ,RESOL,INTEN,IMIN,FWIDTH
REAL*4 SPEC,BROD
INTEGER*4 NPTS,I,J,M,N
C
RESOL=(FWIDTH)/FLOAT(NPTS-1)
IF (ABS(HW).LT.ABS(0.5*RESOL)) GO TO 61
IMIN=0.00001
DO 20 I=1,NPTS
20  BROD(I)=0.0
C GAUSSIAN BROADENING
XK=-2.7726/(HW*HW)
DO 60 I=1,NPTS
BROD(I)=BROD(I)+SPEC(I)
J=1
INTEN=IMIN+0.00001
50  IF (INTEN.LT.IMIN) GO TO 60
RJ=J*RESOL
INTEN=SPEC(I)*EXP(XK*RJ*RJ)
M=I-J
N=I+J
IF (M.GT.0) BROD(M)=BROD(M)+INTEN
IF (N.LE.NPTS) BROD(N)=BROD(N)+INTEN
J=J+1
GO TO 50
60  CONTINUE
61  CONTINUE
DO 62 I=1,NPTS
62  SPEC(I)=BROD(I)
RETURN

```

```
END
C
SUBROUTINE SHOW(SPEC,NPOINTS,FSTART,FWIDTH)
C
IMPLICIT REAL*4(A-H,O-Z)
C
INTEGER*4 NPOINTS,NP
REAL*4 SPEC(0:1023),FSTART,FWIDTH,FX,FSTEP
CHARACTER*20 FILEN,FILEP
COMMON/FILES/FILEN,FILEP
C
FSTEP=(FWIDTH)/FLOAT(NPOINTS-1)
OPEN(UNIT=8,FILE=FILEP,STATUS='NEW')
FSTEP=(FWIDTH)/FLOAT(NPOINTS-1)
WRITE (8,5) NPOINTS
5  FORMAT(1X,I4)
DO 10 NP=0,NPOINTS-1
    FX=(FSTEP*NP+FSTART)/1000.
10  WRITE (8,20) FX,SPEC(NP)
20  FORMAT(1X,F10.4,2X,F10.6)
RETURN
END
C
SUBROUTINE EXIT
C
STOP
END
```

## References

1. Pake, G.E. J. Chem. Phys. **1948**, 16, 327.
2. Pound, R.V. Phys. Rev. **1950**, 79, 685.
3. Bloembergen, N.; Rowland, T.J. Phys. Rev. **1955**, 97, 1679.
4. Abragam, A. Principles of Nuclear Magnetism; Oxford University Press: Oxford, 1963.
5. Yannoni, C.S.; Bernier, P.P.; Bethune, D.S.; Mejer, G.; Salem, J.R. J. Am. Chem. Soc. **1991**, 113, 3190.
6. Spiess, H.W., in NMR Basic Principles and Progress; Springer-Verlag: Berlin, 1978. vol. 15, p. 55.
7. Slichter, C.P. Principles of Magnetic Resonance; 3rd ed.; Springer-Verlag: New York, 1990.
8. Jameson, C.J.; Mason, J., in Multinuclear NMR; Mason, J., ed.; Plenum Press: New York, 1987. pp. 51-88.
9. Jameson, C.J., in Specialist Periodical Report - Nuclear Magnetic Resonance; Webb, G.A., ed.; Royal Society of Chemistry: Cambridge, UK, 1984-1991. vol. 13-20.
10. Jameson, C.J., in Multinuclear NMR; Mason, J., ed.; Plenum Press: New York, 1987. pp. 89-131.
11. Cohen, M.H.; Reif, F., in Solid State Physics; Sietz, F.; Turnbull, D., eds.; Academic Press: New York, 1957. vol. 5, p. 321.
12. Smith, J.A.S. Advances in Nuclear Quadrupole Resonance; Heyden and Son, Ltd.: London, 1974. vol. 1.
13. Haeberlen, U. Advances in Magnetic Resonance, Supplement 1; Waugh, J.S., ed.; Academic Press: New York, 1976.
14. Mehring, M. High Resolution NMR in Solids; 2nd ed.; Springer-Verlag: Berlin, 1983.
15. Gerstein, B.C.; Dybowski, C.R. Transient Techniques in NMR of Solids; Academic Press: Orlando, FL, 1985.

16. Ernst, R.R.; Bodenhausen, G.; Wokaun, A. Principles of Nuclear Magnetic Resonance in One and Two Dimensions; Oxford University Press: Oxford, 1987.
17. Munowitz, M. Coherence and NMR; Wiley-Interscience: New York, 1988.
18. Taylor, P.C.; Baugher, J.F.; Kriz, H.M. Chem. Rev. **1975**, 75, 203.
19. Vaughan, R.W. Ann. Rev. Phys. Chem. **1978**, 29, 397.
20. Duncan, T.M.; Dybowski, C. Surf. Sci. Rep. **1981**, 1, 157.
21. (a) Gerstein, B.C. Anal. Chem. **1983**, 55, 782A.  
(b) Gerstein, B.C., in Topics in Carbon-13 NMR Spectroscopy; Levy, G., ed.; John Wiley and Sons: New York, 1984. vol. 4, p. 123.  
(c) Gerstein, B.C. Adv. Coll. Interf. Sci. **1985**, 23, 45.
22. van Willigen, H.; Griffin, R.G.; Haberkorn, R.A. J. Chem. Phys. **1977**, 67, 5855.
23. Zilm, K.W.; Grant, D.M. J. Am. Chem. Soc. **1981**, 103, 2913.
24. Solum, M.S.; Facelli, J.C.; Gan, Z.; Grant, D.M. Mol. Phys. **1988**, 64, 1031.
25. VanderHart, D.L.; Gutowsky, H.S. J. Chem. Phys. **1968**, 49, 261.
26. (a) Pyykkö, P. Chem. Phys. **1977**, 22, 289.  
(b) Pyykkö, P.; Wiesenfeld, L. Mol. Phys. **1983**, 43, 557.
27. Arfken, G. Mathematical Methods for Physicists; 3rd ed.; Academic Press: San Diego, 1985.
28. Lovett, D.R. Tensor Properties of Crystals; Adam Hilger: Bristol UK, 1989.
29. Alderman, D.W.; Solum, M.S.; Grant, D.M. J. Chem. Phys. **1986**, 84, 3717.
30. Oas, T.G.; Drobny, G.P.; Dahlquist, F.W. J. Magn. Reson. **1988**, 78, 408.
31. Cheng, J.T.; Edwards, J.C.; Ellis, P.D. J. Phys. Chem. **1990**, 94, 553.
32. Power, W.P.; Wasylishen, R.E. Ann. Rep. NMR Spectrosc. **1991**, 23, 1.
33. Herzfeld, J.; Berger, A.E. J. Chem. Phys. **1980**, 73, 6021.
34. Press, W.H.; Flannery, B.P.; Teukolsky, S.A.; Vetterling, W.T. Numerical Recipes; Cambridge University Press: Cambridge, UK, 1986. pp.289-293.
35. Fenzke, D.; Maeß, B.; Pfeifer, H. J. Magn. Reson. **1990**, 88, 172.

36. de Groot, H.J.M.; Smith, S.O.; Kolbert, A.C.; Courtin, J.M.L.; Winkel, C.; Lugtenburg, J.; Herzfeld, J.; Griffin, R.G. J. Magn. Reson. **1991**, 91, 30.
37. Nixon, J.F.; Pidcock, A. Ann. Rev. NMR Spectrosc. **1969**, 2, 345.
38. Pregosin, P.S.; Kunz, R.W. NMR Basic Principles and Progress; Diehl, P.; Fluck, E.; Kosfeld, R., eds.; Springer-Verlag: Berlin, 1979. Vol. 16, pp. 16-153.
39. Pidcock, A., in Catalytic Aspects of Metal Phosphine Complexes; Alyea, E.C.; Meek, D.W., eds.; Advances in Chemistry Series 196; American Chemical Society: Washington, D.C., 1982. pp.1-22.
40. Verkade, J.G.; Mosbo, J.A., in Phosphorus-31 NMR Spectroscopy in Stereochemical Analysis, Organic Compounds and Metal Complexes; Verkade, J.G.; Quin, L.D., eds.; Methods in Stereochemical Analysis 8; VCH Publishers, Inc.: Deerfield Beach, FL, 1987. pp.425-463.
41. McConnell, H.M. J. Chem. Phys. **1956**, 24, 460.
42. Ramsey, N.F. Phys. Rev. **1953**, 91, 303.
43. (a) Buckingham, A.D.; Love, I. J. Magn. Reson. **1970**, 2, 338.  
(b) Buckingham, A.D.; Pyykkö, P.; Robert, J.B.; Wiesenfeld, L. Mol. Phys. **1982**, 46, 177.
44. Pyykkö, P. Chem. Rev. **1988**, 88, 563.
45. Lounila, J.; Jokisaari, J. Prog. Nucl. Magn. Reson. Spectrosc. **1982**, 15, 249.
46. Robert, J.B.; Wiesenfeld, L. Phys. Rep. **1982**, 86, 363.
47. Robert, J.B.; Wiesenfeld, L., in Phosphorus-31 NMR Spectroscopy in Stereochemical Analysis, Organic Compounds and Metal Complexes; Verkade, J.G.; Quin, L.D., eds.; Methods in Stereochemical Analysis 8; VCH Publishers, Inc.: Deerfield Beach, FL, 1987. pp.151-183.
48. Jameson, C.J., in Phosphorus-31 NMR Spectroscopy in Stereochemical Analysis, Organic Compounds and Metal Complexes; Verkade, J.G.; Quin, L.D., eds.; Methods in Stereochemical Analysis 8; VCH Publishers, Inc.: Deerfield Beach, FL, 1987. pp.205-230.
49. Emsley, J.W.; Lindon, J.C. NMR Spectroscopy Using Liquid Crystal Solvents; Pergamon Press: Oxford, 1975.

50. (a) Jokisaari, J.; Hiltunen, Y.; Lounila, J. J. Chem. Phys. **1986**, 85, 3198.  
(b) Pulkkinen, A.; Hiltunen, Y.; Jokisaari, J. Liq. Cryst. **1988**, 3, 737.  
(c) Lounila, J.; Ala-Korpela, M.; Jokisaari, J. J. Chem. Phys. **1990**, 93, 8514.
51. (a) Lounila, J.; Diehl, P. J. Magn. Reson. **1984**, 56, 254.  
(b) Lounila, J.; Diehl, P. Mol. Phys. **1984**, 52, 827.  
(c) Lounila, J. Mol. Phys. **1986**, 58, 897.
52. Penner, G.H.; Power, W.P.; Wasylshen, R.E. Can. J. Chem. **1988**, 66, 1821.
53. Alyea, E.C.; Dias, S.A.; Goel, R.G.; Ogini, W.O.; Pilon, P.; Meek, D.W. Inorg. Chem. **1978**, 17, 1697.
54. Whitlow, S.H. Can. J. Chem. **1974**, 52, 198.
55. Alyea, E.C.; Dias, S.A.; Ferguson, G.; Restivo, A.J. Inorg. Chem. **1977**, 16, 2329.
56. Alyea, E.C.; Dias, S.A.; Ferguson, G.; Parvez, M. Inorg. Chim. Acta **1979**, 37, 45.
57. McFarlane, W.; Rycroft, D.S. J. Chem. Soc., Faraday Trans. 2, **1974**, 70, 377.
58. Goggin, P.L.; Goodfellow, R.J.; McEwan, D.M.; Griffiths, A.J.; Kessler, K. J. Chem. Soc., J. Chem. Res. (M) **1979**, 2315.
59. (a) Roberts, P.J.; Ferguson, G.; Goel, R.G.; Ogini, W.O.; Restivo, R.J. J. Chem. Soc. Dalton **1978**, 253.  
(b) Alyea, E.C.; Dias, S.A.; Ferguson, G.; Khan, M.A.; Roberts, P.J. Inorg. Chem. **1979**, 18, 2433.
60. Alyea, E.C.; Ferguson, G.; Restivo, R.J. J. Chem. Soc. Dalton **1977**, 1845.
61. Henry, E.R.; Szabo, A. J. Chem. Phys. **1985**, 82, 4753.
62. Penner, G.H.; Wasylshen, R.E. Can. J. Chem. **1989**, 67, 1909.
63. Buergi, H.B.; Fischer, E.; Kunz, R.W.; Parvez, M.; Pregosin, P.S. Inorg. Chem. **1982**, 21, 1246.
64. Allman, T.; Lenkinski, R.E. Inorg. Chem. **1986**, 25, 3202.
65. (a) Tutunjian, P.N.; Waugh, J.S. J. Chem. Phys. **1982**, 76, 1223.  
(b) Tutunjian, P.N.; Waugh, J.S. J. Magn. Reson. **1982**, 49, 155.

66. Grimmer, A.-R.; Peter, R.; Fechner, E. Z. Chem. **1978**, 18, 109.
67. (a) Grimmer, A.-R.; Müller D.; Neels, J. Z. Chem. **1983**, 23, 140.  
(b) Haubenreisser, U.; Sternberg, U.; Grimmer, A.-R. Mol. Phys. **1987**, 60, 151.
68. Cogne, A.; Grand, A.; Laugier, J.; Robert, J.B.; Wiesenfeld, L. J. Am. Chem. Soc. **1980**, 102, 2238.
69. (a) Nolle, A. Z. Physik B **1979**, 34, 175.  
(b) Balz, R.; Haller, M.; Hertler, W.F.; Lutz, O.; Nolle, A.; Schafitel, R. J. Magn. Reson. **1980**, 40, 9.
70. Viste, A.; Hotokka, M.; Laaksonen, L.; Pyykkö, P. Chem. Phys. **1982**, 72, 225.
71. Fyfe, C.A. Solid State NMR for Chemists; CFC Press: Guelph, Ontario, Canada, 1983.
72. (a) Nelson, J.H.; Rahn, J.A.; Bearden, W.H. Inorg. Chem. **1987**, 26, 2192.  
(b) Rahn, J.A.; O'Donnell, D.J.; Palmer, A.R.; Nelson, J.H. Inorg. Chem. **1989**, 28, 2631.  
(c) Rahn, J.A.; Baltusis, L.; Nelson, J.H. Inorg. Chem. **1990**, 29, 750.
73. Carty, A.J.; Fyfe, C.A.; Lettinga, M.; Johnson, S.; Randall, L.H. Inorg. Chem. **1989**, 28, 4120.
74. Lindner, E.; Fawzi, R.; Mayer, H.A.; Eichele, K.; Pohmer, K. Inorg. Chem., **1991**, 30, 1102.
75. Eckert, H. Ber. Bunsenges. Phys. Chem. **1990**, 94, 1062.
76. Duncan, T.M. A Compilation of Chemical Shift Anisotropies; Farragut Press: Chicago, 1990.
77. Kowalewski, J. Ann. Rep. NMR Spectrosc. **1982**, 12, 82.
78. Bennett, J.; Pidcock, A.; Waterhouse, C.R.; Coggon, P.; McPhail, A.T. J. Chem. Soc. (A) **1970**, 2094.
79. Buchanan, G.W.; Morin, F.G.; Fraser, R.R. Can. J. Chem. **1980**, 58, 2442.
80. Fox, R.B.; Venezky, D.L. J. Am. Chem. Soc. **1953**, 75, 3967.
81. (a) Power, W.P.; Wasylishen, R.E.; Curtis, R.D. Can. J. Chem. **1989**, 67, 454.  
(b) Wasylishen, R.E.; Penner, G.H.; Power, W.P.; Curtis, R.D. J. Am.

- Chem. Soc. **1989**, 111, 6082.
- (c) Curtis, R.D.; Penner, G.H.; Power, W.P.; Wasylishen, R.E. J. Phys. Chem. **1990**, 94, 4000.
- (d) Curtis, R.D.; Schriver, M.J.; Wasylishen, R.E. J. Am. Chem. Soc. **1991**, 113, 1493.
82. Klose, G.; Trahms, L.; Möps, A. Chem. Phys. Lett. **1985**, 122, 545.
83. (a) Oas, T.G.; Griffin, R.G.; Levitt, M.H. J. Chem. Phys. **1988**, 89, 692.  
(b) Copié, V.; Kolbert, A.C.; Drewry, D.H.; Bartlett, P.A.; Oas, T.G.; Griffin, R.G. Biochemistry **1990**, 29, 9176.
84. du Plessis, M.P.; Modro, T.A.; Nassimbeni, L.R. Acta Cryst. **1982**, B38, 1504.
85. Beml, L.; Clark, H.C.; Davies, J.A.; Fyfe, C.A.; Wasylishen, R.E. J. Am. Chem. Soc. **1982**, 104, 438.
86. (a) Robert, J.B.; Wiesenfeld, L. Mol. Phys. **1981**, 44, 319.  
(b) Robert, J.B.; Wiesenfeld, L. J. Magn. Reson. **1980**, 38, 357.
87. Van Calsteren, M.-R.; Birnbaum, G.I.; Smith, I.C.P. J. Chem. Phys. **1987**, 86, 5405.
88. Hauser, H.; Radloff, C.; Ernst, R.R.; Sundell, S.; Pascher, I. J. Am. Chem. Soc. **1988**, 110, 1054.
89. Weller, T.; Franck, U.; Klose, G.; Lochmann, R. Z. Chem. **1982**, 22, 62.
90. Yamasaki, V.A.; Fluck, E. Z. Anorg. Allg. Chem. **1973**, 396, 297.
91. Butcher, F.K.; Deuters, B.E.; Gerrard, W.; Mooney, E.F.; Rothenbury, R.A.; Willis, H.A. Spectrochim. Acta **1964**, 20, 759.
92. Olivieri, A.C. J. Magn. Reson. **1989**, 81, 201.
93. Davies, J.A.; Dutremez, S., submitted for publication.
94. Wasylishen, R.E.; Power, W.P.; Penner, G.H.; Curtis, R.D. Can. J. Chem. **1989**, 67, 1219.
95. Pople, J.A.; Santry, D.P. Mol. Phys. **1964**, 8, 1.
96. Appleton, T.G.; Clark, H.C.; Manzer, L.E. Coord. Chem. Rev. **1973**, 10, 335.
97. Allman, T. J. Magn. Reson. **1989**, 83, 637.

98. Anderson, G.K.; Clark, H.C.; Davies, J.A.; Ferguson, G.; Parvez, M. J. Crystallogr. Spectrosc. Res. **1982**, 12, 449.
99. Pregosin, P.S. Ann. Rep. NMR Spectrosc. **1986**, 17, 285.
100. Cameron, T.S.; Clark, H.C.; Linden, A.; Nicholas, A.M. Inorg. Chim. Acta **1989**, 162, 9.
101. Caldwell, A.N.; Manojlović-Muir, L.; Muir, K.W.; Solomun, T. Eur. Cryst. Meeting **1977**, 210.
102. Kubo, A.; McDowell, C.A. J. Chem. Phys. **1990**, 92, 7156.
103. (a) Eichele, K., Ph.D. Dissertation, Universität Tübingen, 1991.  
(b) Lindner, E.; Fawzi, R.; Mayer, H.A.; Eichele, K.; Hiller, W. Organometallics **1991**, submitted for publication.
104. Del Pra, A.; Zanotti, G. Inorg. Chim. Acta **1980**, 39, 137.
105. Messmer, G.G.; Amma, E.L. Inorg. Chem. **1966**, 5, 1775.
106. Cardin, C.J.; Cardin, D.J.; Lappert, M.F.; Muir, K.W. J. Chem. Soc. Dalton **1978**, 46.
107. McFarlane, W. J. Chem. Soc. (A) **1967**, 1922.
108. Santos, R.A.; Chien, W.-J.; Harbison, G.S.; McCurry, J.D.; Roberts, J.E. J. Magn. Reson. **1989**, 84, 357.
109. Jones, W.H.; Graham, T.P.; Barnes, R.G. Phys. Rev. **1963**, 132, 1898.
110. Baugher, J.F.; Taylor, P.C.; Oja, T.; Bray, P.J. J. Chem. Phys. **1969**, 50, 4914.
111. Taylor, P.C.; Baugher, J.F.; Kriz, H.M. Chem. Rev. **1975**, 75, 203.
112. Bray, P.J.; Gravina, S.J., in Advances in Materials Characterization II; Snyder, R.L.; Condrate, R.A., Sr.; Johnson, P.F., eds.; Plenum Publishing Corp.: New York, 1985. pp.1-29.
113. Barnes, R.G.; Torgeson, D.R.; Bray, P.J. Phys. Stat. Sol. (b) **1988**, 147, K175.
114. (a) Gornostansky, S.D.; Stager, C.V. J. Chem. Phys. **1967**, 46, 4959.  
(b) Gornostansky, S.D.; Stager, C.V. J. Chem. Phys. **1968**, 48, 1416.
115. Spiess, H.W.; Haas, H.; Hartmann, H. J. Chem. Phys. **1969**, 50, 3057.
116. Segel, S.L.; Creel, R.B. Can. J. Phys. **1970**, 48, 2673.

117. Creel, R.B.; Segel, S.L.; Schoenberger, R.J.; Barnes, R.G.; Torgeson, D.R. J. Chem. Phys. **1974**, 60, 2310.
118. Mooibroek, S.; Wasylshen, R.E.; Dickson, R.; Facey, G.; Pettitt, B.A. J. Magn. Reson. **1986**, 66, 542.
119. Douglass, D.C.; Peterson, G.E. J. Am. Ceram. Soc. **1986**, 69, 48.
120. Eaton, D.R.; Buist, R.J.; Sayer, B.G. Can. J. Chem. **1987**, 65, 1332.
121. Nolle, A. Z. Physik A **1977**, 280, 231.
122. (a) Kundla, E.; Samoson, A.; Lippmaa, E. Chem. Phys. Lett. **1981**, 83, 229.  
(b) Samoson, A.; Kundla, E.; Lippmaa, E. J. Magn. Reson. **1982**, 49, 350.
123. Oldfield, E.; Kirkpatrick, R.J. Science **1985**, 227, 1537,
124. (a) Oldfield, E.; Timken, H.K.C.; Montez, B.; Ramachandran, R. Nature **1985**, 318, 163.  
(b) Han, O.C.; Timken, H.K.C.; Oldfield, E. J. Chem. Phys. **1988**, 89, 6046.
- i25. Lefebvre, F.; Amoureux, J.-P.; Fernandez, C.; Derouane, E.G. J. Chem. Phys. **1987**, 86, 6070.
126. Samoson, A.; Lippmaa, E.; Pines, A. Mol. Phys. **1988**, 65, 1013.
127. Buerger, M.J. Elementary Crystallography; Wiley: New York, 1967.
128. Chu, P.J.; Gerstein, B.C. J. Chem. Phys. **1989**, 91, 2081.
129. France, P.W. J. Magn. Reson. **1991**, 92, 30.
130. Varty, T.; Brown, R.J.C.; Temme, F.P. Z. Naturforsch. **1990**, 45a, 550.
131. Detellier, C., in NMR of Newly Accessible Nuclei; vol.2; Academic Press: New York, 1983. pp.105-151.
132. Miller, J.J. Z. Krist. **1938**, 99A, 32.
133. Morris, A.J.; Kennard, C.H.L.; Moore, F.H.; Smith, G.; Montgomery, H. Cryst. Struct. Comm. **1981**, 10, 529.
134. von Meerwall, E.D. Comp. Phys. Commun. **1977**, 13, 107.
135. Fukushima, E.; Roeder, S.B.W. Experimental Pulse NMR; Addison-Wesley: Reading, MA, 1981. pp.106-112.

136. Guerts, F.M.M.; Kentgens, A.P.M.; Veeman, W.S. Chem. Phys. Lett. **1985**, 120, 206.
137. Janssen, R.; Veeman, W.S. J. Chem. Soc., Faraday Trans. 1 **1988**, 84, 3747.
138. Samoson, A.; Lippmaa, E. J. Magn. Reson. **1988**, 79, 255.
139. Man, P.P.; Klinowski, J.; Trokiner, A.; Zanni, H.; Papon, P. Chem. Phys. Lett. **1988**, 151, 143.
140. Goc, R.; Fiat, D. Phys. Stat. Sol.(b) **1987**, 140, 243.
141. Haase, A.R.; Kerber, M.A.; Kessler, D.; Kronenbitter, J.; Kruger, H.; Lutz, O.; Muller, M.; Nolle, A. Z. Naturforsch. **1977**, 32a, 952.
142. Andrew, E.R., in The Time Domain in Surface and Structural Dynamics; Long, G.J.; Grandjean, F., eds.; Kluwer Academic Publishers: Norwell, MA, 1988. pp.31-48.
143. Oas, T.G.; Hartzell, C.J.; Dahlquist, F.W.; Drobny, G.P. J. Am. Chem. Soc. **1987**, 109, 5962.
144. (a) France, P.W. J. Magn. Reson. **1979**, 34, 585.  
(b) France, P.W. J. Magn. Reson. **1980**, 40, 311.
145. Mooibroek, S., Ph.D. Thesis, Dalhousie University, 1987.
146. (a) Kennedy, M.A.; Ellis, P.D. Concepts Magn. Reson. **1989**, 1, 35.  
(b) Kennedy, M.A.; Ellis, P.D. Concepts Magn. Reson. **1989**, 1, 109.  
(c) Kennedy, M.A., Ph.D. Thesis, University of South Carolina, 1989.
147. Volkoff, G.M.; Petch, H.E.; Smellie, D.W.L. Can. J. Phys. **1952**, 30, 270.
148. Volkoff, G.M. Can. J. Phys. **1953**, 31, 820.
149. (a) Liechti, O. J. Magn. Reson. **1988**, 80, 71.  
(b) Liechti, O.; Kind, R. J. Magn. Reson. **1989**, 85, 480.